

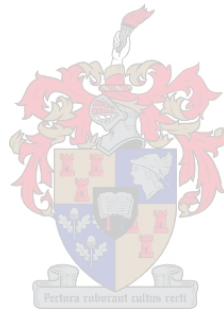


UNIVERSITEIT•STELLENBOSCH•UNIVERSITY  
jou kennisvennoot • your knowledge partner

# Comparative study of the equivalent moment factor between international steel design specifications

by

Hermanus Johannes Wessels Smalberger



Thesis presented in fulfilment of the requirements for the degree of  
Master of Science in Engineering  
in the Faculty of Engineering at Stellenbosch University

Supervisor:

Mr. Etienne van der Klashorst

December 2014

# Declaration

By submitting this thesis electronically, I declare that the entirety of the work contained therein is my own, original work, that I am the sole author thereof (unless to the extent explicitly otherwise stated), that reproduction and publication thereof by Stellenbosch University will not infringe any third party rights and that I have not previously in its entirety or in part submitted it for obtaining any qualification.

Signature: \_\_\_\_\_  
HJW Smalberger

Date: November 2014

# Synopsis

Lateral-torsional buckling (LTB) is an important failure mode that needs to be taken into account during the design of steel beams. The fundamental equation for determining the elastic critical moment of a beam was derived with the assumption that the beam is subjected to a uniform bending moment distribution. Loads on steel structures generate a great variety of bending moment distributions. The effect of the bending moment distribution is taken into account by a parameter known as the equivalent moment factor. The procedure outlined in the South African National Standard for limit-states design of hot-rolled steel work, SANS 10162-1:2011, for determining the equivalent moment factor was originally developed for a bending moment that is uniformly or linearly distributed, however it is currently used for all bending moment distributions.

A Finite Element (FE) model was developed in this investigation for determining the equivalent moment factor. The numerical model included residual stresses and initial geometric imperfections commonly found in hot-rolled steel beams. To validate the assumptions made during the development of the FE model an in-depth experimental investigation was conducted on simply supported beams. Three different load configurations were considered in the experimental study in order to simulate various bending moment distributions. A comparison of the equivalent moment factor between the numerical results and the results obtained from various steel specifications, including SANS 10162-1:2011, was carried out in an attempt to quantify the positive and negative attributes of the various methods employed by steel design specifications.

The experimental investigation concluded that the FE model is able to successfully represent a simply supported beam with realistic characteristics that include residual stresses and imperfections. The comparative study illustrated that for a bending moment distribution with a constant moment gradient, SANS 10162-1:2011 provides excellent results. However, for the other distributions considered in this investigation highly conservative results were obtained for the equivalent moment factor. The relevance of these findings were made clear by considering three design cases found in steel structures. The resistance moment of the beams in each of these cases was calculated according to each of the steel specifications. It was found that the use of a highly conservative procedure for determining the equivalent moment factor can lead to the uneconomical design of a structure.

# Samevatting

Laterale-torsie knik is 'n belangrike falings modus wat in ag geneem moet word tydens die ontwerp van staal balke. Die fundamentele vergelyking vir die bepaling van die elastiese kritieke moment van 'n balk is afgelei met die aanname dat die balk onderworpe is aan 'n eenvormige buigmoment verdeling. Belastings op staalstrukture genereer 'n groot verskeidenheid van buigmoment verdelings. Die effek van hierdie buigmoment verdelings word in ag geneem deur 'n parameter wat bekend staan as die ekwivalente moment faktor. Die prosedure uiteengesit in die Suid-Afrikaanse Nasionale Standaard vir die ontwerp van warm-gewalste staalwerk, SANS 10162-1:2011, vir die bepaling van hierdie faktor is oorspronklik ontwikkel vir 'n buigmoment wat uniform of linieêr verdeel is oor die lengte van die balk, maar dit word tans gebruik vir alle buigmoment verdelings.

'n Eindige Element (FE) model is ontwikkel in hierdie ondersoek vir die bepaling van die ekwivalente moment faktor. Die numeriese model sluit die residuele spannings en aanvanklike geometriese imperfeksies wat in die algemeen teenwoordig is in warm-gewalste profiele in. Die aannames wat gemaak is tydens die ontwikkeling van die FE model is bevestig met 'n in diepte eksperimentele ondersoek oor die gedrag van eenvoudig opgelegde balke. Drie verskillende las konfigurasies is oorweeg in die eksperimentele studie om verskeie buigmoment verspreidings na te boots. 'n Vergelyking van die ekwivalente moment faktor tussen die numeriese resultate en die resultate verkry van verskeie staal spesifikasies, insluitend SANS 10162-1:2011, is uitgevoer in 'n poging om die positiewe en negatiewe eienskappe van die verskillende metodes wat gebruik word in verskillende staal ontwerp spesifikasies, te kwantifiseer.

Die eksperimentele ondersoek het tot die gevolgtrekking gelei dat die FE model in staat is om 'n eenvoudige opgelegte balk te verteenwoordig, met realistiese eienskappe wat residuele spannings en imperfeksies insluit. Die vergelykende studie toon dat SANS 10162-1:2011 uitstekende resultate bied vir 'n buigmoment verdeling met 'n konstante moment gradiënt. Dit was egter gevind dat vir ander verdelings wat in hierdie ondersoek oorweeg is, SANS 10162-1:2011 hoogs konserwatiewe resultate bied. Die toepaslikheid van hierdie bevindinge is duidelik gemaak deur drie ontwerp gevalle wat algemeen in staalstrukture gevind word te bestudeer. Die weerstandsmoment is in elk van die gevalle bereken volgens elke staal spesifikasies. Daar is gevind dat die gebruik van 'n hoogs konserwatiewe prosedure vir die bepaling van die ekwivalente moment faktor kan lei tot die ontwerp van 'n onekonomiese struktuur.

# Acknowledgements

I would like to express my gratitude to the following individuals that contributed to the completion of the thesis:

- My parents, for their continuing support and love for which I am truly thankful.
- Chantel Olivier, for her patience and support during the late hours and long weeks.
- Mr. Etienne van der Klashorst, for guiding me through this research project and assisting me in solving any problems which I encountered.
- Mr. Johan van der Merwe, for his assistance and advice during the construction of the experimental setup.
- Greg Mitchell from FEAS (pty), for his technical assistance during the development of the finite element model.
- Peter Cupido, Herschen Adonis and Charlton Ramat for their assistance during the experimental investigation.
- All my friends, for their encouragement and support over the two years and for making the bad times better. I thank each one of you personally:
  - Charlie De La Harpe
  - Dawie de Klerk
  - Diederick Dippenaar
  - Louwrens Mostert
  - Petrus Theart
  - Philip Piek
  - Rudi van Wyk
  - Ryno Bakkies Barnard
- Lastly and most importantly, I would like to thank my Heavenly Father for giving me the ability and intelligence to complete this thesis.

# Contents

<b>List of Figures</b>	<b>ix</b>
<b>List of Tables</b>	<b>xiii</b>
<b>1 Introduction</b>	<b>1</b>
1.1 Background . . . . .	2
1.2 Research objectives . . . . .	3
1.3 Scope and limitations . . . . .	4
1.4 Research methodology . . . . .	5
1.4.1 Finite Element Analyses . . . . .	5
1.4.2 Experimental testing . . . . .	6
1.4.3 Comparison of the equivalent moment factor . . . . .	6
1.5 Research outline . . . . .	6
<b>2 Literature review</b>	<b>8</b>
2.1 Introduction . . . . .	8
2.2 Lateral-torsional buckling . . . . .	8
2.3 Elastic and inelastic buckling . . . . .	10
2.3.1 Residual stresses . . . . .	10
2.3.2 Initial imperfections . . . . .	11
2.4 Elastic critical moment . . . . .	12
2.4.1 Equivalent moment factor . . . . .	14
2.4.2 Load with respect to the shear centre . . . . .	16
2.4.3 Supports and restraints . . . . .	17
2.5 Design approach of different specifications . . . . .	19
2.5.1 SANS 10162-1:2011 . . . . .	19
2.5.2 ANSI/AISC 360-05 . . . . .	21
2.5.3 EN 1993-1-1 . . . . .	23
2.5.3.1 $C_1$ and $C_2$ factors . . . . .	24
2.5.3.2 General case . . . . .	25
2.5.3.3 Special case . . . . .	25

2.5.4	CSA S16-09 . . . . .	26
2.5.4.1	The effective length factor . . . . .	27
2.5.5	Comparison of steel specifications . . . . .	28
2.6	Finite Element Analysis . . . . .	28
2.6.1	Linear analysis . . . . .	29
2.6.2	Nonlinear analysis . . . . .	30
2.6.3	Solution of nonlinear equilibrium equations . . . . .	31
2.6.4	Finite element models . . . . .	32
2.6.4.1	Finite elements . . . . .	32
2.6.4.2	Mesh generation and refinement . . . . .	34
2.7	Lateral-torsional buckling experiments . . . . .	36
2.7.1	Experimental setup . . . . .	36
2.7.2	Measuring systems . . . . .	39
2.7.3	Load applications . . . . .	41
2.8	Literature overview and conclusions . . . . .	42
<b>3</b>	<b>Finite Element Analysis</b>	<b>45</b>
3.1	Introduction . . . . .	45
3.2	Model development . . . . .	45
3.2.1	Model description . . . . .	46
3.2.2	Elements and mesh configuration . . . . .	48
3.2.3	Material properties . . . . .	48
3.2.4	Boundary conditions . . . . .	51
3.2.5	Initial geometric imperfections . . . . .	52
3.2.6	Residual stresses . . . . .	54
3.2.7	Load conditions . . . . .	56
3.2.8	Analysis method . . . . .	57
3.3	Preliminary validation . . . . .	58
3.4	Conclusion . . . . .	60
<b>4</b>	<b>Experimental design</b>	<b>61</b>
4.1	Introduction . . . . .	61
4.2	Motivation for experimental research . . . . .	61
4.3	Experimental design overview . . . . .	62
4.3.1	Conceptual design . . . . .	62
4.3.2	Actuator support structure . . . . .	63
4.3.3	Support conditions . . . . .	64
4.3.4	Lever arm design . . . . .	66
4.4	Testing configurations . . . . .	68
4.4.1	End moment and distributed load . . . . .	68

4.4.1.1	Measurement equipment . . . . .	70
4.4.2	Tests involving the Gravity Load Simulator (GLS) . . . . .	72
4.4.2.1	Measurement and load application equipment . . . . .	73
4.4.2.2	Point load at mid-span . . . . .	74
4.4.2.3	Two point loads at overhung ends . . . . .	75
4.4.3	Measuring of initial imperfections . . . . .	77
4.5	Experimental limitations . . . . .	79
4.6	Conclusion . . . . .	80
<b>5</b>	<b>Experimental results</b>	<b>82</b>
5.1	Introduction . . . . .	82
5.2	Comparison between experimental and numerical results . . . . .	82
5.2.1	Simply supported beam with end moment and distributed load . . . . .	83
5.2.2	Simply supported beam with point load at mid-span . . . . .	86
5.2.3	Simply supported beam with two point loads at overhung ends . . . . .	87
5.3	Conclusion . . . . .	90
<b>6</b>	<b>Comparison of the equivalent moment factor</b>	<b>92</b>
6.1	Introduction . . . . .	92
6.2	Comparison of $C_b$ for various bending moment distributions . . . . .	92
6.2.1	Moment distribution type 1 . . . . .	93
6.2.2	Moment distribution type 2 . . . . .	94
6.2.3	Moment distribution type 3 . . . . .	96
6.2.4	Moment distribution type 4 . . . . .	97
6.3	Relevance of results . . . . .	98
6.3.1	Simply supported beam . . . . .	99
6.3.2	Crane girder . . . . .	100
6.3.3	Portal frame rafter beam . . . . .	101
6.4	Conclusion . . . . .	102
<b>7</b>	<b>Conclusion and recommendations</b>	<b>104</b>
7.1	Conclusions . . . . .	104
7.2	Recommendations . . . . .	108
7.3	Concluding statement . . . . .	109
<b>A</b>	<b>Derivation of the Elastic Critical Moment</b>	<b>115</b>
<b>B</b>	<b>Geometric imperfections of test specimens</b>	<b>120</b>
<b>C</b>	<b>Experimental Results</b>	<b>123</b>
<b>D</b>	<b>Sample calculation for determining <math>C_b</math></b>	<b>131</b>



---

D.1	End moment and distributed load . . . . .	131
<b>E</b>	<b>Determination of the moment resistance</b>	<b>133</b>
E.1	Simply supported beam . . . . .	133
E.1.1	SANS 10162-1:2011 . . . . .	134
E.1.2	CSA S16-09 . . . . .	134
E.1.3	AISC 360-05 . . . . .	135
E.1.4	EN 1993-1-1 . . . . .	136
E.2	Crane girder . . . . .	138
E.2.1	General problem outline . . . . .	138
E.2.2	SANS 10162-1:2011 . . . . .	139
E.2.3	CSA S16-09 . . . . .	140
E.2.4	AISC 360-05 . . . . .	140
E.2.5	EN 1993-1-1 . . . . .	141
E.3	Rafter beam . . . . .	143
E.3.1	General problem outline . . . . .	143
E.3.2	SANS 10162-1:2011 . . . . .	144
E.3.3	CSA S16-09 . . . . .	145
E.3.4	AISC 360-05 . . . . .	147
E.3.5	EN 1993-1-1 . . . . .	149
<b>F</b>	<b>Detail drawings of experimental setup</b>	<b>152</b>

# List of Figures

1.1	Lateral-torsional buckling of a cantilever . . . . .	2
1.2	The Marcy Pedestrian Bridge . . . . .	3
2.1	I-beam with central concentrated load . . . . .	9
2.2	Interaction between instability and plasticity . . . . .	10
2.3	Residual stresses in I-beam . . . . .	11
2.4	Lateral buckling strength of simply supported I-beam . . . . .	12
2.5	Beam failure curve . . . . .	12
2.6	Bifurcation of the equilibrium . . . . .	13
2.7	Quarter-Point Method . . . . .	15
2.8	Applied loads on top and bottom flanges . . . . .	16
2.9	Results for centrally-loaded beam . . . . .	17
2.10	End support conditions for a beam . . . . .	18
2.11	Uniformly distributed load with equal end moments . . . . .	20
2.12	Beam strength vs. Unbraced length . . . . .	23
2.13	Point of application of transverse load . . . . .	24
2.14	Fallacy of assuming that an inflection point is a brace point . . . . .	27
2.15	Comparison between moment capacities for EN1993-1-1, AISC 360-05, SANS 10162-1:2011 and CSA S16-09 for a beam subjected to a uniform moment. . . . .	28
2.16	Newton-Raphson and Arc-length method . . . . .	32
2.17	I-beam constructed from three plates . . . . .	33
2.18	Thin-walled channel loaded by transverse tip force $P$ in the plane of the web . . . . .	34
2.19	Refinement possibilities . . . . .	35
2.20	Bending moment distribution in an experimental beam setup . . . . .	36
2.21	Schematic elevation of test rig . . . . .	37
2.22	Buckled shape of compression flange . . . . .	37
2.23	Section S-S . . . . .	38
2.24	Support system . . . . .	39
2.25	Deflection monitor system at mid-span . . . . .	40
2.26	Displacement device for measuring displacement . . . . .	40

2.27 Gravity Load Simulator . . . . .	41
2.28 Buckled shape of compression flange with GLS at both ends . . . . .	41
3.1 Cross section of IPE200 . . . . .	46
3.2 Beam model layout . . . . .	47
3.3 Shear distribution through section . . . . .	49
3.4 Material model for S355JR steel . . . . .	50
3.5 Idealized simply supported boundary conditions . . . . .	51
3.6 Coupling Constraint . . . . .	52
3.7 Straightness tolerance . . . . .	53
3.8 Ultimate capacity with varying imperfection mode and magnitude . . . . .	53
3.9 Imperfection shapes and failure modes at UL . . . . .	54
3.10 Residual stress contours and distribution for I-section (half span only) . . . . .	55
3.11 Residual stress distribution from Abaqus . . . . .	55
3.12 Effect of residual stresses on ultimate load capacity . . . . .	56
3.13 Loading configurations for FE study . . . . .	57
3.14 Moment capacities for a simply supported beam . . . . .	59
4.1 Concept for applying end moment . . . . .	62
4.2 General layout of experimental setup . . . . .	63
4.3 Force distribution throughout support structure . . . . .	64
4.4 Support frame 1 (pinned) . . . . .	65
4.5 Support components . . . . .	66
4.6 Reaction forces at hinges . . . . .	67
4.7 Lever arm components . . . . .	67
4.8 Loading configurations for experimental work . . . . .	68
4.9 Test layout for end moment and distributed load . . . . .	69
4.10 Before and after the test was conducted . . . . .	70
4.11 Geometric variables to measure applied end moment and end rotation . . . . .	70
4.12 Transducer at actuator end support . . . . .	71
4.13 Transducer at support frame 1 . . . . .	72
4.14 Load application equipment . . . . .	73
4.15 Transducer at actuator end support . . . . .	74
4.16 Point load at mid-span . . . . .	75
4.17 Initial and deformed state . . . . .	75
4.18 Beam with overhung ends . . . . .	76
4.19 Beam with overhung ends . . . . .	76
4.20 Restraint at support . . . . .	77
4.21 Geometric imperfection of test specimens . . . . .	78
4.22 Measuring of imperfections . . . . .	78

4.23	Recorded imperfections of test specimen B8 . . . . .	79
4.24	Additional rotation of the support frame relative to the test specimen . . . . .	80
5.1	End moment and distributed load . . . . .	83
5.2	End moment and distributed load . . . . .	84
5.3	LTB due to single end moment and distributed load . . . . .	85
5.4	Point load at mid-span . . . . .	86
5.5	Single point load at midspan . . . . .	86
5.6	LTB due to point load at mid-span . . . . .	88
5.7	Two point loads at overhung ends . . . . .	88
5.8	Test specimen B12 . . . . .	89
5.9	LTB due to point loads at overhung ends . . . . .	90
6.1	Moment distribution type 1 . . . . .	93
6.2	$C_b$ results for moment distribution type 1 . . . . .	94
6.3	Moment distribution type 2 . . . . .	94
6.4	$C_b$ results for moment distribution type 2 . . . . .	95
6.5	Simply supported beam subjected to double curvature due to equal end moments applied in the same direction . . . . .	96
6.6	Moment distribution type 3 . . . . .	96
6.7	$C_b$ results for moment distribution type 3 . . . . .	97
6.8	Moment distribution type 4 . . . . .	97
6.9	$C_b$ results for moment distribution type 4 . . . . .	98
6.10	Steel beam ( $457 \times 191 \times 98$ ) with uniformly distributed load . . . . .	99
6.11	Rafter bending moment diagram . . . . .	101
A.1	Beam subjected to arbitrary loads in $yz$ plane . . . . .	115
A.2	Beam subjected to arbitrary loads in $yz$ plane (Top view) . . . . .	116
A.3	I-beam subjected to moments . . . . .	117
B.1	Recorded imperfections of test specimen B1 . . . . .	120
B.2	Recorded imperfections of test specimen B2 . . . . .	120
B.3	Recorded imperfections of test specimen B3 . . . . .	121
B.4	Recorded imperfections of test specimen B4 . . . . .	121
B.5	Recorded imperfections of test specimen B5 . . . . .	121
B.6	Recorded imperfections of test specimen B6 . . . . .	122
B.7	Recorded imperfections of test specimen B7 . . . . .	122
B.8	Recorded imperfections of test specimen B8 . . . . .	122
C.1	Test specimen B7 . . . . .	124
C.2	Test specimen B8 . . . . .	124

---

C.3	Test specimen B9 . . . . .	125
C.4	Test specimen B10 . . . . .	125
C.5	Test specimen B1 . . . . .	126
C.6	Test specimen B2 . . . . .	126
C.7	Test specimen B3 . . . . .	127
C.8	Test specimen B4 . . . . .	127
C.9	Test specimen B5 . . . . .	128
C.10	Test specimen B6 . . . . .	128
C.11	Test specimen B12 . . . . .	129
C.12	Test specimen B13 . . . . .	129
C.13	Test specimens B12 & B13 . . . . .	130
E.1	W610×217 . . . . .	138
E.2	Crane girder . . . . .	138
E.3	Bending moment distribution along girder . . . . .	139
E.4	Typical portal frame . . . . .	143
E.5	Rafter bending moment diagram . . . . .	143

# List of Tables

2.1	Types of sections and their properties . . . . .	9
2.2	Length factors for end support conditions . . . . .	19
2.3	Table 1 in SANS 10162-1:2011 . . . . .	20
2.4	Recommended values for imperfection factor for lateral-torsional buckling curves . . . . .	25
2.5	Recommended values for lateral buckling curves for cross sections . . . . .	25
2.6	Selection of lateral-torsional buckling curve for cross sections . . . . .	26
3.1	Cross-sectional properties . . . . .	47
4.1	Rotation of beam end for the two methods of measuring the end rotation . . . . .	72
6.1	Moment resistance for simply supported beam . . . . .	99
6.2	Crane girder properties . . . . .	100
6.3	Moment resistance for crane girder . . . . .	100
6.4	Moment resistance for rafter beam segment 1 . . . . .	101
6.5	Moment resistance for rafter beam segment 2 . . . . .	101
6.6	Moment resistance for rafter beam segment 3 . . . . .	102
A.1	Cosines of angles between axes in figure A.1 and A.2 . . . . .	116

# Nomenclature

A-L	Arc-Length
ASD	Allowable Flexural Strength
CAD	Computer-Aided Drawing
DOF	Degrees of Freedom
FE	Finite Element
FEA	Finite Element Analysis
FEM	Finite Element Methods
GC	General Case
GLS	Gravity Load Simulator
LRFD	Load and Resistance Factor Design
LTB	Lateral-Torsional Buckling
N-R	Newton-Raphson
RS	Residual Stresses
SC	Special Case
UL	Ultimate Load
$b$	Flange width [mm]
$C_b$	Equivalent moment factor
$C_w$	Warping constant [mm <sup>6</sup> ]
$E$	Young's modulus / Modulus of elasticity [GPa]

---

$\varepsilon_e$	Engineering strain [mm mm <sup>-1</sup> ]
$\varepsilon_t$	True strain [mm mm <sup>-1</sup> ]
$f_y$	Yield stress [MPa]
$G$	Shear modulus [GPa]
$h$	Section height [mm]
$I_{yy}$	Moment of inertia, about y-axis [mm <sup>4</sup> ]
$J$	St. Venant's torsion constant [mm <sup>4</sup> ]
$K$	Effective length factor
$\kappa$	Ratio of smaller moment to larger moment
$L$	Gross length, length of member [mm]
$M$	Applied moment [kN m]
$M_{cr}$	Elastic critical moment [kN m]
$M_p$	Plastic moment [kN m]
$M_r$	Resistance moment [kN m]
$M_y$	Yield moment [kN m]
$P$	Applied point load [kN]
$r_y$	Radius of gyration, about y-axis [mm]
$\sigma_e$	Engineering stress [MPa]
$\sigma_r$	Residual stress [MPa]
$\sigma_t$	True stress [MPa]
$\sigma_y$	Yield stress [MPa]
$t_f$	Flange thickness [mm]
$t_w$	Web thickness [mm]
$W$	Distributed line load [kN m <sup>-1</sup> ]
$Z_e$	Elastic section modulus [mm <sup>3</sup> ]



# Chapter 1

## Introduction

For the design of steel beams it is required to determine the capacity of beams that are prone to lateral-torsional buckling (LTB). The calculation usually involves taking into account the bending moment distribution along the beam through a parameter known as the equivalent moment factor. This factor is then simply multiplied with the critical elastic moment capacity as derived by Timoshenko et al. (1961). Although this is the general procedure, each steel specification has a different method of determining the equivalent moment factor.

The method described in SANS 10162-1:2011 was originally developed for the use of a bending moment distribution with a constant gradient or a uniform moment distribution as far back as 1955, however the equation in SANS 10162-1:2011 is currently still used for any moment distribution. During the period of this research study, the decision was made to adopt relevant parts of the Canadian Steel Standard (CSA, 2014) as the latest version of the South African code for the design of hot-rolled steelwork. This adoption may be considered overdue due to the fact that the erroneous use of the equivalent moment factor that is presented in SANS 10162-1:2011 was corrected in the 2009 edition of CSA S16, as based on the research by Driver et al. (2010). The Canadian Standard still also uses an approach similar to that of the current version of SANS 10162-1:2011, but also provides a more accurate method for bending moment distributions other than a linear or uniform one.

The current method for determining the equivalent moment factor was investigated in-depth and compared to various steel specifications by Driver et al. (2010) and concluded that the approach followed by SANS 10162-1:2011 yields conservative results and in some cases un-conservative results. However, few of the numerical models, if any, considered during the investigation by Driver et al. (2010) have been validated by an experimental study. This study to an extent duplicates existing research, but introduces new experimental work and independent finite element analysis to motivate the addition of a more complex design method.

The objective of this research thesis is to compare SANS 10162-1:2011 and other notable steel design specifications, including the Canadian Standard, with numerical results in order to determine the accu-

racy of the different methods. The following sections present the background of the investigation and describe the problem statement. The research scope and objectives are presented in Sections 1.2 and 1.3 respectively. The research methodology followed in this investigation is discussed in Section 1.4 and an overview of the thesis contents and research investigation process is presented in Section 1.5.

## 1.1 Background

Steel is a popular and efficient building material and is constantly used to create new structures, it has been utilized for over a century in the construction of buildings and bridges. One of the main reasons why steel is such a popular building material is because it usually takes less time to construct a steel structure when compared to a concrete structure. The ductile behaviour of steel, coupled with its high tensile capacity, also adds to the popularity of this building material.

Beams are structural elements that are found in most structures in various shapes and sizes. They are capable of withstanding loads primarily by resisting bending and shear. Over the years many different types of steel sections have been developed to be used as beams, of which the most popular is the I-section. I-beams subjected to flexural bending have greater strength and stiffness in the plane in which the load is applied, which is generally perpendicular to the strong axis, rather than in the plane of the minor axis (Mohebkah, 2011). If a beam does not have the sufficient stiffness or lateral support the beam can fail in a mode that is referred to as lateral-torsional buckling (LTB), as shown in figure 1.1.



Figure 1.1: Lateral-torsional buckling of a cantilever (Trahair et al., 2008)

When failure does occur due to LTB the consequences can be devastating. In 2002 the Marcy pedestrian bridge in New York collapsed during construction due to LTB, as shown in figure 1.2. The composite bridge consisted of a steel tub girder and concrete slab. Failure occurred during the casting of the deck, injuring nine workers and killing one (Peraza, 2008). Incidents like this illustrate the importance of understanding the behaviour of structures and ensuring the structural integrity of its members as a whole. Where the capacity of a beam is insufficient, it is the designer's responsibility to provide bracing

systems or increase the member size.



Figure 1.2: The Marcy Pedestrian Bridge (Peraza, 2008)

Different countries adopt their own design standards and they may vary substantially from one another in the way that they characterize the physical bending resistance. Fundamentally all design standards use the same approach to determine the capacity of a beam prone to LTB, the procedure is either explicitly or implicitly based on the calculation of a member's elastic critical moment,  $M_{cr}$  (Galambos et al., 2008). South Africa is currently in the process of updating the existing steel specification for the design of hot-rolled steelwork. To better understand the reason behind the decision for adopting the Canadian Standard it is worth noting the origin of the current steel code, SANS 10162-1:2011, which was adopted from previous versions of the S16 code.

It is clear that South Africa is moving towards the design philosophy of Northern America, where The United States of America, Canada and Mexico all adopt a similar design approach in their codes. This is also reflected by Part 2 of the steel code, SANS 10162-2:2011, which was adopted from the Australian Standard due to the similarities between the two countries with regards to cold-formed steel construction. It is worth mentioning that the Australian Standard is fundamentally based on the North American Standard, which was developed according to the existing knowledge base of The United States of America and Canada.

## 1.2 Research objectives

The following research objective can be identified:

- To determine how the approach of SANS 10162-1:2011, with regards to the equivalent moment factor, compares to other steel specifications.

This research investigation aims to compare SANS 10162-1:2011 with other international steel design specifications. Its main objective is to highlight both positive and negative attributes of SANS 10162-1:2011 in comparison with other specifications. Apart from this, there are also the following principal objectives:

- To add to the existing database of experimental studies concerning LTB.
- To investigate the failure phenomenon that is LTB.
- To develop a finite element (FE) model that is able to accurately simulate the behaviour of steel beams.
- To compare experimental test results and numerical results.
- To evaluate the computational effort of SANS 10162-1:2011 compared to other steel specifications.
- To illustrate the relevance of the results obtained by the comparison.

### 1.3 Scope and limitations

The variety of support conditions and span configurations a beam can be exposed to makes this research field rather broad. Therefore, for this investigation only beams that are simply supported was considered. The aim of this investigation was to subject the beam to a purely elastic deformation up to the buckling point, which requires a large span. For this reason and the fact that only certain lengths are available from steel merchants, the span concerned during this investigation is 6.5 m.

The experimental work carried out during this investigation was conducted on IPE200 sections. The size of this section makes it large enough for use in practice, but also small enough to subject it to LTB in a lab environment. The IPE200 is also a class 1 section which eliminates the possibility of local buckling occurring. A total number of 13 tests were carried out, due to time and financial restrictions. The testing program was as follows:

- Four tests with an end moment and distributed load.
- Six tests with a single point load at mid-span.
- Three tests with two end moments.

A beam can be subjected to a large number of load configurations that can greatly influence the behaviour of the beam. In this study four different types of load configurations were applied to the numerical model for the comparison of the steel specifications. Three of the four correspond to the configurations mentioned above, the fourth configuration was not possible to simulate in the experimental study. These four configurations were specifically chosen in order to evaluate the performance of SANS 10162-1:2011 and the other codes. Unlike the load configurations in the three experimental tests, all vertical loads were

applied at the shear centre of the numerical model, in order to eliminate the effect of taking account of a destabilizing load.

The steel design specifications considered in this study are the following:

- SANS 10162-1:2011
- AISC 360-05
- CSA S16-09
- EN 1993-1-1

The FE model is used to apply various load configurations to the beam in order to simulate the various bending moment distributions. From this the numerical value of the equivalent moment factor can be determined. To conclude, this research includes experimental and numerical investigations to determine the equivalent moment factor for a simply supported beam subjected to various bending moment distributions.

## 1.4 Research methodology

This section presents the research methodology and hypothesis for this thesis. The research consists of Finite Element Analyses (FEA) and experimental investigations in order to determine the equivalent moment factor for a simply supported beam. The research hypothesis can be summarized in the following statement:

*The equation used in SANS 10162-1:2011 to determine the equivalent moment factor was originally developed for a bending moment distribution with a constant gradient, however its continuing use for all types of distributions leads to highly conservative results and in some cases un-conservative results.*

This research can be broken down into four different stages. Firstly, a thorough literature review was conducted in order to determine and quantify the potential variables that can contribute to the LTB of a beam, as well as a study of previous experimental investigations. Secondly, a FE model was developed that is able to simulate the behaviour of steel beams in order to determine the equivalent moment factor. The third stage includes an experimental investigation which provides insight into the behaviour of simply supported beam in order to validate the FE model. Finally, the comparison of the equivalent moment factor, by which the comparative performance of the steel specifications is evaluated.

### 1.4.1 Finite Element Analyses

FEA can be used to study the behaviour of steel beams subjected to various load configurations and boundary conditions. The FE model developed in this study also includes the effects of residual stresses, initial imperfections and a material model based on the true stresses and strains. The deliverables for this model are to:

1. Accurately simulate the behaviour of a steel beam.
2. Determine the equivalent moment factor for various bending moment distributions based on numerical results.
3. Serve as a database for future work.

This FE model provides a tool for further investigation of steel beams, including larger sections, different support conditions and other load configurations.

### 1.4.2 Experimental testing

A full scale experimental study, comprising of three different testing configurations was conducted in order to study the behaviour of a simply supported steel beam. The experimental results will aim to validate the numerical model. A total of thirteen tests were carried out, which consisted of four tests for a non-linear distribution, six tests for a bi-linear distribution and three tests for a uniform distribution. The main deliverables of the experimental work are to:

1. Study the behaviour of a simply supported beam.
2. Validate the assumptions made during the development of the FE model.
3. Add to the database of existing experimental setups concerning LTB.

### 1.4.3 Comparison of the equivalent moment factor

The comparison of steel specifications against each other as well as numerical results, gives a direct indication of the conservatism, or lack thereof, of the specifications under consideration. The comparison of the equivalent moment factor considers four different bending moment distributions. The relevance of the results obtained are presented through various examples commonly found in structural engineering practice. The main deliverables of the comparison are to:

1. Compare the different methods for obtaining the equivalent moment factor.
2. Compare the calculation complexity of each specification.
3. Illustrate the relevance of the results through practical examples.

The comparative study will give insight and motivation for the decision of adopting a new steel design specification.

## 1.5 Research outline

This first chapter presented a short background on the importance of steel beam design and the failure mode of LTB. The scope of the investigation was discussed along with the methodology that was followed

in order to complete this study.

Chapter 2 presents the literature review conducted for this study. It defines the LTB phenomenon as well as factors that contribute to this failure mode. A detailed discussion on the procedure followed for beam design of all four steel specifications is presented. Previous experimental work and finite element modelling concerning LTB are discussed.

Chapter 3 discusses the development of the FE model. All the assumptions made for the model to behave like a real steel beam are presented.

Chapter 4 presents and discusses the experimental design as well as the three different tests conducted in this investigation.

Chapter 5 presents the results obtained from the experimental tests and numerical analyses. The chapter discusses the validation process of the FE model.

Chapter 6 presents the comparison of the equivalent moment factor between the steel specifications and the numerical model. It also discusses the relevance of the results obtained.

Chapter 7 concludes the thesis with a summary of the conclusions gathered throughout this study as well as recommendations for future work.

Chapter 7 is followed by a series of appendices, which include the derivation of the elastic critical moment, geometric imperfections of test specimens and experimental results. Also included in the appendices are the calculations carried out in order to determine the resistance moment and  $C_b$  together with a complete set of CAD drawings for the experimental setup.

## Chapter 2

# Literature review

### 2.1 Introduction

This chapter reviews a large body of knowledge that provides the framework for guiding this investigation as well as relevant information with regards to lateral-torsional buckling (LTB) and factors that contribute to this phenomenon. The basic definition for LTB is discussed along with external factors, e.g. end supports and bracing, as well as internal factors that can induce this type of buckling, such as residual stresses and geometric imperfections. The design for LTB according to the various steel codes under consideration are discussed in detail, as this is the focus point of this investigation. Published research on LTB experiments and finite element modelling (FEM) are also presented as a point of departure for the experimental and numerical work that were done during this study.

### 2.2 Lateral-torsional buckling

Lateral-torsional buckling is a failure mode that may often be the controlling factor in steel beam design. LTB occurs when a steel beam is subjected to a bending moment with respect to its major axis and the applied moment  $M$  reaches the elastic buckling moment,  $M_{cr}$ , when the beam buckles by deflecting laterally and twisting (Trahair et al., 2008). Beams are especially prone to this type of buckling during the construction phase, when braces are either absent or different in type from the permanent bracing system (Galambos et al., 2008).

When LTB occurs the line of action of the load moves with the cross section, but remains vertical, as shown in figure 2.1. The case where the load acts above the centroid is more dangerous than that of the loading applied to the shear centre because of the additional torque which increases the twisting of the beam and decreases its resistance to buckling (Ho et al., 2002). The two deformations are interdependent, i.e. lateral deflection increases twisting and twisting increases lateral deflection, therefore the buckling deformations are coupled which makes the analysis of this type of failure complex. In deriving design



rules for beams based on considerations of lateral buckling certain simplifications are essential (Kirby et al., 1979).

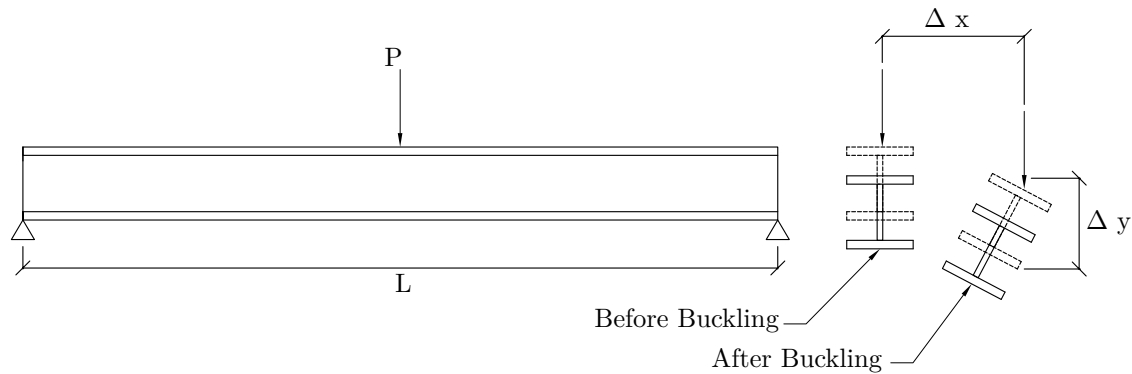


Figure 2.1: I-beam with central concentrated load

Table 2.1: Types of sections and their properties

Section Properties	Square	Flat bar	H-Section	I-Section	Rectangular Hollow Section
A	1	1	1	1	1
I <sub>xx</sub>	1	25	12.45	45.59	16.94
I <sub>yy</sub>	1	0.04	3.2	3.2	8.1
J	1	0.04	0.034	0.033	4.731

The problem of lateral instability can be minimized by a sensible choice of section. Kirby and Nethercot illustrated this by taking five different types of sections as shown in table 2.1. Although each has the same cross-sectional area, the values of their flexural and torsional properties relative to those of the unit square exhibit considerable variation. They found that the flat bar and the I-section to be the least stable. Although the rectangular hollow section exhibits a very large degree of lateral stability, it is more common to use I-sections because they are easier to produce and particularly easier to join to other members (Kirby et al., 1979).

Lateral-torsional buckling can also be avoided by:

1. Providing properly spaced and designed lateral and/or torsional bracing.
2. Connecting open-section beam groups intermittently by triangulated lacing or diaphragms.
3. Ensuring that the required design moment does not exceed the critical value (Galambos et al., 2008).

The principal variable affecting LTB is the distance between lateral and/or torsional restraints. Other variables include the type and position of the loads, the restraints at the ends and the intermediate positions along the beam axis, continuity at supports, residual stresses and initial imperfections.

## 2.3 Elastic and inelastic buckling

The failure of a perfectly straight beam is initiated when the additional stresses induced by elastic buckling cause first yield. However, a perfectly straight beam of intermediate slenderness may start yielding before the elastic buckling moment is reached, because of the combined effects of the in-plane bending stresses and any residual stresses, and may subsequently buckle inelastically (Trahair et al., 2008).

Only in cases for which the elastic critical moment is less than the moment at first yield, i.e.  $M_{cr} < M_Y$ , will lateral buckling be a purely elastic phenomenon. If  $M_{cr} > M_Y$  buckling will not occur until after the appearance of some plastic zones. The limiting case will correspond to the beam that is sufficiently stocky for it to attain its fully plastic moment  $M_p$ . This interaction between plasticity and instability is summarized in figure 2.2. Three distinct regions may be observed:

1. Beams of high slenderness ( $\sqrt{M_p/M_{cr}} > 1.1$ ) which fail by elastic lateral buckling at  $M_{cr}$ .
2. Beams of intermediate slenderness ( $1.1 > \sqrt{M_p/M_{cr}} > 0.4$ ) for which collapse is by inelastic lateral buckling at loads below  $M_{cr}$ .
3. Stocky beams ( $0.4 > \sqrt{M_p/M_{cr}}$ ) which are capable of attaining  $M_p$  without buckling (Kirby et al., 1979).

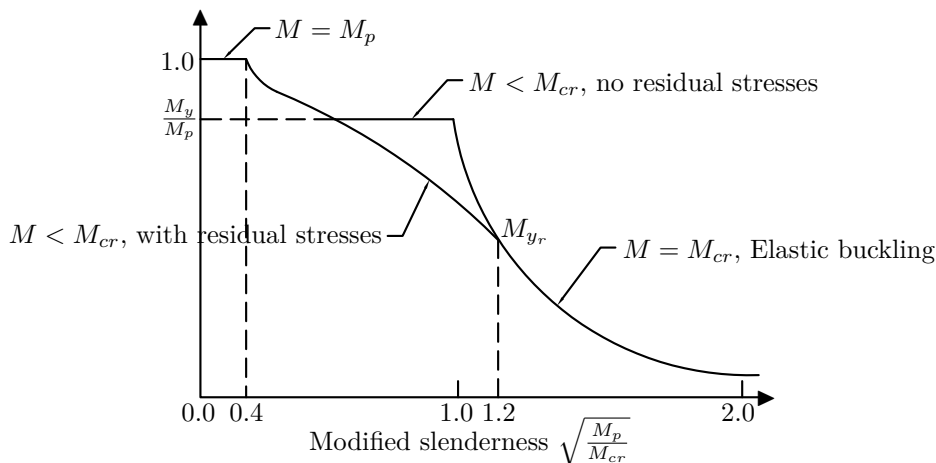


Figure 2.2: Interaction between instability and plasticity (Kirby et al., 1979)

### 2.3.1 Residual stresses

It is normally assumed that a structural element that bears no load is free from stress and strain. However, in reality stresses and strains exist that are created during the manufacturing process of these elements. Hot-rolled steel members are subjected to large thermal expansions during the manufacturing process that result in yield level strains occurring within these members. Because the subsequent cooling is not uniform throughout the element, self equilibrating internal stress patterns are formed. These stresses are known as residual stresses as shown in figure 2.3.

The distribution and magnitude of residual stresses are functions of a variety of factors, including hot

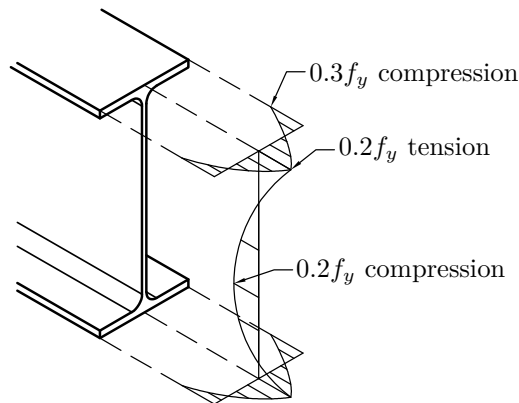


Figure 2.3: Residual stresses in I-beam

rolling, welding and flame cutting. The residual stresses due to cold straightening are usually localized and can in most cases be neglected (Galambos, 1968). Residual stresses in beams cause yielding to be initiated at lower moments and once started, yielding spreads gradually through the cross section as the moment is increased. As shown in figure 2.2 the elastic range now starts at a moment  $M_{y_r}$  and is increased at the expense of the elastic range. The presence or absence of residual stresses has no effect on the value of  $M_p$  and the plastic range is virtually unaffected (Kirby et al., 1979).

The flange-tip residual stresses are comparatively high in hot-rolled beams, especially those with high ratios of flange to web area, and so the inelastic buckling is initiated comparatively early in these beams. The residual stresses in hot-rolled beams decrease away from the flange tips and so the extent of yielding increases and the effective rigidities steadily decrease in an approximately linear fashion as the slenderness increases, as can be seen in figure 2.4 (Trahair et al., 2008). Residual stresses can be greatly reduced by stress-relieving the member, but is usually only done in cases where it will make a positive contribution to the economy of the structure (Galambos, 1968).

### 2.3.2 Initial imperfections

Behaviour of a thin-walled structure may be strongly influenced by imperfection in geometry or misalignment in connections. Imperfections are often introduced during manufacture or assembly, and may be overlooked in analysis because they are small and their magnitude and location are unknown. Yet their presence may greatly reduce the load-carrying capacity of the structure (Cook et al., 2002).

In order to examine the effect of either the presence of an initial lack of straightness or of eccentricity in the applied loading, it is convenient to consider first the case where the beam is both free of residual stresses and very slender such that  $M_{cr} \ll M_Y$ . The “imperfect” beam’s lateral deflection and twist increase continuously from the start of loading, tending to become very large as the applied moment approaches  $M_{cr}$ . These additional deformations produce additional stresses and for very slender beams failure will occur almost immediately after the maximum stress in the beam reaches the material yield

stress (Kirby et al., 1979).

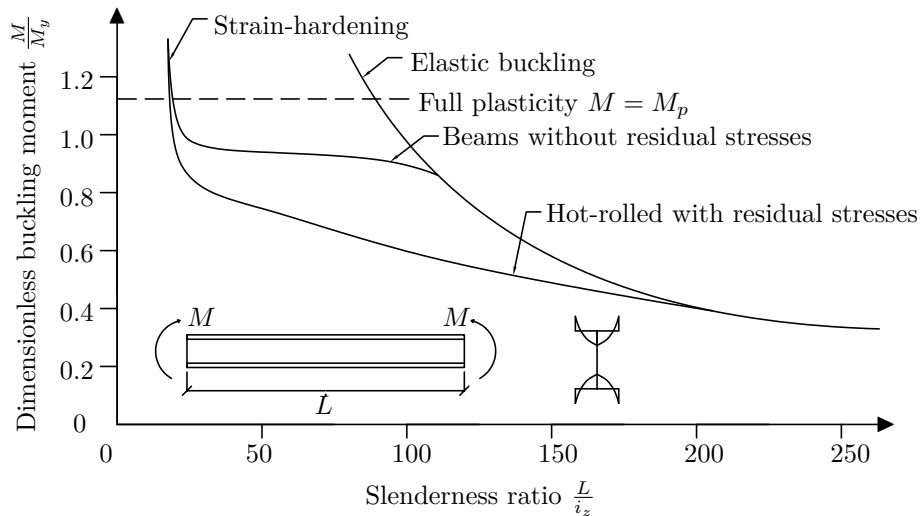


Figure 2.4: Lateral buckling strength of simply supported I-beam (Trahair et al., 2008)

This form of failure by limiting the stress to yield magnitude is shown in figure 2.5. In the case of beams of intermediate slenderness, a small amount of stress redistribution is possible after yielding and the prediction by the limiting stress approach will be conservative. When the presence of residual stresses is allowed for in calculating the values of the applied loads at which yielding is initiated, it is found that the approach becomes conservative, even for very slender beams (Kirby et al., 1979).

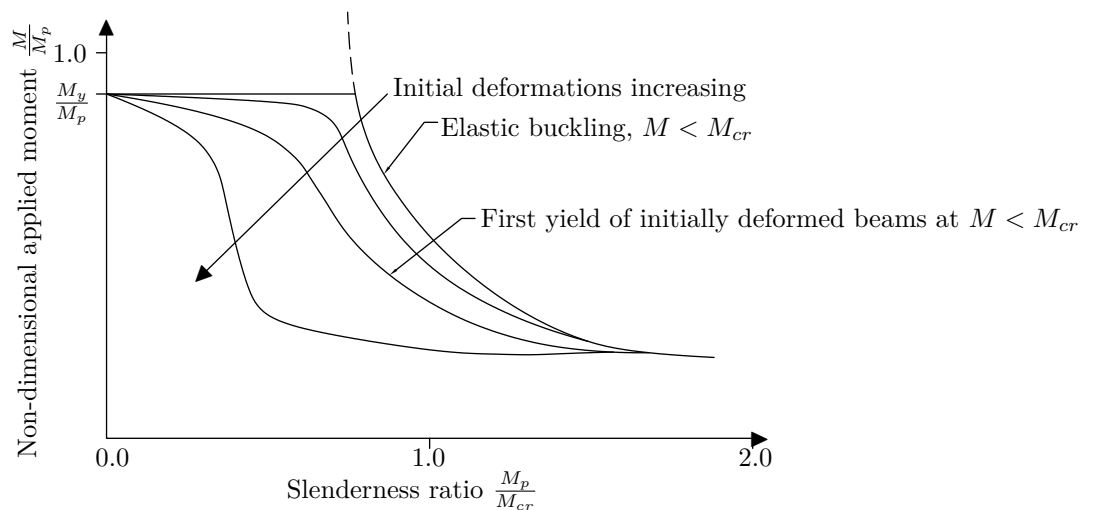


Figure 2.5: Beam failure curve (Kirby et al., 1979)

## 2.4 Elastic critical moment

Inelastic instability may often be preceded by a phenomenon called buckling or bifurcation of the equilibrium. The structure begins to deform in a characteristic pattern of the type of structure and loading

as the load is increased from zero, as seen in figure 2.6. At point A in figure 2.6 bifurcation of the equilibrium occurs. This is where the critical load is reached and the deformation configuration suddenly changes into a different pattern. The actual load-deformation curve then consists of two stable branches: curve OA, the pre-buckling branch, and curve AC, the post-buckling branch (Galambos, 1968).

The lateral buckling is of importance in the design of beams without lateral support, provided the flexural rigidity of the beam in the plane of bending is large in comparison with the lateral bending rigidity. As long as the load on such a beam is below the critical value, the beam will be stable. As the load is increased, a condition is reached at which a slightly deflected form of equilibrium becomes possible. The plane configuration of the beam is now unstable, and the lowest load at which this critical condition occurs represents the critical load for the beam, point A in figure 2.6 (Timoshenko et al., 1961).

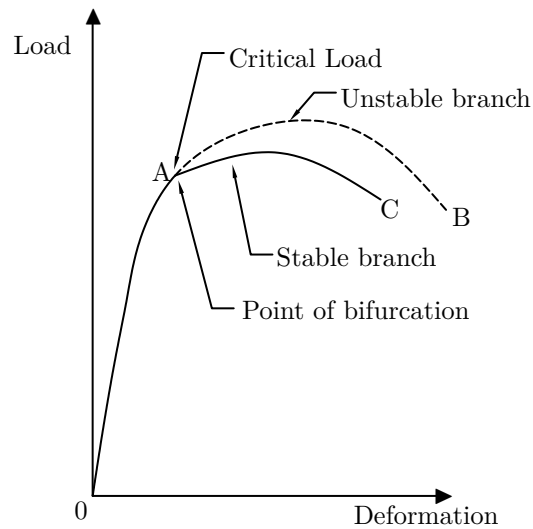


Figure 2.6: Bifurcation of the equilibrium (Galambos, 1968)

Research developments have been followed by the realization of updated design codes and standards. Based on limit state design procedure, modern steel structures codes, such as AISC LRFD, BS 5950-1, and the Eurocode 3, provide design procedures to assess the lateral-torsional buckling resistance of beams. As a first step in these procedures, it is generally required to determine the elastic critical buckling moment of the beam. Initial imperfections and residual stresses, like the ones mentioned before, are usually taken into account through the use of buckling curves (Serna et al., 2006).

For a doubly-symmetric beam subjected to a uniform moment about the strong axis along its length, the critical lateral-torsional buckling capacity ( $M_{cr}$ ) can be expressed as in equation 2.1. A full derivation by Timoshenko et al. (1961) can be seen in Appendix A.

$$M_{cr} = \frac{\pi}{L} \sqrt{EI_y C \left( 1 + \frac{C_1 \pi^2}{C L^2} \right)} \quad (2.1)$$

Where  $C = GJ$  is the torsional rigidity and  $C_1 = EC_\omega$  is the warping rigidity.

The boundary conditions assumed in this equation are such that both ends are restrained against both

lateral displacement and twist of the beam's cross section, while restraining neither weak-axis rotation nor warping of the cross section, and the potential for interaction buckling is negated (Driver et al., 2010). The unbraced length of a beam, that is to say the length between lateral supports, has the greatest influence on the elastic critical moment. Previous research has shown that the following factors can also influence  $M_{cr}$ :

1. The internal moment distribution between brace points.
2. The elevation of the applied load with respect to the shear centre.
3. The degree of lateral, rotational and warping restraints at the brace points.
4. The potential for less critical adjacent unbraced segments to restrain buckling (Nethercot et al., 1971).

### 2.4.1 Equivalent moment factor

In practice beams will be subjected to a whole range of different loading conditions, which will in turn produce a variety of different bending moment distributions. Kirby et al. (1979) states that the case of a uniform bending moment distribution is rarely found in practice, which is the most severe moment distribution that can be applied to a beam segment. However, the case of two equal point loads applied to a beam is often found in practice and subjects the segment between the two point loads to a uniform bending moment distribution. It is widely accepted by most structural design steel specifications that the effect of a non-uniform moment distribution can be approximated by simply multiplying equation 2.1 with an equivalent moment factor,  $C_b$ . Since a non-uniform moment distribution is less severe than a uniformly distributed moment, the value of this factor is always greater than or equal to one (Driver et al., 2010).

Non-uniform moment distribution between brace points can be categorized into three groups:

1. Linear moment distributions arising when there are no loads or moments applied between brace points.
2. Non-linear moment distribution with multiple constant moment gradient regions.
3. Non-linear moment distribution with continuously varying moment gradients.

There are multiple methods for estimating the equivalent moment factor. In this study the following two methods will be considered, each of which will be discussed separately:

1. Methods developed for unequal end moments only (Salvadori, 1955).
2. Methods developed for a general moment distribution (Kirby et al., 1979).

#### Methods developed for unequal end moments only:

Equation 2.2 is used to approximate the effect of a constant moment gradient (linear moment bending diagram) between brace points. This equation was developed by Salvadori in 1955 using the Rayleigh-

Ritz method to determine interaction curves for I-beams simply supported in the weak plane under thrust and unequal end moments (Salvadori, 1955).

$$C_b = 1.75 + 1.05\kappa + 0.3\kappa^2 \leq 2.3 \quad (2.2)$$

The parameter  $\kappa$  is the ratio of the smaller factored moment to the larger factored moment at opposite ends of the unbraced length (SABS, 2011). This parameter assesses the influence of the variation in flange forces between the two ends. If a beam flange is subjected to a bending-induced compression that varies between lateral supports, the degree of variation dictates the tendency of the beam to buckle elastically. The case where the flange force varies between tension and compression makes the beam less susceptible to LTB. That is why the  $\kappa$  parameter is positive when the beam segment is in double curvature and negative when in single curvature (Zuraski, 1992).

Driver et al. (2010) conducted a study on the critical evaluation of the  $C_b$  factor. They compared the Canadian national steel specification, CAN/CSA-S16-05 (upon which SANS 10162-1:2011 is based) with the BS 5950-1, AISC specification and the Australian Standard (AS4100), as well as with the work conducted by other researchers on the equivalent moment factor. They found that the procedure currently used in the Canadian design standard produces unacceptable results for the majority of the bending moment distributions considered. Equation 2.2 gave very conservative results for many common cases, but it also gave frequent non-conservative results (Driver et al., 2010).

#### Methods developed for a general moment distribution:

Kirby et al. (1979) developed an equation that is applicable to all types of bending moment distributions. Equation 2.3 is known as the quarter-point method, where the variables include the moments at quarter distances along the beam and the maximum moment of the beam segment, as shown in figure 2.7. The main function of these four segments is to describe the degree of non-uniformity of the moment along the unbraced length of the beam.

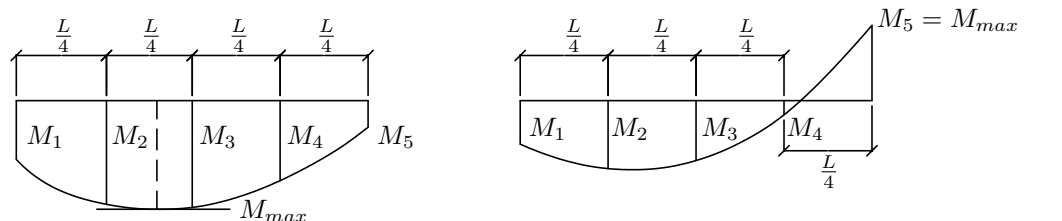
$$C_b = \frac{12M_{max}}{3M_2 + 4M_3 + 3M_4 + 2M_{max}} \quad (2.3)$$


Figure 2.7: Moments at quarter distances used in the quarter-point method (Kirby et al., 1979)

Equation 2.3 is independent of the end moments, unless the maximum moment is located at one or at both ends of the beam segment. Various researchers, most notably Serna et al. (2006), investigated the quarter-

point method. Serna presented a set of results obtained using both finite elements and finite differences. A number of moment distributions were considered, including linear moment, uniformly distributed loading and concentrated load, each with one and two end moments. The results confirmed that values given by design codes, besides being too conservative in many cases, do not properly approximate cases with constraints to lateral bending and warping, which might be non-conservative (Serna et al., 2006). Serna developed an expression, equation 2.4, that renders values that are significantly closer to numerical results than those provided by the similar expression of equation 2.3.

$$C_b = \sqrt{\frac{35M_{max}^2}{9M_2^2 + 16M_3^2 + 9M_4^2 + M_{max}^2}} \quad (2.4)$$

### 2.4.2 Load with respect to the shear centre

When a beam is subjected to a system of transverse loads its LTB capacity is not only dependent on the arrangement of the loads within the span, but also on the height of the applied load on the beam. In practice the applied load on a beam is in general either at the top flange, shear centre or the bottom flange. The runway for a crane girder is a common example for a load applied to the top flange of a beam, whereas bottom-flange loading can be illustrated by a runway beam with the hoist suspended from the bottom flange (Kirby et al., 1979).

If the load is applied above the shear centre, as in the case for top flange loading, the load causes an additional torsional moment in the element which in turn increases the beam's cross-sectional rotation even further, as shown in figure 2.8(a). Logic then dictates that the opposite is true if the load is applied to the bottom flange as in figure 2.8(b). The applied load creates a restoring moment which instead of increasing the effect of LTB, works against the rotation of the beam to decrease the effect of LTB.

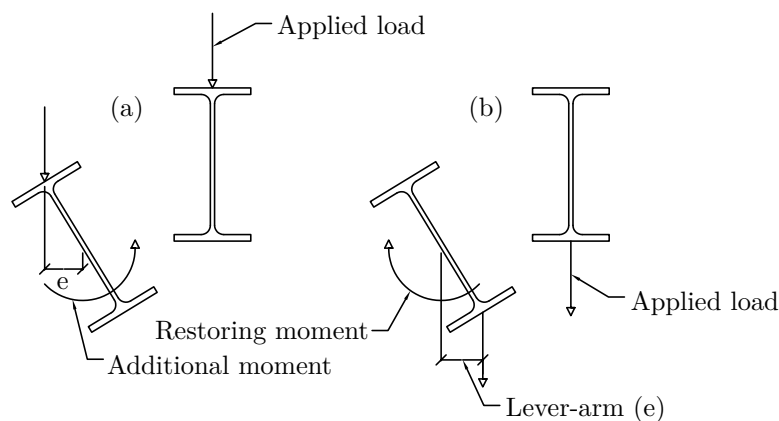


Figure 2.8: Applied loads on top and bottom flanges

To illustrate this effect, Kirby et al. (1979) conducted tests for a particular case of a centrally-loaded beam. The results are shown in figure 2.9. The graph shows how the level of load application influences the lateral stability of the beam. In figure 2.9 the non dimensional ratio  $(\frac{L^2 GJ}{EC_w})$  is a measure of the contribution of warping to the torsional resistance of the beam. If the transverse loading is applied in



such a way that twisting of the loaded cross section is prevented, then the actual level of application of the loading will have no effect (Kirby et al., 1979).

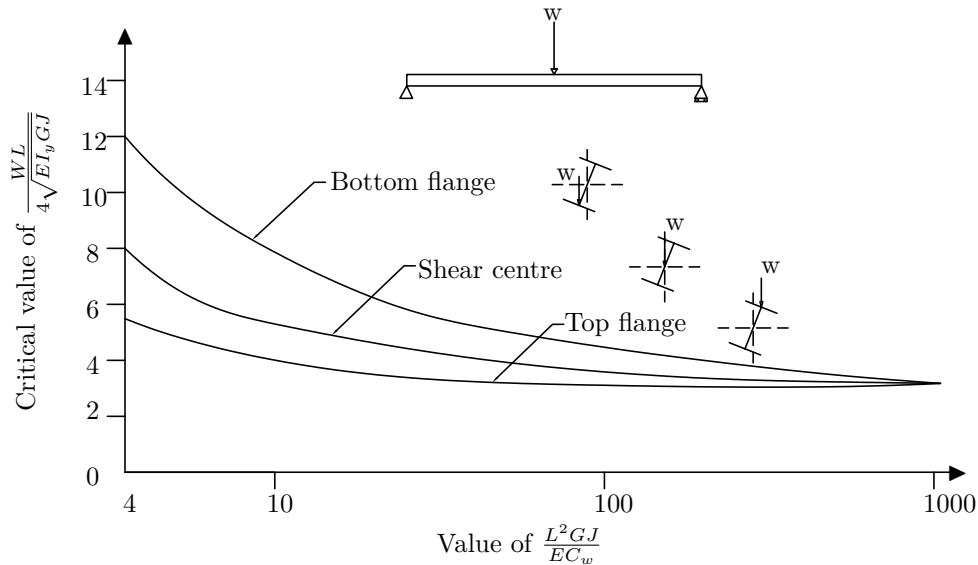


Figure 2.9: Results for centrally-loaded beam (Kirby et al., 1979)

To compensate for this effect the different steel specifications have their own procedures to take into account the effect of the variation in the level of application of the loading on the beam. These procedures will be discussed in detail in Section 2.5.

### 2.4.3 Supports and restraints

For the derivation of equation 2.1 it was assumed that the supports are capable of preventing both lateral deflection and twisting. These support conditions provide the lowest measure of lateral restraint and consequently yield the lowest value of  $M_{cr}$ . It is possible that a beam can be supported in such a way that other, more beneficial or even less beneficial supports can be assumed. By increasing the lateral stability of a beam with more beneficial end supports, one can notably reduce the mass of a beam.

Three deformations take place during LTB, namely twisting, lateral bending and warping. From this one can see that a number of support conditions are possible. Nethercot et al. (1971) investigated the effect of end restraints on the lateral stability of a beam. They considered four types of end support conditions, as seen in figure 2.10; these are:

1. Those which completely prevent both lateral deflection and twist but offer no restraint either to warping or lateral bending. (Type I)
2. Those which completely prevent lateral deflection, twisting and warping, but offer no restraint to lateral bending. (Type II)
3. Those which completely prevent lateral deflection, twisting and lateral bending, but offer no restraint to warping. (Type III)

4. Those which completely prevent lateral deflection, twisting, warping and lateral bending. (Type IV)

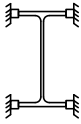
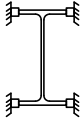
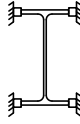
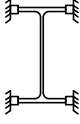



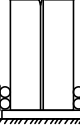
	Type I	Type II	Type III	Type IV
	Simply supported	Warping fixed	Lateral bending fixed	Completely fixed
				
				
Lat. disp:	Prevented: $u = 0$	Prevented: $u = 0$	Prevented: $u = 0$	Prevented: $u = 0$
Lat. bend:	Free: $\frac{d^2 u}{dz^2} = 0$	Free: $\frac{d^2 u}{dz^2} = 0$	Prevented: $\frac{du}{dz} = 0$	Prevented: $\frac{du}{dz} = 0$
Twisting:	Prevented: $\phi = 0$	Prevented: $\phi = 0$	Prevented: $\phi = 0$	Prevented: $\phi = 0$
Warping:	Free: $\frac{d^2 \phi}{dz^2} = 0$	Prevented: $\frac{d\phi}{dz} = 0$	Free: $\frac{d^2 \phi}{dz^2} = 0$	Prevented: $\frac{d\phi}{dz} = 0$

Figure 2.10: Possible end support conditions for a beam (Nethercot et al., 1971)

In a situation where the ends of the beam are completely fixed and a uniform moment is applied, the beam buckles laterally in a mode which requires the formation of inflexion points at quarter points along the unsupported length (Timoshenko et al., 1961). This situation is identical to the Euler buckling of a strut which is built in at each end. When using the basic equation for simple supports (equation 2.1) a length equal to half the span must be employed. Nethercot et al. (1971) suggested a similar solution to that of Timoshenko whereby an effective length needs to be determined depending on the end conditions of the beam, which is then used in equation 2.1.

Nethercot et al. (1971) first suggested two separate length factors, as shown in table 2.2.  $K_1$  and  $K_2$  reflects the two possible types of end fixity, lateral bending restraint and warping restraint, for a beam under a uniform moment. For other forms of applied loading the problem is complicated by the fact that  $K_1$  and  $K_2$  are frequently not even approximately constant, but vary with the proportions of the beam. This imprecision was brought out in the BS 449 specification. BS 449 first made the approximation  $K_1 = K_2 = k$ , leading to the following interpretation of the effective length (Kirby et al., 1979):

$$l = kL \quad (2.5)$$

Equation 2.5 represents the length of a beam of similar section subjected to similar loading which would have the same elastic critical moment as the beam in question. Where  $k$  is:

1. Ends unrestrained against lateral bending  $k = 1.00$
2. Ends partially restrained against lateral bending  $k = 0.85$
3. Ends practically fixed against lateral bending  $k = 0.70$

Nethercot and Kirby give two reasons for the conservative choice of  $k$ . First, fully fixed end supports against rotation and warping are hardly ever possible and secondly, these values recognize the effect of different types of loading. For example, the  $k$ -value for a central point load applied at the level of the centroid with a completely fixed end support is theoretically 0.63 and not 0.70 as used for design purposes (Kirby et al., 1979).

Table 2.2: Length factors for end support conditions

Type of end condition	K1	K2
Simply Supported	1.00	1.00
Warping Fixed	0.92*	0.48*
Completely Fixed	0.50	0.50

\*Approximate Value

## 2.5 Design approach of different specifications

In the preceding sections different variables that influence the load carrying capacity of a beam segment prone to LTB were discussed. Each of these variables has a significant impact on the critical moment of a beam. In order to take into account the variety of conditions a beam can be exposed to, design specifications need to include all of these variables in a simple manner in order to prevent confusion and reduce human error, while at the same time providing a safe design methodology.

In this study the following specifications will be compared:

1. SANS 10162-1:2011 (SABS, 2011)
2. ANSI/AISC 360-05 (AISC, 2005)
3. EN 1993-1-1 (CEN, 2005)
4. CSA S16-09 (CSA, 2009)

Each of the above mentioned specifications utilizes a different approach to calculate the LTB capacity of a beam. The methodology of each specification will be discussed in this section.

### 2.5.1 SANS 10162-1:2011

The design for laterally unsupported members is given in §13.6 in SANS 10162-1:2011. The code specifies an equation, equation 2.6, for the critical elastic moment similar to that of Timoshenko et al. (1961). The difference lies in how the code takes account for the loading conditions and support conditions at the beam ends.

$$M_{cr} = \frac{\omega_2 \pi}{KL} \sqrt{EI_y GJ + \left(\frac{\pi E}{KL}\right)^2 I_y C_w} \quad (2.6)$$

The  $\omega_2$  parameter in equation 2.6 is the equivalent moment factor, more generally known as  $C_b$ . This parameter is calculated with the equation for an unbraced beam segment subjected to end moments, equation 2.2. The only difference in SANS 10162-1:2011 in comparison to the equation developed by Salvadori is that the upper limit is 2.5 instead of 2.3. The code states that  $\omega_2$  is equal to equation 2.2 for unbraced beam segments subjected to end moments, or  $\omega_2 = 1.0$  when the bending moment at any point within the unbraced length is larger than the larger end moment or when there is no effective lateral support for the compression flange at one of the ends of the unsupported length (SABS, 2011).

As mentioned in Section 2.4.1,  $\kappa$  is the ratio of the smaller end moment to the larger end moment at opposite ends of the unbraced length and positive for double curvature and negative for single curvature (SABS, 2011). The code however gives no indication of how to account for triple curvature, which typically occurs when a uniformly distributed load is applied along with two equal end moments, as in figure 2.11.

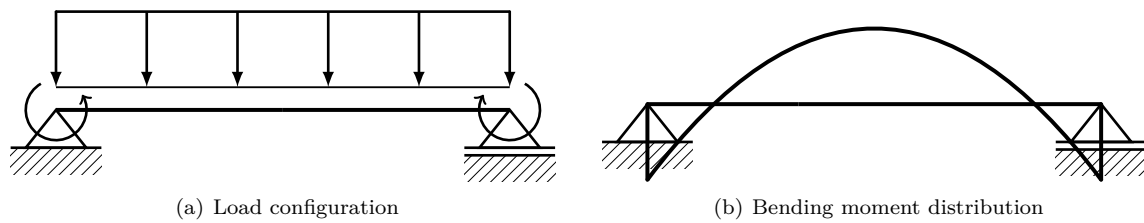


Figure 2.11: Uniformly distributed load with equal end moments

Equation 2.6 also accounts for the level of the applied load and the end restraints of the beam by using the  $K$  parameter, which is known as the effective length factor. This parameter can be found in Table 1 in SANS 10162-1:2011.

Table 2.3: Table 1 in SANS 10162-1:2011

Restraint Against Lateral Bending at Supports	Effective Length Factor $K$	
	Loading Condition	
	Normal	Destabilizing
Unrestrained	1.00	1.20
Partially Restrained	0.85	1.00
Practically Fixed	0.70	0.85

Table 2.3 offers a series of end restraints, which range from unrestrained to fully fixed, as discussed in Section 2.4.3. As the fixity of the end supports increases  $K$  reduces, in other words the buckling length of the beam decreases as indicated by Timoshenko et al. (1961). In SANS 10162-1:2011 Section 10.2.1, it is also stated that the  $K$  factor in table 2.3 must be increased by 20% where the beam ends are not restrained against torsion (SABS, 2011).

Table 2.3 also take into consideration the level of application of the load. The  $K$  factor for normal loading basically means that the load is applied at the shear centre of the section or below the shear centre, i.e.

the load doesn't cause an additional moment about the centroid. The  $K$  factor for destabilising loading is for the case where the load is applied above the shear centre and the load causes an additional moment about the shear centre and increases the rotation of the beam.

When continuous lateral support is not provided to the compression flange of a member subjected to uni-axial strong axis bending, the factored moment resistance,  $M_r$ , may be taken as follows (SABS, 2011):

a) for doubly symmetric class 1 and 2 sections, except closed square and circular sections

- when  $M_{cr} > 0.67M_p$

$$M_r = 1.15\phi M_p \left(1 - \frac{0.28M_p}{M_{cr}}\right) \text{ but not greater than } \phi M_r$$

- when  $M_{cr} \leq 0.67M_p$

$$M_r = \phi M_{cr}$$

b) for doubly symmetric class 3 and class 4, except closed square and circular sections, and for channels:

- when  $M_{cr} > 0.67M_y$

$$M_r = 1.15\phi M_y \left(1 - \frac{0.28M_y}{M_{cr}}\right) \text{ but not greater than } \phi M_r$$

- when  $M_{cr} \leq 0.67M_y$

$$M_r = \phi M_{cr}$$

The 0.67 factor in the equations accounts for the effects of residual stresses that initiate inelastic buckling and is based on the research by Galambos (1963).

## 2.5.2 ANSI/AISC 360-05

Chapter F in ANSI/AISC 360-05 contains provisions for calculating the flexural strength of members subject to simple bending about one principle axis (AISC, 2005). In this study only members with a compact section will be considered, i.e. members that classify as class 1 sections. The ANSI/AISC 360-05 provides ten different procedures (F2-F12) for members in bending, where each of these procedures is applicable to a certain type of cross section, i.e. compact, slender, non-compact and square and rectangular circular hollow sections.

Under general provisions (F1) the procedures for determining the load and resistance factor design (LRFD) and the allowable flexural strength (ASD) are given. They are as follows:

- LRFD =  $\phi_b M_n$ , where  $\phi_b = 0.90$
- ASD =  $\frac{M_n}{\Omega_b}$ , where  $\Omega_b = 1.67$

The equation for determining the LTB modification factor, or more commonly known, the equivalent moment factor  $C_b$ , is stated as in section F1:

$$C_b = \frac{12.5M_{max}}{2.5M_{max} + 3M_A + 4M_B + 3M_C} R_m \leq 3.0 \quad (2.7)$$

Equation 2.7 is very similar to equation 2.3 that was developed by Kirby et al. (1979), with the only difference being the coefficients for the moments that are slightly higher.  $R_m$  in equation 2.7 is the cross section's mono-symmetry parameter, which equals 1.0 for doubly-symmetric sections. In section F2 provisions are specified to determine the nominal flexural strength ( $M_n$ ) of doubly-symmetric compact I-shaped members and channels bent about their major axis. This section provides three different equations for  $M_n$ , they are:

$$M_n = M_p = F_y S_x \quad (2.8)$$

$$M_n = C_b \left[ M_p - (M_p - 0.7F_y S_x) \left( \frac{L_b - L_p}{L_r - L_p} \right) \right] \leq M_p \quad (2.9)$$

$$M_n = F_{cr} S_x \leq M_p \quad (2.10)$$

$$F_{cr} = \frac{C_b \pi^2 E}{\left( \frac{L_b}{r_{ts}} \right)^2} \sqrt{1 + 0.078 \frac{J}{S_x h_o} \left( \frac{L_b}{r_{ts}} \right)^2} \quad (2.11)$$

where

$F_y$  is the specified minimum yield stress of the type of steel being used.

$S_x$  is the plastic section modulus about the x-axis.

$J$  is the St. Venant's torsion constant.

$r_{ts}$  is the effective radius of gyration.

$h_o$  is the distance between flange centroids.

$L_p$  is the limiting laterally unbraced length for the limit state of yielding.

$L_b$  is the length between points that are either braced against lateral displacement of compression flange or braced against twist of the cross section.

$L_r$  is the limiting laterally unbraced length for the limit state of inelastic LTB (AISC, 2005).

The limiting lengths  $L_p$  and  $L_r$  are determined as follows:

$$L_p = 1.76 r_y \sqrt{\frac{E}{F_y}} \quad (2.12)$$

$$L_r = 1.95r_{ts} \frac{E}{0.7F_y} \sqrt{\frac{Jc}{S_x h_o}} \sqrt{1 + \sqrt{1 + 6.76 \left( \frac{0.7F_y S_x h_o}{E Jc} \right)^2}} \quad (2.13)$$

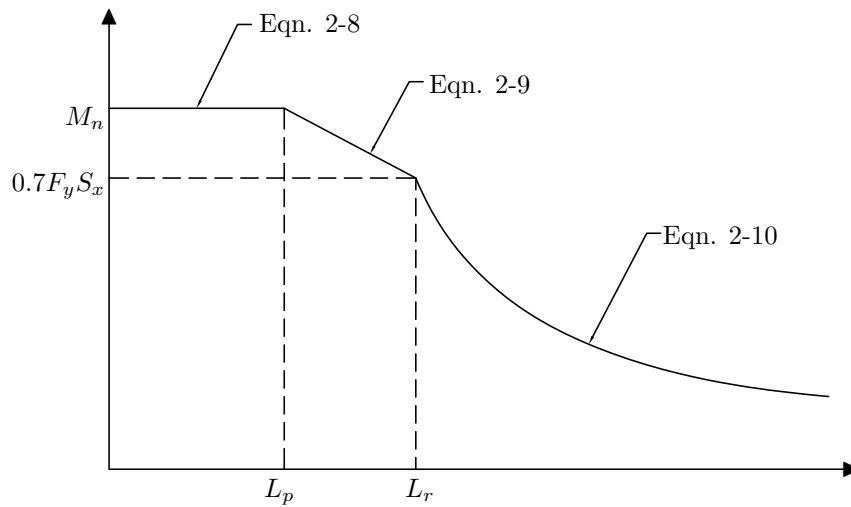


Figure 2.12: Beam strength vs. Unbraced length (AISC, 2005)

As can be seen in figure 2.12 equations 2.8-10 are each applicable for a certain length of the beam. First, equation 2.8 applies when  $L_b \leq L_p$ , where the limit state of LTB does not apply. This equation is generally used when stocky beams are under consideration and the beam behaves plastically. Secondly, equation 2.9 applies only when  $L_p < L_b \leq L_r$ . In this region the strength is limited by inelastic buckling. Lastly, on the far right of the curve equation 2.10 is applicable, where  $L_b > L_r$ . In this region elastic buckling is limiting the strength of the beam.

### 2.5.3 EN 1993-1-1

In EN 1993-1-1 two methods are given for the determination of the lateral-buckling resistance of a beam namely the general case (GC) and the special case (SC). The GC can be used for all sections, while the SC is specifically used for rolled sections of standard dimensions. As with any design of a structural element the maximum applied moment ( $M_{Ed}$ ) first needs to be determined by an elastic analysis (if the beam is statically indeterminate), or by statics (if the beam is statically determinate) (Trahair et al., 2008). In section 6.3.2.1 of EN 1993-1-1 it is stated that a laterally unrestrained member subjected to major axis bending should be verified against lateral-torsional buckling as follows for both cases:

$$\frac{M_{Ed}}{M_{b,Rd}} \leq 1,0 \quad (2.14)$$

$$\bar{\lambda}_{LT} = \sqrt{\frac{W_y f_y}{M_{cr}}} \quad (2.15)$$

$$M_{cr} = C_1 \frac{\pi^2 EI_z}{(kL)^2} \left\{ \sqrt{\left(\frac{k}{k_w}\right)^2 \frac{I_w}{I_z} + \frac{(kL)^2 GI_t}{\pi^2 EI_z} + (C_2 z_g)^2} - C_2 z_g \right\} \quad (2.16)$$

where

$k$  is an effective length factor for out-of-plane bending (usually 1.0).

$k_w$  is an effective length factor for warping (usually 1.0).

$z_g$  is the distance between the point of load application and the shear centre, as shown in figure 2.13.

$C_1$  and  $C_2$  are coefficients depending on the loading and end restraint conditions (NCCI, 2008).

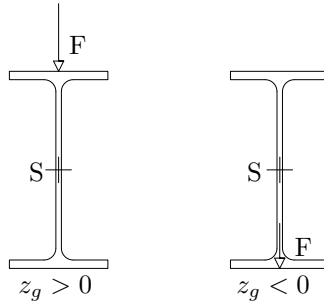


Figure 2.13: Point of application of transverse load

The elastic critical moment is then calculated by using equation 2.16 (Trahair et al., 2008). EN 1993-1-1 does not provide an explicit expression for the  $M_{cr}$ , but equation 2.16 is found in NCCI (2008). This document is part of a set of non-contradicting complementary information provided by the Steel Construction Institute (SCI) in the UK. The modified slenderness ratio is then calculated afterwards by using equation 2.15 (CEN, 2005). For the rest of the procedure for both the GC and SC it is necessary to calculate  $\alpha_{LT}$ ,  $\beta$  and  $\bar{\lambda}_{LT,0}$ . The steps and equations necessary to determine these parameters for each method will be discussed separately.

### 2.5.3.1 $C_1$ and $C_2$ factors

The  $C_1$  and  $C_2$  factors depend on various parameters that include section properties, support conditions and the moment diagram (NCCI, 2008). There are three different categories for which a beam can be classified when determining these factors, namely:

- Member with end moments only;
- Member with transverse loading;
- Member with end moments and transverse loading.

For each of these categories separate values for  $C_1$  and  $C_2$  need to be determined according to the bending moment diagram for the beam under consideration. In NCCI (2008) various bending moment distributions are presented with corresponding graphs for the determination of  $C_1$  and  $C_2$  values.



### 2.5.3.2 General case

In equation 2.14  $M_{Ed}$  is the design value of the moment and  $M_{b,Rd}$  is the design buckling resistance moment (CEN, 2005). To calculate the resistance moment of a beam, the reduction factor ( $\chi_{LT}$ ) and section modulus ( $W_y$ ) are required as shown in equation 2.17.

$$M_{b,Rd} = \chi_{LT} W_y \frac{f_y}{\gamma_{M1}} \quad (2.17)$$

Section 6.3.2.2 in EN 1993-1-1 describes the procedures for the reduction factor. For bending members of constant cross section, the value of  $\chi_{LT}$  for the appropriate non-dimensional slenderness  $\bar{\lambda}_{LT}$ , should be determined from equation 6.56 in EN 1993-1-1:

$$\chi_{LT} = \frac{1}{\Phi_{LT} + \sqrt{\Phi_{LT}^2 - \bar{\lambda}_{LT}^2}} \text{ but } \chi_{LT} \leq 1, 0$$

where

$$\Phi_{LT} = 0.5[1 + \alpha_{LT}(\bar{\lambda}_{LT} - 0, 2) + \bar{\lambda}_{LT}^2]$$

The imperfection factor ( $\alpha_{LT}$ ) is determined from the buckling curves provided in EN 1993-1-1. The buckling curves are a function of the reduction factor and non-dimensional slenderness,  $\bar{\lambda}_{LT}$ . In the clause two tables, reproduced here as tables 2.4 and 2.5, are given to determine the imperfection factor.

Table 2.4: Recommended values for imperfection factor for lateral-torsional buckling curves

Buckling Curve	a	b	c	d
Imperfection factor $\alpha_{LT}$	0.21	0.34	0.49	0.76

Table 2.5: Recommended values for lateral buckling curves for cross sections using eq. (6.56)

Cross section	Limits	Buckling Curve
Rolled I-sections	$h/b \leq 2$	a
	$h/b > 2$	b
Welded I-sections	$h/b \leq 2$	c
	$h/b > 2$	d
Other cross sections	-	d

### 2.5.3.3 Special case

As mentioned before, the SC is similar to the GC. The difference between the two methods becomes apparent in the determination of the reduction factor,  $\chi_{LT}$ . In section 6.3.2.3 equation 6.57 is used for the determination of the reduction factor for the SC. The equation is as follows:

$$\chi_{LT} = \frac{1}{\Phi_{LT} + \sqrt{\Phi_{LT}^2 - \beta \bar{\lambda}_{LT}^2}} \text{ but } \{\chi_{LT} \leq 1, 0 \text{ and } \chi_{LT} \leq \frac{1}{\bar{\lambda}_{LT}}\}$$

where

$$\Phi_{LT} = 0.5[1 + \alpha_{LT}(\bar{\lambda}_{LT} - \bar{\lambda}_{LT,0}) + \beta \bar{\lambda}_{LT}^2]$$

The parameters  $\bar{\lambda}_{LT,0}$  and  $\beta$  and any limitation of validity concerning the beam depth or h/b ratio may be given in the National Annex. The following values are recommended for rolled sections or equivalent welded sections (CEN, 2005):

$$\begin{aligned}\bar{\lambda}_{LT,0} &= 0.4 \text{ (maximum value)} \\ \beta &= 0.75 \text{ (minimum value)}\end{aligned}$$

Table 2.6 gives the recommendations for buckling curves to determine the imperfection factor  $\alpha_{LT}$  in a similar fashion as with the GC.

For both of these methods LTB effects may be ignored and only cross-sectional checks apply, if the following statements are true:

$$\bar{\lambda}_{LT} \leq \bar{\lambda}_{LT,0}$$

or

$$\frac{M_{Ed}}{M_{cr}} \leq \bar{\lambda}_{LT,0}^2$$

Table 2.6: Selection of lateral-torsional buckling curve for cross sections using equation. (6.57)

Cross section	Limits	Buckling Curve
Rolled I-sections	$h/b \leq 2$	b
	$h/b > 2$	c
Welded I-sections	$h/b \leq 2$	c
	$h/b > 2$	d

#### 2.5.4 CSA S16-09

Clause 13.6 in CSA S16-09 provides the provisions for the design of laterally unsupported beam members. SANS 10162-1:2011 is based on previous versions of this steel specification and there are still some similarities that exist between these two specifications. For the design of Class 1 and 2 sections, except closed square and circular sections CSA S16-09 is still in close agreement with SANS 10162-1:2011. However, a major difference between the two specifications is in the determination of the equivalent moment factor and determining the effective length of a beam segment prone to LTB.

In clause 13.6 it is stated that where the bending moment distribution within the unbraced segment is effectively linear, the equivalent moment factor,  $\omega_2$  may be determined in a similar manner as discussed in Section 2.5.1 above (CSA, 2009). For any other bending moment distribution equation 2.18 must be used, which also employs the quarter-point method. Where  $M_{max}$ ,  $M_a$ ,  $M_b$  and  $M_c$  are defined as in figure 2.7.

$$\omega_2 = \frac{4M_{max}}{\sqrt{M_{max}^2 + 4M_a^2 + 7M_b^2 + 4M_c^2}} \leq 2.5 \quad (2.18)$$

The inclusion of equation 2.18 in the Canadian steel code was greatly influenced by the work conducted by Driver et al. (2010). Driver et al. (2010) demonstrated that the method for calculating  $\omega_2$  specified in

previous editions of the Canadian Standard and SANS 10162-1:2011, produces highly erroneous results in some common situations (Driver et al., 2010). With regard to the loading position on the beam which can have a significant effect on the capacity of the beam, as discussed in Section 2.4.2, the Canadian code provides a simple and conservative effective length approach for top flange loading. For loads applied at the level of the top flange,  $M_{cr}$  may be determined using  $\omega_2 = 1.0$  and using an effective length, for pinned-ended beams, equal to  $1.2L$  and, for all other cases,  $1.4L$  (CSA, 2009). For other positions of the load or unusual loading and other support conditions the designer must consult the Guide to Stability Design Criteria for Metal Structures (Ziemian, 2010).

#### 2.5.4.1 The effective length factor

The parameter  $L$  in equation 2.5, which is similar to the equation for the elastic critical moment in CSA S16-09, is the length of the unsupported member. It is generally taken as the distance between lateral supports (CSA, 2013) and methods of computing effective lengths are given by Kirby et al. (1979), as discussed in Section 2.4.3. At this point it is important to address a common misconception that has often been applied inappropriately in stability design. An inflection point of the bending moment diagram cannot be considered as a brace point (Ziemian, 2010). Figure 2.14 illustrates the fallacy of assuming that an inflection point is a brace point for a doubly symmetric I-section beam. The buckled shape of the  $2L$  beam shows that the top flange and bottom flange move laterally in opposite directions at the mid-span inflection point. For the mid-span of the  $2L$  beam to be considered as a brace point, the movement of both flanges must be restrained either by lateral or torsional bracing (Ziemian, 2010). The Canadian code does not explicitly give information on the effective lengths. It is up to the designer to consult documents like Kirby et al. (1979) and Schmitke (1984) for methods of computing the effective length. Schmitke (1984) gives a summary of the effective lengths for single-span, cantilevers and continuous beams. It also summarizes the work conducted by Kirby et al. (1979) as well as other researchers.

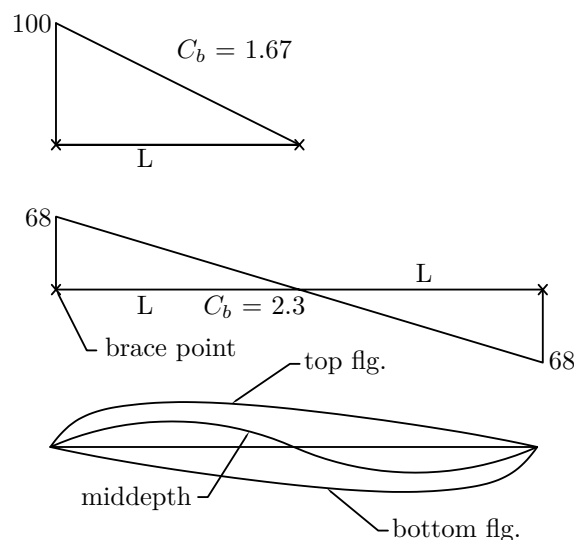


Figure 2.14: Fallacy of assuming that an inflection point is a brace point Ziemian, 2010

### 2.5.5 Comparison of steel specifications

Figure 2.15 shows the ratio of the resisting moment to the plastic moment for various lengths of a beam subjected to a uniform moment. The resulting  $C_b$  value for a uniform moment distribution is equal to 1.0 as discussed in Section 2.4.1. This makes the comparison in figure 2.15 independent of how the equivalent moment factor is determined. The calculation procedure for SANS 10162-1:2011 and CSA S16-09 is the same as indicated by the black graph line in figure 2.15. For the larger region of the elastic zone, that is to say the region with high slenderness ratio, the values for the codes are in good agreement. The dispersion comes as soon as the length of the beam enters the inelastic buckling range.

In this investigation only LTB that occurs in the elastic region will be considered. Given that the steel codes, independent of the  $C_b$  determination, are in good agreement in this region, only the difference in the calculation procedure for determining  $C_b$  will be evaluated. This will make the investigation independent of the procedure that is followed by the above mentioned codes for determining the resistance moment if LTB is not purely in the elastic zone.

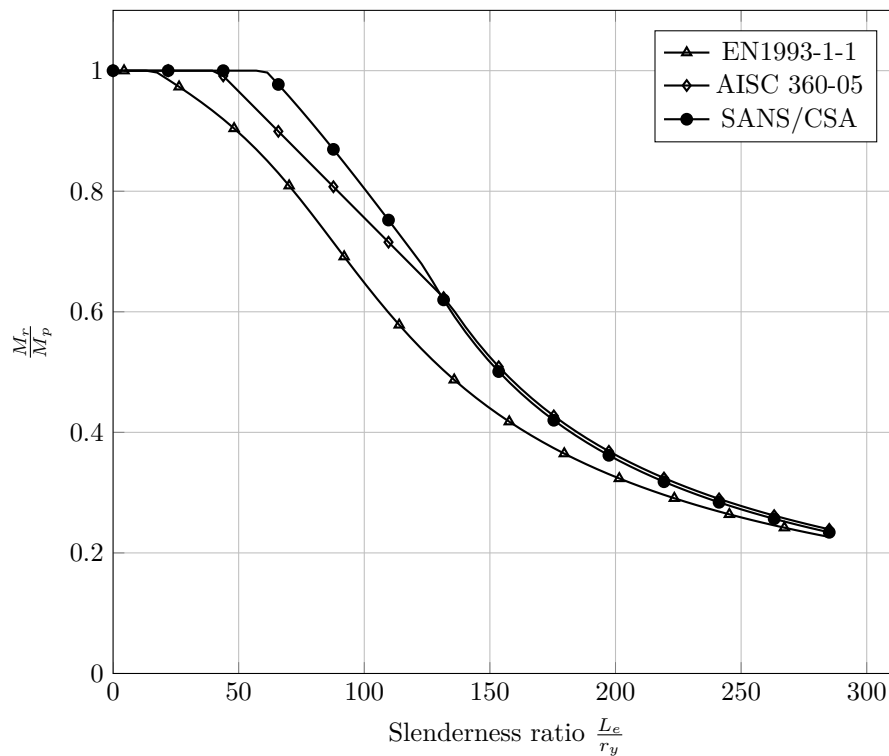


Figure 2.15: Comparison between moment capacities for EN1993-1-1, AISC 360-05, SANS 10162-1:2011 and CSA S16-09 for a beam subjected to a uniform moment.

## 2.6 Finite Element Analysis

Finite element analysis (FEA), also called the finite element method (FEM), is a method for numerical solution of field problems. Mathematically, a field problem is described by differential equations or by an integral expression. Individual finite elements can be visualized as small pieces of a structure. The word

“finite” distinguishes these pieces from infinitesimal elements used in calculus. In finite elements a field quantity is allowed to have only a simple spatial variation. The actual variation in the region spanned by an element is almost certainly more complicated, so FEA provides an approximate solution (Cook et al., 2002).

Elements are connected at points called nodes. The assemblage of elements is called a finite element structure, where the word “structure” is used to describe a body or a region. The particular arrangement of elements is called a mesh. Numerically, a FE mesh is represented by a system of algebraic equations to be solved for unknowns at nodes. Nodal unknowns are values for the field quantity and, depending on the element type, perhaps also its first derivatives. The solution for nodal quantities, when combined with the assumed field in any given element, completely determines the spatial variation of the field in that element. Although FEA is not an exact solution, the solution can be improved by using more elements to represent the structure (Cook et al., 2002). Equation 2.19 represents a simple matrix formulation that can be applied to FEA, where  $[K]$  is called either the structure stiffness matrix or the global stiffness matrix,  $\{D\}$  is the global degrees of freedom (DOF) or displacement vector, and  $\{R\}$  is the global load vector.

$$[K]\{D\} = \{R\} \quad (2.19)$$

As mentioned before, exact agreement is generally not achieved by an FE model of a plane or solid continuum where element displacement fields are only approximate. Regardless of the number or types of elements used, the computational procedure for time-independent FEA is as follows:

1. Generate matrices that describe element behavior.
2. Connect elements together, which implies assembly of element matrices to obtain a structure matrix.
3. Provide some nodes with loads (nodal loads).
4. Provide other nodes with boundary conditions, e.g. support conditions.
5. The structure matrix and the array of loads are parts of a system of algebraic equations. Solve these equations to determine nodal values of field quantities.
6. Compute the gradients; which in structural mechanics are usually the strains (Cook et al., 2002).

### 2.6.1 Linear analysis

Buckling is defined as a condition in which loads are large enough to destroy the stability of an equilibrium configuration (Cook et al., 2002). The main characteristic of buckling is the loss of stiffness and is not modeled by the usual linear finite element analysis.

In order to determine the buckling load of structure, it is necessary to solve a eigenvalue-eigenvector equation. Equation 2.20 is an eigenvalue problem whose smallest root ( $\lambda_{cr}$ ) defines the smallest level of external load for which there is bifurcation (Cook et al., 2002). Bifurcation means that a reference

configuration of the structure and an infinitesimally close configuration are both possible at the same load (Cook et al., 2002).

$$([\mathbf{K}] + \lambda_{cr}[\mathbf{K}_\sigma]_{ref}) \{\delta\mathbf{D}\} = \{\mathbf{0}\} \quad (2.20)$$

A certain buckling mode is associated with each load factor, which is represented by  $\{\delta\mathbf{D}\}$  in equation 2.20. Because the magnitude of  $\{\delta\mathbf{D}\}$  is indeterminate in a linear buckling problem, it defines a shape but not amplitude (Cook et al., 2002). The terms between the round brackets comprise a net stiffness,  $[\mathbf{K}_{net}]$ . Because  $[\mathbf{K}_{net}]\{\delta\mathbf{D}\}$  is zero, the stresses of critical intensity reduce the net stiffness to zero with respect to buckling mode  $\{\delta\mathbf{D}\}$  (Cook et al., 2002). This is represented in mathematical terms by equation 2.21.

$$\det([\mathbf{K}_{net}]) = \det([\mathbf{K}] + \lambda_{cr}[\mathbf{K}_\sigma]_{ref}) = \mathbf{0} \quad (2.21)$$

## 2.6.2 Nonlinear analysis

Most civil engineering structures behave in a linear elastic fashion under service loads. Exceptions are slender structures such as some suspension systems or arches, and structures subject to early localized yielding or cracking. Prior to reaching their limit of resistance, almost all structures exhibit significant nonlinear response. The term “nonlinearity” means that the response is not directly proportional to the action that produces it.

In nonlinear analysis an attempt is made to improve the analytical simulation of the behavior of the structure in some respect. The fundamental aim is to improve the quality of design by providing the engineer with a more reliable prediction of the performance of a system that is being designed. In a linear-elastic analysis the material is assumed to be unyielding and its properties invariable, and the equation of equilibrium is formulated on the geometry of the unloaded structure, or on an initial reference configuration. Deformations are assumed to be so small as to be insignificant in their effect on the equilibrium and mode of response of the system (McGuire et al., 1999).

When considering geometric nonlinearity, the structural material is treated as elastic but the effects of deformations and finite displacements in formulating the equation of equilibrium are included. It is also possible to consider material nonlinearity, i.e. the effect of changes in member material properties when subjected to loads. A general option is to include the effects of both geometric and material nonlinearity in the analysis. The sources of nonlinearity for each class are as follows (McGuire et al., 1999):

- Geometric effects:
  1. Initial imperfection, such as member camber and out-of-plumb erection.
  2. The  $P - \Delta$  effect, a destabilizing moment equal to a gravity load times the horizontal displacement it undergoes as a result of the lateral displacement of the supporting structure.
  3. The  $P - \delta$  effect, the influence of axial force on the flexural strength of an individual member.

- Material effects:
  1. Plastic deformation of steel structures
  2. Cracking or creep on reinforced concrete structures
  3. Inelastic interaction of axial force, bending, shear and torsion
- Combined effects:
  1. Plastic deformation plus  $P - \Delta$  and  $P - \delta$  effects
  2. Connection deformation
  3. Panel zone deformation
  4. Contribution of infilling and secondary systems to strength and stiffness (McGuire et al., 1999)

In first-order inelastic analysis the equation of equilibrium is written in terms of the geometry of the un-deformed structure. When destabilizing effects of finite displacement are relatively insignificant, first-order inelastic analysis can produce an excellent representation of simple elastic-plastic behavior. In second-order inelastic analysis the equation of equilibrium is written in terms of the geometry of the deformed structure, i.e. the stiffness and the loads become functions of displacement or deformation. It has the potential for accommodating all of the geometry, elastic and material factors that influence the response of the structure (McGuire et al., 1999).

### 2.6.3 Solution of nonlinear equilibrium equations

Various solution techniques exist for nonlinear analyses in finite element modelling. The two most common solution methods are however the Newton-Raphson (N-R) method and the Arc-length method (A-L), as shown in figure 2.16. The N-R method is described as a way of generating the  $P$  versus  $u$  curve, whose shape is not known at the outset (Cook et al., 2002). The calculation procedure uses the tangent stiffness, which is defined as  $k_t = dP/du$  and represent the slope of the  $P$  versus  $u$  plot. A convergence criterion based on the maximum norm of the incremental displacement is adopted. In the incremental-iterative process, each load step consists of the application of an increment of the external loads and subsequent iteration to restore equilibrium (Mohebkhah, 2011). Although this method is not guaranteed to converge for all nonlinear problems, continued iteration typically causes forced errors to decrease, successive displacement increments  $\Delta u$  to approach zero and the updated solution  $u_1$  to approach the correct value (Cook et al., 2002).

The A-L method is a form of N-R iteration in which, within each new level of external load, iterative increments of load and displacement are adjusted in such a way that iterative steps,  $1A$ ,  $aB$ ,  $bC$ , and so on cause points  $A$ ,  $B$ ,  $C$ , etc. to lie on a curve of radius  $\Delta L$  centered at initial point 1 (Cook et al., 2002).

The method incorporates a way to keep the process from doubling back on itself when the curve acquires

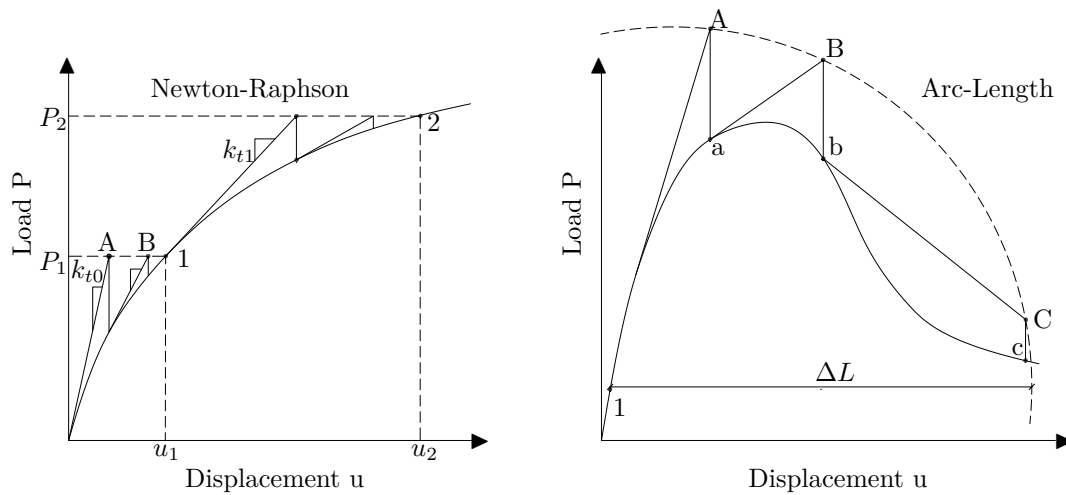


Figure 2.16: Newton-Raphson and Arc-length method (Cook et al., 2002)

a negative slope. Computed displacements correspond to a load that is adjusted by computation and is slightly less than the load level used to start the process (Cook et al., 2002).

## 2.6.4 Finite element models

In modelling the analyst seeks to exclude redundant detail, but includes all essential features so the analysis of the model is not unnecessarily complicated, yet provides results that describe the actual problem with sufficient accuracy. It is important to realize that FEA is simulation, not reality. Even very accurate FEA may be at odds with physical reality if the mathematical model is inappropriate or inadequate (Cook et al., 2002).

A mathematical problem is an idealization, in which geometry, material properties, loads and boundary conditions are simplified based on the analyst's understanding of what features are important or unimportant in obtaining the results required. In a stress analysis a material may be regarded as homogeneous, isotropic and linearly elastic, although in reality common materials are otherwise. Also a load distributed over a small area may be regarded as a concentrated point load, which in reality is not possible. Modelling decisions like the ones mentioned precede the FEA.

Modelling of thin-walled structures is fairly common and much literature is available on the different finite element variables that play a role in the modelling of these structures. From the literature a general procedure can be established in order to develop a finite element model.

### 2.6.4.1 Finite elements

In finite element modelling the user has a number of options when it comes to the type of element that can be used for modelling. The most frequently used elements are shells, solids and wires. Each of these elements have a specific purpose and care must be taken when deciding which element is appropriate for the model under consideration. It is very important to understand how the structure will behave



and how the elements are able to behave. In more complicated models a combination of these elements can be used, but this introduces new complications in the form of adding rigid elements to connect the dissimilar elements.

Shell elements are commonly used when creating a thin-walled model e.g. an I-beam. A shell can be defined as a body whose thickness is much smaller than its other dimensions. As with all types of elements available in finite modelling, this element too has its advantages and disadvantages. Probably the most significant attribute of shells is that they have both translational and rotational degrees of freedom (DOF). This sets them apart from solid elements which only have translational DOF.

When modelling thin-walled structures it is best to avoid the use of solid 3D elements. If 3D elements were made thin in only the thickness direction there would be problems with shear locking and ill-conditioning, but if these problems were avoided by using a great number of compact 3D elements, the finite element structure would have far too many DOF. To avoid too many DOF the elements used in the model are based on plate theory. Again, depending on the type of plate theory adopted, special formulation devices may be needed to avoid shear locking (Cook et al., 2002).

Most researchers have modeled thin-walled structures by simply constructing the cross section of say an I-beam with three plates and extruding the section to the desired span, see figure 2.17. The technique has been used extensively in the modelling of LTB of hot-rolled sections such as I-beams and channel sections.

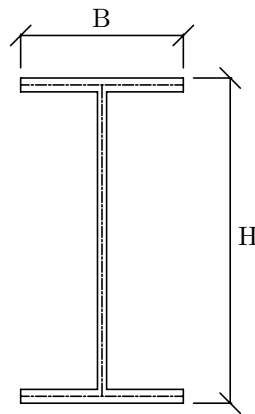


Figure 2.17: I-beam constructed from three plates

In the case of Lim (2003), an I-beam subjected to a linear moment gradient was modeled by using beam elements to investigate various support conditions. In a basic stress analysis deformation and stress in straight members are subjected to stretching, bending, and twisting. However, thin-walled structures often have additional deformation modes which may produce the largest deformation. These additional modes cannot be represented by standard beam elements (Cook et al., 2002).

A typical example of this is a cantilever beam with a load  $P$  applied at a position which is not through the shear centre, see figure 2.18. If the load was applied through the shear centre the beam would bend without twisting. In this case however the beam will bend as well as twist and the cross section will

become contorted as predicted by the St. Venant's torsion theory. Due to the fact that the beam is fixed at one end, i.e. preventing warping at this end, the amount of twisting is reduced and introduces normal stresses that are not predicted by elementary beam theory (Cook et al., 2002).

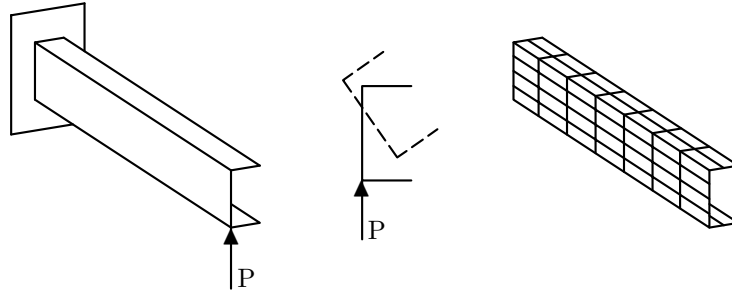


Figure 2.18: Thin-walled channel loaded by transverse tip force  $P$  in the plane of the web (Cook et al., 2002)

For a problem such as the one in figure 2.18 a standard beam element is incapable of providing either the correct torsional stiffness or the correct stresses. Even if  $P$  is directed through the shear centre so that the beam does not twist, a thin-walled open cross section with wide flanges displays a shear lag effect (Cook et al., 2002). This behaviour can also not be represented by a standard beam element. To improve on this the beam must be modelled as in figure 2.18, where the individual elements display both membrane and bending stiffness.

#### 2.6.4.2 Mesh generation and refinement

Mesh generation is a technique that is used to divide a complex problem into smaller elements, such as the ones mentioned above. Elements that display satisfactory geometry may not serve well in an analysis, because they are badly shaped for the analytical purposes under consideration. The solution to the problem tends to be more accurate when elements are compact, without great elongation, skew or warping. The degree of degradation caused by by these distortions varies with element type, mesh arrangement and the physical problem being investigated. Distortion usually degrades field gradients such as stresses more than it degrades displacements, natural frequencies or mode shapes (Cook et al., 2002).

If such a situation arises where the mesh generation causes elements to be distorted, there are certain methods one can use to improve the results of the analysis by revising the mesh. The main goal is to achieve the necessary accuracy by using only as many DOF as necessary. In the revision of a mesh one typically refines the mesh, but it can be that the revision of the mesh involves coarsening in some regions (Cook et al., 2002). The various refinement methods include  $h$ -refinement,  $p$ -refinement and  $r$ -refinement.

In  $h$ -refinement the  $h$  refers to a linear dimension that characterizes the size of an element, such as largest

span, or the square root of the area of a plane element, or the cube root of the volume of a solid element. When employing  $h$ -refinement the mesh is refined by adding elements of the same type, see figure 2.19(a). In the case of a  $p$ -refinement, the  $p$  refers to the degree of the highest complete polynomial in the element field quantity. A  $p$ -refinement consists of increasing  $p$  within the elements without changing the number of elements. This can be done by adding nodes on existing inter-element boundaries, see figure 2.19(b). The last method is the  $r$ -refinement, where the  $r$  stands for rearrange. It consists of the relocating of nodes without changing the number of elements or the polynomial degree of their field quantities see figure 2.19(c) (Cook et al., 2002).

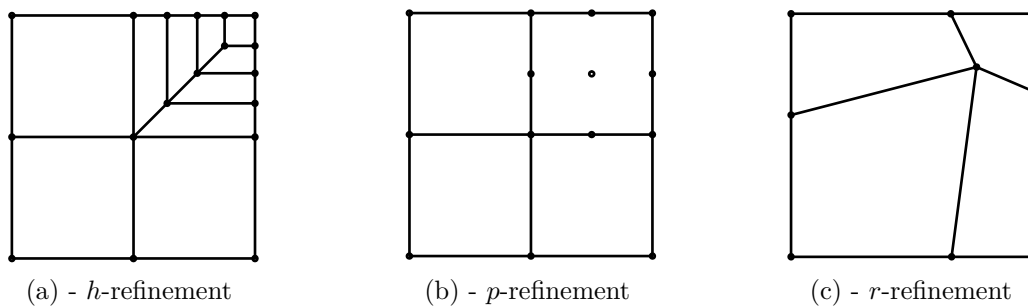


Figure 2.19: Refinement possibilities (Cook et al., 2002)

These methods are commonly used when modelling structures with irregular geometry where, for example, elements can get distorted near edges which are not straight. In this study however the beam that was modelled had a simple cross section, but the modelling of the flange-web intersection becomes more complex when using solid elements due to the fillet radii. As mentioned in the previous section, most researchers have modeled these types of beam by using shell elements. Mesh density in FEA is one of the parameters that can be used for tuning the model to be as accurate as possible. A general rule of thumb is to have at least six elements across the thickness of an structural member. This is necessary in order to accurately simulate the stresses over the cross section of the element. For beam element some researchers used nine integration points through the thickness of the elements to model the distribution of flexural residual stresses in the beam section and the spread of plasticity through the thickness of the elements (Anapayan et al., 2012). Mohebkah (2011) used four elements across the width of the flanges and eight elements over the height of the web. In the investigation of Yuan (2004) it was necessary to have 16 elements for the web and 10 elements for the flanges, which is double that of Mohebkah (2011). It must be kept in mind that the more dense the mesh is, the longer the run time of the analysis will be. It is thus very important to optimize the model according to the type of analysis and the objective of the model.

## 2.7 Lateral-torsional buckling experiments

Experimental results in a research project provides one with insight of what happens in reality. Much research has been conducted in the field of LTB, but a variety of experimental tests are still lacking. However, the experimental setups that do exist can provide influential insight for the design of a probable and realistic experimental setup that can improve on the experiments already conducted. Experiments for LTB are usually designed in order to simulate a certain moment bending diagram in order to determine the load carrying capacity of the beam segment under consideration.

### 2.7.1 Experimental setup

In the design of a testing apparatus considerable effort must be made to ensure that the boundary conditions and the application of the loads are as close as possible to a theoretical model. The boundary conditions have a significant effect on the effective length of a beam, as discussed in Section 2.4.3, which in turn influences the capacity of the beam. In most of the experimental setups that have been investigated, the researchers all simulate one type of bending moment distribution, as shown in figure 2.20. The test setup is based on the conventional four point bending test. Figure 2.21 shows the elevation view of the testing apparatus designed by Barnard (1996) which is basically a beam supported at two interior supports. The beam has two overhung ends to which a point load is applied at each end that produces two end moments at the interior supports, which in turn generates a uniform bending moment distribution across the span B-D.

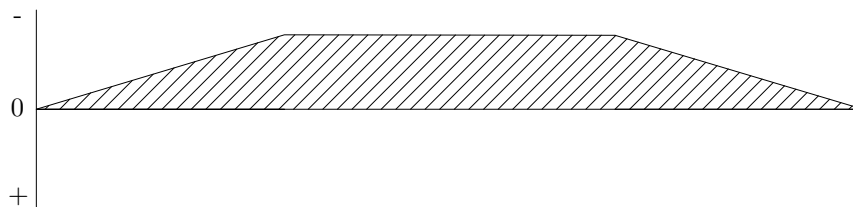


Figure 2.20: Typical bending moment distribution in an experimental beam setup (Barnard, 1996)

O'heachteirn et al. (1988) provided a restraint arrangement at the supports to accommodate any longitudinal movement of the test beam. This restraint also allowed it to warp but not twist within the loading yoke. Using the lateral support with the roller and spherical bearing supporting the test girder vertically, provides the setup with simply-supported conditions (O'heachteirn et al., 1988). The simply supported condition provided in the test rig, at points A, B, D and E in figure 2.21, allows for the compression flange to buckle in a configuration of the shape shown in figure 2.22. The test girder was supported vertically by load cells on spherical bearings at the end supports A and E, and by a roller knuckle bearing at the intermediate supports B and D. The reaction at the central point C was provided by a portal frame, where the vertical legs are anchored to the strong-floor. Lateral deflection and rotation of the test beam at the supports were prevented by using the loading yoke, as shown in figure 2.22 (O'heachteirn et al., 1988).

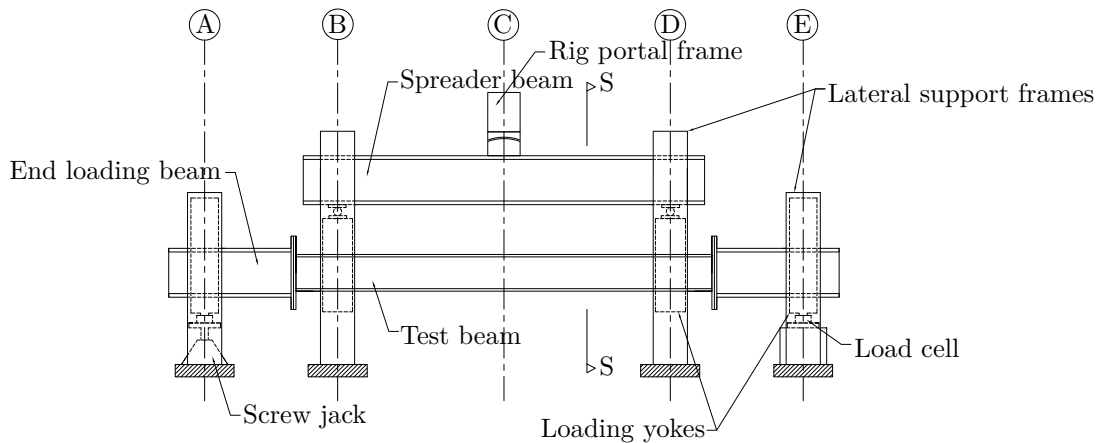


Figure 2.21: Schematic elevation of test rig, refer to O'hEachteirn et al. (1988)

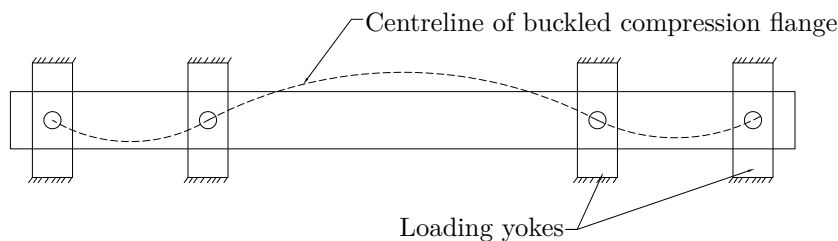


Figure 2.22: Buckled shape of compression flange (O'hEachteirn et al., 1988)

In addition, four corner stud bearings were attached to the outside of each vertical member of the loading yoke, one stud located at each corner. The studs were bored onto a lateral support plate which was secured to a rigidly braced support portal frame, thus preventing lateral deflection as well as rotation of the loading yoke about the vertical or longitudinal axis. A translation and a rotation bearing were provided between the outside of each of the vertical members of the loading yoke and the inside of the support portal frame. By adding both translation and rotation bearings and the four corners stud bearings, the loading yoke is prevented from moving laterally and longitudinally and from rotating about either the vertical or longitudinal axis while being free to slide vertically and to rotate about the girder's major axis (O'hEachteirn et al., 1988).

The flanges of the test beam inside the loading yoke were clamped by a flange clamping plate, to which two longitudinally oriented rails were welded. These rails plus the surface of the plate between them, formed the base plate component of another translation plus rotation bearing, as shown in figure 2.23. A spherical bearing was located between the top cylinder runner component of this bearing and a girder alignment assembly, the purpose of which was to provide rigid and accurate packing in the loading yoke. Longitudinal sliding movement of the test girder was prevented only at support B by adding stop-blocks to prevent longitudinal translation of the translation plus rotation bearing directly above and below each girder (O'hEachteirn et al., 1988).

Similar experimental setups have been used by other investigators, all based on the design by O'hEachteirn et al. (1988). Researchers, Kankanamge (2010), Barnard (1996) and Galambos (1968), adopted the con-

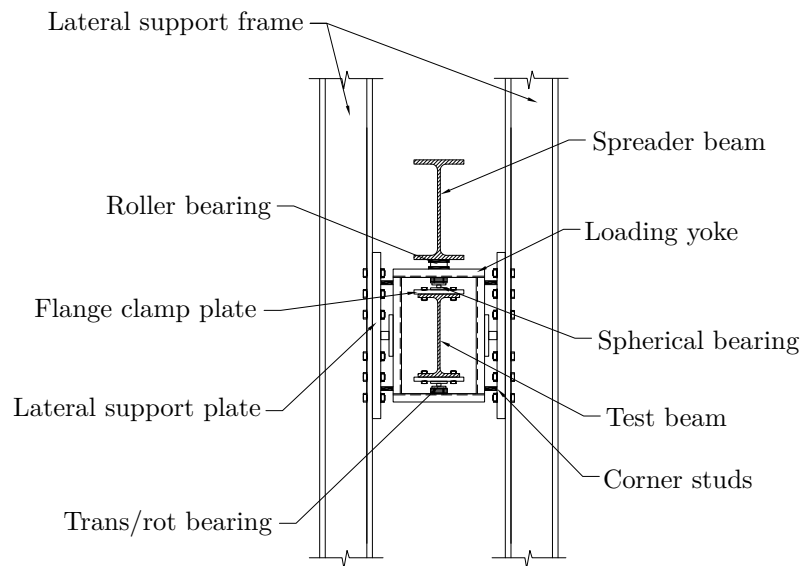


Figure 2.23: Section S-S from figure 2.21 (O'hEachteirn et al., 1988)

cept developed by O'hEachteirn et al. (1988) in order to subject a beam to LTB with the same boundary conditions and the same bending moment distribution across the beam segment under consideration. Minor differences were made by Kankanamge (2010) in order to examine a cold-formed lip channel. The loading system used ensured that the test beam was loaded through the shear centre of the mono-symmetric section. Hydraulic jacks were supported on a rail system which had the capability of moving in either parallel or perpendicular directions to the beam span (Kankanamge, 2010). A support system for both ends of the test beam similar to the loading yoke of O'hEachteirn et al. (1988) was implemented in order to provide the setup with the necessary simply-supported boundary condition as shown in figure 2.24.

Trahair (1993) gives a formal definition of all the DOF that must be allowed and restrained at a beam's end in order for it to be described as a simply supported end. In this definition it is stated that the end must be unrestrained for warping. It is not possible to simulate perfect simply supported boundary conditions in a controlled environment, but they can be simulated with a certain degree of restraint, which when designed correctly, is negligible. The beam that was tested by O'hEachteirn et al. (1988) and Barnard (1996) acts like a continuous beam that has four supports and three spans, as shown in figure 2.22. When beams are continuous throughout a series of lateral supports, A, B, D and E in figure 2.21, interaction buckling occurs and the segment that tends to buckle first, segment B-D, is restrained by the adjoining segments, segment A-B and D-E (Trahair, 1968).

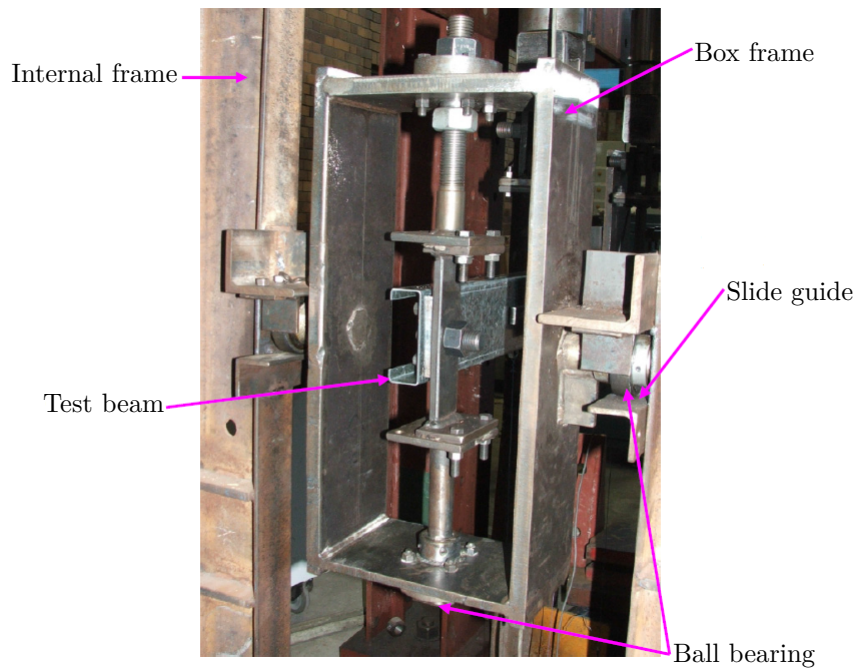


Figure 2.24: Support system (Kankanamge, 2010)

### 2.7.2 Measuring systems

The lack of experiments in the field of LTB research can also be attributed to the fact that accurately measuring the deflections of a beam moving in two simultaneous directions, i.e. laterally and vertically, is a difficult barrier to overcome. The experimental setups available all simulate a uniform moment distribution across the beam. With a uniform moment it is obvious that the maximum displacement will occur in mid-span, whereas with other moment distributions the maximum deflection is not so easily determinable.

Researchers, O'hEachteirn et al. (1988) and Barnard (1996), measured the deflections at mid-span by using electrical displacement transducers, and the loads and reactions were measured using electrical load cells. The vertical and horizontal deflections as well as the rotation about the longitudinal axis at mid-span were measured by using a deflection monitor frame, see figure 2.25. The designers of the experimental setup ensured that the loading and instrumentation systems were designed to allow the straining system gradually to load the test girder to collapse on a continuous basis, without pause (O'hEachteirn et al., 1988). The system in figure 2.25 consists of a lightweight deflection monitoring frame connected through a system of hard-drawn steel wires and pulleys to three displacement transducers. The displacements and rotation of the cross section can then be determined through simple geometry by evaluating the changes in distance between the stationary pulleys and the moving attachment points on the deflection monitoring frame (O'hEachteirn et al., 1988).

This measuring apparatus is not very reliable for various reasons. Although steel wires are used, there is a certain degree of deformation that occurs and causes the wires to lengthen. Another degree of uncertainty is the friction force that is generated at the pulleys. This force can hinder the wires from

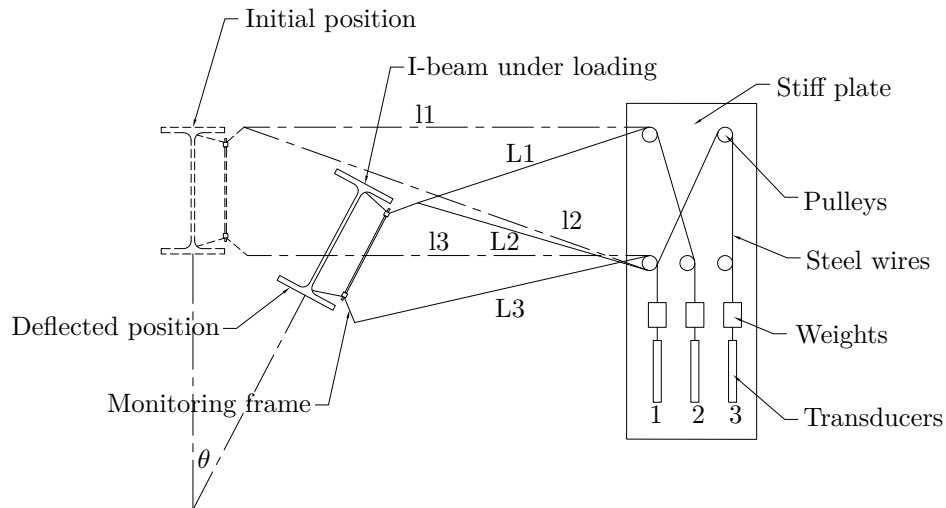


Figure 2.25: Deflection monitor system at mid-span (O'heachteirn et al., 1988)

displacing smoothly as the beam undergoes LTB, which can have a significant influence for accurate readings. The tension weights also provide a certain degree of lateral force to the beam, although it is relatively small.

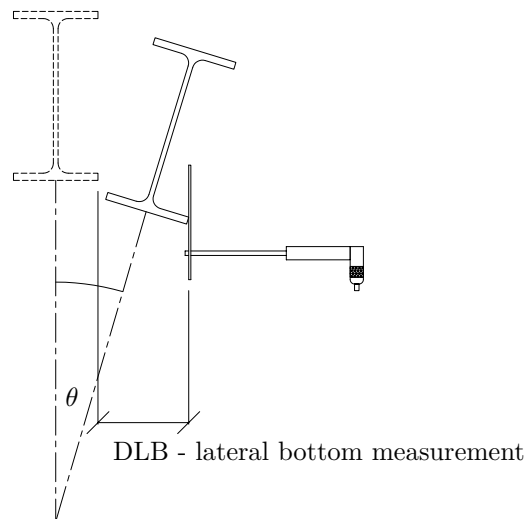


Figure 2.26: Displacement device for measuring displacement (Piloto, 2000)

Figure 2.26 illustrates the concept used by Piloto (Piloto, 2000). The horizontal deflection is measured by using a metal plate fixed to a transducer. As the beam undergoes LTB the beam pushes against the plate and the transducer measures the horizontal displacement. The arising issue with this concept is that the plate lacks rigidity. Because transducers are fragile equipment they cannot carry a big transverse load, which will be the case if a thicker plate is attached to the end. This lack of rigidity can influence the recorded data if the lateral movement of the beam bends the plate.



### 2.7.3 Load applications

In order to simulate gravity loads it is crucial that the applied load remains vertical as the beam starts to rotate as shown in figure 2.1. Hanging weights is an effective way of accomplishing a gravitational load, but the weights can get rather big if larger forces are needed. The fact that a load-driven test is performed makes the use of weights rather dangerous. An alternative method to hanging weights is to use what is called a gravity load simulator (GLS), see figure 2.27, which is based on the Robert's straight-line motion (Heck, 1923). The GLS allows for the testing of large structures which sway laterally under load. This is an effective method for applying a point load, or where more than one GLS is available, a series of point loads. The mechanisms that are described eliminate the restraining effect of the loads and the lateral bracing on test specimens permitted to sway (Yarimci, 1966). This modification allows the ends of the beam to translate laterally and reduces the effect of interaction buckling by reducing the stiffness provided by the end spans. This is shown in figure 2.28.

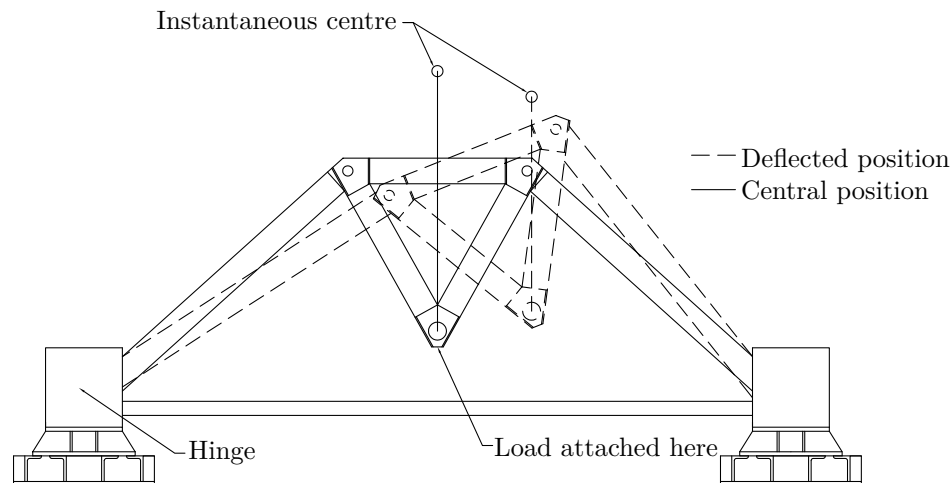


Figure 2.27: Gravity Load Simulator (Yarimci, 1966)

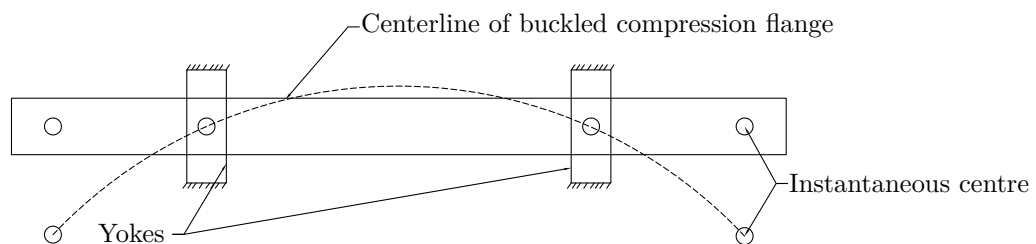


Figure 2.28: Buckled shape of compression flange with GLS at both ends

The mechanism is symmetrical and consists of three main members, the two inclined straight arms connected by a rigid triangular member. The two inclined arms are connected by pins at both ends and permit plane motions with one degree of freedom. For the type of mechanism shown, equilibrium requires that the line of action of the load pass through the instantaneous centre, i.e. the intersection of the two arms. In order for the load to be vertical, the loading device should be attached at the point along the

perpendicular bisector of the top width that is directly below the instantaneous centre (Yarimci, 1966). In addition to the lateral mobility of the GLS, it also consists of translational DOF in the longitudinal direction in order to accommodate the longitudinal displacement of a beam.

The application of the force is achieved through the use of a hydraulic pump or actuator. The magnitude of the load that can be applied is only governed by the size of the gravity-load simulator itself and by the force that can be generated by a hydraulic pump or actuator.

## 2.8 Literature overview and conclusions

This literature review includes a large volume of knowledge which relates to LTB and the factors that contribute to this buckling phenomenon. A conclusion is given below that highlights the most important aspects in the design of beams against LTB. Also contained in this conclusion is the possible application of the concepts discussed above in this investigation.

- It is important to understand the deformations that are induced by LTB. When the applied moment reaches the elastic critical moment the beam buckles by deflecting laterally and twisting (Trahair et al., 2008). These two deformations are interdependent which increases the complexity of an analysis of this type of failure.
- When considering a steel beam subjected to a bending moment distribution along its length, then depending on its length, three regions can be observed. Beams with a high slenderness will fail at  $M_{cr}$ . For beams of intermediate slenderness, some yielding occurs before the beam fails. Stocky beams are capable of reaching the plastic moment of the section without buckling (Kirby et al., 1979).
- There are two factors that greatly influence the ultimate load carrying capacity of beams, i.e. residual stress and geometric imperfections. These two factors will be taken into account in the numerical model that will be developed in this investigation.
- Timoshenko et al. (1961) derived an equation for the elastic critical moment for a beam subjected to a uniform moment. In order to account for the variety of bending moment distributions that can be present in a beam, this equation is simply multiplied by a moment modification factor  $C_b$ . This factor is generally determined by using what is called the quarter-point method, which describes the degree of non-uniformity of the moment along the length of the beam.
- The research conducted by Driver et al. (2010), provides a baseline for this investigation. Driver concluded that the method for determining the equivalent moment factor based on the equation by Salvadori (1955), gave poor results in cases where a linear distribution was absent. Also, the work done by Serna et al. (2006) concludes that the results for  $C_b$ , even when the quarter-point method in its raw form is used, can yield very conservative and even non-conservative results.
- The position of the applied load directly influences the load bearing capacity of a steel beam

undergoing LTB. Loads that are applied above or below the shear centre cause additional and restoring moments, respectively.

- Each steel specification discussed above has a different procedure for calculating  $C_b$ . Most notable is the Canadian code, CSA 16-09 which employs both the quarter-point method as well as the equation developed by Salvadori (1955). The CSA S16-09 has been updated with this modification based on the research conducted by Driver et al. (2010) and Serna et al. (2006).
- In order to fully model the nature of LTB it is necessary to take into account  $P-\delta$  effects. To model these non-linearities a non-linear analysis must be carried out by using the Arc-length method. Shell elements have been used with great success to model thin-walled structures such as I-beams (Serna et al., 2006). These types of elements will be considered in the development of the numerical model. With regards to the mesh size, according to Yuan (2004) it is advisable to have 10 elements across the flanges and 16 elements along the web (Yuan, 2004). The mesh size will be varied in the analysis in order to determine the accuracy while taking into account the computing time of a finer mesh.
- Previous experimental work has been conducted on LTB of beams, most notably O'Eachteirn et al. (1988). They investigated the bending capacity of a beam subjected to a uniform moment distribution. The lateral bending of the beam is similar to that of a continuous beam, which is in contradiction to the definition of a simply supported beam. The ends of the beam are restrained to a certain degree to prevent free rotation about the vertical axis of the cross section.
- However, the test setup of O'Eachteirn et al. (1988) provides invaluable information of how to allow for the rotation of the beam under loading, whilst still supporting the structure. They designed a loading yoke (frame) to which the beam is fixed. The frame is supported by bearings to allow rotation for in-plane bending, while the beam is supported on bearings to allow for out-of-plane bending. A frame similar to this will be designed for the experimental work to be conducted in this study.
- Because of the complex nature of LTB the displacement measuring remains a concern. A measuring device comprising of a series of pulleys and transducers was used by O'Eachteirn et al. (1988). This method of recording the displacement takes into account the vertical and lateral displacement of the beam as it undergoes LTB. This mechanism however has its drawbacks in the form of friction resistance by the pulley, elongation of the steel wires and the additional lateral load on the beam itself.
- A GLS was developed at Lehigh University in order to test structures that are permitted to sway (Yarimci, 1966). The load applied by the GLS is able to move with the structure as it sways laterally under load (Yarimci, 1966). This apparatus can be used to replace the loading yokes at the end of the beam in figure 2.21 to reduce the effect of restraining the rotation of the beam end about the weak axis. The GLS can also be used to apply a point load between the supports without contributing any lateral restraint to the beam.

- As a final conclusion, the paper by Driver et al. (2010) provides valuable data for the comparison of the equivalent moment factor. The FE modelling conducted by researchers, Serna et al. (2006) and Yuan (2004), confirms that using shell elements for modelling an I-beam renders satisfactory results. Although some factors are contrary to the definition of a simply supported beam, the experimental work conducted by O'Eachteirn et al. (1988) provides invaluable insight into the design of a simply supported beam setup.

## Chapter 3

# Finite Element Analysis

### 3.1 Introduction

The purpose of this chapter is to present and discuss the finite element analyses (FEA) that were undertaken in this investigation in order to study the behaviour of a simply supported beam that undergoes LTB. The failure of a steel beam through the mechanism of LTB is a fundamental failure case in steel structures. This subject has been studied for many years by various researchers, however there are still many issues that need to be addressed.

With the development of powerful computers and software packages, the nature of this type of failure can be studied in detail. To date many researchers have used FEA to determine the ultimate load capacity of steel beams and compared this to the results obtained from steel codes. However, only a few of these models have been validated by experimental work. The goal of the numerical study is to develop a FE model in order to study the behaviour of a steel beam subjected to various bending moment distributions by using the software package Abaqus. Abaqus is a general-purpose FEA program for use in the numerical modelling of structural response (*High performance software* 2013).

This chapter will present the model development undertaken in this study and includes the modelling assumptions and considerations that were employed during the investigation, i.e. element type, material properties and boundary conditions. Furthermore, the inclusion of initial imperfections is presented along with a sensitivity study of these imperfections as well as the modelling of residual stresses. This chapter is closed with a preliminary validation of the numerical model to assist in the design of the experimental setup.

### 3.2 Model development

The model developed in this study is able to simulate the behaviour of a steel beam that undergoes LTB due to a series of imposed loads. The beam under consideration assumes idealized simply supported

conditions that will be replicated as accurately as possible in the experimental setup. From the discussion in Section 2.5.5 the length of the beam will be chosen so that the slenderness ratio will fall in the elastic region. In this region the beam will undergo global buckling with the formation of some plastic zones only after the ultimate load is reached. Another factor to consider for the beam length is the availability of stock at the steel merchants. This is of importance due to the fact that this numerical model needs to be validated by a series of experimental tests with similar parameters, including member length and section size. The section size of the model is chosen as a standard IPE200, shown in figure 3.1. The reasoning behind the choice of section is that it is commonly found in practice and makes the experimental work relevant to the industry.

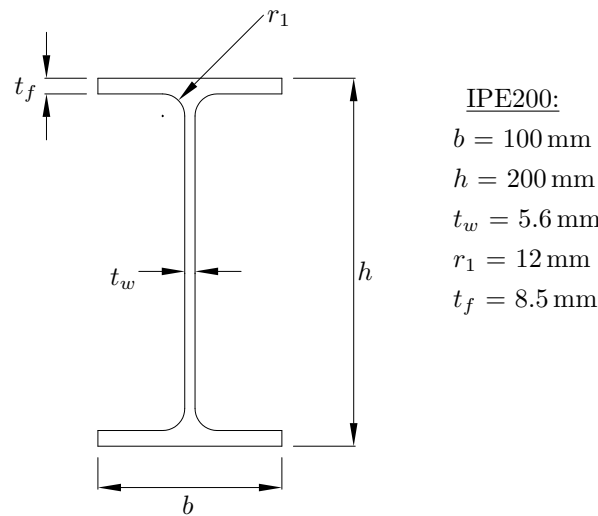


Figure 3.1: Cross section of IPE200 (de Clercq, 2010)

Included in this FE model are variables such as residual stresses and geometric imperfections that can have a significant effect on the capacity of a steel beam as shown by Kirby et al. (1979) in Section 2.3. The following section describes the development of the steel beam model.

### 3.2.1 Model description

As already mentioned the model in this study will be a simply supported IPE200 beam with a total span of 6.3 m. The cross section and support conditions are of such a nature that symmetric modelling is allowed, but the loading condition on the beam is not symmetrical, see Section 3.2.5, which eliminates the possibility of symmetric modelling. Figure 3.2(a) illustrates the general layout of the FE model, including the support conditions. The section in this model, shown in figure 3.2, does not include the fillet radii at the intersection of the web and flanges. This modelling consideration is based on the work conducted by Serna et al. (2006) and Yuan (2004) in which satisfactory results were gathered with the exclusion of these radii. The exclusion of the radii can also be attributed by the discussion in Section 2.6.4.1, with regards to the DOF of shell elements.

The cross-sectional properties of this section have been calculated and are shown in table 3.1 along with the properties of the IPE200. A good comparison between the two cross sections can be observed in

table 3.1 with a difference of no more than 5%, except for the St. Venant's torsion ( $J$ ) constant which shows a 27% difference. The significance of the large difference in  $J$  is made apparent by its presence in the equation for  $M_{cr}$ . A reduction in  $J$  will lead to a reduction of the buckling moment of the beam.

The model in figure 3.2(b) consists of the normal beam between the supports, but with two additional spans beyond the supports. This model is required in order to validate the experimental test that consists of a beam with two overhung ends. The different load configurations considered during the experimental study are discussed in Section 4.4.

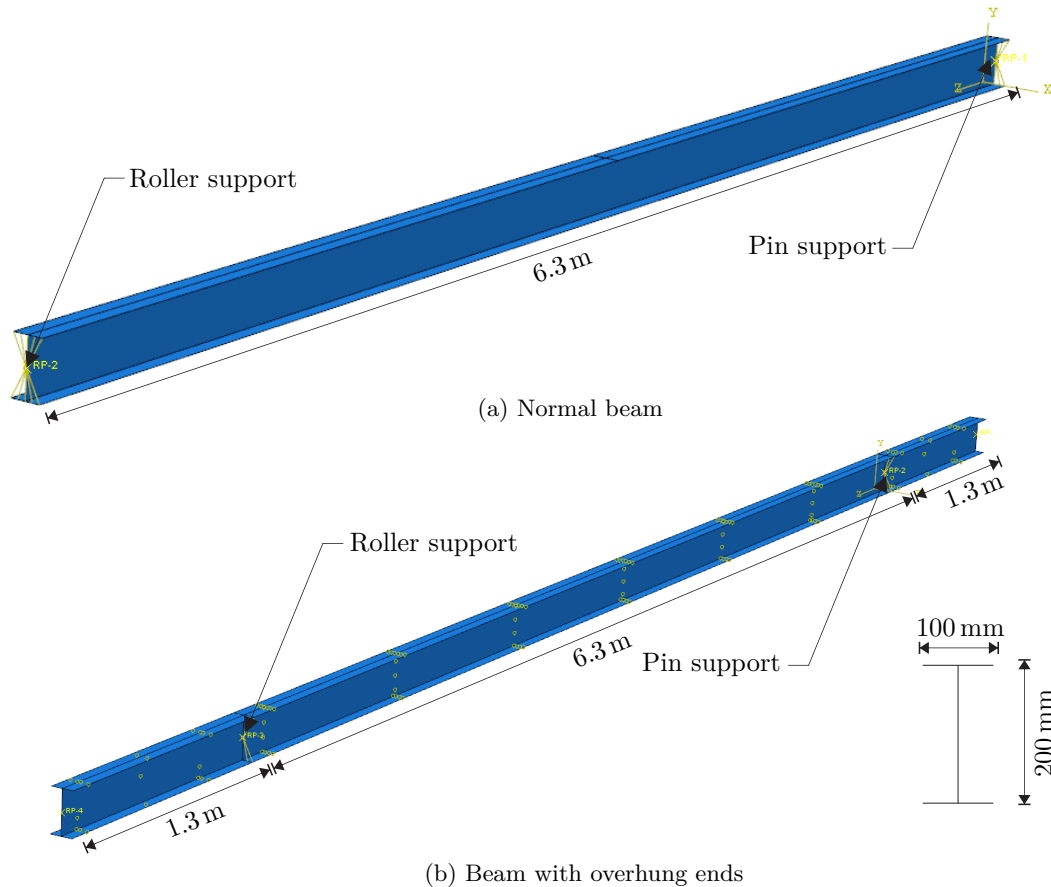


Figure 3.2: Beam model layout

Table 3.1: Cross-sectional properties

	FEM Model	IPE 200	% Difference
Area ( $10^3 \text{ mm}^2$ )	2.72	2.85	4.56
$I_{xx}$ ( $10^6 \text{ mm}^4$ )	18.5	19.4	4.64
$I_{yy}$ ( $10^6 \text{ mm}^4$ )	1.42	1.42	0.00
$Z_x$ ( $10^3 \text{ mm}^3$ )	185	194	4.64
$Z_y$ ( $10^3 \text{ mm}^3$ )	28.4	28.5	0.35
$r_x$ (mm)	82.3	82.6	0.36
$r_y$ (mm)	22.8	22.4	-1.79
$C_w$ ( $10^9 \text{ mm}^6$ )	12.96	13.1	1.07
$J$ ( $10^3 \text{ mm}^4$ )	50.91	70.2	27.48

### 3.2.2 Elements and mesh configuration

From the literature it was found that the most widely used element for an analysis of this type is the shell element. In Section 2.6.4.1 a thin-walled structure is described as a body whose thickness is much smaller than the other dimensions and for this reason the shell element is a promising modelling building block. Apart from that, conventional shell elements have six DOF per node, three translation DOF and three rotational DOF, as opposed to continuum shell elements that only have three translational DOF per node. When modeling the radii by using solid elements, it is necessary to ensure that there are enough elements over the height of the flanges to construct an accurate model. For a model with this particular shape and span, the number of elements required to ensure an accurate model will lead to an unrealistic computing time, further motivating the decision to use shell elements and the exclusion of the fillet radii.

The shell element chosen in this study is Abaqus's S4R element, which is a 4-node doubly curved shell. Element type S4R accounts for finite membrane strains and arbitrary large rotations, which makes them suitable for large-strain analysis. S4R shells can also allow transverse shear deformation, however the shear deformation becomes very small when the shell thickness reduces. As the thickness of these elements decreases they change from using thick shell theory to becoming discrete Kirchhoff thin shell elements (Dassault Systèmes, 2010).

The total shear carried by the flanges is negligible when compared to the web's contribution, see figure 3.3. For this reason the S4R element is sufficient to take into account the shear deformation that occurs during bending. The orientation of the elements in the web allows the shear deformation to take place through the length and width of shell and not through the thickness. The S4R element also uses reduced integration to form the element stiffness. The reduced integration provides accurate results in comparison to the general fully integrated S4 shell, with the added advantage that the running time of the analysis is significantly reduced, especially in three dimensions.

The mesh configuration used in this study is very simple. The fact that the geometry of the model is not complicated makes the meshing rather straight forward. The element shape is quad-dominated due the straight sides of the beam and the sharp corners at the flange-web intersections. In order to provide a sufficient mesh density there are eight elements across the width of the flange and 16 elements along the height of the web. Mohebkhah (2011) suggested four elements across the flange and eight elements for the web, which for this investigation is rather coarse. The mesh in this model is similar to the density suggested by Yuan (2004).

### 3.2.3 Material properties

A key objective in this study is to validate the numerical model by experimental work. For this reason it is crucial that the material properties of the numerical model are similar to that of the test specimens. Material properties are often presented in graphical form through the use of stress-strain curves. These curves are determined by clamping one end of a specimen, e.g. dog-bone or rod, in a loading frame and



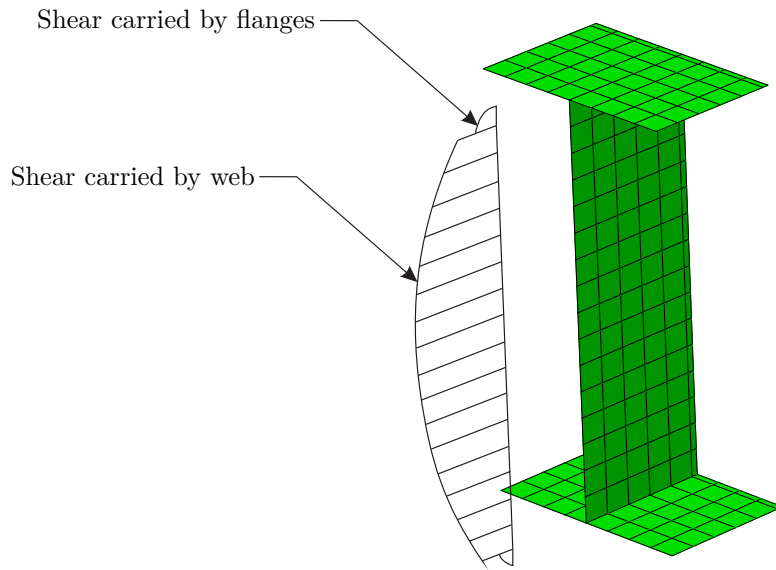


Figure 3.3: Shear distribution through section

subjecting the other end to a controlled displacement. The curve obtained is a plot of  $\sigma_e$  against  $\epsilon_e$  or better known as engineering stress and strain, respectively.

Abaqus however expects the input in the material module to be true stress ( $\sigma_t$ ) and true strain ( $\epsilon_t$ ). The difference between  $\sigma_e$  and  $\sigma_t$  is that the true stress is calculated as  $\sigma_t = P/A$ , where  $A$  is the reduced area of the specimen caused by molecular flow, and  $\sigma_e = P/A_0$ , where  $A_0$  is the original cross-sectional area. A measure of strain often used in conjunction with the true stress takes the increment of strain to be the incremental increase in displacement  $dL$  divided by the current  $L$  (Roylance, 2001):

$$d\epsilon_t = \frac{dL}{L} \rightarrow \epsilon_t = \int_{l_0}^L \frac{1}{L} dL = \ln \frac{L}{L_0} \quad (3.1)$$

Where  $\ln \frac{L}{L_0}$  is called the “true” or “logarithmic strain”. The ratio  $L/L_0$  is the extension ratio, denoted as  $\lambda$ . The relations between the true and engineering measurements are shown in equations 3.2a and 3.2b, respectively and were developed using  $\lambda$ . The modulus of elasticity is determined by dividing the first nonzero true stress by the first nonzero true strain. The true strain is converted into true plastic strain by using equation 3.3. The true stress and true plastic strain are then used to define the material properties in Abaqus. The elastic parameters for the material are  $E = 200$  MPa and  $\nu = 0.3$ .

$$\sigma_t = \sigma_e(1 + \epsilon_e) = \sigma_e \lambda \quad (3.2a)$$

$$\epsilon_t = \ln(1 + \epsilon_e) = \ln \lambda \quad (3.2b)$$

$$\epsilon_{pl} = \epsilon_t - \frac{\sigma_t}{E} \quad (3.3)$$

Two different material models were considered for the numerical investigation, as shown in figure 3.4. The characteristic yield stress of S355JR steel is 355 MPa which corresponds to the 5% percentile of the steel's probability density function. Thus, there is a 95% probability that the beams available from steel merchants have a yield stress higher than the characteristic value. In an attempt to approximate the material model of the test specimen, it was decided that a value around the mean of the distribution should also be considered for the yield stress. A series of tensile tests were conducted by Karmazinova et al. (2012) in order to determine the influence of the steel yield strength value on structural reliability for a steel grade of S355JR. From these tests the mean yield stress for a Log-Normal distribution was determined as 452 MPa.

Both the characteristic yield stress and mean yield stress were considered in this investigation, to illustrate the effect of a beam's material properties. Figure 3.4 shows the stress-strain curves for a yield stress of 355 MPa and 452 MPa. Both the engineering and the true measurements are included in figure 3.4 for each yield stress. The data for the engineering measurements for a yield stress of 355 MPa was obtained by Fisher (2002).

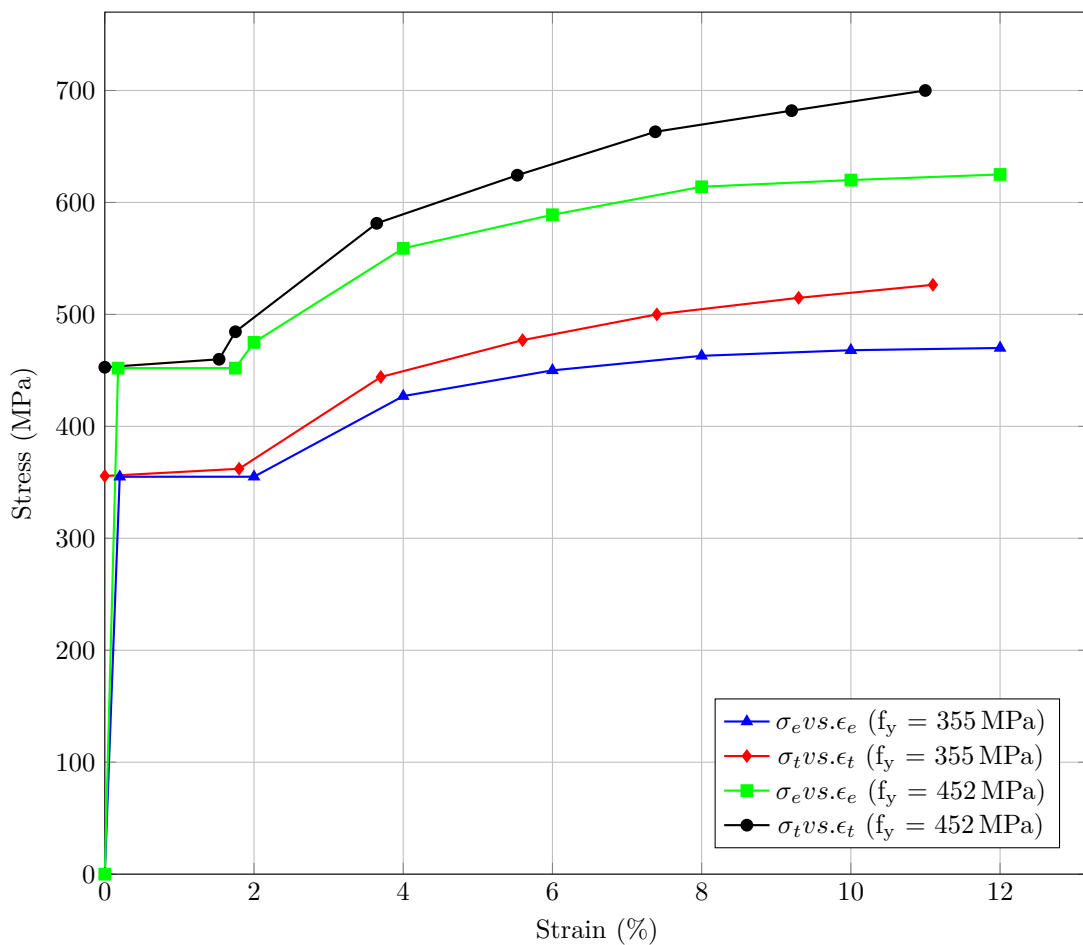


Figure 3.4: Material model for S355JR steel

### 3.2.4 Boundary conditions

As shown in figure 3.2 the beam is simply supported by a roller support and a pin support at the far end. It must be kept in mind that in reality no support conditions are completely fixed or completely pinned, there is always some restraint or lack thereof. Precaution will be taken during the experimental work to ensure that these types of boundary conditions are simulated as closely as possible in the FEA. The theoretical buckling analyses assumes idealized boundary conditions and it is important to ensure that these conditions are replicated as closely as possible for comparison purposes. According to Trahair (1993), the idealized pin support boundary conditions are required to satisfy the following requirements, see figure 3.5:

- Simply supported in plane: both ends fixed against in-plane vertical deflection but unrestrained against in-plane rotation, also one end fixed against longitudinal displacement.
- Simply supported out-of-plane: both ends fixed against out-of-plane horizontal deflection and twist rotation, but unrestrained against minor axis rotation and warping displacement (Trahair, 1993).

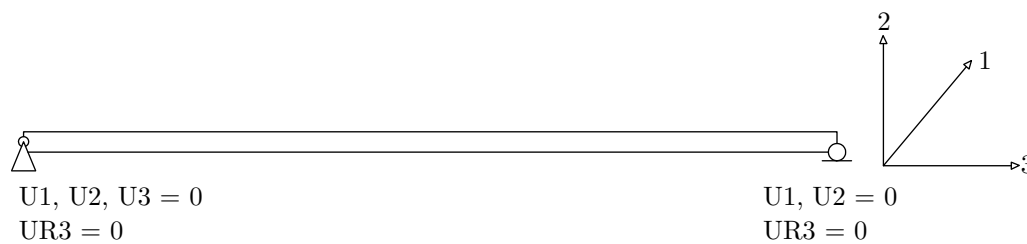


Figure 3.5: Idealized simply supported boundary conditions (Trahair, 1993)

The supports at the ends of the beam are located at the centroid of the section, which is the point where the moments will be applied. The applied moment at this point needs to be distributed smoothly throughout the cross section of the beam, whilst still providing the conditions given by Trahair (1993). The centroid of the beam will serve as a reference node as this is the point where the beam is supported and the load is applied. A type of constraint needs to be implemented that will make this reference point the master node and slave the rest of the surface of the cross section to this node, as depicted figure 3.5. Abaqus provides two types of coupling constraints that are of interest in this investigation, namely kinematic coupling and distributing coupling.

The kinematic coupling constrains the motion of the coupling nodes to the rigid body motion of the reference node. Kinematic constraint is imposed by eliminating the DOF at the coupling nodes (Dassault Systèmes, 2010). It basically acts like an infinitely stiff plate fixed to the end of the beam and it was found that this type of constraint can increase the warping restraint, resulting in an increase in capacity. The distributing coupling constraint provides a method called structural coupling. The structural coupling method couples the translation and rotation of the reference node to the translation and rotation motion of the coupling nodes. This distributing coupling then inherits the average stiffness of the nodes to which it is attached. This type of constraint is particularly suited for the bending behaviour of shells when

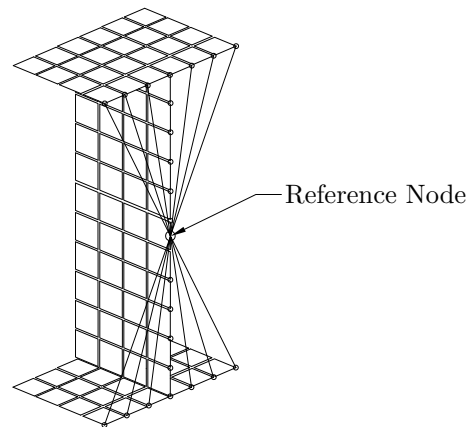


Figure 3.6: Coupling Constraint

the constraint spans small distances (Dassault Systèmes, 2010). For this constraint to be active it is necessary for all rotational DOF to be active. Once the ends of the beam are constrained as described, the conditions defined by Trahair (1993) can be implemented at the reference node to allow for idealized simply supported boundary conditions, as in figure 3.5.

### 3.2.5 Initial geometric imperfections

Every steel beam that is produced has some form of geometric imperfection that can be caused by the production process or even by the handling of these members. Very little data is available on these imperfections and the data available does not indicate how these imperfections trigger LTB. The two aspects of geometric imperfections that are important are the shape of the imperfection as well as the magnitude. The imperfections in steel beams are random and it is possible that these random imperfections only initiate the buckling deformation, but the ultimate load capacity if the beam is mainly determined by the primary buckling mode (Yuan, 2004).

SANS 2001:CS1 provides documentation on fabrication and erection of building materials. In table 3 of this document permissible deviations in rolled components after fabrication is given. According to table 3 in SANS 2001:CS1:

- $\Delta = L/1000$  or 3 mm whichever is the greater, see figure 3.7

In order to better understand the behaviour of a beam a sensitivity analysis was carried out using the model in figure 3.2(a) with a varying degree of imperfection shape and magnitude. The beam was loaded with a single point load in the middle of the beam at the centroid of the cross section. At this point it is worth mentioning that residual stresses were not modeled for the investigation of the initial imperfections. The ultimate capacity of the beam was determined for two different initial geometric imperfections, the 1st and 2nd eigenmode, with varying magnitudes. Figure 3.8 illustrates the degree of variation between the two imperfections, as well as the difference in the ultimate load capacity for different magnitudes of the imperfections. From the results in figure 3.8 it can be concluded that the initial mode of the imperfection

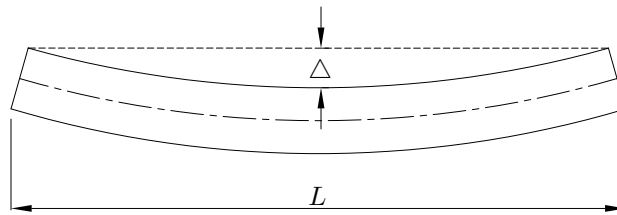


Figure 3.7: Straightness tolerance of a beam in plan view (SABS, 2005)

as well as the magnitude dictate the ultimate capacity of the beam. By using the tolerance given by SABS (2005) ( $L/1000$ ) the magnitude of the imperfection to be used in this investigation is 6.3 mm.

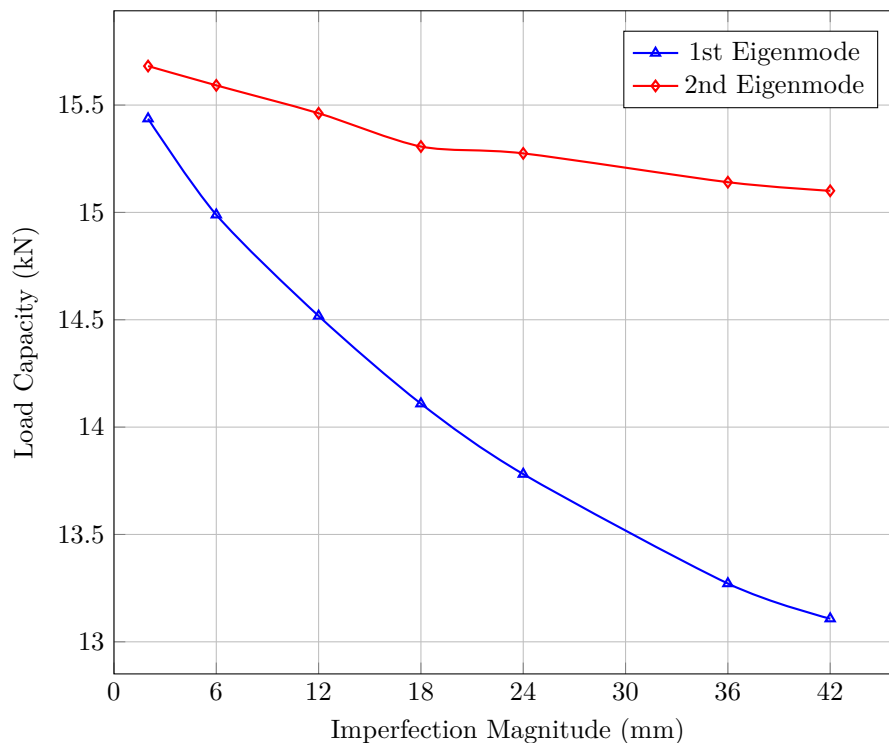


Figure 3.8: Ultimate capacity with varying imperfection mode and magnitude

Figure 3.9 shows the failure of the beam at the ultimate load (UL). It should be noted that only half of the span is shown in figure 3.9 for illustration purposes. Although the initial imperfection was different the ultimate failure mode was the same for both imperfections, but at different ultimate loads. Based on the results given above it can be concluded that the imperfection shape and its magnitude play a crucial role in the capacity of a steel beam and care must be taken when implementing an imperfection. For the geometric imperfection used in this investigation it was decided that the 1st eigenmode gave the most conservative results although the difference between the two modes with a magnitude of 6.3 mm ( $L/1000$ ) was only 3.9%.

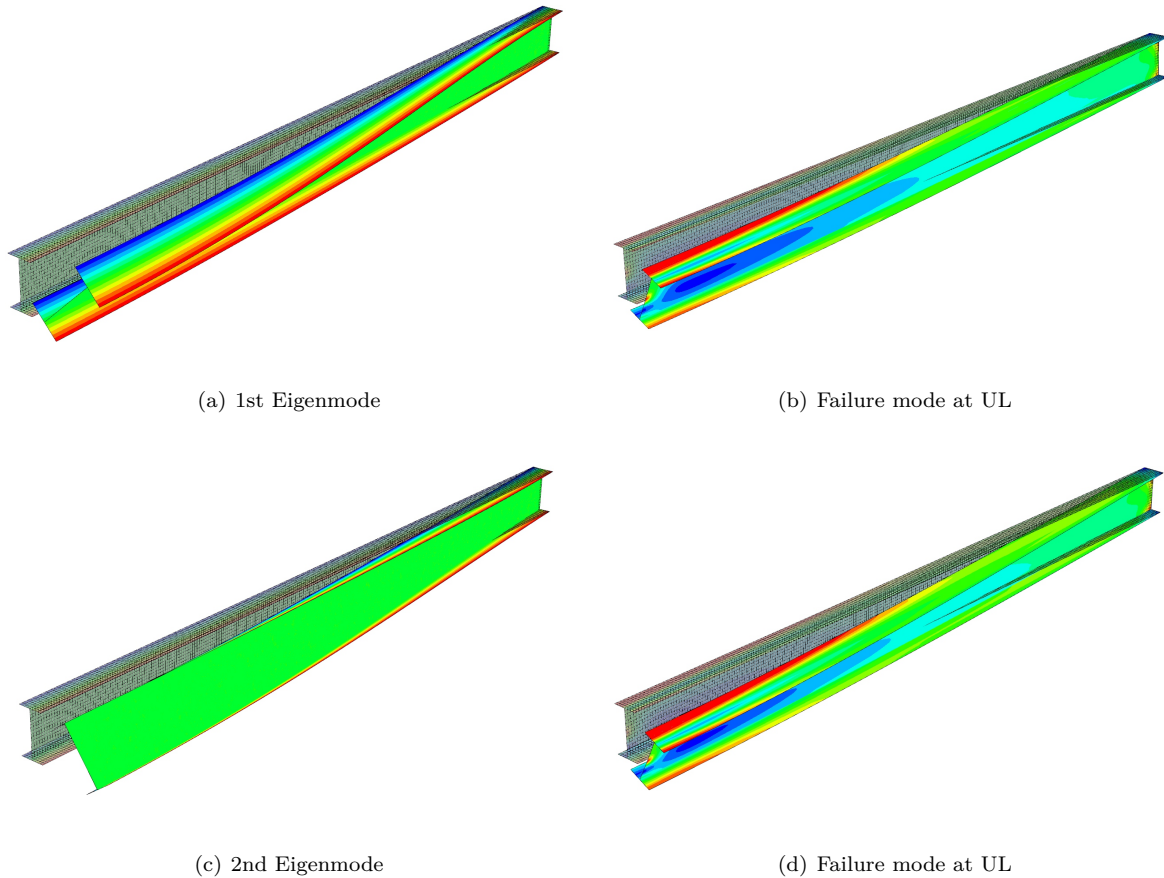


Figure 3.9: Imperfection shapes and failure modes at UL

### 3.2.6 Residual stresses

Residual stresses in hot-rolled steel members arise due to the effect of differential cooling that takes place during the manufacturing process. These stresses are known to have an effect on the member's stiffness and cause the yielding point and ultimate load to be reduced as stated in Section 2.3.1. The stress distribution in these members may vary due to the variations in the production process, e.g. where the residual stresses in the upper flange are often higher than the stresses in the lower flange due to the cooling effect (Yuan, 2004). The residual stresses in hot-rolled sections are constant through the thickness of plates while the membrane component is in the longitudinal direction.

In order to model the residual stresses an idealized stress distribution needs to be assumed. The ECCS (1984) recommends that for a hot-rolled I-section the distribution of residual stresses must be taken as shown in figure 3.10. With the yield stress being 355 MPa and the depth to width ratio being larger than 1.2, the value for  $\sigma_r$  used in this model is  $\approx 107$  MPa and for a yield stress of 452 MPa,  $\sigma_r \approx 135$  MPa. The residual stresses were assigned to the defined element sets of the member as an initial stress field, with the direction of the stress in the global S33 direction. By introducing residual stresses, the model is in a numerical non-equilibrium state. A static load step first needs to be completed before applying any loads to allow the model to restore equilibrium to the system. The contour plot in figure 3.10 is after this

equilibrium step was completed, which is why the contours do not extend to the end of the beam. From Abaqus the residual stresses were plotted, as shown in figure 3.11, which show the distribution across the flange and web of the model. It is clear that the distributions in figure 3.11 resembles a more accurate model, since the stress distributions are non-linear across the elements.

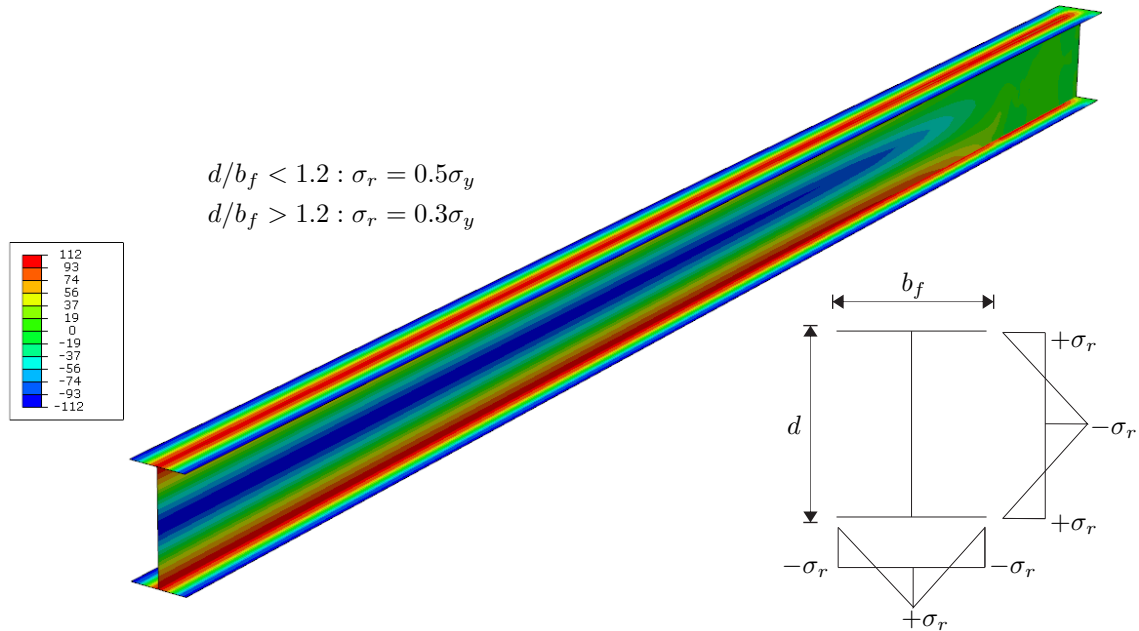


Figure 3.10: Residual stress contours and distribution for I-section (half span only)

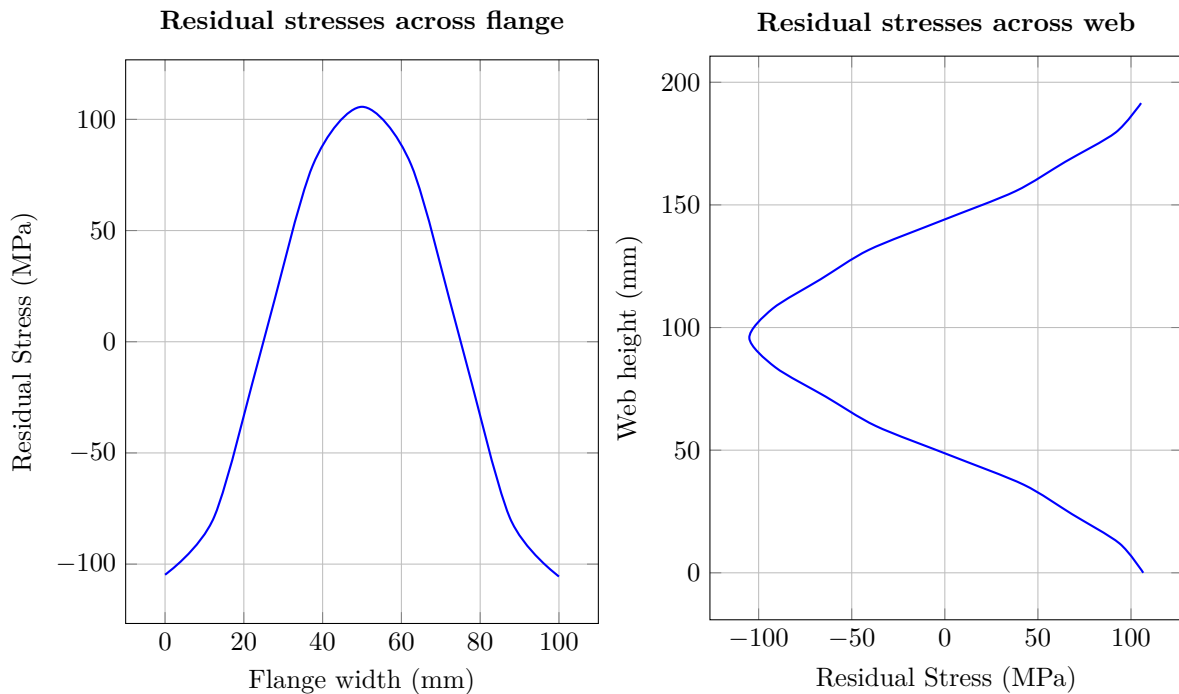


Figure 3.11: Residual stress distribution from Abaqus

As mentioned before, the residual stresses impact the yielding point and the ultimate load carrying capacity of steel members. This reduction in capacity is determined by the magnitude of these initial stresses. A study was performed in Abaqus to determine the influence of residual stresses for two different

types of loadings on the beam model described in Section 3.2.1. The first loading on to the beam was two end moments applied in the opposite direction. The second loading was a point load applied at the centroid of the beam in the middle of the span. The results for the two cases are shown in figure 3.12. In the both cases it can be seen that yielding occurs in an earlier stage for the case with residual stresses (RS) and that the ultimate load is reduced. The ultimate load for the case of the two end moments reduced by 4% and in the case of the point load it was reduced by nearly 10% due to the presence of residual stresses. This shows that the modelling of residual stresses can have a significant impact on the load capacity of steel beams.

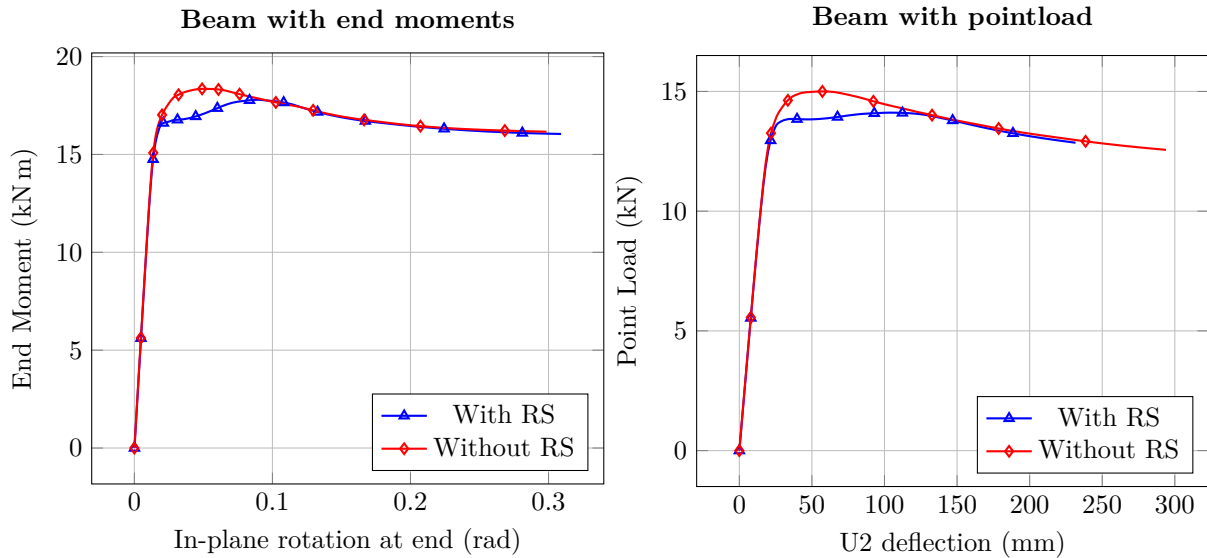


Figure 3.12: Effect of residual stresses on ultimate load capacity

### 3.2.7 Load conditions

This investigation involves four different types of loading configurations in order to generate different moment distributions along the beam. The configuration in figure 3.13(a) involves two end moments with a parameter  $-1 \leq \kappa \leq 1$ . When  $\kappa = -1$  the beam is subjected to the fundamental case of a uniform bending moment distribution. This distribution was assumed in the derivation of the elastic critical moment, see Appendix A. The loading for  $\kappa = -1$  can therefore be seen as the control distribution for this investigation. The applied moment is located at the reference node of the coupling constraint as described in Section 3.2.4. The load configuration in figure 3.13(b) involves a point load  $P$  that is applied to the centroid of the beam. The parameter  $a$  is the location of the point load along the length of the beam for values  $0 < a \leq 0.5$ . The importance of this configuration is to evaluate the steel codes for a beam with a bilinear bending moment distribution with zero end moments.

The beam in figure 3.13(c) is simultaneously subjected to a end moment and a distributed load applied to the centroid of the beam. The magnitude of the end moment,  $\frac{\beta WL^2}{8}$ , is derived from the fixed end moment of a propped cantilever beam with a distributed load, which is equal to  $\frac{WL^2}{8}$ . The parameter  $\beta$  is varied between  $-1$  and  $2$  in order to change the distribution across the beam and induce double



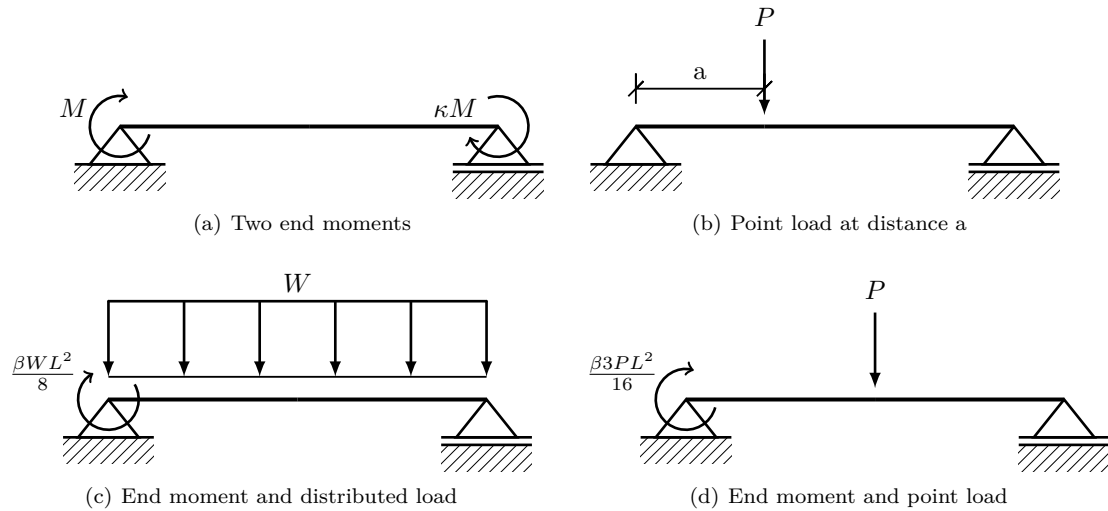


Figure 3.13: Loading configurations for FE study

curvature for values larger than 0. The significance of this configuration is that the bending moment distribution is non-linear for which equation 2.2, which is used in SANS 10162-1:2011, was not initially designed for. This distribution has the potential to highlight the flaws of using equation 2.2. The last configuration, figure 3.13(d), is similar to that of (c), except that the distributed load is replaced by a point load  $P$  applied at the middle of the span on the centroid of the beam. As the value  $\beta$  is increased from -1 to 2, the largest moment switches from the interior to the end of the beam. This effects the value of the equivalent moment factor and can therefore also be used to critically evaluate the steel codes under consideration.

### 3.2.8 Analysis method

Two types of analysis must be performed in order to determine the ultimate load capacity of the beam subjected to the four loading configurations mentioned above. Firstly, an elastic buckling analysis was performed in which the eigenmodes are requested in the step, which will be used in the non-linear analysis as the initial imperfections. Also, the material parameters used in the buckling analysis are the Young's modulus and the poisson's ratio as defined in Section 3.2.3. Following the buckling analysis is the non-linear analysis which employs the Arc-length solution technique. In Abaqus the Riks method is used to observe the post-buckling behaviour of the beam. The following parameters were used for the non-linear analysis:

- maximum number of increments = 100,
- initial increment size = 1,
- minimum increment size =  $1 \times 10^{-5}$ ,
- maximum increment size =  $1 \times 10^{36}$ ,
- enable automatic increment reduction.

The following summary presents the procedure for preparing the non-linear analysis:

1. Define the geometry and assign the web and flange sections.
2. Mesh the model.
3. Define the material properties, create the coupling constraints and define the support conditions and loads.
4. Create a buckling step and define the buckling analysis parameters.
5. In the keywords editor create a .fil file for initial imperfections by using the \*NODE FILE keyword before \*End Step.
6. Run the buckling analysis to generate the eigenmodes for the initial imperfection.
7. Define the plasticity properties of material.
8. Create a Static, General step for the equilibrium of the system due to the predefined stress field of the residual stresses.
9. Create a Riks step and define the parameters.
10. Define the residual stresses at the element sets by using the \*INITIAL CONDITIONS, TYPE = STRESS keywords in the predefined fields module.
11. Import the initial imperfection by using the \*IMPERFECTION keyword before the first step. Input for the \*IMPERFECTION keyword is as follows:
  - FILE = job-name (buckling analysis),
  - STEP = 1 (first step),
  - 1, 6.3 (mode shape number and magnitude, respectively)
12. Run the non-linear analysis.

### 3.3 Preliminary validation

The preceding sections described the development of the numerical model, including the effect of initial geometric imperfections and residual stresses. The validation of the assumptions and modelling considerations mentioned above are of utmost importance for this investigation. A preliminary validation process was implemented to determine the validity of the model so that the bending capacity of the beam can be determined for the design of the experimental setup discussed in Chapter 4. This however is not the final validation and the model will only be declared adequate after comparing the experimental results to the numerical results.

The method of determining the adequacy of the model includes the comparison of the results computed with Abaqus and the results obtained from the design codes, as well as the fundamental linear buckling

equation developed by Timoshenko et al. (1961), see equation 3.4. The dimensionless moment capacities for the four design codes with a varying beam slenderness are shown in figure 3.14, along with the results obtained from the non-linear analysis using Abaqus. In this particular case the load configuration in figure 3.13(a) was used with  $\kappa = -1$ , generating a uniform moment. The cross-sectional properties shown in table 3.1 were used to calculate the resisting moment according to the four steel specifications.

$$M_{cr} = \frac{\pi}{L} \sqrt{EI_y GJ \left( 1 + \frac{EC_\omega \pi^2}{GJ L^2} \right)} \quad (3.4)$$

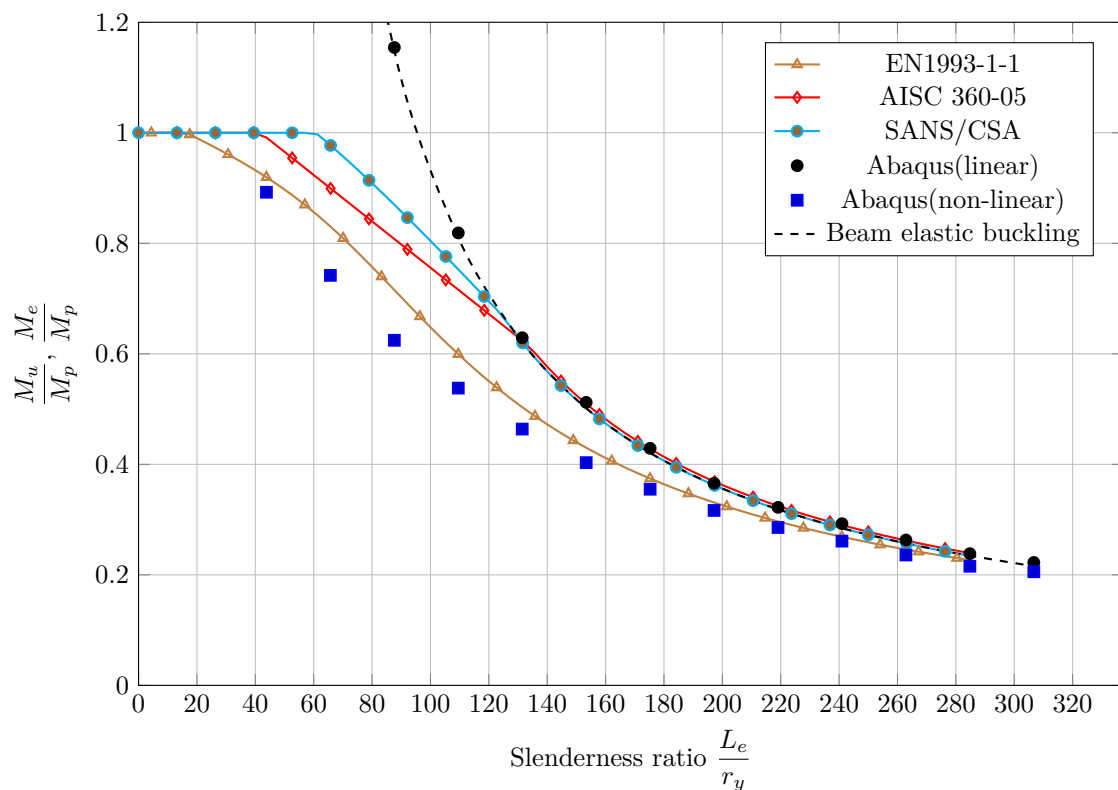


Figure 3.14: Moment capacities for a simply supported beam

From figure 3.14 it can be seen that the linear analysis agrees well with the elastic beam theory. It is clear that the difference between the design codes in the elastic-plastic range becomes significant. This can be due to different approximations used in the design codes such as effective lengths and partial factors. The non-linear analysis in Abaqus agrees reasonably well with the EN 1993-1-1 and follows the general trend of the three design curves. In the numerical investigation of Yuan (2004) similar results were found using a non-linear analysis. However, these results were compared to the ABCB (1998), the Australian steel design code, in which the numerical results showed good agreement with the ABCB (1998). According to Yuan (2004) the reason for the good agreement is that the Australian beam curve was derived from the test results of 159 hot-rolled beams. This preliminary validation shows that the beam model described in this chapter is able to simulate realistic beam behaviour.

## 3.4 Conclusion

A FE model was developed with the goal to capture realistic beam behaviour, that will be validated by an experimental investigation carried out on IPE200 beams. The cross-sectional properties of the FE model and that of the IPE200 are very similar. However, the St. Venant's torsion constant ( $J$ ) is 27% less than that of the IPE200. This must be kept in mind as it reduces the beam capacity when using the FE model in comparison to the real IPE200, because of its presence in the design equation. The sensitivity analysis that was carried out for the initial imperfections provided valuable information on the effect of the imperfection shape and magnitude. The results obtained from this analysis shows that the failure mode at the ultimate moment is independent of the initial imperfection, which was also concluded by Yuan (2004). The 1st eigenmode provides the most conservative results and is used as the imperfection mode shape with a magnitude of 6.3 mm in the numerical model.

The presence of residual stresses in the beam shows a significant effect on the load carrying capacity of the member. It was found that these stresses can reduce the capacity of a beam by 10% which causes the beam to yield at an earlier stage. As for the magnitude of these stresses, a value of  $0.3\sigma_y$  was assumed as suggested by the ECCS (1984). The stress distribution across the flanges and web of the beam model resemble a non-uniform distribution. This captures the residual pattern well due to the fact that the cooling effect is also non-uniform through the elements of the beam as mentioned in Section 2.3.1.

The simply supported boundary conditions, as defined by Trahair (1993), are implemented using a structural coupling constraint that reduces the warping restraint at the beam ends. The most important outcome is the result of the preliminary validation. It was concluded that these boundary conditions are satisfactory as the linear analysis corresponded well to the elastic beam theory. The inclusion of the initial imperfection and the residual stresses in the non-linear analysis allowed for a good correspondence with the design codes. Thus, it can be concluded that the beam model is able accurately simulate a simply supported beam, although the final validation is dependent on the experimental results presented in Chapter 5.

## Chapter 4

# Experimental design

### 4.1 Introduction

This chapter presents a detailed discussion of the experimental work done in this investigation. All the beams that were tested during the experimental investigation were simply supported IPE200 beams. The motivation for the experimental work is presented, followed by an overview of the experimental design. The overview of the design includes the most important aspects such as the conceptional design, the support structure for the actuator and the support conditions for the test beam. The design of the lever arm mechanism is also discussed along with the three different loading configurations considered in the experimental investigation. Lastly, a short discussion is presented on the limitations that were observed during the experimental work. A full set of detail drawings of the experimental setup are presented in Appendix F.

### 4.2 Motivation for experimental research

As is the case with most research investigations, the validation of results remains a crucial part of the investigation. Validation of results gives confidence to the researcher, but more importantly it gives credibility to the research gathered. In the modern age computer software is readily available, but most software packages are still not completely reliable, which can be one reason for incorrect results. Computer software can also be used incorrectly if the methods employed by the software are not completely understood by the user, leading to incorrect results.

The experimental research conducted during this study aims to validate the numerical model that was presented in Chapter 3. A validated numerical model allows for further investigation and can be used to determine the equivalent moment factor for various load configurations. The experimental work also aims to contribute to the existing database of experimental tests performed in the field of LTB. In this investigation certain limitations and errors that were experienced are presented, as well as promising new

findings that can further be investigated and improved upon by other researchers.

## 4.3 Experimental design overview

The testing apparatus used during this investigation provided several complex barriers that had to be overcome. The concept of the design is rather simple, but it involves a number of crucial elements that had to be well thought out and designed. The most crucial design aspects of the test setup are presented and discussed in this section, which includes the support structure for the actuator, the support frames for the test beam and the lever arm mechanism for applying the end moment. It should be kept in mind that all tests performed in this investigation assume simply supported conditions for the test beam. It must be made clear that the design of the test setup was mostly governed by the geometry of the existing elements available, i.e. support columns in the structures lab.

### 4.3.1 Conceptual design

In Section 2.4.1 it is mentioned that the equation in SANS 10162-1:2011 to determine  $C_b$  was developed for a constant moment gradient and is in fact not applicable to non-linear moment distributions. From this the concept of applying a single end moment was created. The single end moment is able to produce a linear bending moment distribution along the beam and a non-linear distribution when a distributed load is added. The concept for creating this end moment is very simple, it consists of a force that is applied to a lever arm, as shown in figure 4.1. This concept evolved into the experimental setup depicted in figure 4.2, which illustrates all the major components.

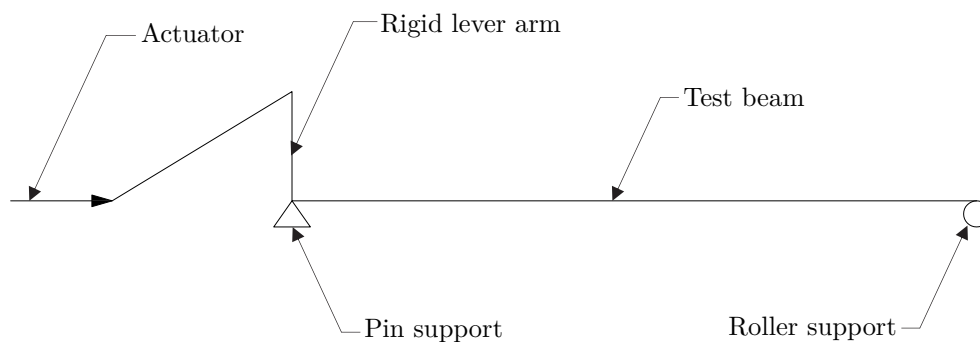


Figure 4.1: Concept for applying end moment

The actuator provides an axial force that is transferred through a pushrod connected to the rigid lever arm (support frame 1). This horizontal force at the top of the lever arm together with the offset distance provided by the lever arm, generating an end moment at the pinned end of the beam. It was decided that the force generated by the actuator and the reaction at the pin support should be enclosed in a single support structure to avoid any slip that might occur if the actuator and the support of the test beam were separated. The support structure for the actuator was designed as a frame to keep all the forces

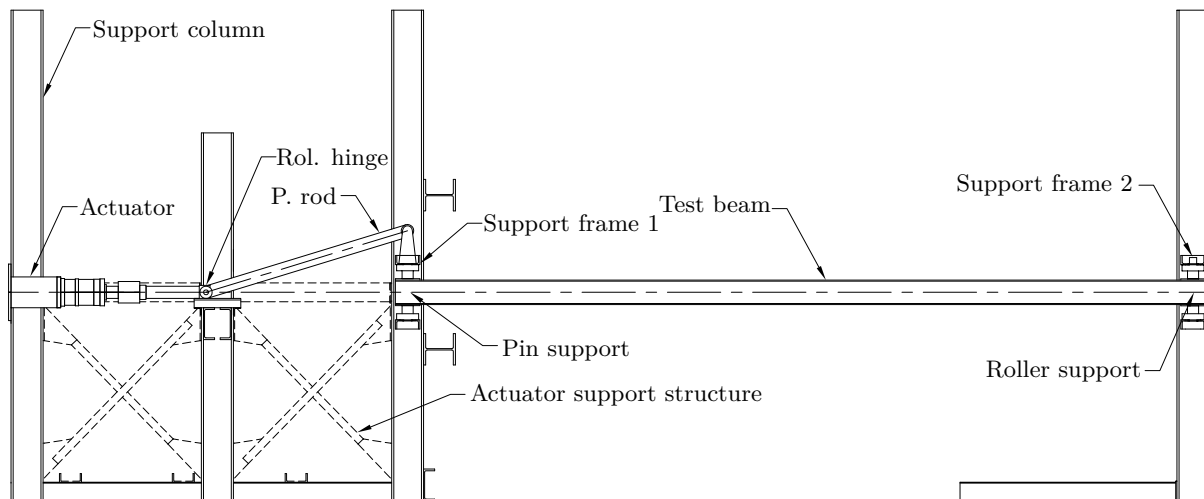


Figure 4.2: General layout of experimental setup

enclosed in a single system, where the pinned end support forms part of the frame. The end supports for the beam (support frame 1&2) had to be designed while keeping in mind the definition of a simply supported beam as stated by Trahair (1993). The complexity of the support conditions were increased due to the fact that the force applied by the actuator had to be distributed through the support frame at the pinned end to the test beam. The design aspects mentioned above will be discussed in detail in the following sections.

### 4.3.2 Actuator support structure

The concept described above requires the 500 kN servo-hydraulic actuator to be mounted horizontally, which created the need for a support structure in the form of a braced frame. The goal of this frame is not only to provide a mounting support for the actuator, but also keep the forces generated by the actuator in an enclosed system, as shown in figure 4.3. The forces are spread throughout the frame, thus eliminating the potential for slip to occur as opposed to the actuator and the pin support being two separate structures. The frame is fixed to the floor by cross beams that span across the bottom chord of the frame and are bolted to the floor, refer to DWG 6 in Appendix F.

Lateral stability of the support structure is provided at each of the three support columns in the form of support frame 1, two channels at the roller hinge and the end support for the actuator, refer to figure 4.2. The end support of the actuator consists of an end plate fixed to two beams, which in turn are bolted to the two support columns at the end of the braced frame, refer to DWG 3. This end support was designed according to the serviceability limit state due to the importance of preventing any additional deflections at the end of the frame. Avoiding any additional deflections, where possible, was of great importance for measuring the end rotation of the beam and in determining the applied end moment, which is described in Section 4.4.1.1.

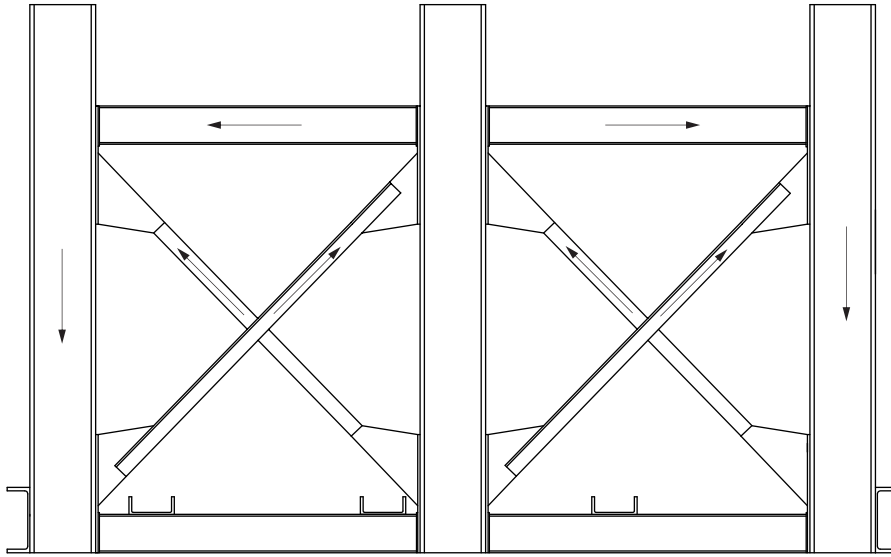


Figure 4.3: Force distribution throughout support structure

### 4.3.3 Support conditions

A single span simply supported beam is a basic and common occurrence in the field of structural engineering. It usually doesn't take much effort to solve unknown variables associated with this type of scenario when compared to multi-span beams or beams with different end conditions. However, to duplicate the boundary conditions in a controlled environment, whilst ensuring that the requirements for a simply supported beam are satisfied, is more complex than the theoretical model.

The complication arises when the test specimen needs to be fixed in such a way that it is physically supported at its ends and that the boundary conditions at the ends are in agreement with that of a simply supported beam. With simply supported boundary conditions the beam must be able to rotate about the strong and weak axis of the cross section, while still being supported so that the ends of the test specimen can withstand the reaction forces due to the applied loads. As mentioned in Section 3.2.4, for simply supported boundary conditions both ends of the beam need to be fixed against in-plane vertical deflection, unrestrained against in-plane rotation and one end must also be fixed against longitudinal displacement. Also both ends must be fixed against out-of-plane horizontal deflection and torsion, but unrestrained against minor axis rotation and warping. A support frame was designed, resulting from the experimental work conducted by Kankanamge (2010) and O'hEachteirn et al. (1988), that allows the test specimen to rotate about the strong and weak axis of the cross section, see figure 4.4. The support frames at both ends are the same, however the difference comes in where the one end is pinned and the other end is supported on a roller to allow for translation in the longitudinal direction.

Simply supported conditions in an experimental setup will always provide some sort of restraint. In order to reduce the restraint due to friction as much as possible, bearings were placed at positions where either rotation or translation were present. The support frame, constructed from four channels that are welded



together, is supported by steel pins to allow for rotation about the x-axis, as defined in figure 4.4. Each pin is fitted into a roller bearing that is located in a bearing housing milled from a steel block. The test beam is bolted to two plates, onto which a shaft is welded, and the space between the test beam and plates is filled by using shim plates. This shaft pushes against a thrust bearing located at the top and bottom of the support frame. The thrust bearings allow the beam to rotate about the y-axis, as shown in figure 4.4. As mentioned above, the design for both support frames is the same, except for the translation DOF in the longitudinal direction at the roller end support. The combination of rotation about both axes and the test beam being bolted in at the support frames, restrains the following DOF, where directions 1, 2 and 3 is x, y and z (longitudinal direction), respectively:

- Pin support end
  - Translation: U1, U2, U3
  - Rotation: UR3
- Roller support end
  - Translation: U1, U2
  - Rotation: UR3

The restrained DOF are in agreement with those which were defined by Trahair (1993).

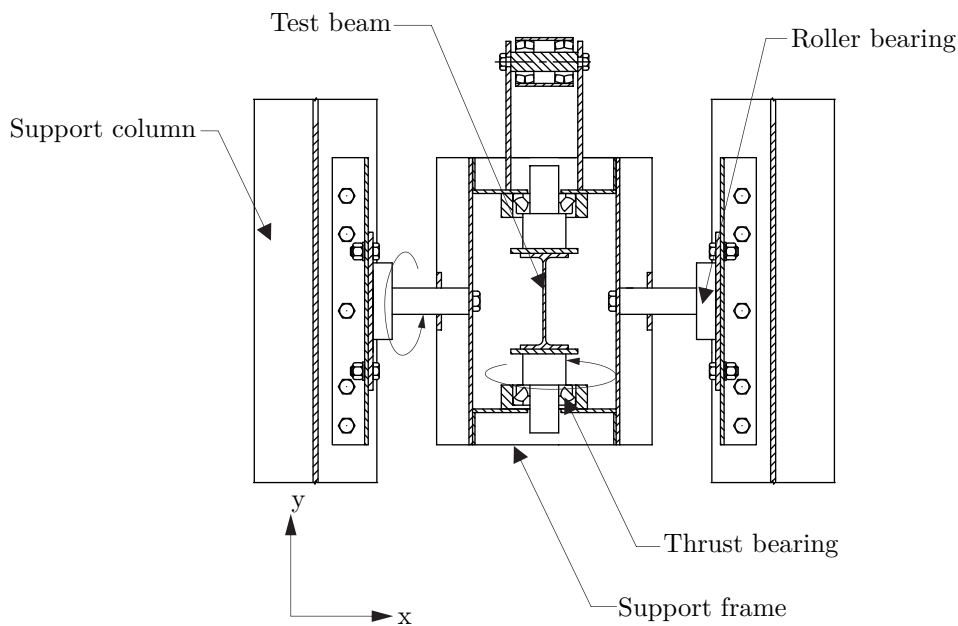
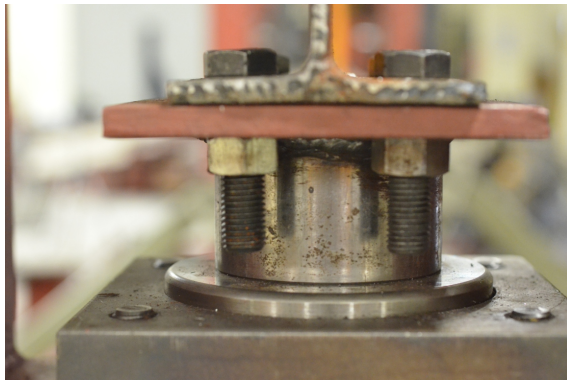


Figure 4.4: Support frame 1 (pinned)

Figure 4.5 illustrates the components that make up the support frame. Included in this figure is the thrust bearing configuration that allows rotation about the y-axis, shown in figure 4.5(a). In figure 4.5(c) it can be seen how the test beam is bolted to the plates that connect the shafts to the thrust bearings. The end condition of support frame 2 is shown in figure 4.5(b), where the roller bearing allows the beam to displace in the longitudinal direction (U3). The pin support described above is shown in figure 4.5(d),

where the steel pin is fitted into a roller bearing that is located in a bearing housing, which is fixed to the support columns.



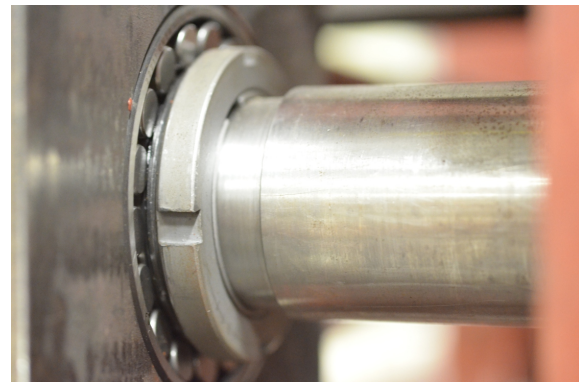
(a) Thrust bearing configuration



(b) Roller bearing at roller support



(c) Support frame



(d) Steel pin fitted into bearing

Figure 4.5: Support components

#### 4.3.4 Lever arm design

The concept of applying a single end moment is described in Section 4.3.1 above. The application of the end moment consists of horizontal force provided by an actuator, that is transferred through an inclined push rod fixed to a hinge connected to support frame 1. This force, together with the lever arm  $L$ , generates an end moment applied to the pinned end of the test beam. The general layout of the lever arm mechanism is shown in figure 4.6, along with the reaction forces at the three hinges.

The actuator used in this experimental study had to develop to an axial force only. A transverse force applied to the piston of the actuator can severely damage the seals. This design consideration had to be overcome by making use of a series of hinges to avoid any bending moments that can induce transverse loads at the actuator's end. The push rod in figure 4.6 is fitted with a sleeve at each end, which contains two roller bearings, refer to DWG 8. The one end of the push rod is connected to two steel plates that are welded to support frame 1. A pin is fitted through the sleeve and bolted to the two plates which form the lever arm hinge, figure 4.7(a). The other end of the push rod is connected to a steel end box constructed from three steel plates, which forms the roller hinge, figure 4.7(b). A steel pin, running through the sleeve and steel box, is fitted with four roller bearings that are able to move along the roller tracks provided

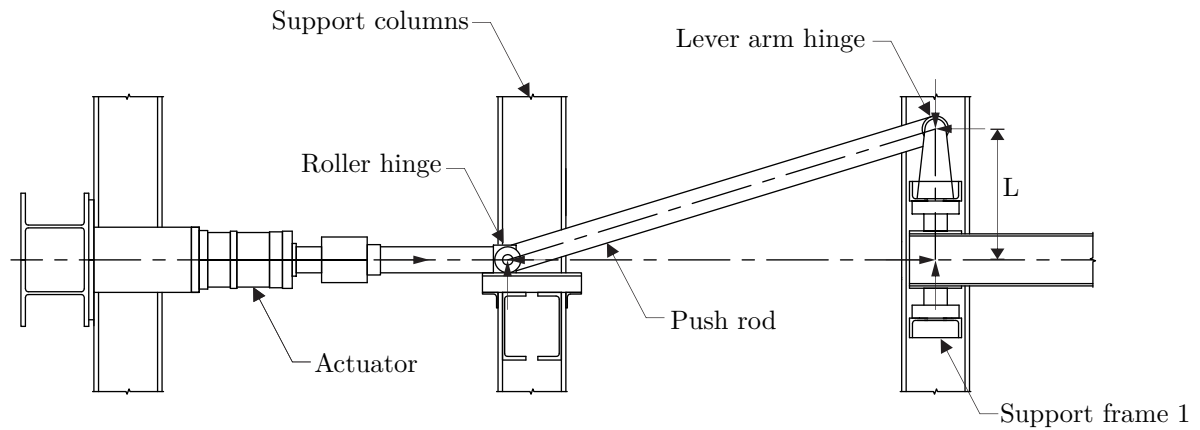
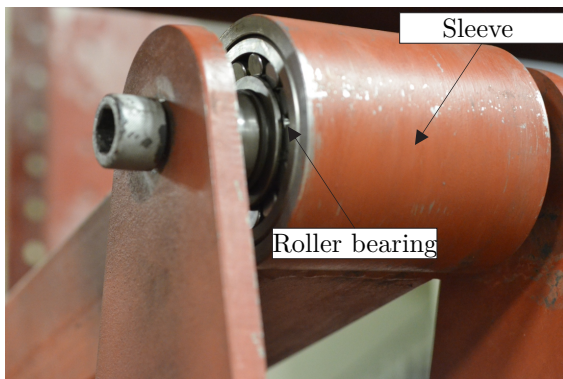
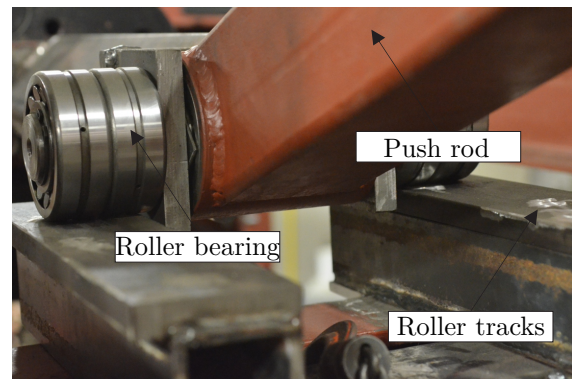


Figure 4.6: Reaction forces at hinges

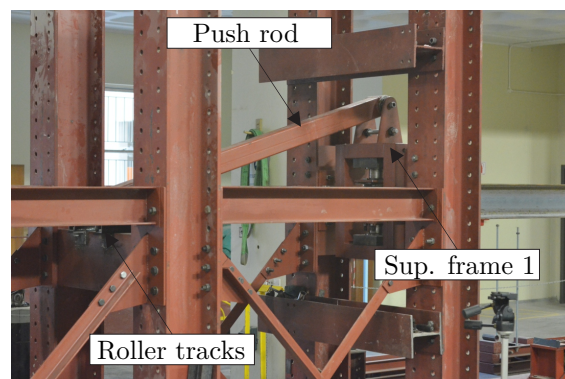
between the two central support columns. The steel end box is welded to square tube that is bolted to the end of the actuator.



(a) Lever arm hinge



(b) Roller hinge



(c) Lever arm assembly

Figure 4.7: Lever arm components

The roller hinge shown in figure 4.7(b) absorbs the vertical reaction that is generated at the lever arm hinge and in this process ensures that the actuator is subjected only to an axial force. The horizontal force at the lever arm hinge, a distance “L” from the pinned support, creates an end moment about the major axis of the test beam. The vertical force at the lever arm hinge generates a moment in the opposite direction, which is relatively small in comparison. The geometry of the lever arm mechanism, together

with the displacement measurement from the actuator, is used to determine the applied moment as well as the rotation of support frame 1, this will be discussed in Section 4.4.1.

## 4.4 Testing configurations

During the experimental investigation three different types of load configurations were applied to the simply supported beam, as shown in figure 4.8. The test specimen under consideration in this investigation is an IPE200 section with a total length of 6.5 m. However, due to the design of the support frame and the beam being bolted in at the support frame, the effective length of the beam is taken as 6.3 m. The first and most complicated configuration, figure 4.8(a), consists of a single end moment applied together with a distributed load. The second and third load configurations were carried out with the use of a gravity load simulator (GLS). In figure 4.8(b), a single point load is applied at mid-span using the GLS, while the third configuration, figure 4.8(c), employs two GLSs for applying a point load at each end. The last test is based on the work conducted by O'hEachteirn et al. (1988). A detailed discussion of each of the load configurations is presented in this section.

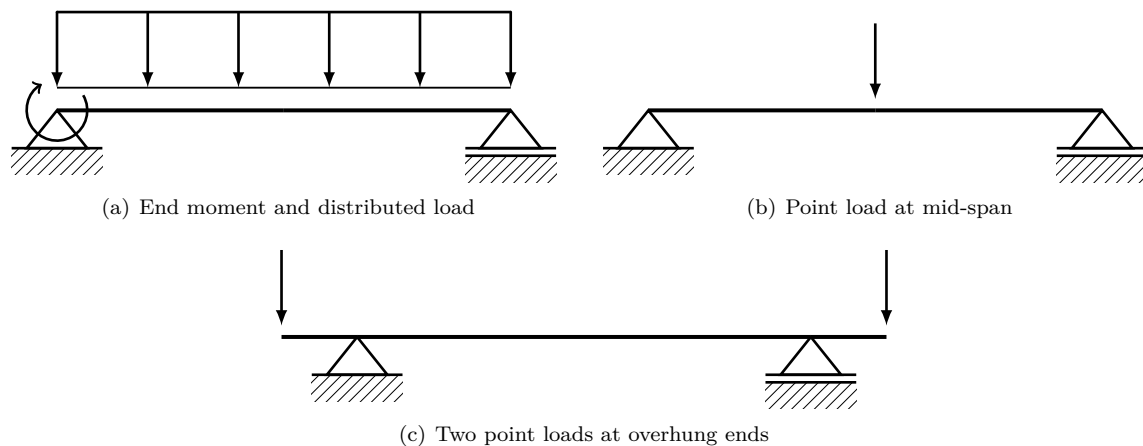


Figure 4.8: Loading configurations for experimental work

### 4.4.1 End moment and distributed load

It was mentioned in Section 4.2 that this research aims to contribute to the existing database of LTB experimental research. The literature reviewed failed to present an experiment where a single end moment was applied to a simply supported beam. This load configuration then represents an evolution in the design for an experimental setup employing a single end moment. A distributed load, together with an end moment provides a non-linear bending moment distribution along the beam, which aims to validate the FE model with a similar load configuration, as discussed in Section 3.2.7.

The preceding sections describe the lever arm mechanism that is used to generate the end moment using a 500 kN actuator. To apply a distributed load along a beam without providing any lateral restraint was a difficult barrier to overcome. The distributed load in this investigation was simulated by using a

series of point loads spaced apart along the beam. The point loads were applied by using 100 kg lead weights hanging from weight frames, as shown in figure 4.9. The frames were located at the top flange of the IPE200 beam and held in position by milled down M12 bolts, refer to DWG 3, that were placed inside drilled pilot holes. Applying the point loads in this manner ensures that the load remains vertical as the beam undergoes LTB. Although there was a total number of 23 weights available, only 12 were eventually used for safety reasons. The 12 lead weights together with the frames gave a total distributed load of  $2 \text{ kN m}^{-1}$  along the beam.

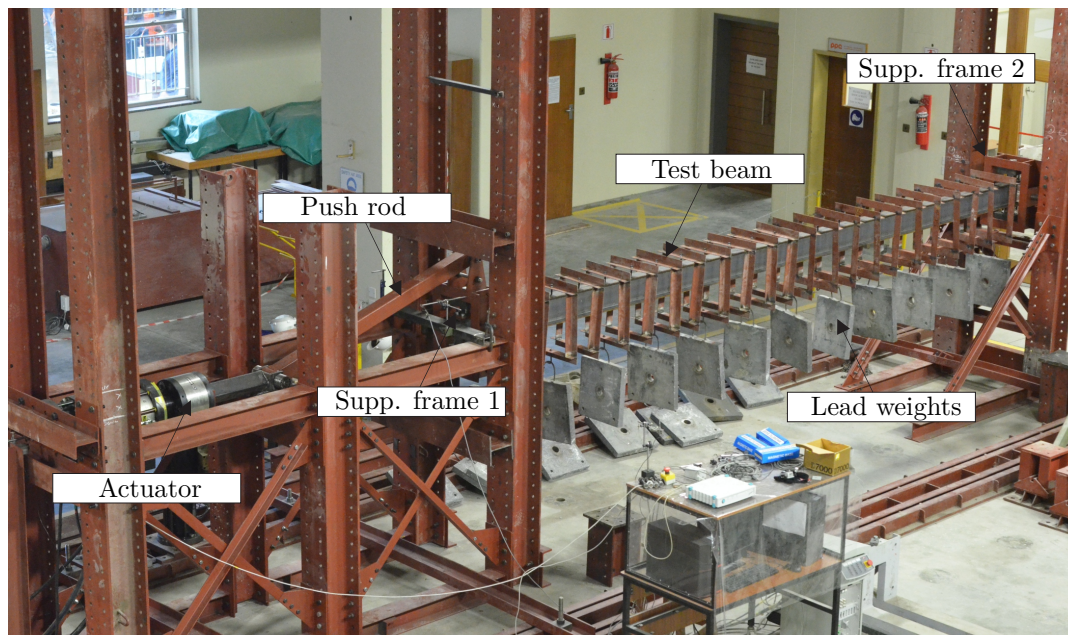
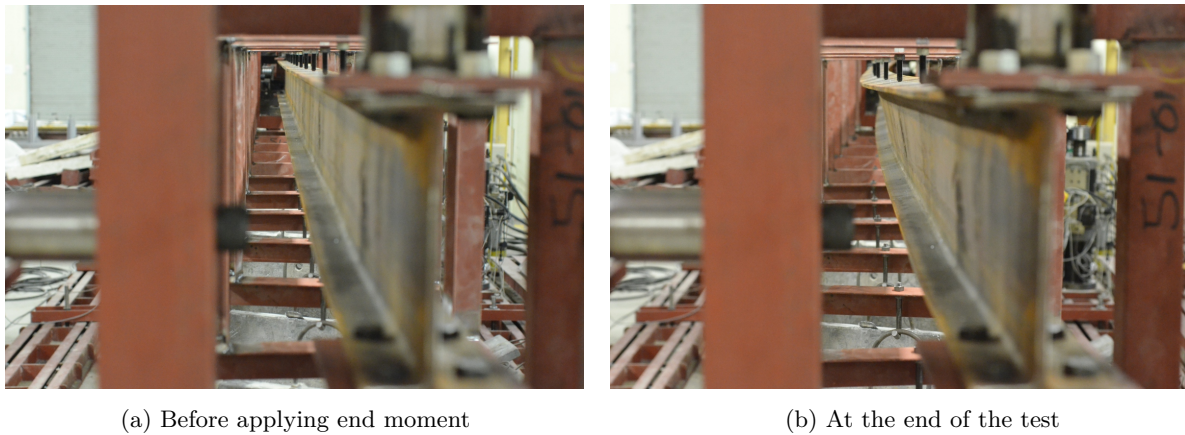


Figure 4.9: Test layout for end moment and distributed load

The test procedure for this load configuration involved firstly placing the lead weights on the frames. The actuator was then used to apply a constant axial displacement at a rate of  $4 \text{ mm s}^{-1}$  in order to generate the end moment. The test was monitored using the displacement control function, which adjusts the force applied by the actuator to constantly meet the required displacement rate. A load vs. deflection graph was plotted during the test in order to physically evaluate when the beam failed due to a loss in stiffness, i.e. a reduction in the force was observed together with an increase in deflection.

In figure 4.10 two stages of the test are shown. The beginning of the test, figure 4.10(a), shows a slight vertical deflection of the beam due the applied distributed load. Figure 4.10(b) shows the results at the end of the test, where it can clearly be seen that the beam failed due to LTB. It can also be observed in both figures that the bolts of the weight frames remain vertical and cause an additional destabilizing effect. The test was successfully carried out and it proved that it is possible to subject a simply supported beam to a single end moment in an experimental situation. Although the test was successful, a number of limitations and areas of concern were observed. These limitations will be discussed in Section 4.5.



(a) Before applying end moment

(b) At the end of the test

Figure 4.10: Before and after the test was conducted

#### 4.4.1.1 Measurement equipment

This particular load configuration presented a difficult task in terms of measuring the deflection and applied end moment. Due to the fact that the applied end moment is a function of the axial force provided by the actuator and magnitude of the lever arm, it was not possible to employ a direct measurement of the applied end moment. A geometric approach had to be implemented in order to determine the rotation of the beam end and the magnitude of the applied moment. Figure 4.11 illustrates the geometry of the lever arm mechanism in the initial and deformed state. In order to determine the end moment and the rotation only the displacement of the actuator ( $x$ ) and the axial force ( $F$ ) were recorded.

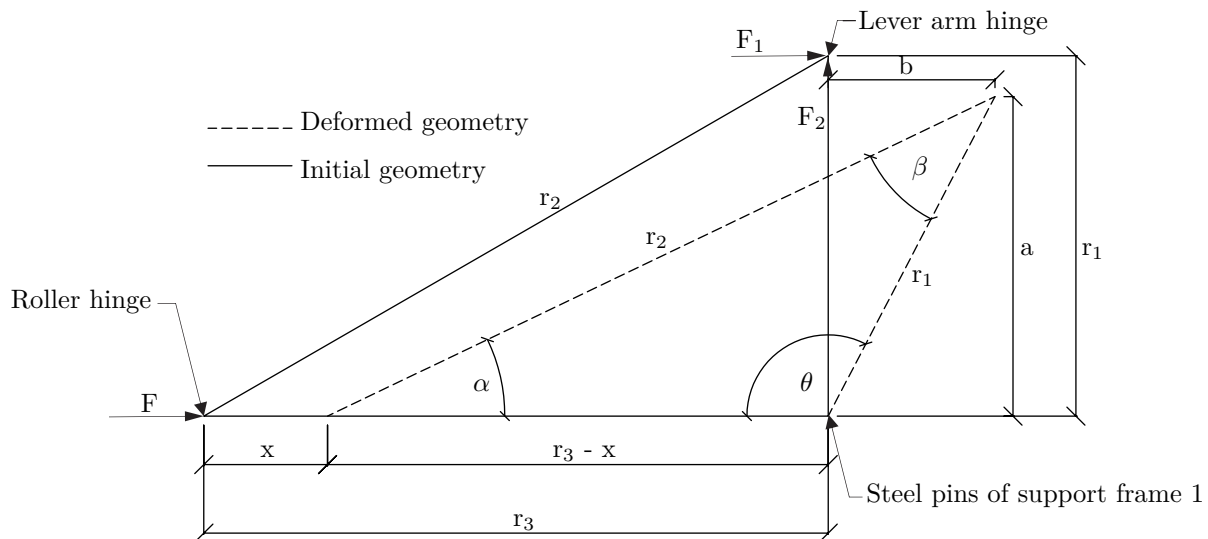


Figure 4.11: Geometric variables to measure applied end moment and end rotation

The variables,  $r_1$  and  $r_2$ , which are known, remain constant throughout the entire test as these are support frame 1 and the push rod, respectively. The displacement measurement from the actuator's transducer is used to determine the deformed geometry of the lever arm mechanism. Equations 4.1-4.3 are used to determine the angles  $\theta$ ,  $\beta$  and  $\alpha$  by using the variables defined in figure 4.11. These three angles

are then used to determine the force components,  $F_1$  and  $F_2$ , due to the axial force  $F$  at the lever arm hinge. The dimensions  $a$  and  $b$  are calculated using basic trigonometry and provide the lever arms for  $F_1$  and  $F_2$ , respectively. The moments generated,  $F_1a$  and  $F_2b$ , are in opposite directions and the applied end moment is taken as the resultant moment, i.e.  $F_1a - F_2b$ . The dimension  $b$  is relatively small in comparison to  $a$ , thus making the moment generated by  $F_2$  small in comparison to  $F_1a$ .

$$\cos \theta = \frac{r_1^2 + (r_3 - x)^2 - r_2^2}{2r_1(r_3 - x)} \quad (4.1)$$

$$\cos \beta = \frac{r_1^2 - (r_3 - x)^2 + r_2^2}{2r_1r_2} \quad (4.2)$$

$$\cos \alpha = \frac{r_2^2 + (r_3 - x)^2 - r_1^2}{2r_2(r_3 - x)} \quad (4.3)$$

It was also necessary to measure the deflection of the end support to which the actuator was fixed due to the reaction at this point, as shown in figure 4.12. The displacement recorded at this point was always less than 1 mm, but was still incorporated into the calculation described above by using  $x$ , as in figure 4.11, as the resultant displacement of the actuator's transducer and the displacement of the end support.

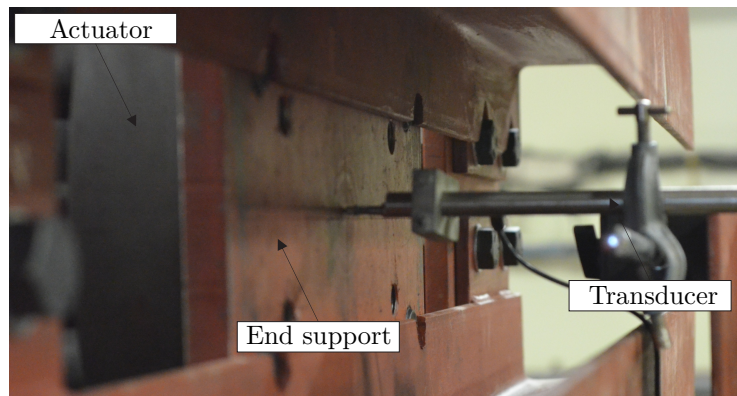


Figure 4.12: Transducer at actuator end support

The preceding method described for determining the end moment and the rotation at the pin support had to be validated to ensure that the calculations used in the method were correctly executed. In order to validate this method, it was decided that the rotation at the pin support had to be determined in such a manner that is completely independent of the variables used in the method described above. A transducer was used to measure the horizontal displacement,  $\delta_h$  in figure 4.13, of support frame 1. The vertical distance ( $L$ ) between the point where the tip of the transducer made contact with support frame 1 and the centreline of the steel pins of the support frame was measured. The rotation ( $\theta$ ) was then calculated by using equation 4.4.

$$\theta = \arctan \frac{\delta_h}{L} \quad (4.4)$$

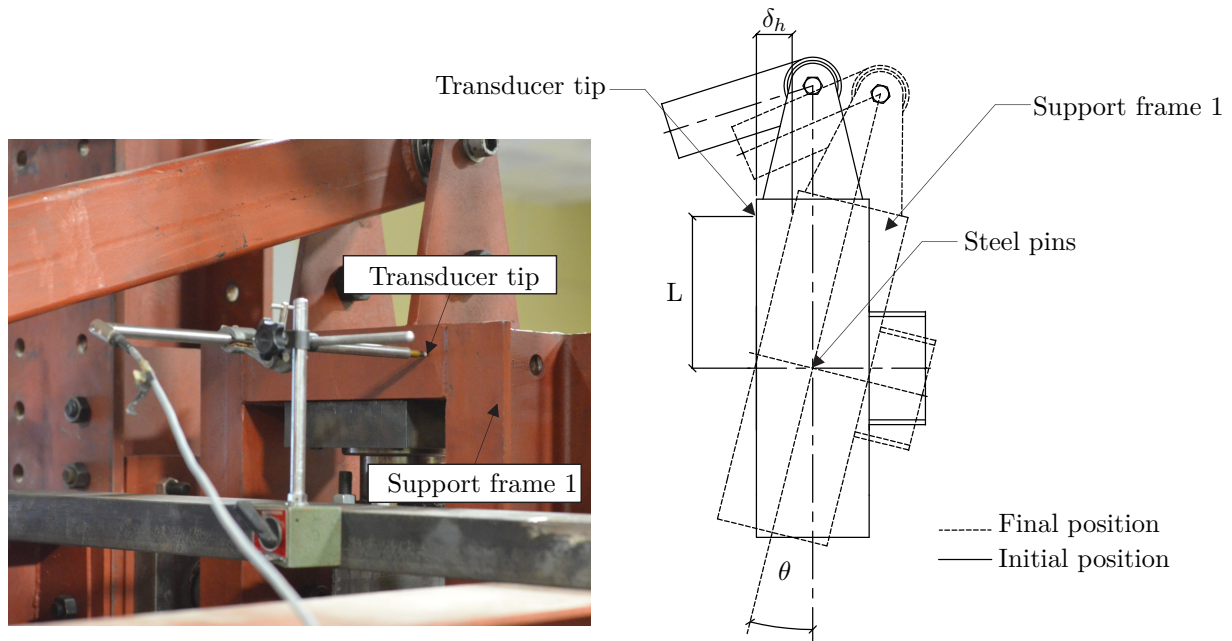


Figure 4.13: Transducer at support frame 1

The two methods showed similar results for the rotation of the beam end. A total of four tests were carried out using the load configuration of an end moment and distributed load. Table 4.1 shows the rotation at the end of the beam as determined according to the two methods described above. The difference in rotation between the two methods was always less than 5%, proving that the approach followed to determine the applied end moment and the rotation of the beam was correctly implemented and that the results obtained are trustworthy.

Table 4.1: Rotation of beam end for the two methods

Beam	Rotation at the beam end (degrees)		Difference (%)
	Using actuator transducer	Transducer at support frame 1	
1	3.03	3.14	3.5
2	3.44	3.51	2.0
3	2.61	2.72	4.0
4	3.69	3.75	1.6

#### 4.4.2 Tests involving the Gravity Load Simulator (GLS)

In Section 2.2 it was stated that when a beam undergoes LTB, the line of action of the load moves with the cross section, but remains vertical. In order to test structures permitted to sway, a testing apparatus known as the gravity load simulator was developed. Section 2.7.3 describes how the GLS can be implemented in order to subject a structure to a point load, while allowing the applied load to remain vertical. A significant attribute of the GLS, is that it eliminates the effect of restraint and lateral bracing caused by the load. In this investigation the GLS was used for the two loading configurations depicted in figure 4.8(b) and (c). The method of using the GLS for these two configurations is discussed



in the following sections, together with the equipment that was used for the measurement and the load application.

#### 4.4.2.1 Measurement and load application equipment

The application of the force in the test described in Section 4.4.1 consisted of a computer controlled servo-hydraulic actuator that constantly monitored the displacement rate. The use of the GLS however, calls for a more primitive approach when it comes to the application of the load. A detailed discussion of the assembly is presented, followed by the mechanism employed to apply the load. The applied load is generated by the use of a hydraulic cylinder that is manually operated by a hydraulic hand pump, as shown in figure 4.14(a) and (b), and is capable of applying a maximum point load of 50 kN. The design of the GLS allows the cylinder to be screwed into a threaded swivel cap at the bottom of the rigid triangle, figure 4.14(c). The swivel allows the triangle to rotate while keeping the load vertical as the beam undergoes LTB.

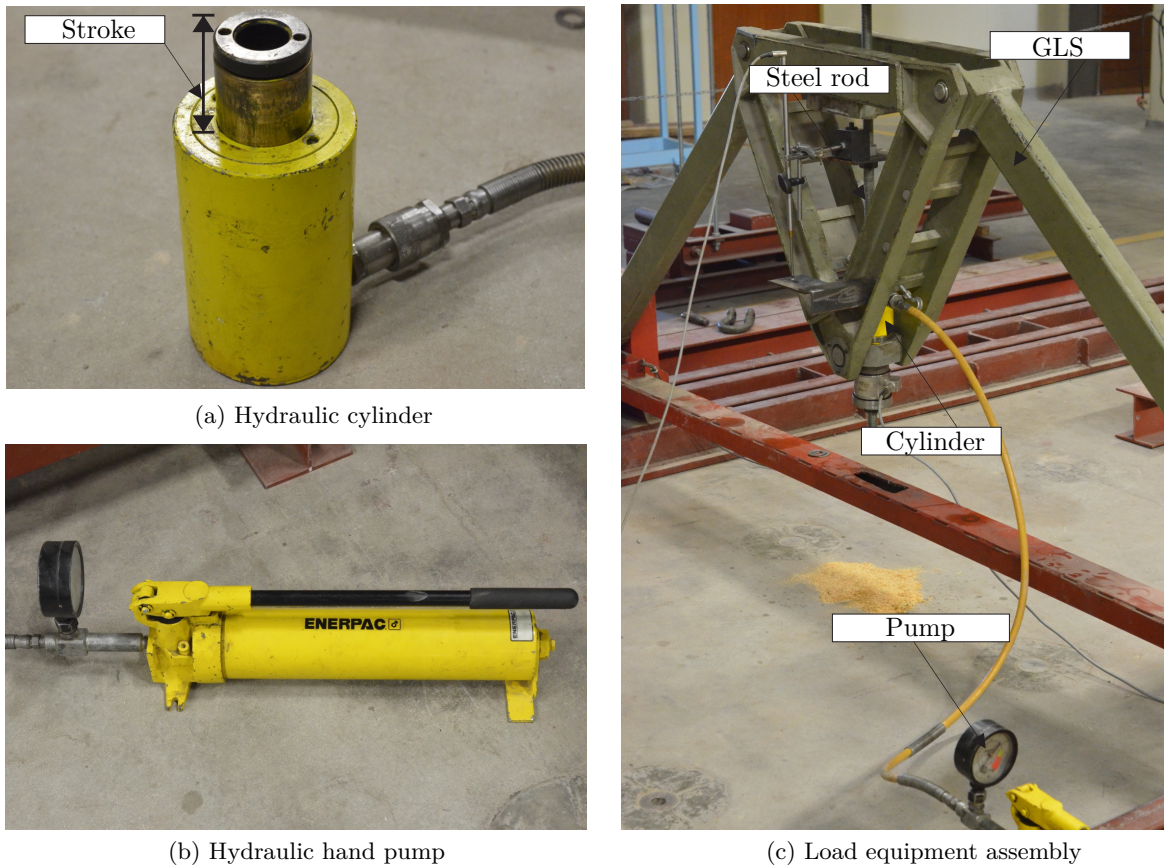


Figure 4.14: Load application equipment

The recorded data for the tests involving the GLS included the magnitude of the applied force as well as the vertical deflection at the point of application. The force was recorded by using a 200 kN load cell, while the deflection was measured using a 100 mm transducer. The assembly of the transducer and the load cell for the GLS are shown in figure 4.15(a) - (c), respectively. The transducer assembly shows the transducer fixed to the steel rod and the tip of the transducer supported by a plate clamped to the swivel.

This arrangement allows the transducer to follow the line of action, i.e. the transducer follows the steel rod, while the plate remains perpendicular to the transducer's tip.

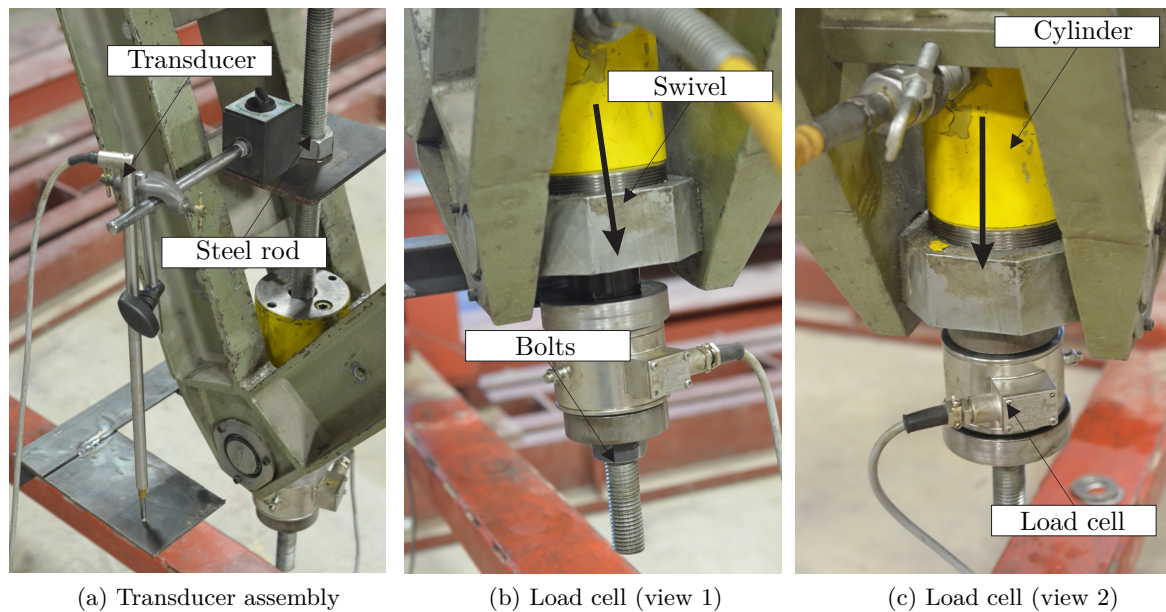


Figure 4.15: Transducer at actuator end support

The load cell is located between two steel plates, of which the bottom plate is secured with a bolt and the top plate is supported by a bush pressing against the cylinder's piston. The mechanism to apply the point load is initiated when the hydraulic pump is manually pumped and the cylinder's piston starts extending. The extending piston presses against the bush which causes a compression force on the load cell that is clamped between the two plates. As the piston extends, the steel rod is pulled downwards, as indicated by the arrow in figure 4.15, creating a point load downwards on the top flange of the beam.

#### 4.4.2.2 Point load at mid-span

The test configuration for a beam subjected to a single point load at mid-span was carried out using the GLS and the equipment described above. A total number of six specimens were tested, all of which were IPE200 sections with a span of 6.3 m. A frame, constructed from channel sections, was fitted with a pointed steel pin and positioned inside a pilot hole on the top flange of the test specimen. The steel rod, connected to the load cell assembly of the GLS, is bolted to the bottom chord of the frame, as shown in figure 4.16. The frame is designed in such a manner that the beam is unrestricted in order to move as it undergoes LTB and the restraining effect of the load is eliminated. As the test beam undergoes LTB the applied point load remains vertical, see figure 4.16, which causes a destabilizing effect as described in Section 2.4.2.

In the preceding section it was mentioned that the transducer assembly was designed in such a manner that the transducer follows the line of action during LTB. This is illustrated in figure 4.17, which shows the initial and deformed state of the GLS during the test. The yellow line resembles the steel rod, while the white line resembles the transducer. From figure 4.17 it can be seen that the transducer remains

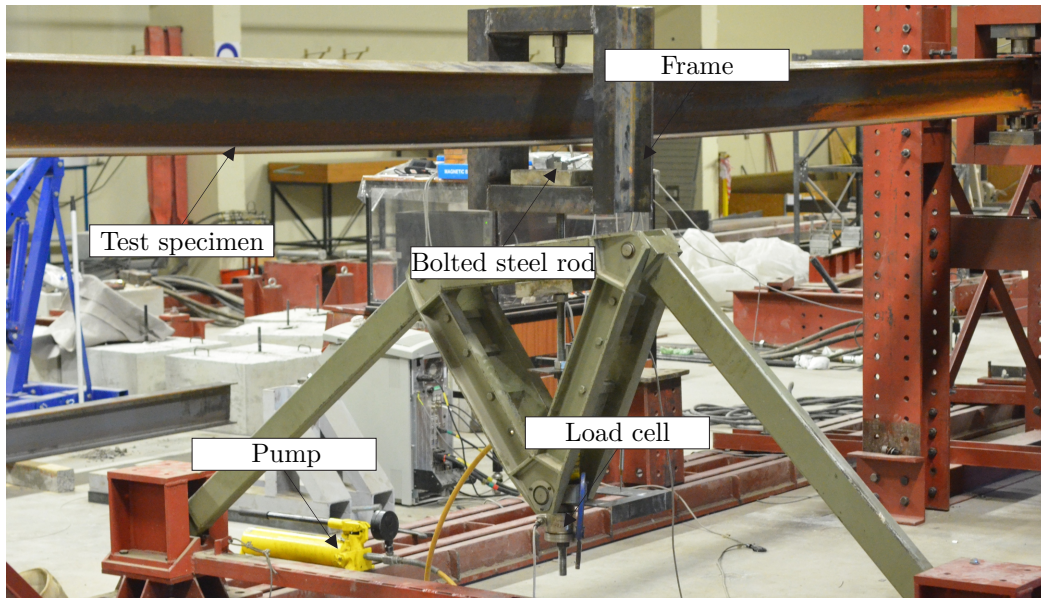


Figure 4.16: Point load at mid-span

parallel to the steel rod during the test and that the plate remains perpendicular to the transducer's tip. This ensures that the displacement measured by the transducer is the absolute vertical deflection of the beam.



(a) Initial state

(b) Deformed state

Figure 4.17: Initial and deformed state

#### 4.4.2.3 Two point loads at overhung ends

The literature review provided invaluable information on experimental tests that were previously carried out and the work by O'hEachteirn et al. (1988) is of special significance. The loading configuration in their test was similar to the one shown in figure 4.18, which includes two point loads applied at both ends of a simply supported beam with overhung ends. The point loads,  $P_1$  and  $P_2$ , at a distance  $l$  from the support generate a moment,  $P_1l$  and  $P_2l$  at the support, respectively. If the magnitude of the point loads are the same, the beam segment between the supports is subjected to a uniform bending moment distribution.

The design of O'hEachteirn et al. (1988) presents one aspect upon which this experimental investigation

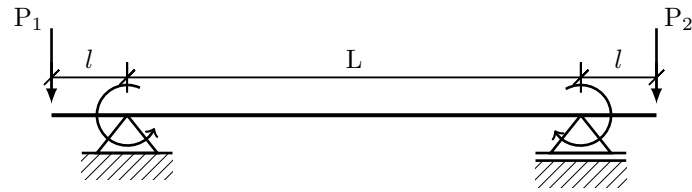


Figure 4.18: Beam with overhung ends

aims to improve, namely the restraint provided by the overhung beam ends. In Section 2.7.1 it is stated that as the beam segment between the supports buckles, it is restrained by the adjoining segments. This is due to the fact that the applied point loads at the ends are not able to displace laterally as buckling occurs. In this investigation a similar test was carried out in order to subject the IPE200 beam to a uniform bending moment distribution. The beam had a total length of 9.5 m, with the cantilever segments each having a length of 1.5 m. The point loads were applied to the top flange of the beam, at a distance of 1.3 m apart for the supports, which corresponds with the distance  $l$  in figure 4.18.

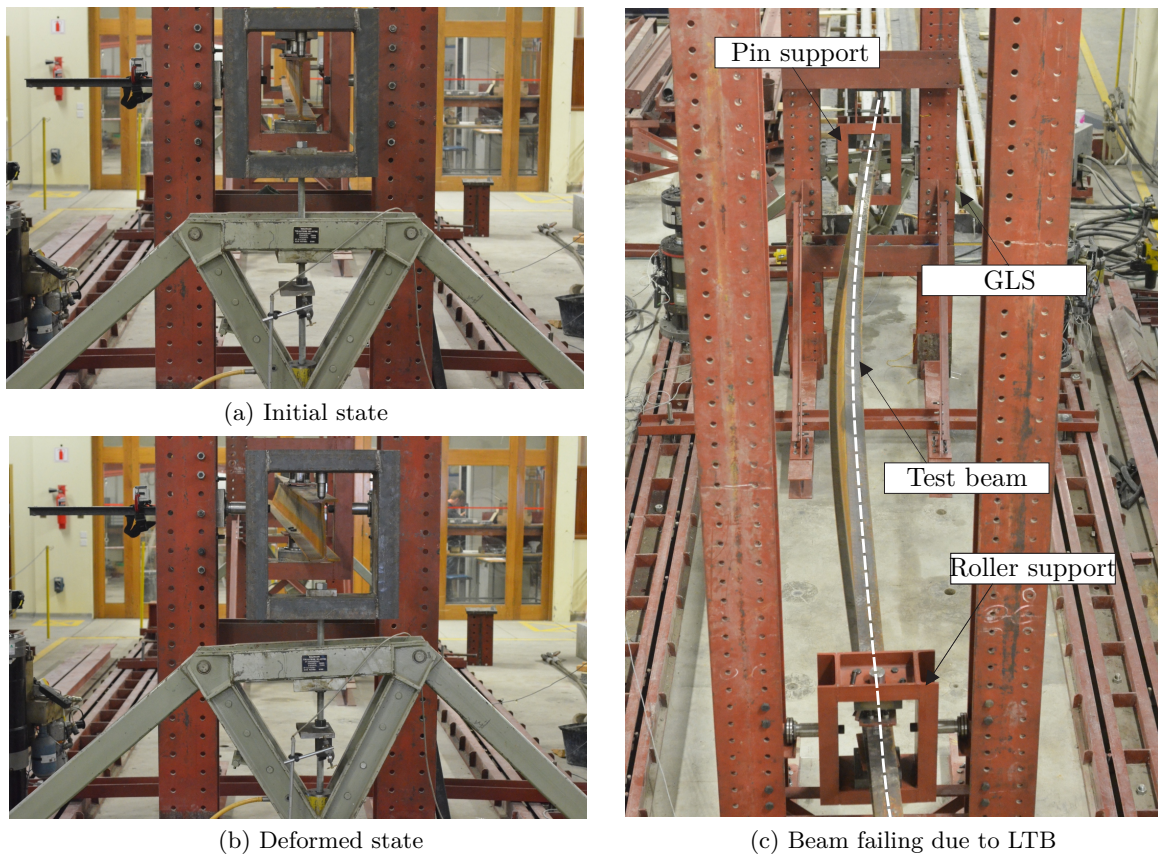


Figure 4.19: Beam with overhung ends

The possibility of the beam failing in shear was never an issue due to the 50 kN capacity of the hydraulic equipment and the factored shear resistance of the IPE200 being 233 kN. To apply the point loads two GLSs were used, one at each end of the beam. The measuring and load application equipment described in Section 4.4.2.1 were used in order to carry out three tests. The initial and deformed state of the GLS is shown in figure 4.19(a) and (b), respectively. These figures illustrate how the GLS allows the applied point load to displace laterally as the beam undergoes LTB. The effect that this mobility has is made

clear in figure 4.19(c). The white dashed line is plotted on the centre of the top flange to highlight the buckled shape of the beam. The shape of the buckled beam shows that the adjoining segments have a negligible restraining effect on the beam segment between the supports, although a small degree of restraint is present at the support itself, as shown in figure 4.20. The effect of this restraint will be made clear in Chapter 5.

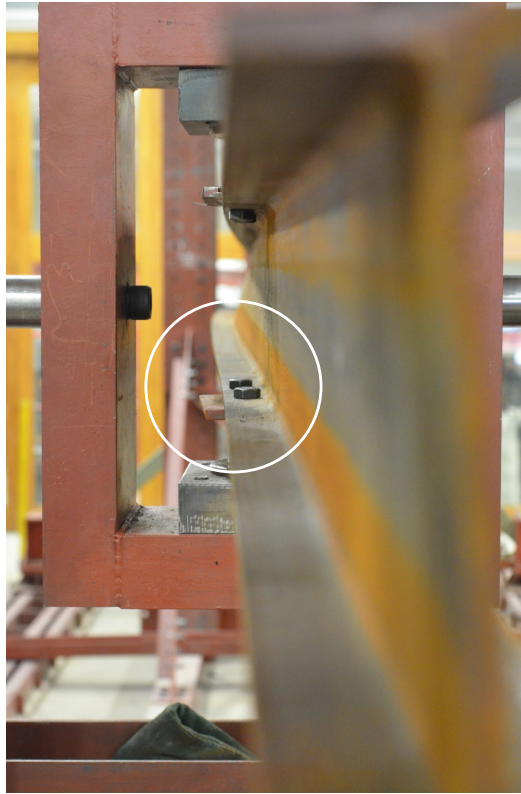


Figure 4.20: Restraint at support

### 4.4.3 Measuring of initial imperfections

The influence of initial geometric imperfections in a steel beam was shown to have a significant impact on the load carrying capacity, refer to Section 3.2.5. The assumption made in FE analyses is that all the beams have the same geometric irregularities, which in reality is not true. It was observed that a few specimens had significant geometrical imperfections before the tests were carried out, as shown in figure 4.21. Figure 4.21 shows that the beam is relatively straight, except at the end where the beam exhibits an out-of-straightness imperfection highlighted by the white circles. This observation motivated the decision to measure the initial imperfections of the test specimens in an attempt to quantify the magnitude of these imperfections.

In order to measure the imperfections it was necessary to position an object next to the beam that was perfectly straight. A steel cable was fixed to the two ends of the beam at the same offset distance and using a nut and bolt, as in figure 4.22(b), the cable was pre-stressed to a point where lateral deflection was

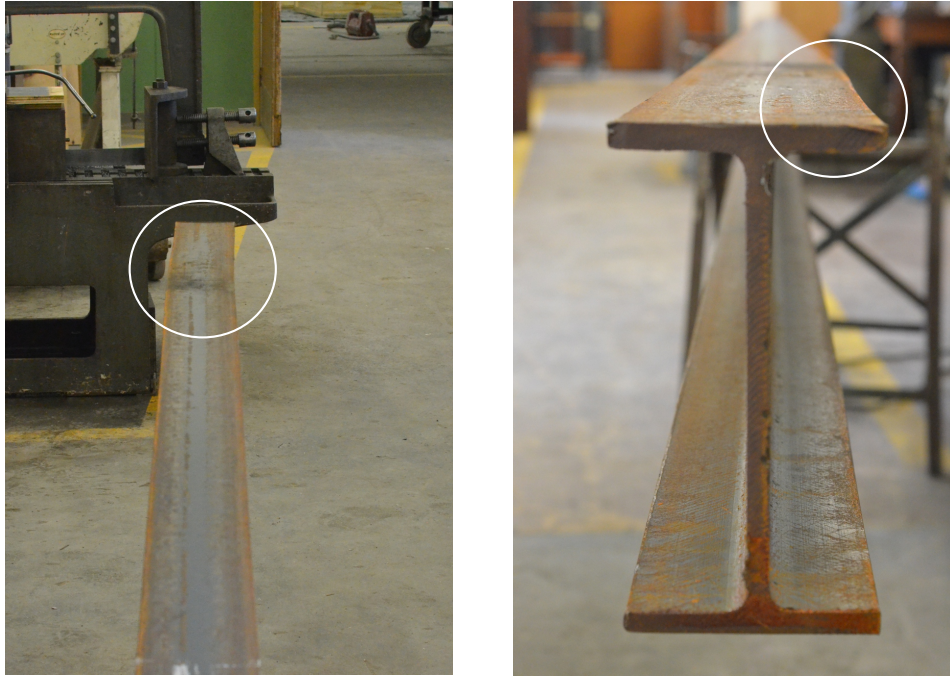


Figure 4.21: Geometric imperfection of test specimens

absent due to contact with the laser. A total of 22 measurements were recorded at mid-section height, at constant intervals along the length of the beam. The readings were determined by using a laser positioned against the pre-stressed cable, as shown in figure 4.22(a).

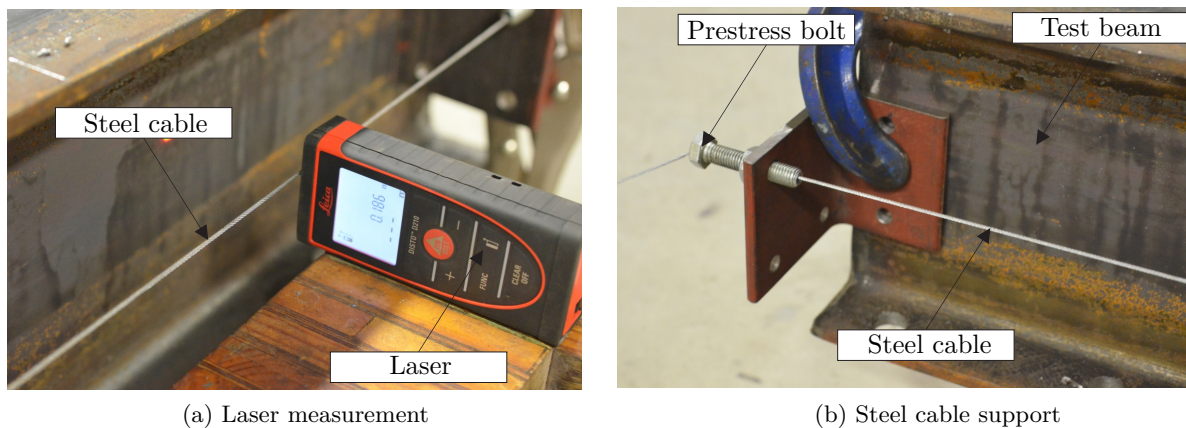


Figure 4.22: Measuring of imperfections

A total number of thirteen beams were tested during this investigation of which the imperfections of only eight beams were recorded. The reason for this is that the method for determining the imperfections, as described above, was only implemented at a later stage. Figure 4.23 shows the imperfection magnitudes for test beam B8, which exhibited the largest imperfections of the measured beams. It can be seen that the largest imperfection, recorded at mid-span, is 6 mm, which is almost equal to the tolerance of  $L/1000$ . Appendix B presents a series of graphs similar to the one in figure 4.23 for each of the remaining test specimens that were measured. Although the imperfection shape and magnitude varies between the

different specimens, the general shape of the imperfection resembles that of the 1<sup>st</sup> eigenmode, except that of specimen B6. This validates the assumption made in Section 3.2.5 for using the 1<sup>st</sup> eigenmode as the initial imperfection and  $L/1000$  as the imperfection magnitude.

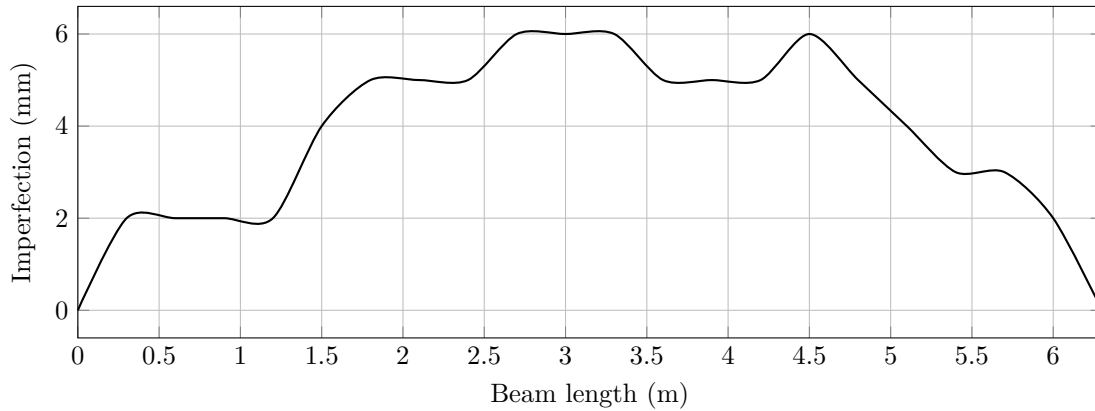


Figure 4.23: Recorded imperfections of test specimen B8

## 4.5 Experimental limitations

This section provides a short discussion on the limitations and sources of error that were observed during experimental testing. A significant flaw encountered during the tests involving the end moment mechanism, was a lack of rigidity in support frame 1. Section 4.3.4 describes how the axial force is used together with the lever arm mechanism in order to apply the end moment to the specimen. In the description it is mentioned that the force provided by the actuator is transmitted to support frame 1, which in turn rotates to apply the end moment. The error observed in this mechanism was that support frame 1 experienced an additional rotation to the rotation of the test specimen. This additional rotation originates due to the thrust bearings rotating the steel block housings, resulting in a lack of rigidity between the support frame and the test specimen.

The additional rotation mentioned above is illustrated in figure 4.24, where it can be seen that the support frame rotates while the test specimen remains horizontal. As the frame rotates only the bottom part of the bearing rotates with the support frame, resulting in a concentrated force applied to the ball bearings as indicated by the black arrows in figure 4.24. This force applied to the thrust bearings is not equally distributed along all the ball bearings, causing a significant increase in friction for the out-of-plane rotation.

In Section 4.3.3 it is mentioned that the space between the test specimen and the plates is filled using shim plates. A problem encountered when using this method, was that if the space was too tightly packed, the thrust bearings would pinch and the rotation of the support frame would be restrained. The bearing would only release when the beam underwent a significant vertical deflection, resulting in a sudden lateral deflection of the beam.

Two other limitations were observed during the tests involving the GLS. Firstly, the piston stroke of

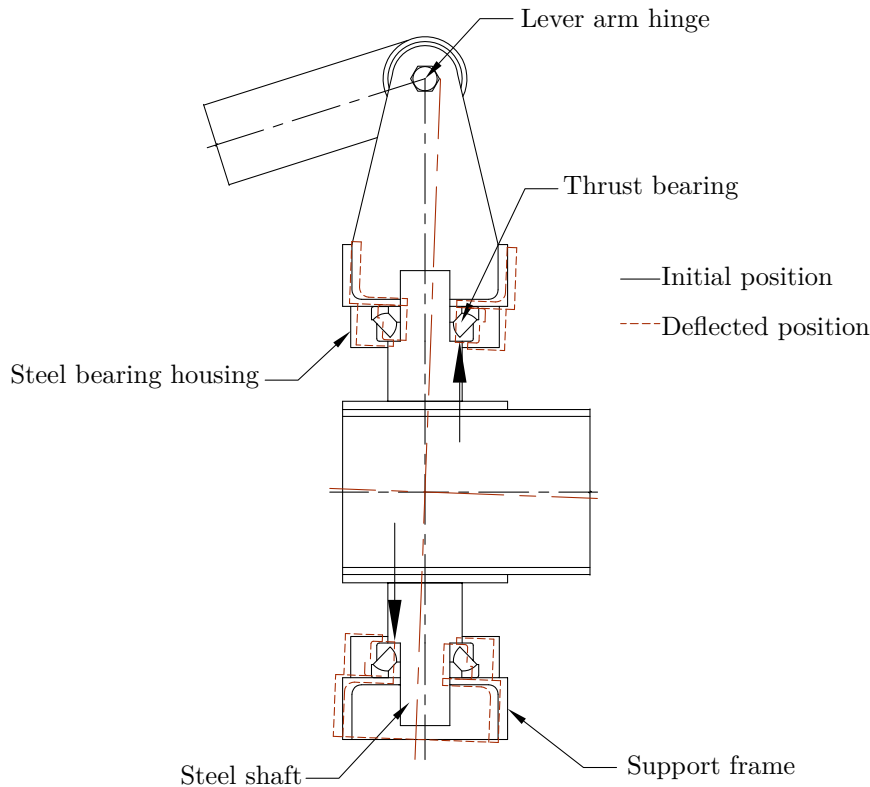


Figure 4.24: Additional rotation of the support frame relative to the test specimen

the cylinder is limited and if this limit is reached during the test, the piston must first be reset before continuing the test. Secondly, the manually operated hand pumps made it difficult to apply the same point load simultaneously, resulting in a non-uniform bending moment distribution. This can be attributed to various factors, including the pump rate, which is uncontrolled, or a difference in the oil pressure between the pumps. In Chapter 5 the experimental results are presented where the impact of these limitations and errors will be highlighted.

## 4.6 Conclusion

The experimental work conducted during this investigation consisted of three different load configurations applied to a simply supported IPE200 beam. A total number of thirteen beams were tested of which four were subjected to an end moment together with a distributed load, six subjected to a point load at mid-span and three subjected to a point load at each end. This investigation then provides a variety of tests, where failure of all the beams was due to LTB, contributing to the research field of LTB.

The support frames that were used in the tests successfully simulated the behaviour of simply supported conditions, although a small degree of restraint was observed during the tests involving the overhung ends. In two tests the space between the plates and the test beam was too tightly packed and caused the thrust bearing to pinch, restricting the beam to rotate about the vertical axis. The tests concerning the end moment and distributed load proved that it is possible to apply a single end moment to a beam in



order to induce LTB. However, a significant flaw that was observed during these tests was the rotation of the thrust bearing inside the bearing housings. The force applied to support frame 1 to generate the end moment proved to be too concentrated for the degree of rigidity present between the test beam and the thrust bearings. The additional rotation of the support frame resulted in a concentrated force clamping down on the ball bearings and increasing the friction for the out-of-plane rotation of the beam.

Two methods were used in the measuring of the beam end rotation, in which both depended on different recorded data. The difference between the two methods was less than 5%, illustrating that a good approximation of the beam end rotation can be determined. The assembly of the transducer in the tests involving the GLS was able to move with the line of action, which allowed the recorded measurement to reflect only the absolute vertical deflection of the beam. The GLSs allowed the applied load at the top flange to move along with the beam, while remaining vertical and in this process the effect of restraints was eliminated.

In previous experiments where point loads were applied to a beam with overhung ends, the applied point loads created a significant restraint by not being able to move laterally. The GLSs provided lateral mobility in the tests concerning this configuration. The hydraulic pumps used to apply the loads using the GLSs made it difficult to simulate a perfectly uniform moment due to the difference the loads generated by the pumps. The measurement of initial geometric imperfection provided valuable information concerning the imperfection shape and magnitude. The measurements obtained validate the assumption made in Chapter 3 concerning the imperfection shape and magnitude.

## Chapter 5

# Experimental results

### 5.1 Introduction

In the previous two chapters a detailed description was given about the FE and experimental work conducted during this investigation. The goal of the numerical investigation was to develop a FE model in order to determine the equivalent moment factor of a simply supported beam subjected to various bending moment distributions. The experimental work was in turn aimed at validating the assumptions made in the development of the FE model to ensure that the model is able to capture realistic beam behaviour.

The exclusion of any tensile tests in this investigation is motivated by the objectives set out for the experimental program. By studying the behaviour of steel beams, rather than duplicating an ultimate load carrying capacity, makes it possible to include a range of yield stresses and thus reducing the amount of work and resources needed to determine the material properties for every test specimen. This chapter presents the results obtained from the experimental investigation as well as the FE analyses carried out for similar load configurations.

Included in this chapter is a detailed discussion of the comparison between the experimental and numerical results. A summary of each test is given as well as reasons for any discrepancies that might have occurred. A full range of the test data is presented in Appendix C of this document.

### 5.2 Comparison between experimental and numerical results

This section presents the comparison between the experimental results and those obtained by the FE model described in Chapter 3. The FE model was subjected to the same load configurations as described in Section 4.4. It is worth noting that there are some discrepancies between the test specimens and the FE model, as well as sources of error that were observed during the experimental testing.

Table 3.1 lists the cross sectional properties of both the test specimen and the FE model, where it can be seen that the St. Venant's torsion constant ( $J$ ) is significantly lower for the FE model. This parameter has a direct correlation to the load carrying capacity of a steel beam prone to LTB. A reduction in  $J$  will lead to a reduction in the load carrying capacity of the beam. Another factor that can lead to discrepancies between the numerical and experimental results is the difference in material properties. Section 3.2.3 describes the two material models considered during the numerical investigation, namely a model using the characteristic yield stress as well as a model using the mean yield stress. It is expected that the different material properties will be irrelevant within the elastic range, whereafter a difference in load carrying capacity will occur.

The initial geometric imperfections also affect the load carrying capacity of a beam, as shown in Section 3.2.5. The recorded imperfections of the test specimens illustrate an out-of-straightness of less than  $L/1000$  for most of the specimens, refer to Appendix B, which can contribute to a higher ultimate load. A major source of error, presented in Section 4.5, is the additional rotation of the support frame with respect to the test specimen. The additional rotation resulted in an increase in friction for the out-of-plane rotation. It is expected that this lack of rigidity between the support frame and test specimen will have an effect on the experimental results presented in the following sections.

### 5.2.1 Simply supported beam with end moment and distributed load

It was stated in Section 4.4.1 that tests involving a simply supported beam subjected to a single end moment have not previously been conducted, which motivated the design of a test setup that included a single end moment. In order to simulate a non-linear bending moment diagram the test consisted of a single end moment, together with a distributed load of  $2 \text{ kN m}^{-1}$ , as shown in figure 5.1. Although all four test specimens failed due to LTB, certain flaws in the design were observed and the effect of these flaws is presented in this section.

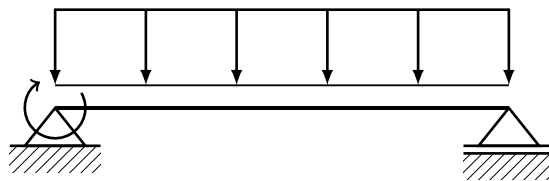


Figure 5.1: End moment and distributed load

The model described in Chapter 3 was subjected to the same load configuration as the test specimens, namely 12 point loads, consisting of lead weights and frames, spaced evenly along the beam's top flange with a magnitude of  $1.05 \text{ kN}$  each, as well as a single end moment. A non-linear analysis was performed, during which the series of point loads were first applied using a Static, General step with 10 increments to simulate the dead weight of the hanging weights. The Riks method was then used to determine the magnitude of the end moment required for the beam to fail due to LTB. The data recorded during the tests was analyzed as described in Section 4.4.1.1, in order to plot the beam end rotation against the applied end moment.

Figure 5.2 shows the experimental results together with the numerical results for the two yield stresses for a beam subjected to a single end moment and distributed load. When considering the experimental results it can be seen that all the specimens exhibited an ultimate load (UL) around 19 kN m, illustrating good consistency of the testing apparatus. All the specimens, except B8, showed similar behaviour up to an end moment of 12.5 kN m, i.e. within the elastic range. Specimen B8 shows a significantly higher UL which is followed by a sudden drop from 27 kN m to 19 kN m. It can also be seen that specimen B8 exhibits a fairly large rotation from 7 kN m, compared to the other specimens.

Although a lack of rigidity between the support frame and test specimens was present for all the tests, the test concerning specimen B8 illustrated a severe lack of rigidity. The large rotation of the support frame in the case of specimen B8 resulted in a large clamping force on the ball bearings, as described in Section 4.5, which restricted the out-of-plane rotation of the beam. As the end moment reached a value of 27 kN m, the friction force was overcome, leading to the sudden drop and failure of the beam due to LTB.

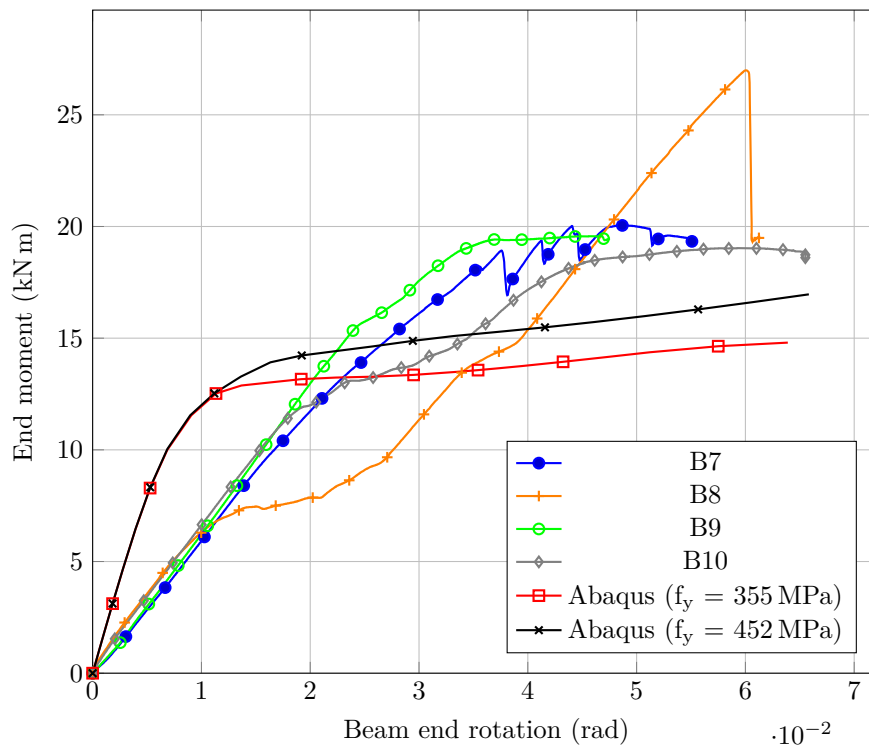


Figure 5.2: End moment and distributed load

The effect of the material properties of a beam can be seen in figure 5.2, where a difference of up to 14% can be observed between the two FE models. However, both FE models exhibit the same behaviour within the elastic range, similar to what was observed with the experimental results. The lack of rigidity is made evident when comparing the experimental and numerical results. When considering an end moment of 10 kN m, the difference in rotation between the test specimens and the FE model is 53%, highlighting the significant lack of rigidity between the test specimens and the support frame. This lack of stiffness in the connection is represented by the distinct difference of the gradients between the numerical and experimental results within the elastic region. The difference in the UL between the test specimens and

the FE model can be attributed to mainly three things, i.e. the lack of rigidity between the test specimens and the support frame, a difference in material properties and the difference of  $J$  between the FE model and the IPE200.

As the support frame rotated relative to the test specimen, it caused an unequally distributed load on the ball bearings. This led to an additional friction force for the out-of-plane rotation which required a larger force to induce buckling of the beam. The application of a concentrated end moment at the support frame amplified the friction force at the thrust bearings, contributing the higher UL. The effect of  $J$  is made apparent with a simple example of a beam subjected to a uniform moment distribution. The elastic critical moment was determined for both the IPE200 and FE model for the beam subjected to a uniform moment distribution. A value of 12.6 % higher than the FE model was determined for the IPE200. This result illustrates that the higher value of  $J$  can contribute to the higher ultimate load of the test specimens.

In figure 5.3 the failure mode of the FE model is illustrated together with the failure mode of the test specimen. The effect of the destabilizing load is clearly made visible in both cases. The lateral deflection of the top flange (compression flange) in the FE model at mid-span is greater than that of the bottom flange, as shown by the legend in figure 5.3(a). A similar observation can be made from figures 5.3(b) and (c) where the top flange exhibits a larger lateral deflection than the bottom flange. Although the moment-rotation curves determined by the numerical and experimental investigation are quite different, the failure mode compares well.

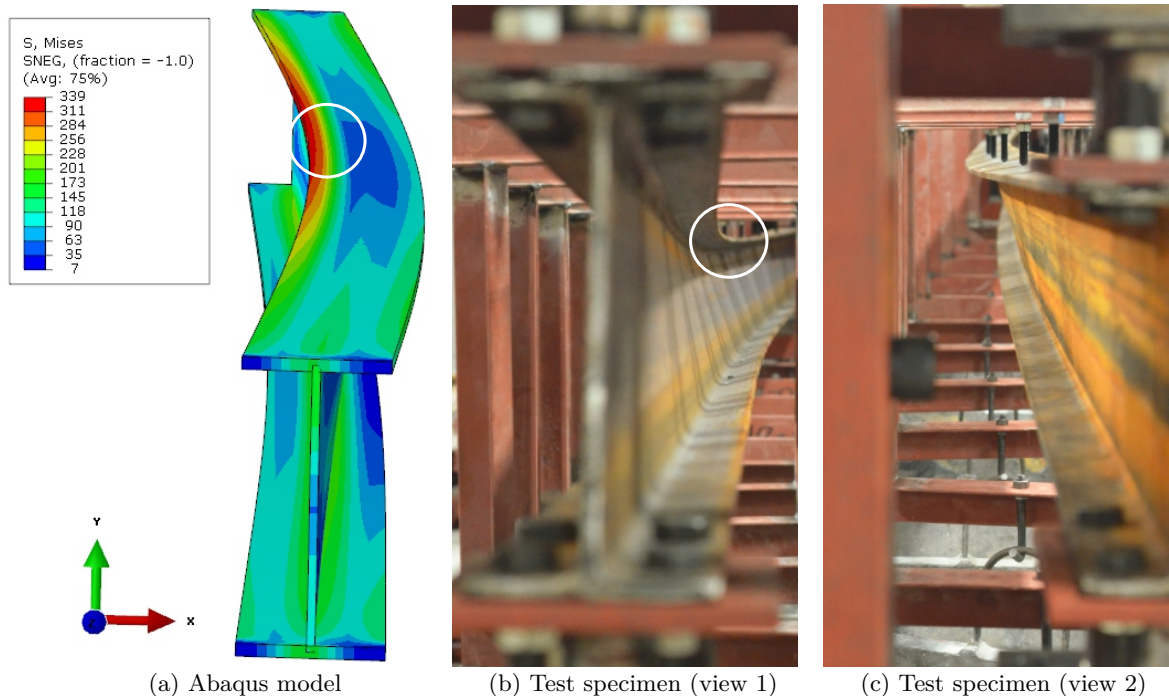


Figure 5.3: LTB due to single end moment and distributed load

### 5.2.2 Simply supported beam with point load at mid-span

The second load configuration consisted of a single point load applied to the top flange of the beam, as shown in figure 5.4. The load was applied by using a GLS that allows the load to move with the beam, while remaining vertical. The experimental results are compared to the results obtained from a non-linear analysis conducted on the FE model subjected to the same load configuration. The data recorded during the tests included the applied point load as well as the vertical deflection of the beam at mid-span. The load was recorded by using a 200 kN load cell and the deflection was measured by using a transducer as described in Section 4.4.2.1. To obtain the load carrying capacity, the load was plotted against the vertical deflection, as shown in figure 5.5.

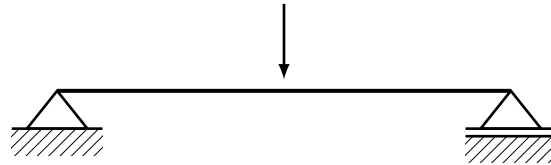


Figure 5.4: Point load at mid-span

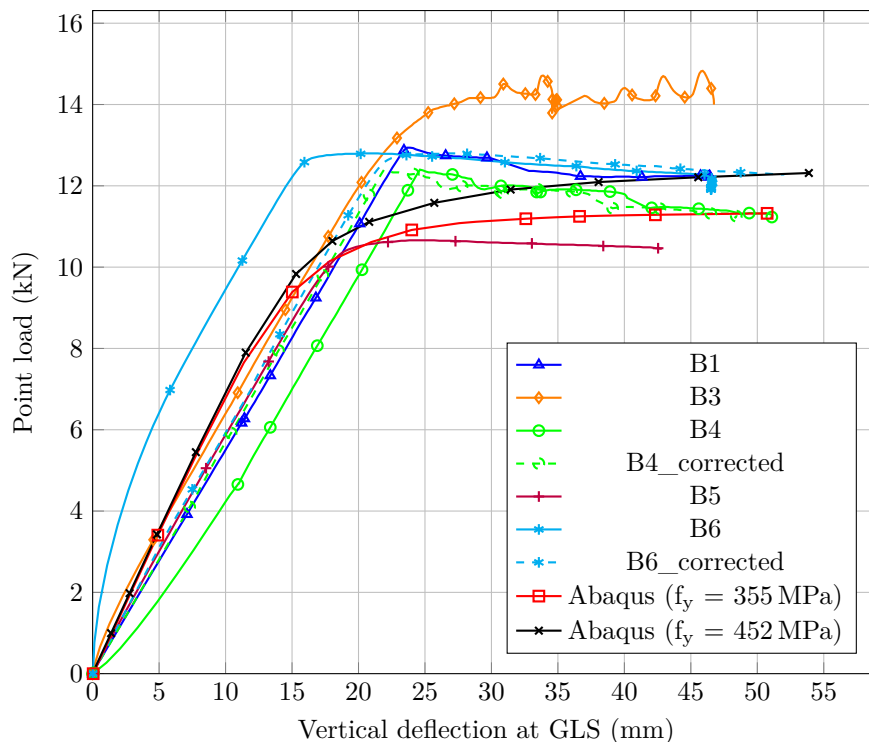


Figure 5.5: Single point load at midspan

The experimental results in figure 5.5 indicate that all the beams fail within the region of 10.5 kN-12.5 kN, except for specimen B3 which reach an UL of about 14 kN. The high UL exhibited by specimen B3 is the result of a restraint occurring at the hydraulic cylinder fixed to the GLS. The cylinder was restricted to rotate by a plate used to support the rigid triangle of the GLS which caused the steel rod, pulling down on the beam, to bend. The bent steel rod made contact with the cylinder opening and resulted in an increase in friction. The fluctuations of the load near the end of the test represents the thread of the

steel rod sliding over the opening in the cylinder. This restriction was removed for the remaining tests. Most of the test specimens shown in figure 5.5 show similar behaviour within the elastic range, similar to what was observed in the previous test. Specimens B4 and B6 both exhibited unusual non-linear behaviour within the elastic region, which raises the question that an error may have occurred with the measurement devices, i.e. transducer and load cell. The data for these two specimens were corrected, depicted by the dashed curves in figure 5.5, to illustrate their behaviour if such an error did not occur. When comparing the extrapolated results with the remaining test specimens, as well as the numerical results, a good agreement within the elastic region can be observed.

The results for the FE model with the two different material models are also shown in figure 5.5. A difference of 10% in load carrying capacity exists between the two FE models as a result of the different material properties. Also, the different material properties are irrelevant within the elastic range with both FE models follow the same trend, similar to the experimental results. The FE models show an UL in the region of 11 kN-12.5 kN which corresponds well to the experimental results. When considering test specimens B6, B4 and B1 a sudden transition can be observed at the buckling point where after the load steadily drops, whereas the FE model exhibits a smooth transition up to the UL. This sudden transition is caused by the rotation of the beam within the support frame. Similar to what was discussed in Section 4.5, an unequally distributed force on the ball bearings causes an increase in friction and restricts the out-of-plane rotation up to a point where the friction can be overcome. The point where this friction is overcome corresponds to the buckling point, whereafter the beam reaches the UL. Specimen B5's UL is lower than the results obtained by the FE model and any of the other specimens. There are two reasons for this occurrence, firstly the point load applied to the top flange can be off centre, causing an additional moment about the shear centre. It is also possible that the yield stress for this particular beam is below 355 MPa, which can have a significant effect on the load carrying capacity as illustrated in figure 5.5.

In figure 5.6 a comparison between the FE model and the test specimen is shown. Similar to what was observed during the test involving the end moment, the top flange shows a significant lateral deflection due to the destabilizing load. Figure 5.6(b) clearly shows that the applied point load remains vertical as the beam undergoes LTB, causing a destabilizing effect. Safety was the governing factor in the duration of the tests involving the GLS due to a concern of the steel loading point slipping off the beam. The beam showed a small degree of plastic deformation at the location highlighted by the white circle in figure 5.6(b). The FE model illustrates that yielding first occurs at this point i.e. the compression side of the compression flange, as shown in figure 5.6(a).

### 5.2.3 Simply supported beam with two point loads at overhung ends

In order to simulate a uniform bending moment distribution along the beam, a point load was applied to each overhung end of the beam, as shown in figure 5.7. The loads were applied using two GLSs, one on each side. The results obtained from the test were compared to the FE model in figure 3.2(b), refer

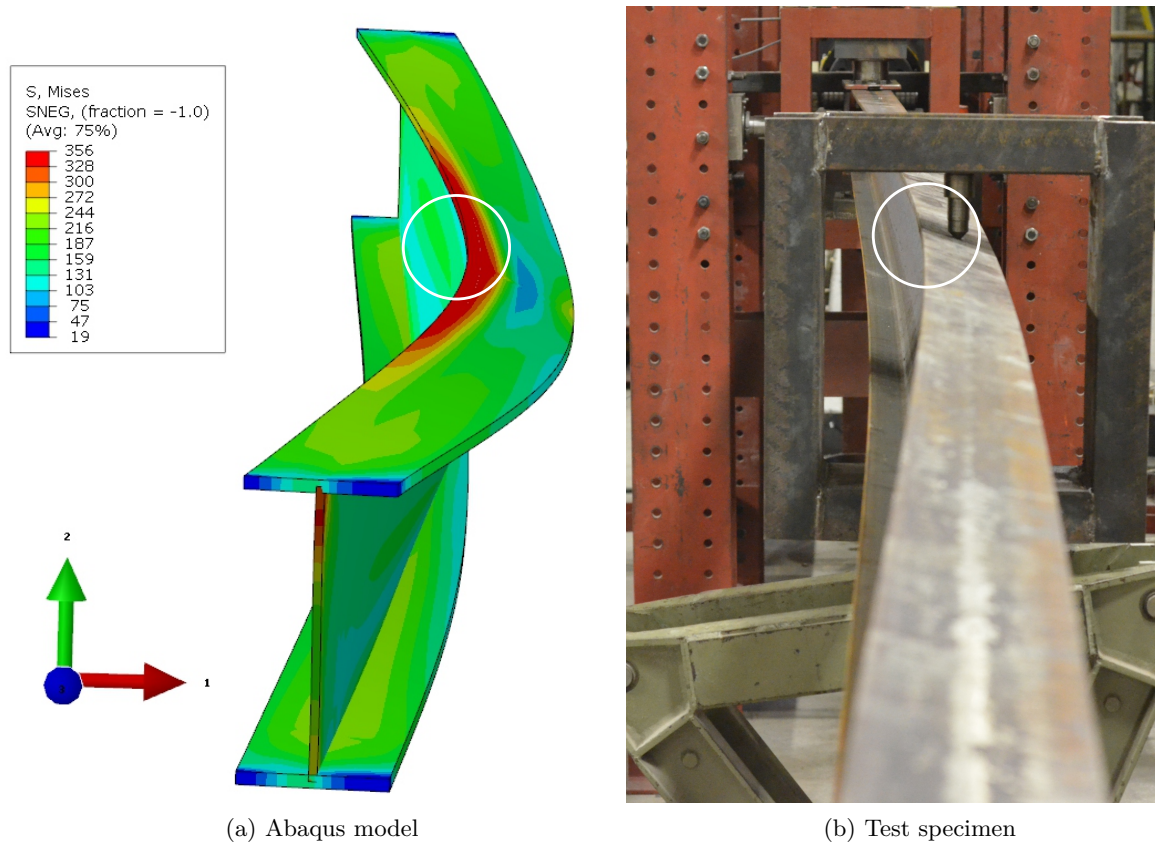


Figure 5.6: LTB due to point load at mid-span

to page 46. This test configuration is based on the experimental work conducted by O'heachteirn et al. (1988), with the improvement of allowing the point load to move laterally as the beam undergoes LTB. A total number of three beams were tested using this load configuration; however the results of only two specimens are presented in this document, due to an error that occurred during the test involving specimen B11.

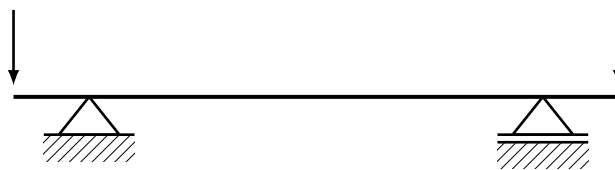


Figure 5.7: Two point loads at overhung ends

The results from the experimental investigation are shown in figure 5.8, together with the numerical results. Only test specimen B12 is presented for illustration purposes, the results for specimen B13 are presented in Appendix C of this document. Although the objective of this test was to simulate a uniformly distributed bending moment, the limitations of the hydraulic pumps made it difficult to accomplish this objective. Figure 5.8 shows a significant difference in the load applied by each pump. Section 4.5 describes the limitations of using hydraulic pumps to apply a load with the GLS. There are a number of reasons for the different loads generated by the different pumps. Firstly, the pumps are manually operated and a difference in pump rate can be present. Secondly, the hydraulic pressure is different for each pump,



which influences the extension of the piston with each pump. If the load at one end is larger, a smaller load is required at the other end to induce LTB, as shown in figure 5.8.

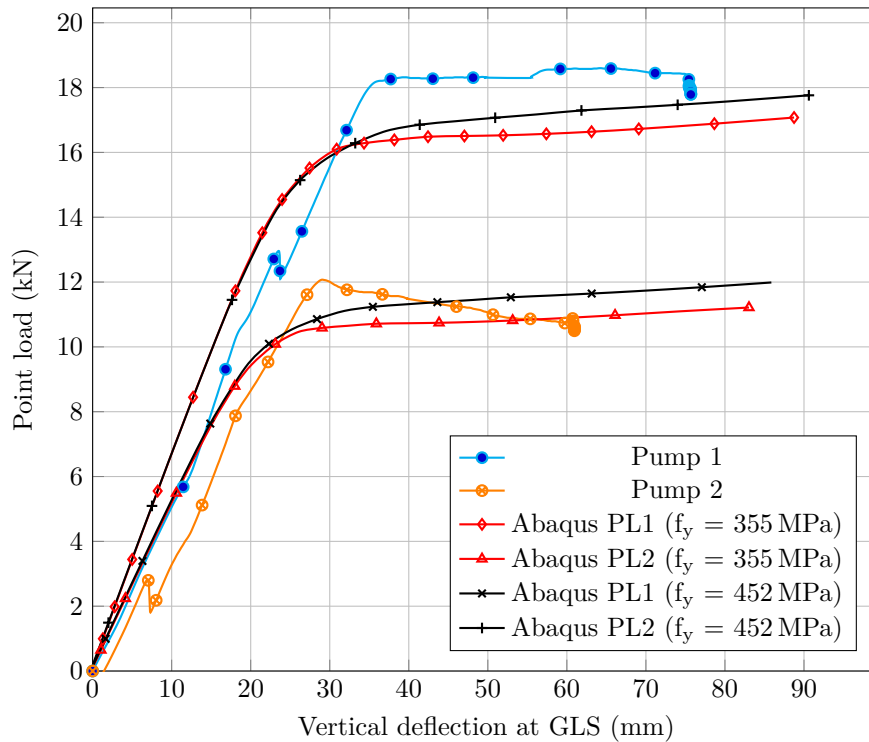


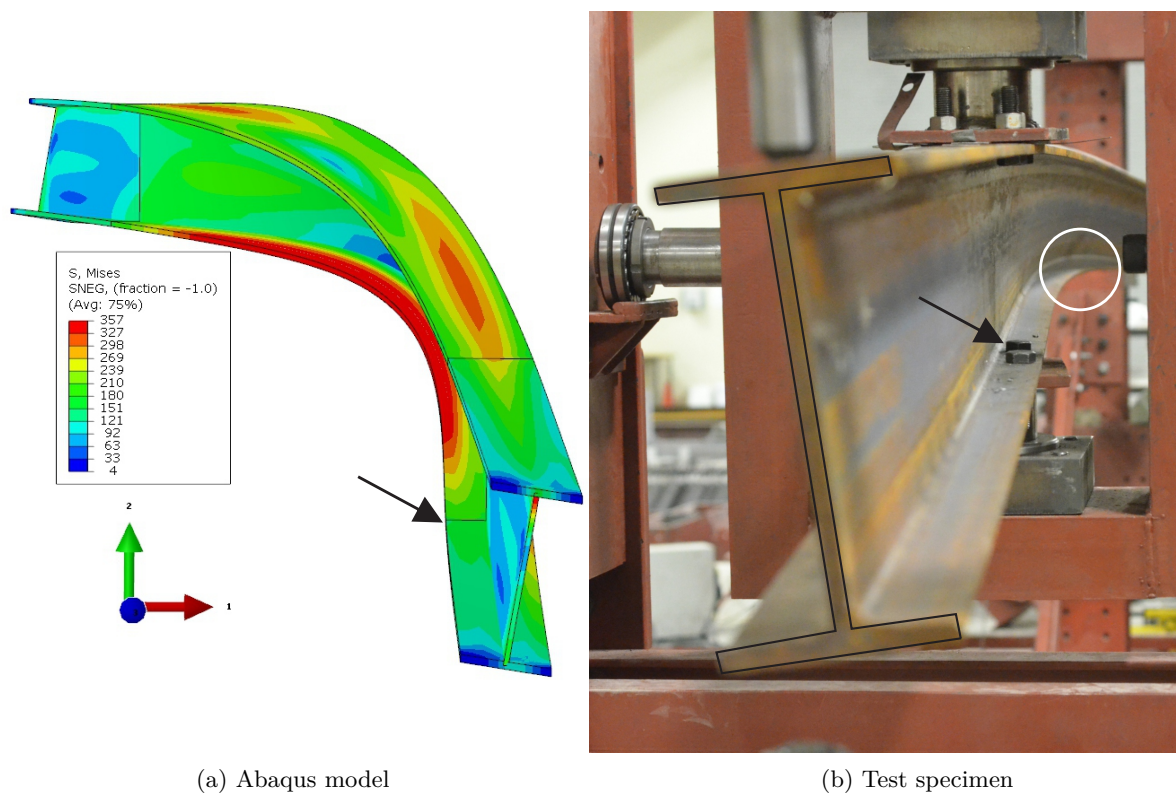
Figure 5.8: Test specimen B12

When considering the experimental results in figure 5.8 it can be observed that for both pumps a sudden transition occurs at the buckling point, similar to the previous test configuration. This rapid change in gradient can again be contributed to the increase in friction for the out-of-plane rotation at the support, resulting from the lack of rigidity between the test specimen and the support frame. As was the case for the previous two test configurations, the effect of the different material properties is made evident by the two FE models, with a difference in the UL amounting to 7% for the numerical results. The different load applied by each pump resulted in two different gradients for the load-deflection graphs within the elastic range. For the two tests conducted (B12 and B13) a good agreement between these two gradients is observed, refer to figure C.13, concluding that the performance of the test configuration was consistent. The numerical results successfully simulated the two different gradients, although the deflection for any given point within the elastic region was less for the FE models. An explanation for this occurrence is that the point loads applied at the overhung ends were off centre, adding an additional moment about the shear centre and causing a larger deflection for the same load as the FE model. Although the test was unsuccessful in simulating a perfectly uniform bending moment, it still provided invaluable information about the behaviour of steel beams subjected to two end moments.

The final buckling mode of the beam is illustrated in figure 5.9, which shows both the FE model and the test specimen. All test specimens showed significant plastic deformation that occurred at the position highlighted by the circle in figure 5.9(b). A similar observation can be made from figure 5.9(a), where the FE model shows that yielding first occurs at the compression side of the compression flange. The

behaviour of the overhung ends of the beam was very similar between the test specimen and the FE model. In both figures 5.9(a) and (b) it can be seen that the cross section at the end undergoes a slight rotation that is initiated by the buckling of the centre span of the beam and increased by the destabilizing effect of the load.

The restraint provided by the supports, as discussed in Section 4.4.2.3, was successfully modelled by the FE model, where an inflection point occurred at the locations indicated by the black arrows for both the test specimen and the FE model. This inflection point occurs at this point due to the torsional restraint provided, where the top and bottom flanges are bolted to the support frame. It is at this point where both flanges are in double curvature resulting in the inflection point. From this it can be concluded that the boundary conditions of the FE model are in agreement with the support frames used in the tests.



(a) Abaqus model

(b) Test specimen

Figure 5.9: LTB due to point loads at overhung ends

## 5.3 Conclusion

During the experimental investigation thirteen tests were carried out on three different types of load configurations, of which all were compared with FE model described in Chapter 3. The experimental study aims to prove that the FE model is able to capture the realistic beam behaviour of a simply supported beam. A number of discrepancies and errors were observed during the course of this investigation that could have a possible impact on the results obtained for the comparison between the experimental and numerical results. These include the material properties, the lack of rigidity between the support frame

and test specimens and the St. Venant's torsion constant.

A total number of four tests were carried out for the load configuration concerning the single end moment and distributed load. All the specimens reached an UL of 19 kN m, illustrating good consistency of the testing apparatus. In all four tests the lack of rigidity between the support frame and test specimens were made evident by the large rotation measured for the specimens. This lack of rigidity results in the bearings rotating within the housings, causing the load to be unequally distributed along the ball bearings and increasing the friction for the out-of-plane rotation. Regardless of this error, a good agreement between the specimens were observed within the elastic range, a similar observation to the numerical results. The difference in material properties proved to have a significant effect on the load carrying capacity after buckling occurs. This, together with the increase in friction caused by the lack of rigidity, contributes to the high UL compared to the numerical results.

For the test concerning the single point load at mid-span, five tests were conducted. All the specimens reached an UL around 11 kN, similar to the numerical results. The friction at the supports were still present for this test, which is represented by the sudden transition occurring at the buckling point, where the FE model showed a smooth transition. As with the previous test, similar behaviour was observed for the specimens within the elastic range, whereafter a dispersion occurs due to the difference in material properties. Similar observations with respect to the additional friction and behaviour within the elastic region can be made for the tests concerning the two point loads at the overhung segments. The support conditions are well represented by the FE model, where a clear inflection point can be observed at the support, similar to the test specimens.

The findings in this chapter, with regard to the boundary conditions, material properties, failure mode of the specimens and load carrying capacity, illustrate that the FE model described in Chapter 3 is sufficient in simulating the behaviour of a simply supported beam. This validation of the FE model ensures that the results obtained from using FEA are reliable and supported by a thorough experimental study. The FE model can further be used for determining the equivalent moment factor for various bending moment distributions when comparing the values obtained from the steel specifications mentioned in Section 2.5.

## Chapter 6

# Comparison of the equivalent moment factor

### 6.1 Introduction

This chapter presents the comparison of the equivalent moment factor between the steel design specifications and numerical results. A total of four different bending moment distributions are considered for the comparative study, including a linear, non-linear and bi-linear distribution. Each of the representative distributions aims to identify the deficiencies and strengths of the various methods used to determine the equivalent moment factor ( $C_b$ ). The steel specifications considered in this study include SANS 10162-1:2011, EN 1993-1-1, AISC 360-05 and CSA S16-9. The FE model described in Chapter 3 was utilized for the determination of the numerical values for  $C_b$  and provides the baseline for the comparison between the steel specifications. The numerical results obtained by Serna et al. (2006) are also included in the comparative investigation.

Included in this chapter is a visual representation that illustrates the comparison between the steel specifications and numerical results for each of the bending moment distributions considered as well as a summary of the significance of the chosen distribution. A discussion of the comparison is given for each distribution, followed by a discussion to highlight relevance of the results, due to the conservatism or lack thereof.

### 6.2 Comparison of $C_b$ for various bending moment distributions

In this section a detailed discussion is presented on the comparison between steel design specifications with regards to the equivalent moment factor. A thorough experimental study was conducted in an attempt to validate the modelling considerations made during the development of the FE model. The FE model used to determine the equivalent moment factor was proven by the experimental study to be

able to capture realistic beam behaviour and provides a reliable baseline for the comparison of the steel specifications. An example of how the  $C_b$  value is calculated according to the FE model and the various steel specifications is available in Appendix D of this document.

### 6.2.1 Moment distribution type 1

This configuration represents a beam subjected to a linear bending moment distribution, with the exception of  $\kappa = -1$ , which represents a uniformly distributed bending moment, as shown in figure 6.1. The value of  $\kappa$  can be interpreted as the ratio of the end moments. There are two main reasons for the selection of this moment distribution. Firstly, it represents the fundamental distribution assumed in the derivation of the elastic critical moment equation. Secondly, it is theoretically the only distribution applicable for the equation employed by SANS 10162-1:2011 for determining  $C_b$ .

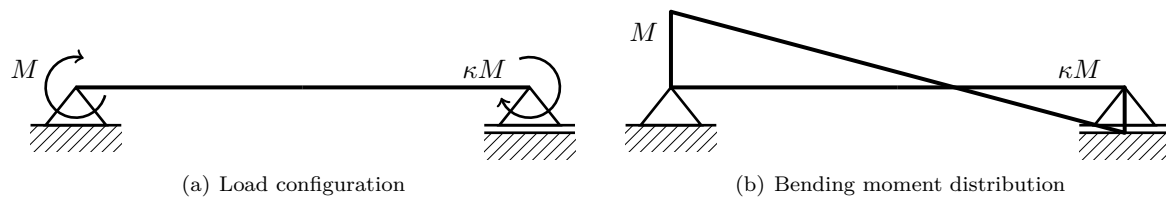
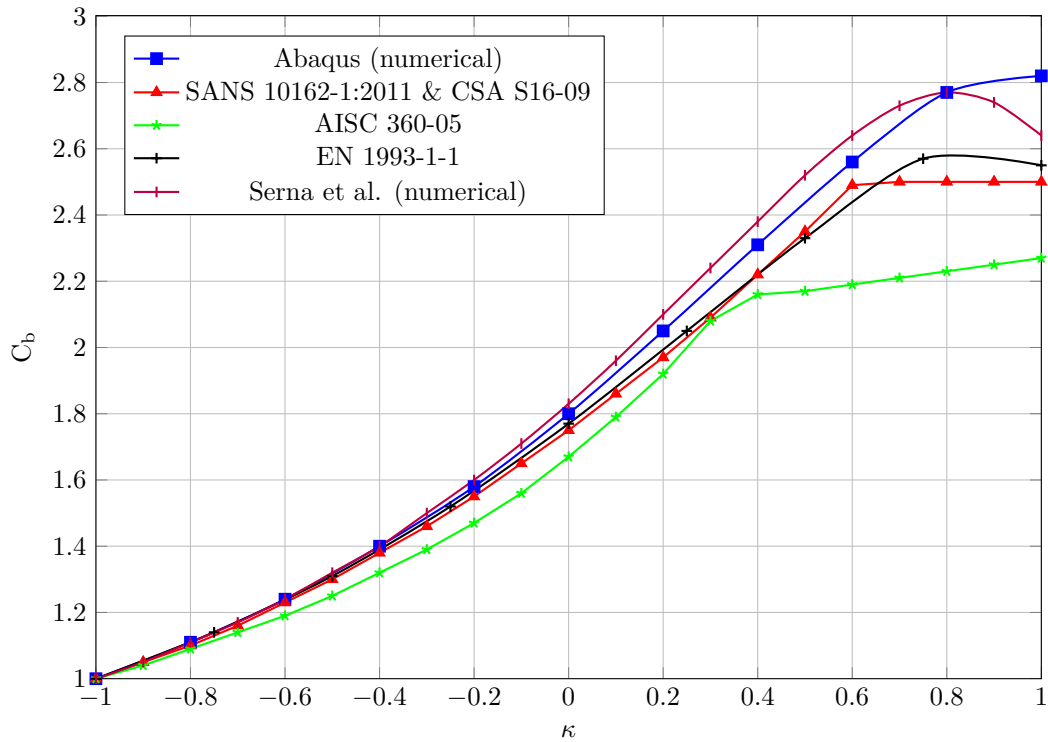


Figure 6.1: Moment distribution type 1

The values for  $C_b$  obtained from the steel specifications and the numerical analysis for moment distribution type 1 are illustrated in figure 6.2. The methods for the different codes show satisfactory correspondence to the numerical results obtained from Abaqus for a  $\kappa$  value smaller than 0.4. At the point where  $\kappa$  is equal to 0.4, the AISC 360-05 shows a significant deviation from the general trend of the results. For  $\kappa$  equal to 1, the quarter-point method of the AISC 360-05 yields the most conservative results, amounting to a difference of 20% when compared to the Abaqus results. From figure 6.2 it can be seen that a deviation between steel specifications and numerical results occur in the region  $0.6 < \kappa < 1$ . Within this region SANS 10162-1:2011 and EN 1993-1-1 provide similar results, with EN 1993-1-1 being slightly higher due to limit of 2.5 for  $C_b$  given in SANS 10162-1:2011. The results determined by the equation in SANS/CSA closely match the numerical values, illustrating the reason for the continuous use of this equation in CSA S16-09.

The two sets of numerical results presented show good agreement, although they are not exactly the same. There are a number of reasons that can lead to the variation of the numerical results obtained. Serna et al. (2006) does not explicitly state the assumptions made during the development of the FE model used in his investigation. It is only stated that the model consists of shell elements and is simply supported. This makes it difficult to quantify the reasons for the difference in the numerical results. Factors that can contribute to a difference in results are the imperfections, material properties of the steel and the type of software package used.


 Figure 6.2:  $C_b$  results for moment distribution type 1

### 6.2.2 Moment distribution type 2

The second moment distribution type consists of a distributed load together with a single end moment, as shown in figure 6.3. The variable  $\beta$  is used to alternate the end moment, for  $\beta$  equal to 0 the beam represents pinned boundary conditions and for  $\beta$  equal to 1.0 a fixed end condition. The range,  $-1 < \beta < 2$ , subjects the beam to single and double curvature with the maximum moment at the end and within the span, this ensures that all possible scenarios are investigated. The non-linear nature of the distribution makes it significant to the research in order to exploit the deficiencies of the equation used in SANS 10162-1:2011, as it was not originally developed for a bending moment distribution of this type.

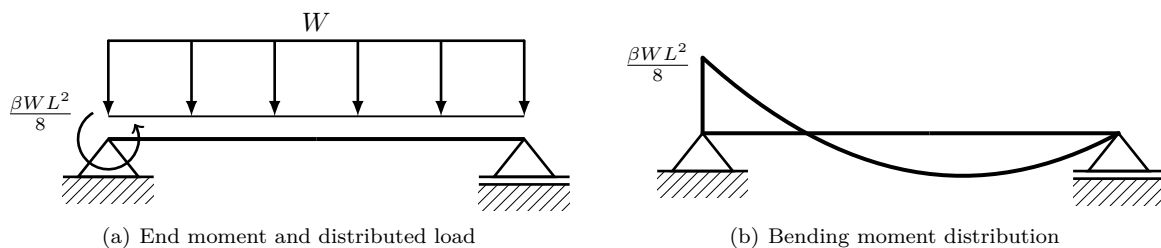


Figure 6.3: Moment distribution type 2

Figure 6.4 presents the  $C_b$  values for moment distribution type 2. The numerical results for this moment distribution show good agreement, with only a difference of 4% between Serna et al. (2006) and the Abaqus results. The values obtained by EN 1993-1-1 correlate well with the numerical results, but show a trend to the non-conservative side for  $\beta > 1.1$ . The Canadian Standard represents an overall good comparison with the numerical results, but again enforces the upper boundary of 2.5 for  $\beta \geq 1.2$ . The

numerical results and the values obtained from the design codes follow a similar trend for  $-1 \leq \beta < 1$ , whereafter a distinct dispersion of the different methods appears. This is similar to the observation made for the previous distribution type and can again be attributed to the effect of double curvature, as shown in figure 6.5. When double curvature becomes significant the outer regions of the beam reaches the moment capacity and start to yield, as shown in figure 6.5. The middle region of the beam is however still fully elastic with relatively small stresses occurring within this region, refer to figure 6.5. For this reason the effect of double curvature leads to an increase in the beam's capacity.

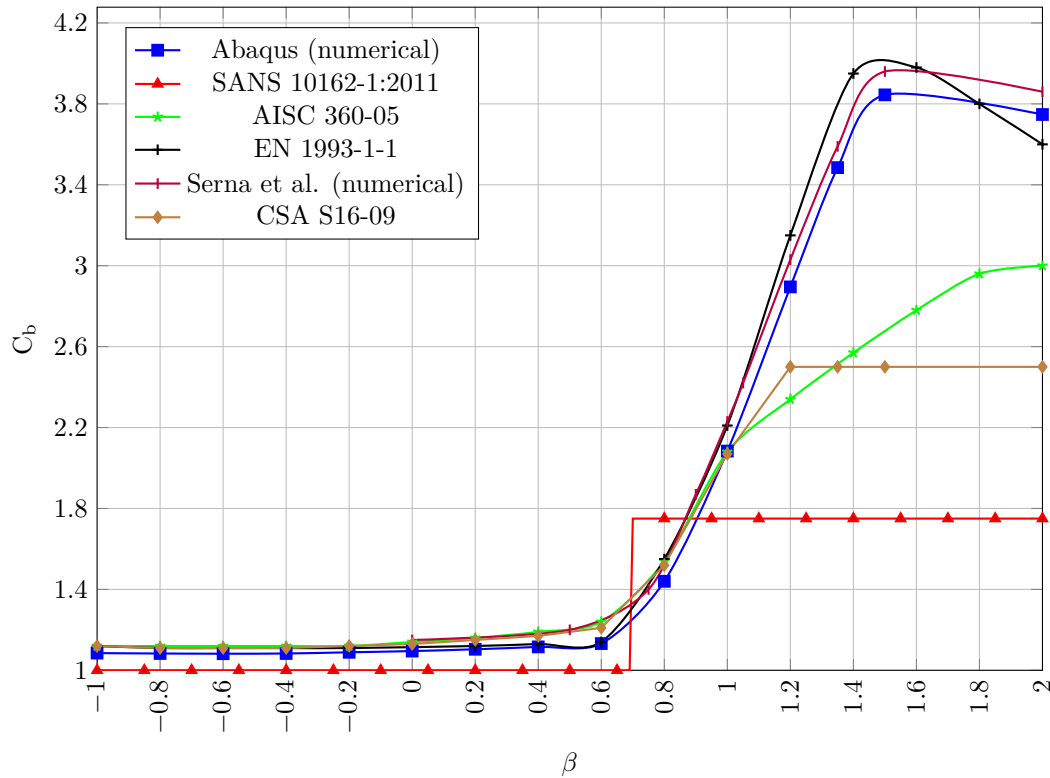


Figure 6.4:  $C_b$  results for moment distribution type 2

The deficiency of the procedure employed by SANS 10162-1:2011 is made clear for this moment distribution. From figure 6.4 it can be seen that SANS 10162-1:2011 fail to follow the general trend of the numerical results or that of the other steel standards. For  $-1 \leq \beta \leq 0.6$ , SANS 10162-1:2011 produce results that are up to 10% less than other steel standards, but also produce a series of non-conservative values of  $C_b$  in the region of  $0.69 \leq \beta \leq 0.87$ . The reason for the poor performance of SANS 10162-1:2011 is due to the fact when the bending moment within the unbraced length is larger than the larger end moment,  $C_b = 1$ , otherwise it is equal to 1.75. This explains the sudden increase from 1 to 1.75 when  $\beta = 0.69$ . The equation of SANS 10162-1:2011 produces results that are extremely conservative for  $1 \leq \beta \leq 2$ , with a difference of up to 53%. This moment distribution type illustrates the South African code's severe lack of ability to accurately take into account the bending moment distribution for beams without a constant moment gradient.

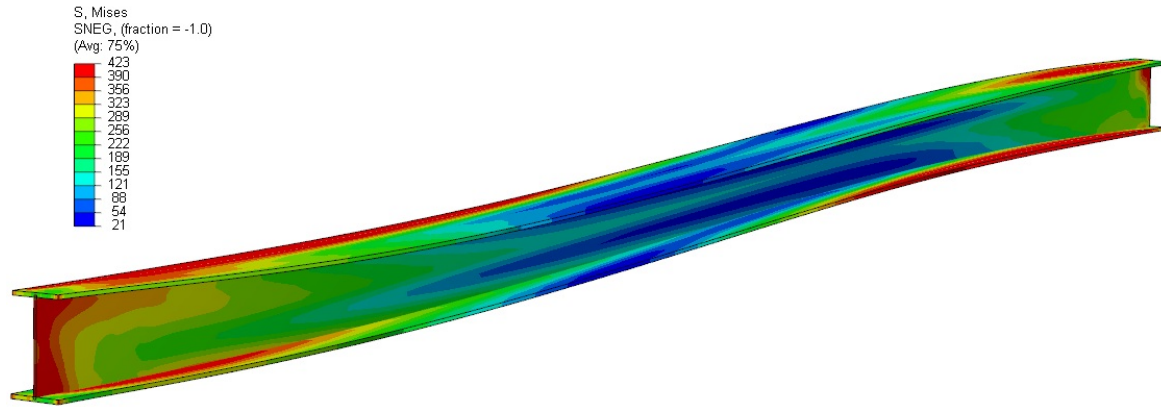


Figure 6.5: Simply supported beam subjected to double curvature due to equal end moments applied in the same direction

### 6.2.3 Moment distribution type 3

Moment distribution type 3 is similar to the previous distribution type, the only difference being the substitution of the distributed load with a single point load at mid-span, as shown in figure 6.6. The parameter  $\beta$  carries out the same role as with moment distribution type 2. This load configuration simulates a bi-linear bending moment, where the maximum moment can be present at the end of the beam or within the unbraced length, depending on  $\beta$ . A configuration of this nature will illustrate that although a linear distribution is present, the varying moment gradients provide difficulties for the procedure suggested by SANS 10162-1:2011.

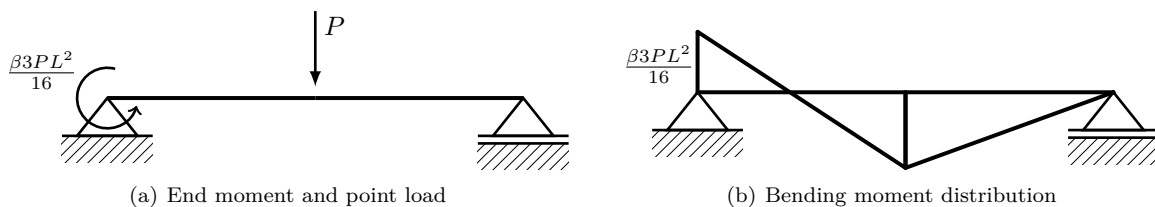
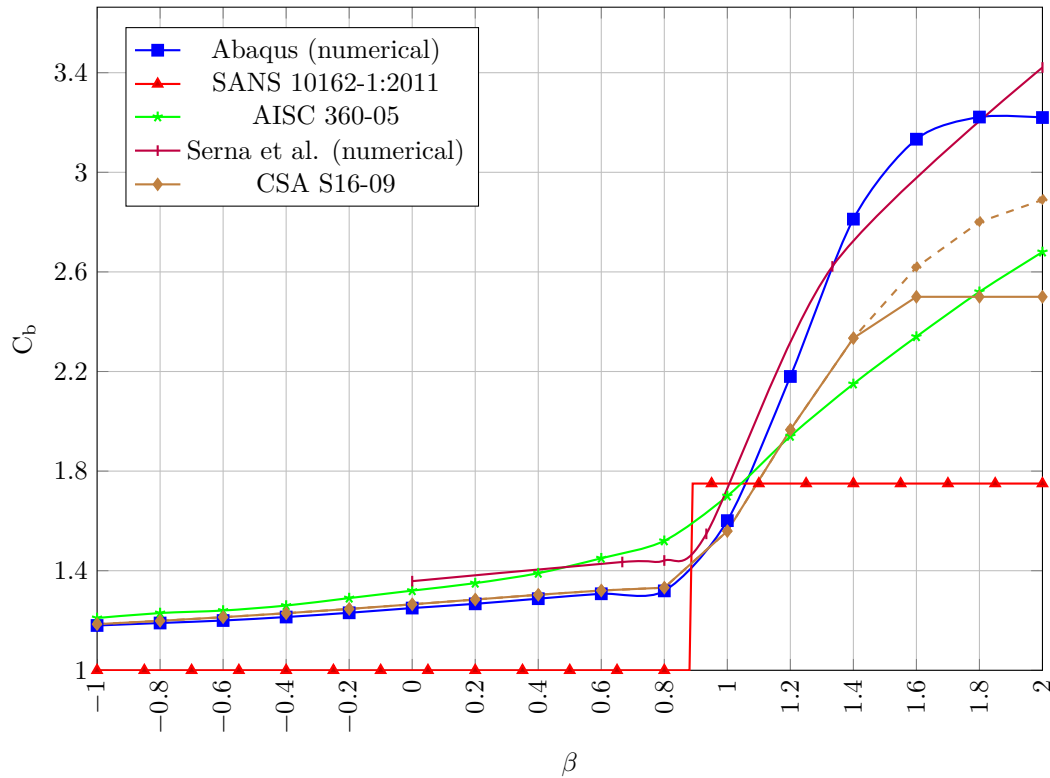


Figure 6.6: Moment distribution type 3

Figure 6.7 shows the comparison of the  $C_b$  values for the load configuration above. A similar trend to the one for moment distribution type 2 is followed by the numerical and quarter-point methods, although the values in the region  $-1 \leq \beta \leq 0.8$  show a steady increase, unlike the previous distribution type. A deviation in the trend of the numerical results occurs when  $\beta < 1.2$ , which again can be due to different modelling considerations; the overall comparison between the Abaqus results and Serna et al. (2006) is satisfactory with a difference of 8%. CSA S16-09 shows excellent agreement with the numerical results obtained from Abaqus. The dashed curve in figure 6.7 is the quarter-point equation of CSA S16-09 without the upper boundary of 2.5 and follows a similar trend to the FE model, with a 17% difference when compared to the Abaqus results. The effect of double curvature is also made clear due to the dispersion of data that occurs when  $\beta \geq 1.0$ . The quarter-point methods make a reasonably good approximation when the effect of double curvature becomes significant.



The  $C_b$  values obtained using SANS 10162-1:2011 again fail to follow the general trend of the numerical and quarter-point methods. SANS 10162-1:2011 suggests a value of 1.0 for  $-1 \leq \beta \leq 0.89$ , due to the same reason mentioned previously, resulting in a difference of up to 13% in this region, when compared to the Abaqus results. A very specific region of non-conservatism is present in the region  $0.89 \leq \beta \leq 1$ , similar to that of moment distribution type 2.


 Figure 6.7:  $C_b$  results for moment distribution type 3

#### 6.2.4 Moment distribution type 4

Moment distribution type 4 consists of a single point load applied to the centroid at various points along the beam, for  $0 < a \leq 0.5$ , as shown in figure 6.8. The use of this configuration allows for the evaluation of  $C_b$  without the effect of double curvature or a non-linear bending moment distribution. It must be noted that previous numerical values for this particular load configuration are unavailable.

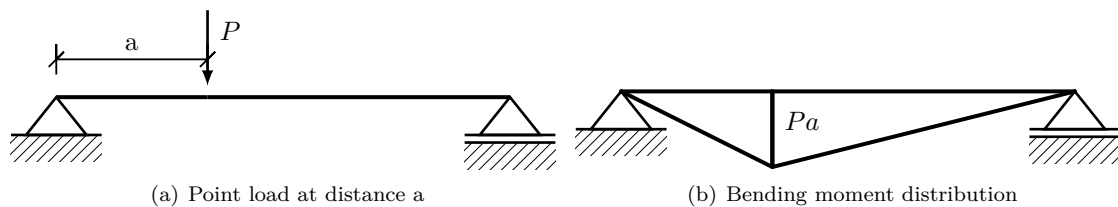


Figure 6.8: Moment distribution type 4

The comparison of the  $C_b$  values for the load configuration above are shown in figure 6.9. The absence of any end moments sets the  $C_b$  value equal to 1.0 for the entire region of  $\frac{a}{L}$ . This produces extremely

conservative results, displaying a maximum of 35 % conservatism and a minimum of 20 %, which is still significant. The quarter-point methods illustrate a reasonably good comparison with the Abaqus results, although a certain degree of non-conservatism is present, amounting to 11 % for  $\frac{a}{L} = 0.34$ . EN 1993-1-1 has a similar approach to SANS 10162-1:2011, assuming a single value, 1.348, for a simply supported beam subject to a single transverse load. This value seems to capture an average of the numerical results of Abaqus, exhibiting conservative and non-conservative results, amounting to 13 % and 7 %, respectively.

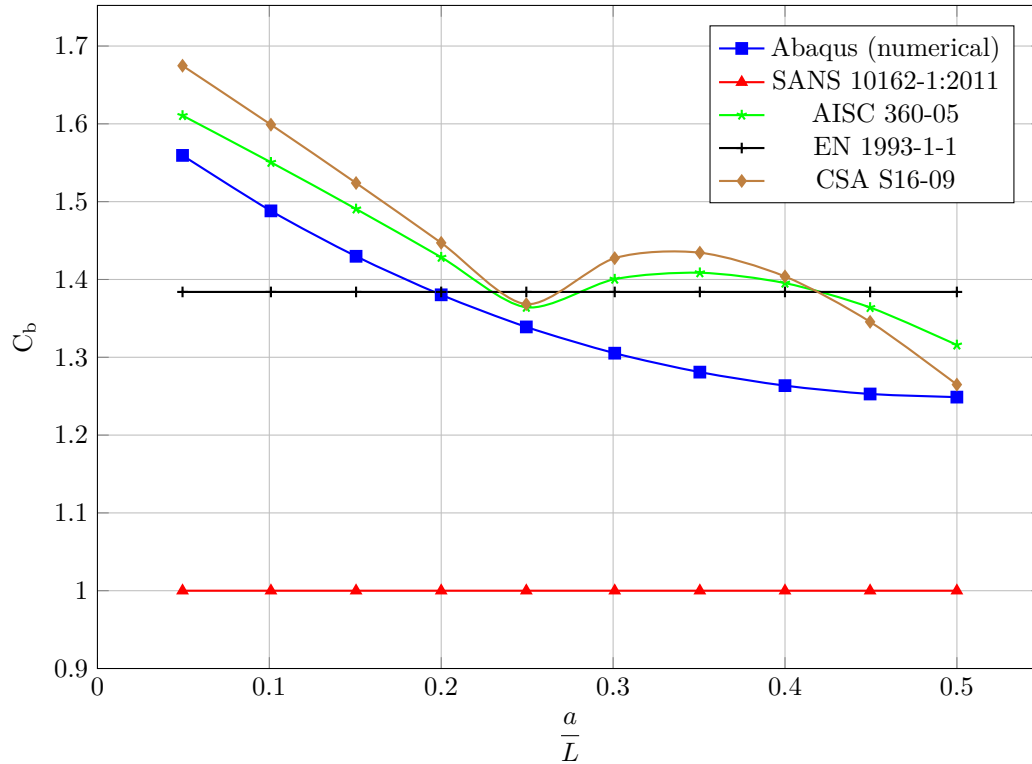


Figure 6.9:  $C_b$  results for moment distribution type 4

### 6.3 Relevance of results

The comparison in the preceding section illustrates that there is a significant difference between the various methods for determining  $C_b$ . The  $C_b$  value is used in the determination of the elastic critical moment ( $M_{cr}$ ) from which the resistance moment is calculated. An extremely conservative  $C_b$  value can lead to an uneconomically designed beam member. This section provides three cases to illustrate the difference in results of the resistance moment for the four different steel specifications. The three cases are practical examples that are commonly found in steel structures to highlight the relevance of the results obtained in Section 6.2. Due to the difference of how the codes handle the position of the load relative to the shear centre, in the following example design calculations, the load was considered to be normal, i.e. not destabilising. A detailed set of calculations are presented in Appendix E of this document.

### 6.3.1 Simply supported beam

The first case considered is relevant to the design of composite beams. The hardened concrete on the steel deck provides lateral support to the top flange along the entire length of the beam. However, during the construction phase when the concrete is being placed on the steel decking it simply acts as an applied dead load, offering no significant lateral restraint. The steel beam needs to be able to resist the bending moments induced by the fresh concrete to avoid a similar failure as in the case of the Marcy Bridge (Peraza, 2008). Therefore, the first case is a simply supported beam subjected to uniformly distributed load, as shown in figure 6.10, simulating the dead and live loads that occur during the construction phase of composite beams. This loading generates a non-linear bending moment distribution along the beam (Brown, 2011).

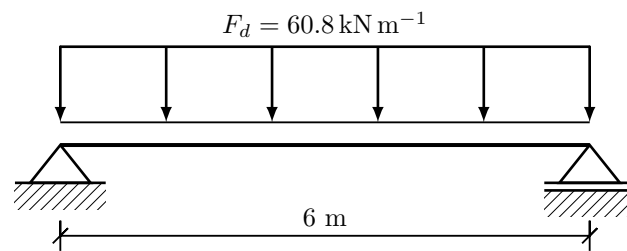


Figure 6.10: Steel beam ( $457 \times 191 \times 98$ ) with uniformly distributed load

The values for the moment resistance are shown in table 6.1. The percentage differences in the table are the difference between the various steel specifications with respect to SANS 10162-1:2011.

Table 6.1: Moment resistance for simply supported beam

Steel specification	$C_b$ value	% difference in $C_b$	$M_r$ (kN m)	% difference in $M_r$
SANS 10162-1:2011	1	0	407	0
CSA S16-09	1.131	12	460	12
AISC 360-05	1.136	12	462	12
EN 1993-1-1	1.127	11	404	0

It is clear from table 6.1 that there is a significant difference between the  $C_b$  values as determined by the various methods of the steel specifications. All of the  $C_b$  values differ with more than 10% from the value suggested by SANS 10162-1:2011, which draws the same conclusion as discussed in Section 6.2, where it was found that SANS 10162-1:2011 is inadequate for a bending moment distribution of a non-linear nature. The calculated moment resistance in table 6.1 illustrates the large degree of conservatism of SANS 10162-1:2011, with a difference of 12% compared to CSA S16-09 and AISC 360-05, which both utilize the more accurate quarter-point method.

Although the  $C_b$  value of EN 1993-1-1 is 11% different from SANS 10162-1:2011, the moment resistance is almost the same. The procedure employed by EN 1993-1-1 after the determination of  $M_{cr}$  is unconventional when compared to the other three steel specifications. It appears that the procedure outlined in EN 1993-1-1 also incorporates a large degree of conservatism that is independent of the  $C_b$  value.

### 6.3.2 Crane girder

The second case considers the design of a runway girder for an overhead gantry crane. Although the design of these girders is often based on serviceability, a calculation concerning the ultimate limit state still needs to be conducted. This particular crane consists of two wheels per rail with a spacing of 3.05 m. Each wheel carries a total load of 169 kN, not including impact loads. It should be noted that the capacity check of the girder is only for bending strength and does not cover other failure modes. As mentioned before, the loads are considered to be normal although it is conceded that the wheel loads applied to the top flange causes destabilising effects. The bending moment distribution that is generated is bi-linear as shown in figure E.3 (MacCrimmon, 2009).

Table 6.2: Crane girder properties (MacCrimmon, 2009)

Design criteria	Value/Units
Simple span?	Yes
Span	10 670 mm
Class of Crane	CMAA Class A
Type of duty	Light
Weight of crane trolley	2721 kg
Bridge wheel per rail	Two
Maximum wheel load	169 kN
Bridge wheel spacing	3050 mm

The values for the moment resistance are shown in table 6.3. The percentage differences in the table are the difference between the steel specifications with respect to SANS 10162-1:2011.

Table 6.3: Moment resistance for crane girder

Steel specification	$C_b$ value	% difference in $C_b$	$M_r$ (kN m)	% difference in $M_r$
SANS 10162-1:2011	1	0	1044	0
CSA S16-09	1.185	16	1478	29
AISC 360-05	1.194	16	1496	30
EN 1993-1-1	1.348	26	1189	12

Due to the fact that the moments within the span are larger than the larger end moment, the value for  $C_b$  is equal to 1.0 according to SANS 10162-1:2011. As in the previous case and the preceding section, this again highlights the highly conservative nature of the approach outlined in SANS 10162-1:2011. The difference in the  $C_b$  values obtained compared to SANS 10162-1:2011 exhibits high percentages, with the  $C_b$  value of EN 1993-1-1 being the highest at 26 %. Although EN 1993-1-1 shows the highest difference in  $C_b$ , the moment resistance differs with only 12 %, which as mentioned above, suggests that the procedure employed by EN 1993-1-1, after the determination of  $M_{cr}$ , includes a high degree of conservatism.

CSA S16-09 and AISC 360-05 produce similar results for both the  $C_b$  value and the moment resistance. The  $C_b$  values obtained using the two quarter-point methods of CSA S16-09 and AISC 360-05 are 16 % different for the value suggested by SANS 10162-1:2011 and the moment resistances calculated using these values exhibit a difference of 30 % compared to SANS 10162-1:2011. From these results it can be seen that a highly conservative  $C_b$  value can lead to an uneconomical design of a structure.

### 6.3.3 Portal frame rafter beam

The final case considered in this investigation is the moment resistance of a rafter beam in a portal frame. The portal frame is shown in figure E.4 in Appendix E. The rafter beam is considered as a significant example due to the bending moment distribution generated by the applied loads. The load case considered in this design consists of the dead loads together with an across wind load. The combination of these loads generates a non-linear bending moment distribution, which produces the double curvature of the rafter beam, see figure 6.11. Three beam segments are considered in this particular case. The segments are taken between points where lateral restraint is provided for the compression flange. The  $C_b$  values and moment resistances of segment 1 through 3 are shown in tables 6.4, 6.5 and 6.6, respectively.

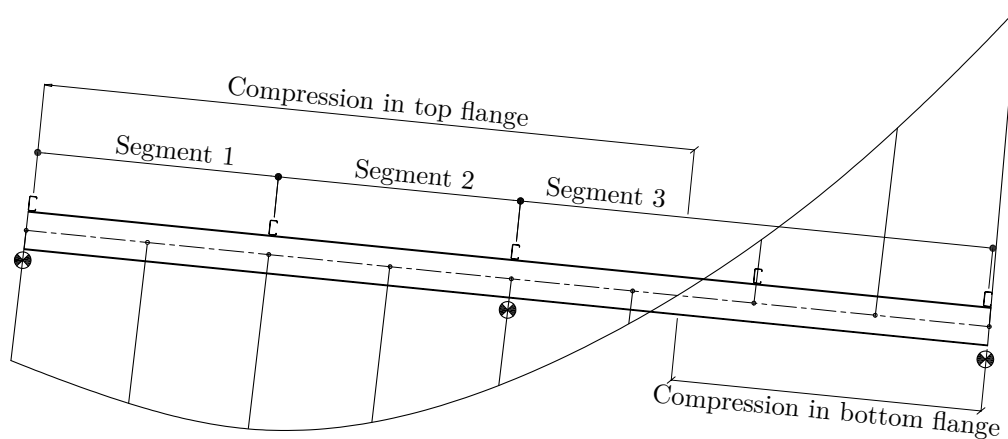


Figure 6.11: Rafter bending moment diagram

Table 6.4: Moment resistance for segment 1

Steel specification	$C_b$ value	% difference in $C_b$	$M_r$ (kN m)	% difference in $M_r$
SANS 10162-1:2011	1.109	0	201	0
CSA S16-09	1.090	2	200	0
AISC 360-05	1.077	3	190	-5
EN 1993	1.120	1	184	-8

Table 6.5: Moment resistance for segment 2

Steel specification	$C_b$ value	% difference in $C_b$	$M_r$ (kN m)	% difference in $M_r$
SANS 10162-1:2011	1.210	0	206	0
CSA S16-09	1.184	2	205	0
AISC 360-05	1.158	4	204	-1
EN 1993	1.220	1	190	-8

The bending moment distribution for segment 1, i.e. between nodes 1 and 3, is effectively a linear distribution. For this reason the  $C_b$  values for all the steel specifications are relatively close, with differences of less than 5%. A similar observation can be made with regard to segment 2, where the values for both  $C_b$  and the resistance moment are in good agreement. However, the resistance moment determined by EN 1993-1-1 yields the most conservative value. In the previous two cases the resistance moment determined using EN 1993-1-1 was close to the conservative result obtained by SANS 10162-1:2011, although

Table 6.6: Moment resistance for segment 3

Steel specification	$C_b$ value	% difference in $C_b$	$M_r$ (kN m)	% difference in $M_r$
SANS 10162-1:2011	2.134	0	154	0
CSA S16-09	2.480	16	170	10
AISC 360-05	2.398	12	175	14
EN 1993	2.420	13	147	-5

the  $C_b$  value was relatively high. From this it can be concluded that the procedure for determining  $M_r$  according to EN 1993-1-1, apart from determining  $M_{cr}$ , yields more conservative results in comparison to CSA S16-09 and AISC 360-05.

The third segment brings forth the inadequacy of SANS 10162-1:2011 when compared to CSA S16-09 and AISC 360-05. The moment distribution is of a non-linear nature and the effect on the  $C_b$  value is made clear in table 6.6, with differences of up to 16%. When comparing the resistance moments between SANS 10162-1:2011, CSA S16-09 and AISC 360-05, it can be seen that SANS 10162-1:2011 produces the most conservative value, being 10% lower than the value obtained using CSA S16-09. The resistance moment obtained from EN 1993-1-1 yields the lowest value, supporting the conclusion made above with regard to the degree of conservatism incorporated in the procedure to determine  $M_r$ .

This section illustrates that an extremely conservative  $C_b$  value can lead to a highly conservative result for the resisting moment. The use of a highly conservative method, as in SANS 10162-1:2011, can lead to a structure with an uneconomical design. The two specifications employing the quarter-point method, CSA S16-09 and AISC 360-05, do not require a significant amount of additional calculation effort, unlike the procedure suggested by EN 1993-1-1, and yield more economical results.

## 6.4 Conclusion

This chapter presented the comparison of the equivalent moment factor ( $C_b$ ) between four different steel design specifications. The four specifications considered in this study were SANS 10162-1:2011, CSA S16-09, AISC 360-05 and EN 1993-1-1. The comparison included four different bending moment distributions (type 1 to 4) in order to differentiate between the strong and weak points of the various methods used in the different steel specifications. The numerical results obtained by Serna et al. (2006) were used together with the results obtained from Abaqus. The comparison between these two sets of numerical data showed good agreement for moment distribution type 1 to 3, with small deviations due to different modelling considerations.

All the steel specifications showed good agreement with the numerical data for moment distribution type 1, with AISC 360-05 being the most conservative. From this it can be concluded that the equation currently presented in SANS 10162-1:2011, is adequate for linear bending moment distribution as discussed in Section 2.4.1. This supports the procedure outlined in CSA S16-09, where this method is still utilized when considering a linear distribution.

For moment distribution type 2 and 3 it was observed that CSA S16-09 and AISC 360-05 show good agreement with the numerical results, although a deviation becomes clear as soon as the effect of double curvature becomes significant. In both moment distribution type 2 and 3, SANS 10162-1:2011 fails to follow the general trend and results in highly conservative results. This illustrates the inadequacy of using this method for bending moment distribution other than a linear distribution. Similar results were obtained in the research conducted by Driver et al. (2010).

The loading configuration of moment distribution type 4 generated a bending moment distribution with the end moments equal to zero, resulting in a  $C_b$  value of 1.0 for SANS 10162-1:2011 which produces highly conservative results. EN 1993-1-1 also present a single value for a loading of this nature, which seems to capture the average of the numerical data from Abaqus. The two quarter-point methods show good agreement with the numerical results although it is slightly on the non-conservative side.

In order to illustrate the relevance of these findings, three cases commonly found in steel design, namely simple span laterally unsupported beams, crane girders and rafter beams were assessed with regard to the resistance moment of the beam. It was found that the extreme conservatism of the equation used to determine  $C_b$  in SANS 10162-1:2011, led to a highly conservative value for the resistance moment compared to CSA S16-09 and AISC 360-05. In the case of the crane girder differences of up to 30% in the resistance moment were obtained. Although the  $C_b$  values obtained by EN 1993-1-1 exhibit a high percentage difference, as with CSA S16-09 and AISC 360-05, the resistance moment shows a large degree of conservatism. This led to the conclusion that the procedure outlined in EN 1993-1-1 incorporates a large degree of conservatism for determining  $M_r$ . It is clear that the use of an excessively conservative method for determining  $C_b$ , can lead to an uneconomical design of a structure.

## Chapter 7

# Conclusion and recommendations

The main research objective of this investigation was to compare the equivalent moment factor as obtained by the use of four different steel design specifications. The basis for the comparative study was in the form of a set of numerical results determined by a FE model that is able to capture realistic beam behaviour. This model was successfully validated by an in-depth experimental study. These investigations are complemented by the literature review in Chapter 2. The development of the FE model used in this investigation was discussed in Chapter 3. Chapter 4 presents the design of the experimental setup used for the validation of the numerical model. The experimental results were presented and discussed in Chapter 5 and the comparison of the equivalent moment factor was presented in Chapter 6.

Section 7.1 of this final chapter presents a summary of the main findings and conclusions that can be drawn from this investigation. The recommendations presented in Section 7.2 include a summary of the notable difficulties encountered in this study as well as aspects that proved to be invaluable to the results gathered during this investigation. Section 7.2 also includes a discussion on the recommended work for future research.

### 7.1 Conclusions

The main finding of this research investigation is summarized as follows:

- It is evident that LTB plays a crucial role in the design of beams of a relatively slender nature. Although research in this field is abundant, a variety of experimental investigations are lacking. The equivalent moment factor used in the equation to determine the buckling resistance of a beam susceptible to LTB has also been investigated by numerous researchers. However, these investigations are all based on numerical data only. From these investigations it was concluded that the equation provided by SANS 10162-1:2011 to determine the equivalent moment factor, presents highly conservative results when compared to other methods.

Concerning the FE modelling of the beam, the following is noted:



- The cross-sectional properties between the FE model and the IPE200 section correspond well even though the radii were not included in the FE model. The only significant difference is the St. Venant's torsion constant ( $J$ ) which is 27% less for the FE model when compared to the IPE200 section. This reduces the load carrying capacity of the FE model in comparison with the IPE200 section used in the experimental study.
- The sensitivity analysis conducted on the initial geometric imperfections proved that the ultimate failure of the beam was independent of the imperfection shape and magnitude. The 1st eigenmode provided the most conservative results. For this reason the first eigenmode was used as the imperfection shape with a magnitude of 6.3 mm, corresponding to the out-of-straightness tolerance of  $L/1000$ .
- Residual stresses present in hot-rolled steel sections were proved to have a significant impact on the ultimate load (UL) of the beam. These stresses were modelled successfully in Abaqus and showed that the presence of these stresses reduce the UL up to 10%. The residual stress distribution across the cross section is of a non-linear nature, which is due to the non-uniform cooling effect that takes place during manufacturing.
- The preliminary validation conducted depicted an excellent correspondence between the linear analysis and the elastic beam theory. From this it can be concluded that boundary conditions modelled in Abaqus fulfilled the requirements laid out for simply supported boundary conditions. The structural constraints implemented in Abaqus adapt the stiffness of the constrained region, rather than simulating a rigid surface across the region. This proved to be satisfactory for beam bending applications. The non-linear analysis showed good agreement with the steel specifications, emphasizing the importance of including residual stresses when attempting to model realistic beam behaviour.

The following can be concluded regarding the experimental program:

- The two support frames used in the experimental setup were able to successfully simulate the behaviour of simply supported boundary conditions, although a small degree of restraint was present at these supports. The lack of rigidity between the support frame and the test specimen resulted in the thrust bearings rotating within the bearing housings. This additional rotation exposed the ball bearing to a concentrated force that was unequally distributed along the ball bearings. These forces increased the friction for the out-of-plane rotation. It was observed that when the packing between the test specimen and plates supporting the shaft was too tightly packed, it also restricted the thrust bearing's rotation. The bearings released as soon as the applied load was large enough to overcome the friction.
- In the experimental study it was proven that it is possible to induce LTB by applying a single end moment, although a significant flaw was encountered during testing. It was evident that the load applied to the lever arm caused the thrust bearings to rotate within the steel block housing, adding an additional rotation of the support frame with respect to the test specimen.
- An unconventional method, dependent on the geometry of the lever arm configuration, was utilized

for determining the applied moment and beam end rotation. This method was validated by using a transducer to directly measure the rotation of the beam end. The difference between the two methods was less than 5%, confirming that the method used for determining the applied end moment was correctly employed.

- The gravity load simulators (GLSs) used during the course of the experimental study provided a method for applying a point load without adding an additional restraint to the beam. The GLSs are able to translate laterally and vertically with the beam, while the applied load remains vertical, causing the necessary destabilizing effect. The added mobility of the GLSs made it possible to test beams with overhung ends while at the same time reducing the restraint provided by the adjacent beam segments. This is an improvement on the experimental work previously conducted by other researchers. The hydraulic pumps used to apply the load using the GLSs, made it difficult to simulate a perfectly uniform moment, due to differences between the pumps.
- Eight test specimens were measured in order to quantify the initial geometric imperfections. Although the imperfection shape and magnitude varies between all the specimens, the general trend resembles an imperfection shape corresponding to the 1st eigenmode. As for the magnitude of these imperfections, it was found that some specimens exhibited a magnitude of  $L/1000$ . The measuring of these imperfections validates the assumptions made in the development of the FE model, with regard to the initial geometric imperfections.
- The testing apparatus used to apply the end moment performed well and from the results gathered good consistency was observed with all beams failing due to LTB at around 19 kN m. However, the additional rotation of the thrust bearings led to a loss of stiffness between the test beam and support frame, which was initially assumed to be rigid. Therefore, the applied moment represents the moment necessary to rotate the support frame and not the test specimen. Although bearings were placed at all locations where translation and rotation were present, there was still some degree of friction that was evident in the results.
- The two material models used for the numerical analyses concluded that the behaviour of a beam within the elastic region is independent of the yield stress, which was similar to the behaviour of the test specimens. The effect of yield stress on the load carrying capacity of the beam is made apparent after the buckling point. All the experimental tests, but one, showed consistently higher UL resistances. The main reasons for the different UL observed in the experimental tests are as follows:
  - The test specimens could have had a higher yield strength.
  - The St. Venant's torsion constant ( $J$ ) is 27% lower for the FE model.
  - The additional friction caused by the lack of rigidity at the supports.

When comparing the physical tests with the numerical simulation the following can be concluded:

- Similarities between the failure modes of the FE model and test specimens were observed. In the

tests concerning the overhung ends, the failure mode was closely resembled by the FE model. The FE model presented a cross section that was slightly rotated at the point where the load was applied, which was similar to the observation made during testing. A small inflection point was observed at the point where the test specimen was bolted to the support frame. A similar inflection point was observed in the deformed shape of the FE model. The FE model illustrated that yielding first starts at the compression side of the compression flange, which was similar to the plastic deformation of the test specimens observed after testing.

- The behaviour of the FE model closely resembled that of the test specimens, although some errors and limitations were observed during testing. An overall good comparison between the numerical results and those obtained during testing, makes it possible to conclude that the FE model developed in this investigation is able to simulate the realistic behaviour of a simply supported beam.

The comparison of the equivalent moment factor lead to the following conclusions:

- The comparison of the equivalent moment factor ( $C_b$ ) was proposed to differentiate between the positive and negative attributes of the different methods used by the various steel design specifications. The comparison included the results obtained from the FE model as well as numerical results obtained from other researchers. The two sets of numerical data showed good correspondence for moment distribution type 1 to 3. Some discrepancies were present and can be the result of different modelling considerations assumed for the two numerical models.
- For the cases of constant moment gradient SANS 10162-1:2011 showed excellent correspondence with numerical results, with AISC 360-05 yielding the most conservative results. This finding concludes that the equation presented in SANS 10162-1:2011 is adequate for bending moment distributions with a constant moment gradient. CSA S16-09 still employs this equation when a linear bending moment distribution is considered, together with a quarter-point method, similar to that of AISC 360-05, for other distributions.
- From the results of moment distribution type 2 and 3 it was evident that SANS 10162-1:2011 failed to follow the general trend of the numerical results or that of the other methods. This deficiency leads to highly conservative results and for a specific region non-conservative results were observed. The quarter-point methods were able to accurately follow the trend of the numerical results up to a point where double curvature becomes significant. Double curvature significantly increases the buckling capacity of a beam due to the middle region of the beam being completely elastic after yielding occurs at the outer regions. SANS 10162-1:2011 also presented highly conservative results for moment distribution type 4 by suggesting a value of  $C_b = 1.0$  due to the absence of end moments. The quarter-point methods showed reasonable agreement with the numerical results, although the values were slightly on the non-conservative side. EN 1993-1-1 suggests a single value for this moment distribution type, which seems to be the average of the numerical results obtained from Abaqus.
- The large degree of conservatism encapsulated in the approach used by SANS 10162-1:2011 was

made relevant by considering three beam design cases commonly found in structural engineering. The resistance moments of the beams for these three cases were determined according to all four steel design specifications. It was found that differences of up to 30 % occurs when comparing SANS 10162-1:2011 with the other steel design specifications. This finding concludes that the effect of a conservative  $C_b$  value can lead to a structural member that is over designed. The compound effect of overly designed members in a structure can have a significant impact on the economy of the structure.

## 7.2 Recommendations

Based on the conclusions and results obtained during this investigation the following recommendations can be made when considering the design and experimental work of beams subjected to LTB:

- The inclusion of residual stresses in the FE model proved to be invaluable in the describing the behaviour of steel beams. The load carrying capacity and post buckling behaviour of the beam is drastically altered when the effect of residual stresses is disregarded. For these reasons it is recommended that the effect of these stresses be taken into account when studying the behaviour of hot-rolled steel sections.
- The support frames used in the experimental study presented a significant flaw. The thrust bearing at the top and bottom of the support frame rotated within the steel block housing, reducing the stiffness of the connection between the test specimen and the support frame. Ideally this connection should be perfectly or nearly rigid in order to accurately measure the beam end rotation and the applied end moment. The design of this connection needs to be altered before utilizing the two support frames in future investigations.
- The method of applying the load when using the GLS (i.e. a hydraulic pump) is effective, but rather primitive. The use of a servo controlled actuator within the GLS will make it possible to subject the beam to a perfectly uniform moment distribution, while eliminating the restraint produced when using a spreader beam configuration. The actuator will also make it possible to apply the load without having to reset the piston, depending on the actuator stroke.
- The test using a concentrated end moment proved to be challenging due to the fact that the setup was unique. In its current configuration, it proved that it is possible to apply a single end moment to a beam to induce LTB, although a number of flaws were encountered. This test configuration is not recommended unless the design of the support frames is revised in order to take into account the concentrated load causing the additional rotation. It is also encouraged that other possibilities, other than the lever arm mechanism, should be considered for applying the end moment. The constraints of the experimental program precluded the correction of the issues mentioned above.
- The work conducted during this investigation illustrates the inadequacy of SANS 10162-1:2011 with regard to beam design. The adoption of a new steel specification should not be based on this premise

alone, but should provide an insight into the negative effect of employing methods that are out of date. Subsequent work should include an in-depth comparative investigation on the economical impact of a structure designed according to various steel specifications as well as studies comparing the design procedures of columns and/or the design of connections.

### **7.3 Concluding statement**

This research investigation presents a thorough literature study and provides an essential framework for future investigations concerning LTB. A detailed FE model, validated by an extensive experimental study, is presented in this research. The FE model is capable of capturing the realistic behaviour of a hot-rolled steel beam and can be utilized for the future research. This research investigation illustrated that the method of determining the equivalent moment factor according to SANS 10162-1:2011 is inadequate and provides highly conservative results. These values directly influence the resistance moment of a steel beam and can result in the design of an uneconomical structure. The inevitable adoption of the latest version of the Canadian Standard will provide South Africa with a method that provides more economical results.

# Bibliography

ABCB (1998). *Steel structures*. AS 4100. Australian building codes board (cit. on p. 59).

AISC (2005). *Specification for structural steel buildings*. ANSI/AISC 360-05. American Institute of Steel Construction. Chicago (cit. on pp. 19, 21–23).

Anapayan, T. and M. Mahendran (2012). “Numerical modelling and design of LiteSteel Beams subject to lateral buckling”. In: *Journal of Constructional Steel Research* 70, pp. 51–64 (cit. on p. 35).

Barnard, H. (1996). “The elastic and inelastic lateral torsional buckling strength of hot rolled type 3CR12 steel beams”. MA thesis. Rand Afrikaans University (cit. on pp. 36–39).

Brown, D. (2011). *Steel Building Design: Worked examples for students*. Ed. by M. Brettle. The Steel Construction Institute (cit. on pp. 99, 133).

CEN (2005). *Eurocode 3: Design of steel structures - Part 1-1: General rules and rules for buildings*. EN 1993-1-1. European Committee for standardization. Brussels (cit. on pp. 19, 24–26).

Cook, R. D. and D. S. Malkus (2002). *Concepts and applications of finite element analysis*. Ed. by W. Anderson. John Wiley & Sons Inc. (cit. on pp. 11, 29–35).

CSA (2009). *Limit states design of steel structures*. CSA S16-09. Canadian Standards Association. Ontario (cit. on pp. 19, 26, 27).

CSA (2013). *Commentary on CSA S16-09*. Tech. rep. Canadian Institute of Steel Construction (cit. on p. 27).

CSA (2014). *Limit states design of steel structures*. CSA S16-14. Canadian Standards Association. Ontario (cit. on p. 1).

- Dassault Systèmes (2010). *Abaqus Analysis User's Manual*. Abaqus 6.11. Dassault Systèmes Simulia Corporation (cit. on pp. 48, 51, 52).
- de Clercq, H. (2010). *Southern African Steel Construction Handbook*. SAISC (cit. on p. 46).
- Driver, R. G. and E. Wong (2010). "Critical evaluation of equivalent moment factor procedures for lateral unsupported beams". In: *Engineering Journal* 47 (cit. on pp. 1, 14, 15, 26, 27, 42–44, 103).
- ECCS (1984). "Ultimate limit state calculation of sway frames with rigid joints". In: *Technical Committee 8* 33, p. 20 (cit. on pp. 54, 60).
- Fisher, J. (2002). *World trade center building performance study*. Tech. rep. Lehigh University (cit. on p. 50).
- Galambos, T. V. (1963). "Inelastic lateral buckling of beams". In: *ASCE* 89 (cit. on p. 21).
- Galambos, T. V. (1968). *Structural members and frames*. Prentice-Hall International (cit. on pp. 11, 13, 37).
- Galambos, T. V. et al. (2008). *Structural Stability of Steel: Concepts and Applications for Structural Engineers*. Wiley (cit. on pp. 3, 8, 9).
- Heck, R. C. H. (1923). *Mechanics of machinery*. McGraw-Hill (cit. on p. 41).
- High performance software* (Nov. 2013). URL: <http://www.ercd.hpc.mil/software/description.html?app=abaqus> (cit. on p. 45).
- Ho, D. and B. Suryatmono (2002). "The moment-gradient factor in lateral-torsional buckling on wide flange steel section". In: *Journal of Construction Steel Research* 58, pp. 1247–1264 (cit. on p. 8).
- Kankanamge, N. D. (2010). "Structural behaviour and design of cold-formed steel beams at elevated temperatures". PhD thesis. Queensland University of Technology (cit. on pp. 37–39, 64).
- Karmazinova, M. and J. Melcher (2012). *Influence of steel yield strength on structural reliability*. Tech. rep. Brno University of Technology (cit. on p. 50).
- Kirby, P. A. and D. A. Nethercot (1979). *Design for structural stability*. Ed. by M. R. Horne. Granada Publishing Limited (cit. on pp. 9–12, 14–19, 22, 27, 42, 46).

- Lim, N.-H. (2003). “Elastic buckling of I-beams under linear moment gradient”. In: *International Journal of Solids and Structures* 40, pp. 5635–5647 (cit. on p. 33).
- MacCrimmon, R. (2009). *Guide for the design of crane-supporting steel structures*. Canadian Institute of Steel Construction (cit. on pp. 100, 138).
- McGuire, W., R. H. Gallagher, and R. D. Ziemian (1999). *Matrix Structural Analysis*. Wiley (cit. on pp. 30, 31).
- Mohebkhah, A. (2011). “Lateral buckling resistance of inelastic I-beams under off-shear center loading”. In: *Thin-Walled Structures* 49, pp. 431–436 (cit. on pp. 2, 31, 35, 48).
- NCCI (2008). *Elastic critical moment for lateral torsional buckling SN003a-EN-EU*. Steel Construction Institute. Berkshire (cit. on p. 24).
- Nethercot, D. A. and K. C. Rockey (1971). “A unified approach to the elastic lateral buckling of beams”. In: *The structural engineer* 49, pp. 321–330 (cit. on pp. 14, 17, 18).
- O’heachteirn, P. and D. A. Nethercot (1988). “Lateral buckling tests on monosymmetric plate girders”. In: *Journal of Construction Steel Research* 11, pp. 241–259 (cit. on pp. 36–40, 43, 44, 64, 68, 75, 88).
- Peraza, D. B. (Feb. 2008). *Avoiding Structural failures during construction*. URL: <http://www.structuremag.org/article.aspx?articleID=527> (cit. on pp. 2, 3, 99).
- Piloto, P. A. G. (2000). *A simple model for lateral torsional buckling resistance of steel I-beams under fire conditions*. Tech. rep. Polytechnic Institute of Braganca (cit. on p. 40).
- Royslance, D. (2001). *Stress-strain curves*. Tech. rep. Massachusetts Institute of Technology (cit. on p. 49).
- SABS (2005). *Construction works-Part CS1: Structural steelwork*. SANS 2001-CS1:2005. South African Bureau of Standards. Pretoria (cit. on p. 53).
- SABS (2011). *The structural use of steel - Part 1: Limit-states design of hot-rolled steelwork*. SANS 10162-1:2011. South African Bureau of Standards. Pretoria (cit. on pp. 15, 19–21).
- Salvadori, M. G. (1955). “Lateral Buckling of I-beams”. In: *American Society of Civil Engineers* 120, pp. 1165–1177 (cit. on pp. 14, 15, 42, 43).



- Schmitke, C. D. (1984). *Effective lengths of lateral unsupported steel beams*. Tech. rep. University of Alberta (cit. on p. 27).
- Serna, M. A. and A. Lopez (2006). “Equivalent uniform moment factor for lateral-torsional buckling for steel members”. In: *Journal for Construction Steel Research* 62, pp. 566–580 (cit. on pp. 13, 15, 16, 42–44, 46, 92–94, 96, 102).
- Timoshenko, S and J. Gere (1961). *Theory of elastic stability*. McGraw-Hill (cit. on pp. 1, 13, 18–20, 42, 59, 115–119).
- Trahair, N. S. (1968). “Interaction buckling of narrow rectangular continuous beams”. In: *Civil Engineering Transactions CE10* 2, pp. 167–172 (cit. on p. 38).
- Trahair, N. S. (1993). *Flexural-Torsional buckling of structures*. E & FN Spon London (cit. on pp. 38, 51, 52, 60, 63, 65).
- Trahair, N. S. et al. (2008). *The behaviour and design of steel structures according to EC3*. Spon Press (cit. on pp. 2, 8, 10–12, 23, 24, 42).
- Yarimci, E. (1966). *Techniques for testing structures permitted to sway*. Tech. rep. Lehigh University (cit. on pp. 41–43).
- Yuan, Z. (2004). “Advanced Analysis of Steel Frame Structures Subjected to Lateral Torsional Buckling Effects”. PhD thesis. Queensland University of Technology (cit. on pp. 35, 43, 44, 46, 48, 52, 54, 59, 60).
- Ziemian, R. D. (2010). *Guide to Stability Design Criteria for Metal Structures, Sixth Edition*. Ed. by R. D. Ziemian. Wiley (cit. on p. 27).
- Zuraski, P. D. (1992). “The significance and application of  $C_b$  in beam design”. In: *Engineering Journal* First quarter, pp. 20–25 (cit. on p. 15).

# Appendices

## Appendix A

# Derivation of the Elastic Critical Moment

The beam in figure A.1 is assumed to be subjected to arbitrary loads acting in the  $yz$  plane, which is the plane of maximum rigidity. We assume that a small lateral deflection occurs under the action of these loads. Then from the differential equations of equilibrium for the deflected beam we can obtain the critical values of the loads. In deriving these equations, we shall use the fixed coordinate axes  $x, y, z$  as shown in the figure A.1 (Timoshenko et al., 1961).

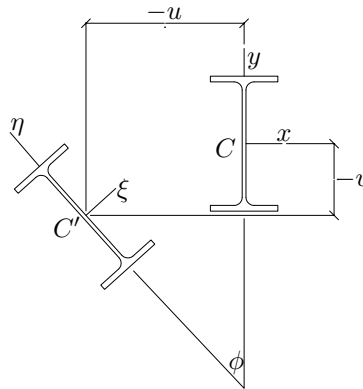


Figure A.1: Beam subjected to arbitrary loads in  $yz$  plane (Timoshenko et al., 1961)

In addition, the coordinate axes  $\xi, \eta, \zeta$  are taken at the centroid of the cross section at any section  $mn$ . The axes  $\xi$  and  $\eta$  are axes of symmetry and hence principal axes of the cross section, and  $\zeta$  is in the direction of the tangent to the deflected axis of the beam after buckling. The deflection of the beam is defined by the components  $u$  and  $v$  of the displacement of the centroid of the cross section in the  $x$  and  $y$  directions, respectively, and by the angle of rotation  $\phi$  of the cross section (Timoshenko et al., 1961).

The angle of rotation  $\phi$  is taken positive about the  $z$  axis according to the right-hand rule of signs, and  $u$  and  $v$  are positive directions of the corresponding axes. Thus the displacements  $u$  and  $v$  of point  $C'$  in

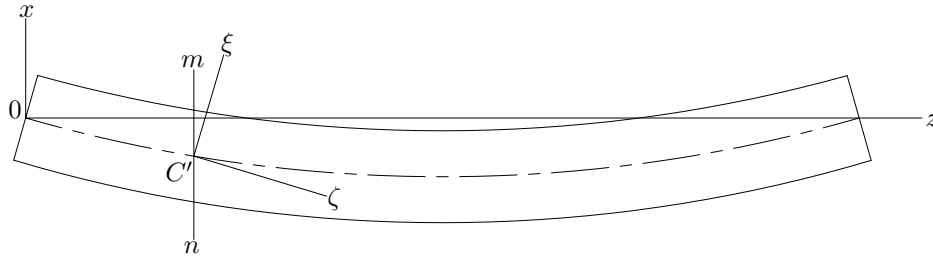


Figure A.2: Beam subjected to arbitrary loads in  $yz$  plane (Top view) (Timoshenko et al., 1961)

figure A.1 are shown negative. The expressions for the cosines of the angles between coordinate axes  $x$ ,  $y$ ,  $z$  and  $\xi$ ,  $\eta$ ,  $\zeta$  will be needed. When the quantities  $u$ ,  $v$ ,  $\phi$  are considered very small, the cosines of the angles between the positive directions of the axes have the values given in table A.1 (Timoshenko et al., 1961).

Table A.1: Cosines of angles between axes in figure A.1 and A.2

Axes	$x$	$y$	$z$
$\xi$	1	$\phi$	$-\frac{du}{dz}$
$\eta$	$-\phi$	1	$-\frac{dv}{dz}$
$\zeta$	$\frac{du}{dz}$	$\frac{dv}{dz}$	1

The curvatures of the deflected axis of the beam in the  $zx$  and  $yz$  planes can be taken as  $\frac{d^2u}{dz^2}$  and  $\frac{d^2v}{dz^2}$ , respectively, for small deflections. For small angles of twist  $\phi$  we can assume that the curvatures in the  $\xi\zeta$  and  $\eta\zeta$  planes have the same values. Thus the differential equations for bending of the beam become:

$$EI_{\xi} \frac{d^2v}{dz^2} = M_{\xi} \quad (\text{A.1})$$

$$EI_{\eta} \frac{d^2u}{dz^2} = M_{\eta} \quad (\text{A.2})$$

In these equations  $I_{\xi}$  and  $I_{\eta}$  are the principal moments of inertia of the cross section about the  $\xi$  and  $\eta$  axes, respectively. The quantities  $M_{\xi}$  and  $M_{\eta}$  represent the bending moments about the same axes, with assumed positive directions. The equation for twisting of the buckled bar is

$$C \frac{d\phi}{dz} - C_1 \frac{d^3\phi}{dz^3} = M_{\zeta} \quad (\text{A.3})$$

where  $C = GJ$  is the torsional rigidity and  $C_1 = EC_{\omega}$  is the warping rigidity. Equation A.3 is valid for a beam of thin-walled open cross section, such as the I-beam in figure A.1. The three differential equations A.1, A.2 and A.3 represent the equations of equilibrium for the buckled beam and from them we can find the critical values of the load.

If an I-beam is subjected to moments  $M_0$  at the ends as in figure A.3, the bending and twisting moments at any cross section are found by taking the components of  $M_0$  about the  $\xi$ ,  $\eta$  and  $\zeta$  axes. Thus, using the



Figure A.3: I-beam subjected to moments Timoshenko et al., 1961

values given in the first column of table A.1, and also considering the positive directions of the moments, we obtain

$$M_\xi = M_0 \quad M_\eta = \phi M_0 \quad M_\zeta = -\frac{du}{dz} M_0 \quad (\text{A.4})$$

Substituting these expression into equations A.1, A.2 and A.3 gives the following equations for  $u$ ,  $v$  and  $\phi$ :

$$EI_\xi \frac{d^2 v}{dz^2} - M_0 = 0 \quad (\text{A.5})$$

$$EI_\eta \frac{d^2 u}{dz^2} - \phi M_0 = 0 \quad (\text{A.6})$$

$$C \frac{d\phi}{dz} - C_1 \frac{d^3 \phi}{dz^3} + \frac{du}{dz} M_0 = 0 \quad (\text{A.7})$$

By differentiating the last equation with respect to  $z$ , and eliminating  $\frac{d^2 u}{dz^2}$  by combining with equation A.6, we obtain the following equation for the angle of twist  $\phi$  (Timoshenko et al., 1961):

$$C_1 \frac{d^4 \phi}{dz^4} - C \frac{d^2 \phi}{dz^2} - \frac{M_0^2}{EI_\eta} \phi = 0 \quad (\text{A.8})$$

or

$$\frac{d^4 \phi}{dz^4} - 2\alpha \frac{d^2 \phi}{dz^2} - \beta \phi = 0 \quad (\text{A.9})$$

where

$$\alpha = \frac{C}{2C_1} \quad \beta = \frac{M_0^2}{EI_\eta C_1} \quad (\text{A.10})$$

The general solution of equation A.9 is

$$\phi = A_1 \sin mz + A_2 \cos mz + A_3 e^{nz} + A_4 e^{-nz} \quad (\text{A.11})$$

in which  $m$  and  $n$  are positive, real quantities defined by the relations:

$$m = \sqrt{-\alpha + \sqrt{\alpha^2 + \beta}} \quad n = \sqrt{\alpha + \sqrt{\alpha^2 + \beta}} \quad (\text{A.12})$$

The constants of integration  $A_1$ ,  $A_2$ ,  $A_3$  and  $A_4$  must be determined from the conditions at the ends of the beam. Assuming that the ends of the beam cannot rotate about the  $z$  axis, figure A.1, but are free to warp, we find that the conditions at the ends are (Timoshenko et al., 1961):

$$\phi = \frac{d^2\phi}{dz^2} = 0 \quad \text{at } z = 0 \text{ and } z = l \quad (\text{A.13})$$

From the conditions at  $z = 0$  we conclude that

$$A_2 = 0 \quad A_3 = -A_4 \quad (\text{A.14})$$

and therefore the angle of twist  $\phi$  can be represented in the form

$$\phi = A_1 \sin mz - 2A_4 \sinh nz \quad (\text{A.15})$$

Now using the conditions at  $z = l$  we obtain the equations

$$A_1 \sin ml - 2A_4 \sinh nl = 0 \quad (\text{A.16})$$

$$A_1 m^2 \sin ml + 2A_4 n^2 \sinh nl = 0 \quad (\text{A.17})$$

Setting the determinant of these equations equal to zero yields

$$(\sin ml)(n^2 \sinh nl + m^2 \sinh ml) = 0 \quad (\text{A.18})$$

Since  $m$  and  $n$  are positive nonzero quantities, we conclude that

$$\sin ml = 0 \quad (\text{A.19})$$

and from equations A.16 and A.17 we also obtain  $A_4 = 0$ . Therefore the form of buckling is given by the equation

$$\phi = A_1 \sin mz \quad (\text{A.20})$$

and the beam buckles in the shape of a sine wave (Timoshenko et al., 1961).

The smallest value of  $m$  satisfying equation A.19 is

$$m = \frac{\pi}{l} \quad (\text{A.21})$$

or, using the expressions in equation A.12

$$\frac{\pi^2}{l^2} = -\alpha + \sqrt{\alpha^2 + \beta} \quad (\text{A.22})$$

Substituting expressions (A.7,A.9,A.10) and solving for the critical value of the moment  $M_0$  from the last equation, we find

$$M_{cr} = \frac{\pi}{L} \sqrt{EI_\eta C \left( 1 + \frac{C_1 \pi^2}{C L^2} \right)} \quad (\text{A.23})$$

## Appendix B

# Geometric imperfections of test specimens

This chapter presents the geometric imperfections of the test specimens, B1-B7, recorded during the experimental investigation. The data was measured as described in Section 4.4.3.

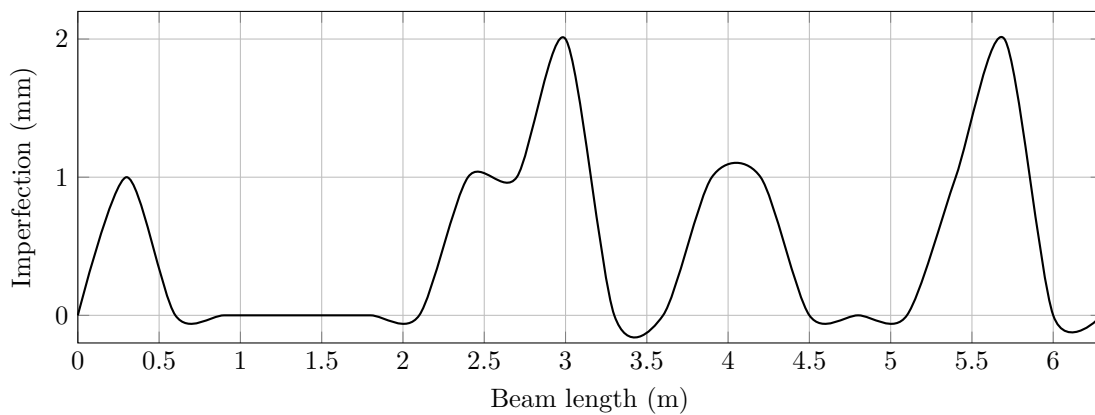


Figure B.1: Recorded imperfections of test specimen B1

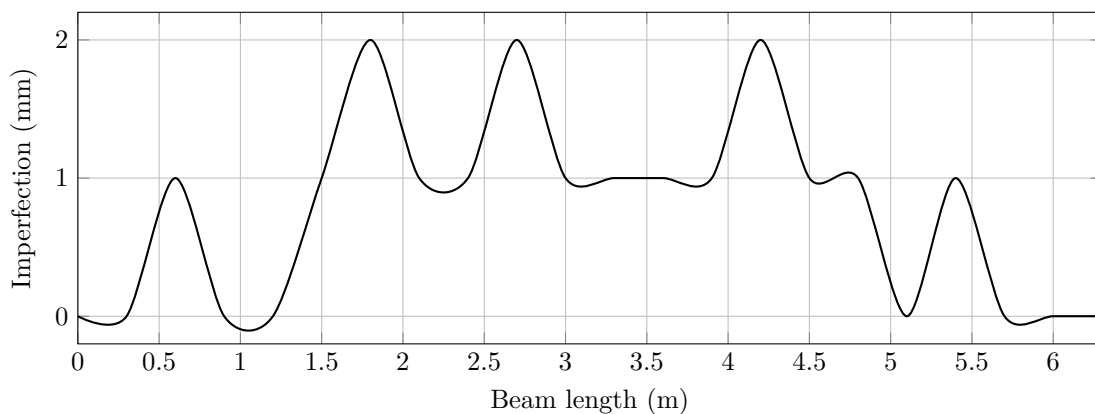


Figure B.2: Recorded imperfections of test specimen B2



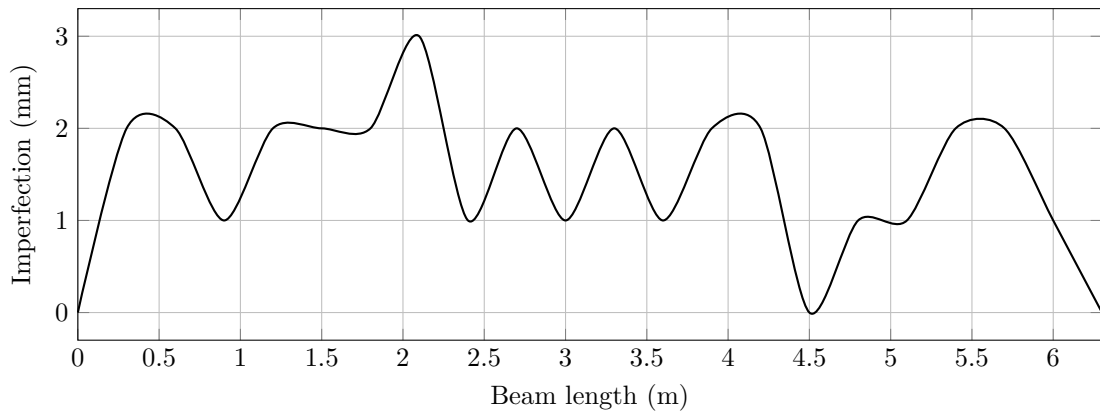


Figure B.3: Recorded imperfections of test specimen B3

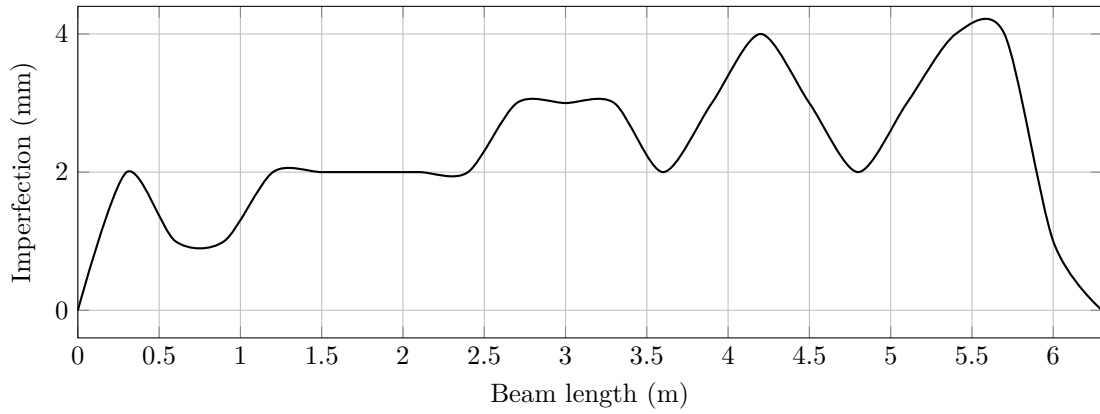


Figure B.4: Recorded imperfections of test specimen B4

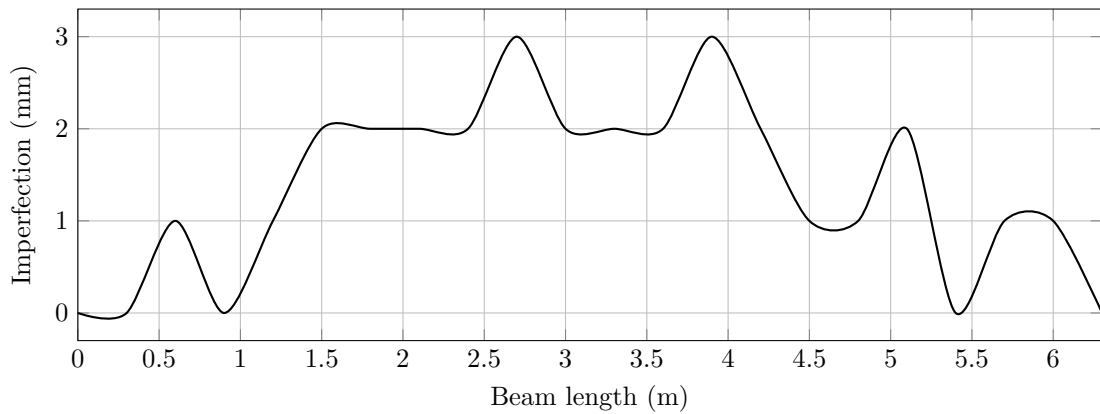


Figure B.5: Recorded imperfections of test specimen B5

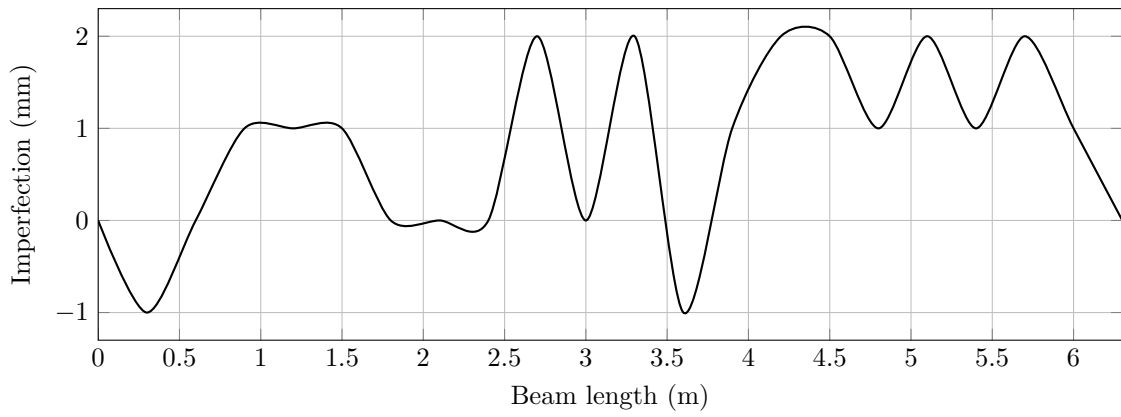


Figure B.6: Recorded imperfections of test specimen B6

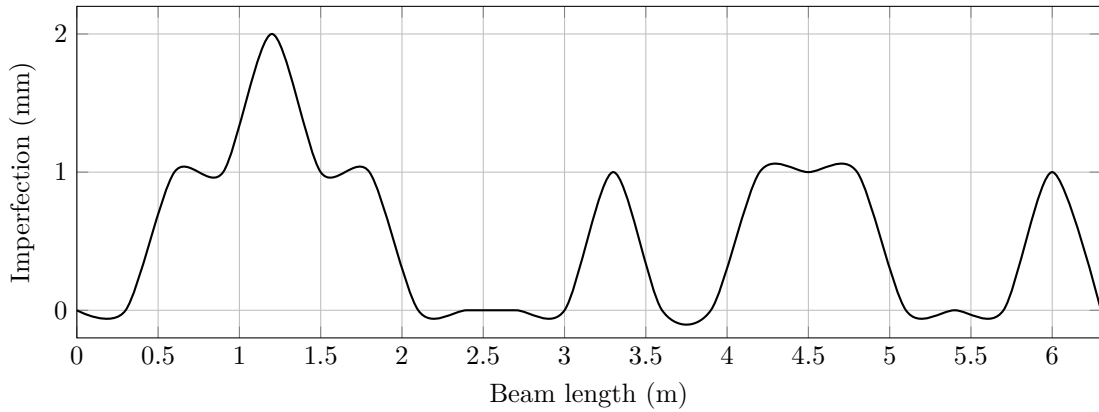


Figure B.7: Recorded imperfections of test specimen B7

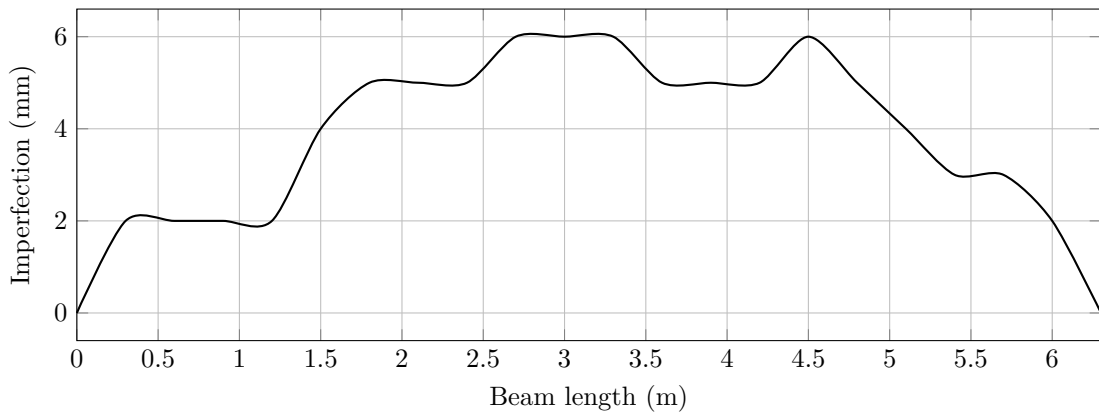


Figure B.8: Recorded imperfections of test specimen B8

## Appendix C

# Experimental Results

The following experimental data is presented in this appendix:

- End moment and distributed load
  - Figure C.1: Test specimen B7
  - Figure C.2: Test specimen B8
  - Figure C.3: Test specimen B9
  - Figure C.4: Test specimen B10
- Point load at mid-span
  - Figure C.5: Test specimen B1
  - Figure C.6: Test specimen B2
  - Figure C.7: Test specimen B3
  - Figure C.8: Test specimen B4
  - Figure C.9: Test specimen B5
  - Figure C.10: Test specimen B6
- Point loads at overhung ends
  - Figure C.11: Test specimen B12
  - Figure C.12: Test specimen B13
  - Figure C.13: Test specimen B12 & B13

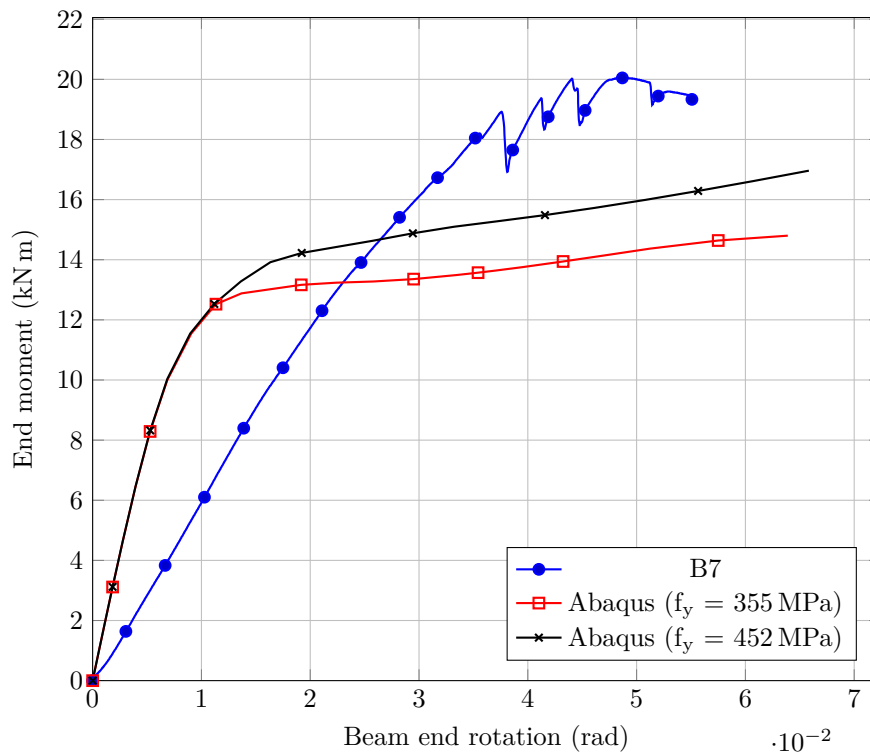


Figure C.1: Test specimen B7

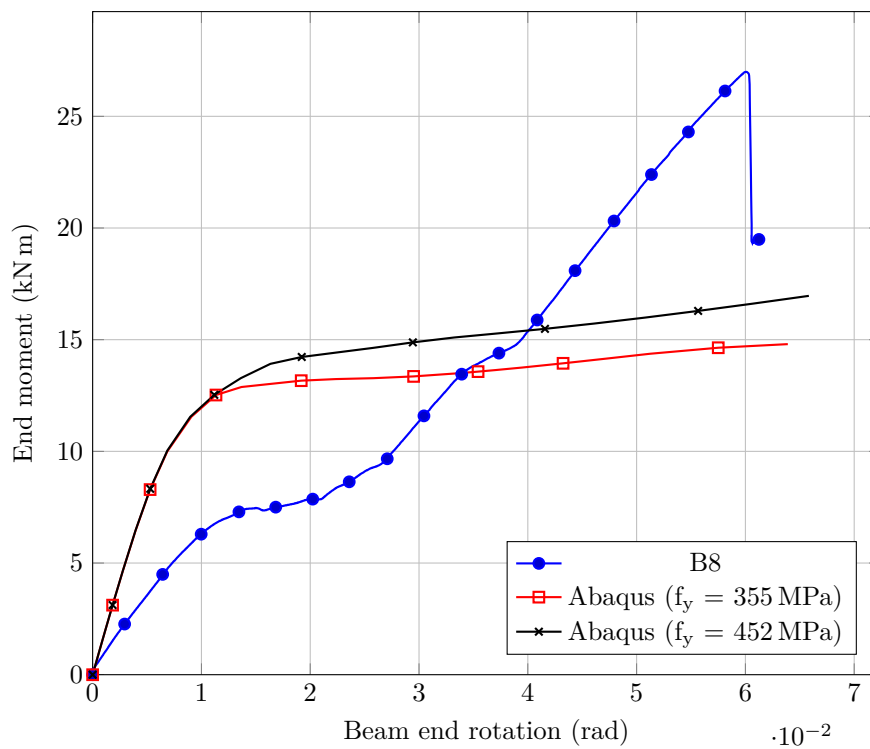


Figure C.2: Test specimen B8

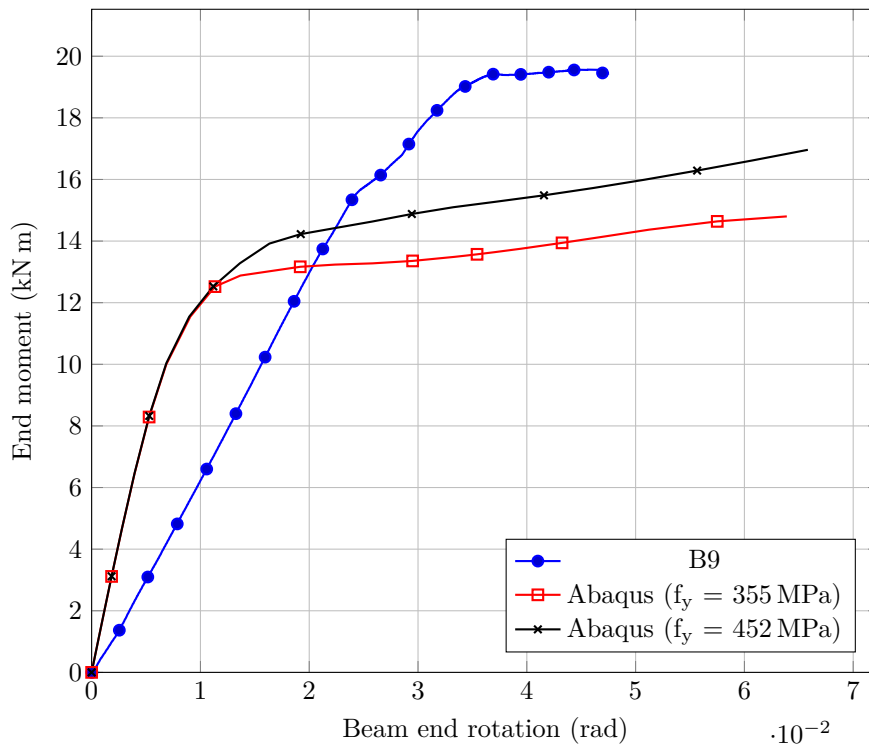


Figure C.3: Test specimen B9

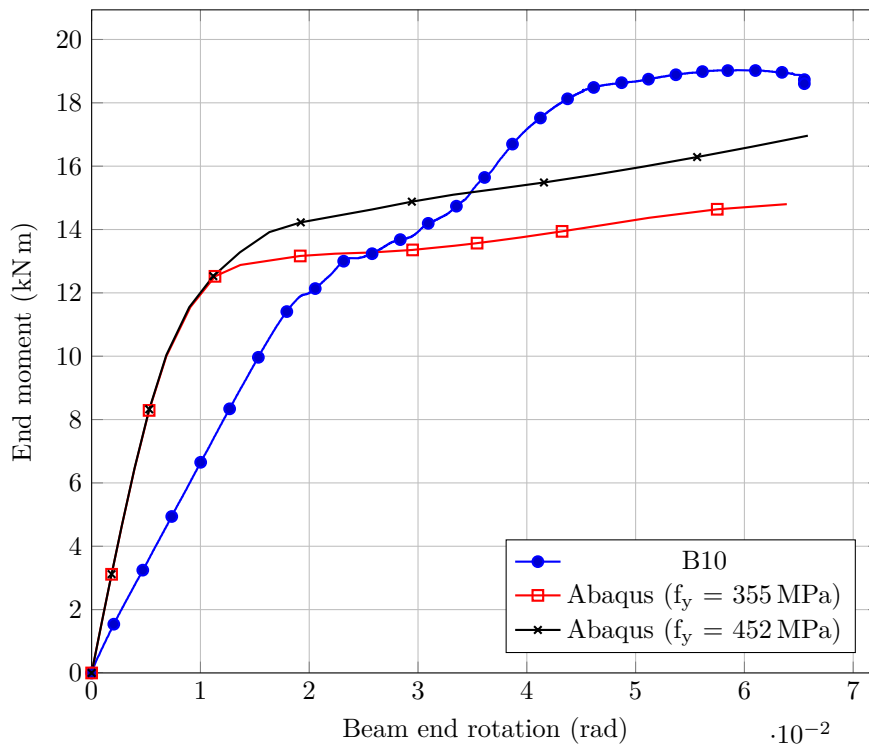


Figure C.4: Test specimen B10

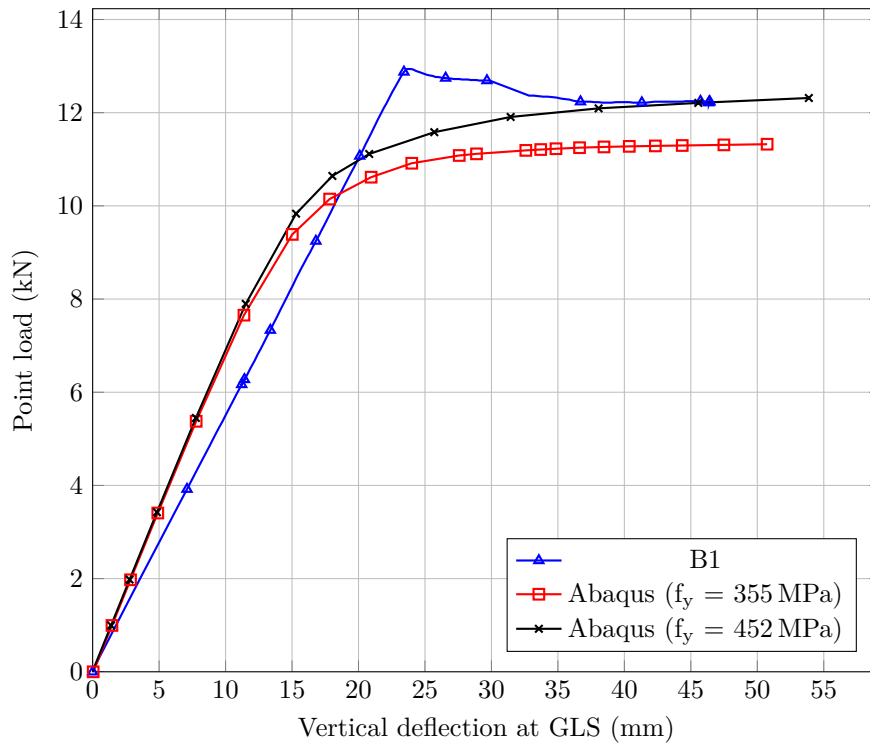


Figure C.5: Test specimen B1

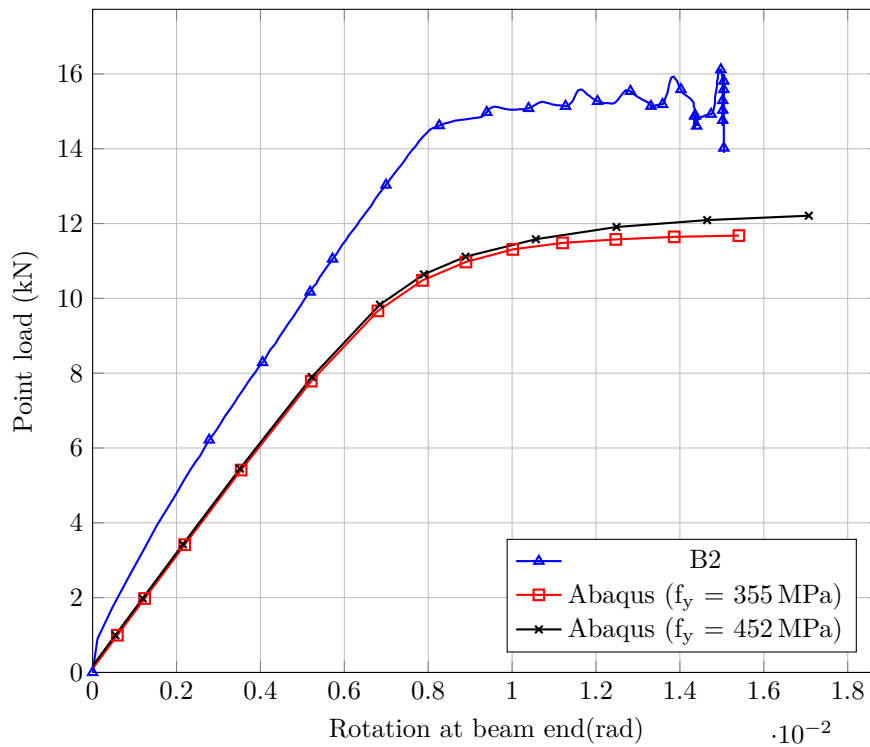


Figure C.6: Test specimen B2

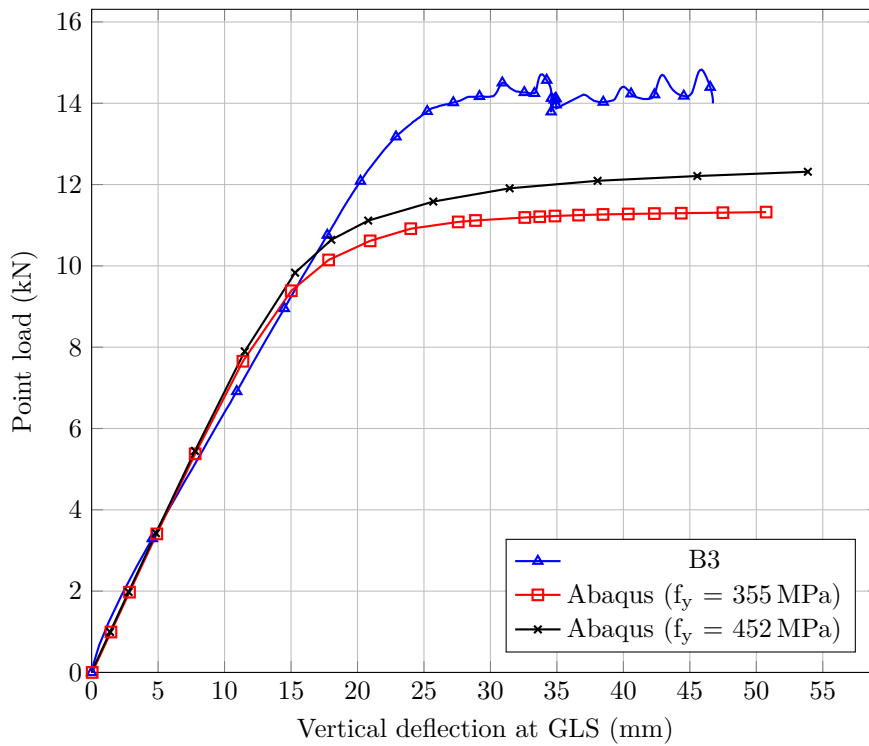


Figure C.7: Test specimen B3

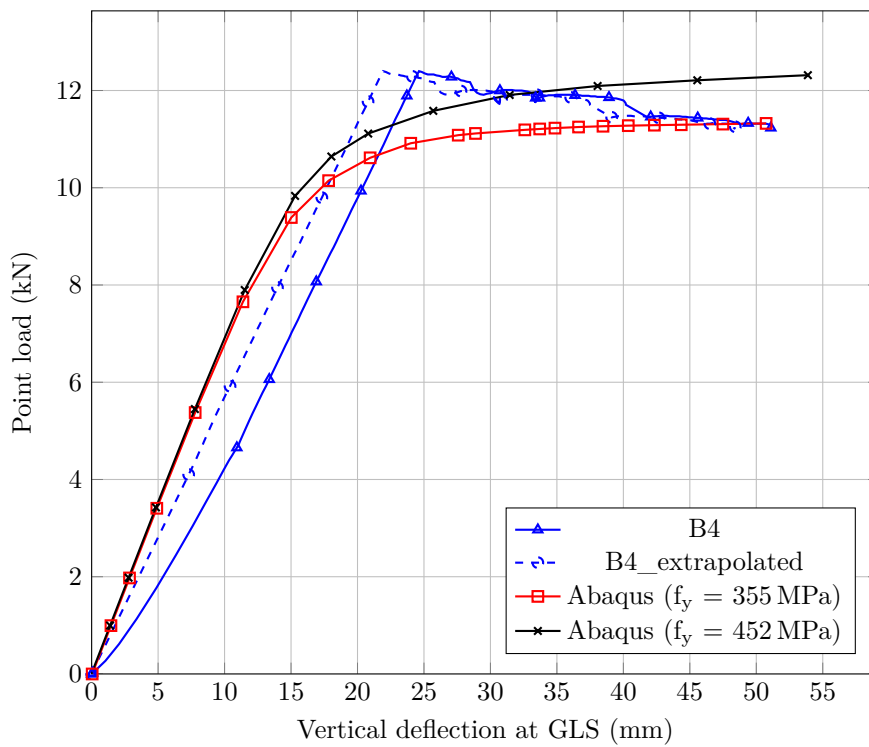


Figure C.8: Test specimen B4

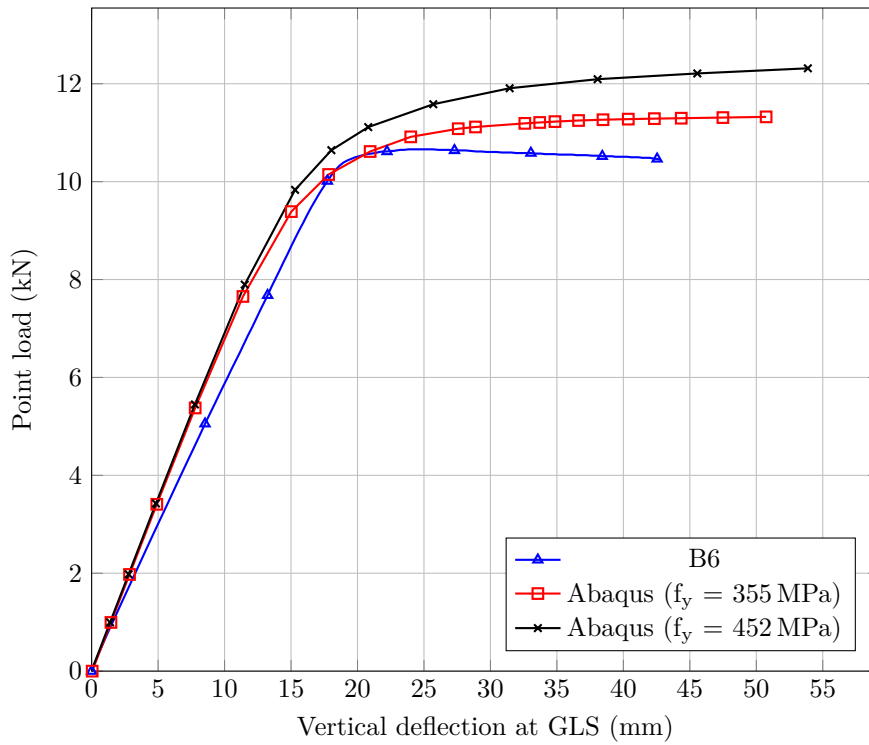


Figure C.9: Test specimen B5

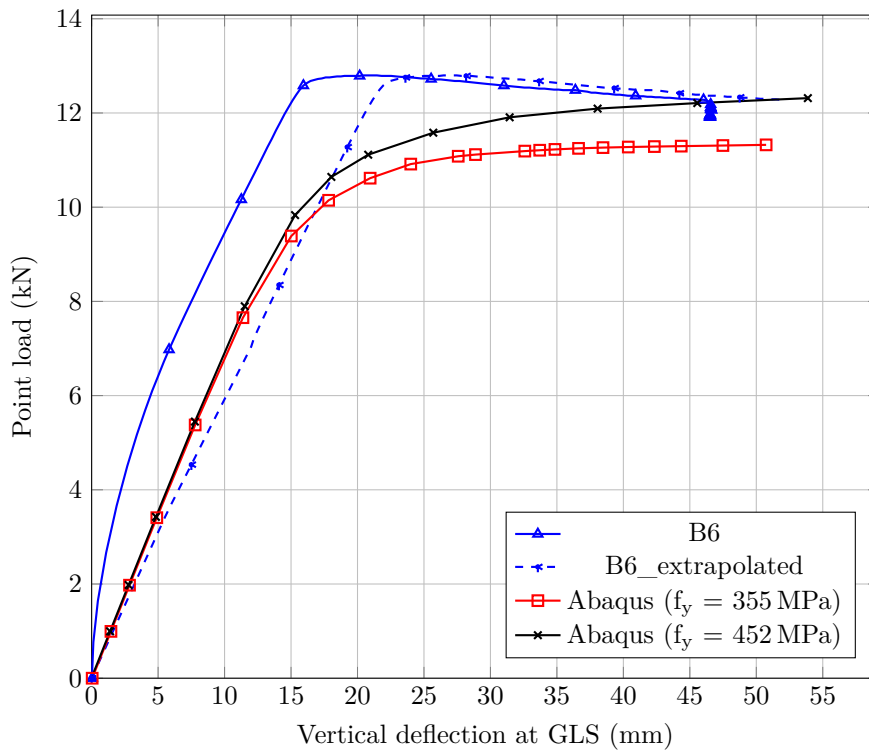


Figure C.10: Test specimen B6



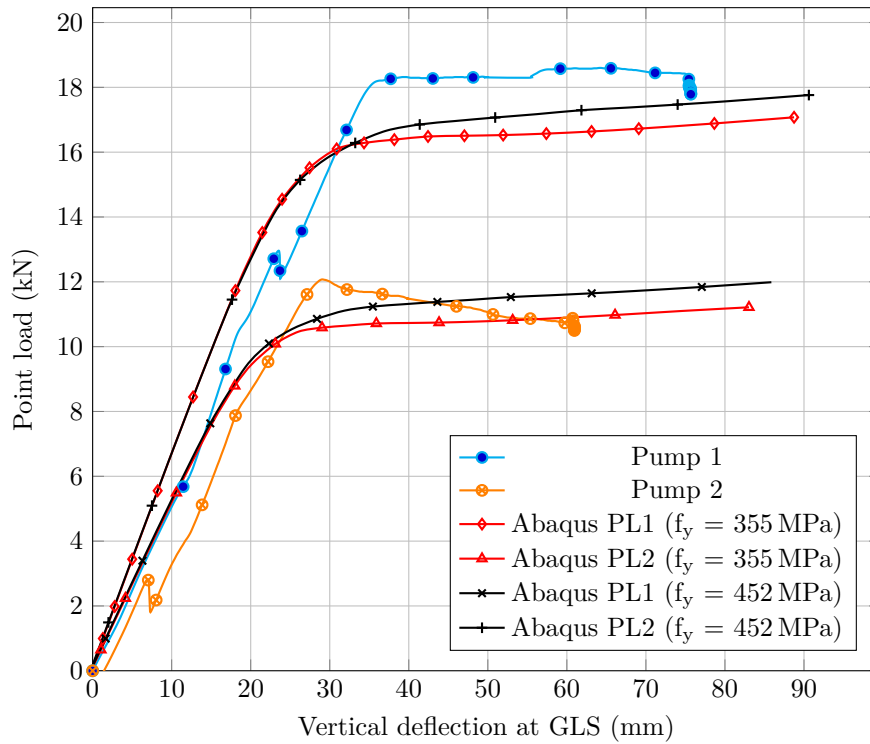


Figure C.11: Test specimen B12

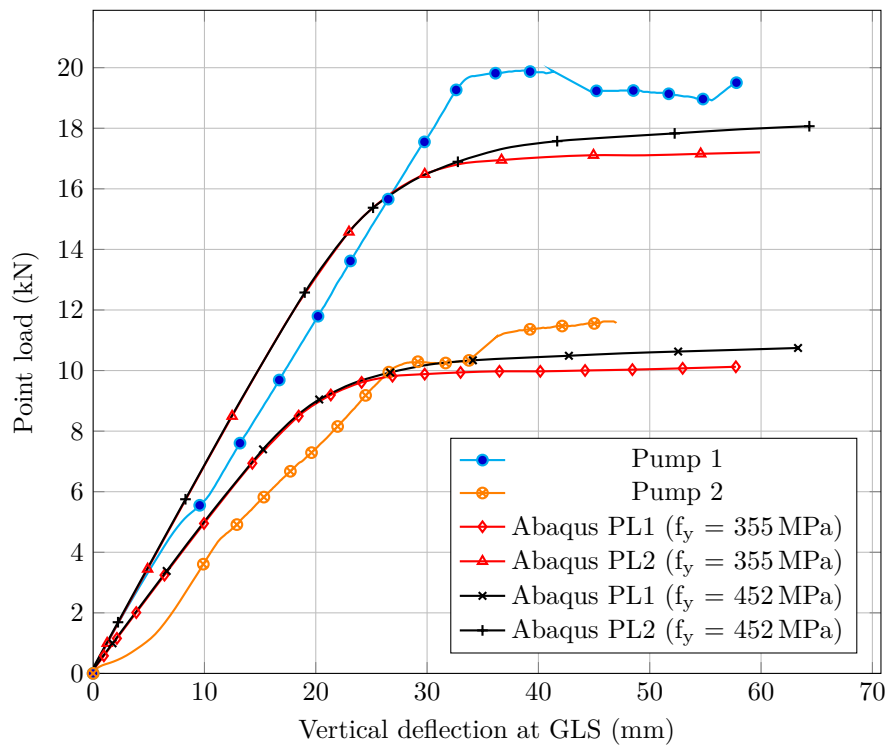


Figure C.12: Test specimen B13

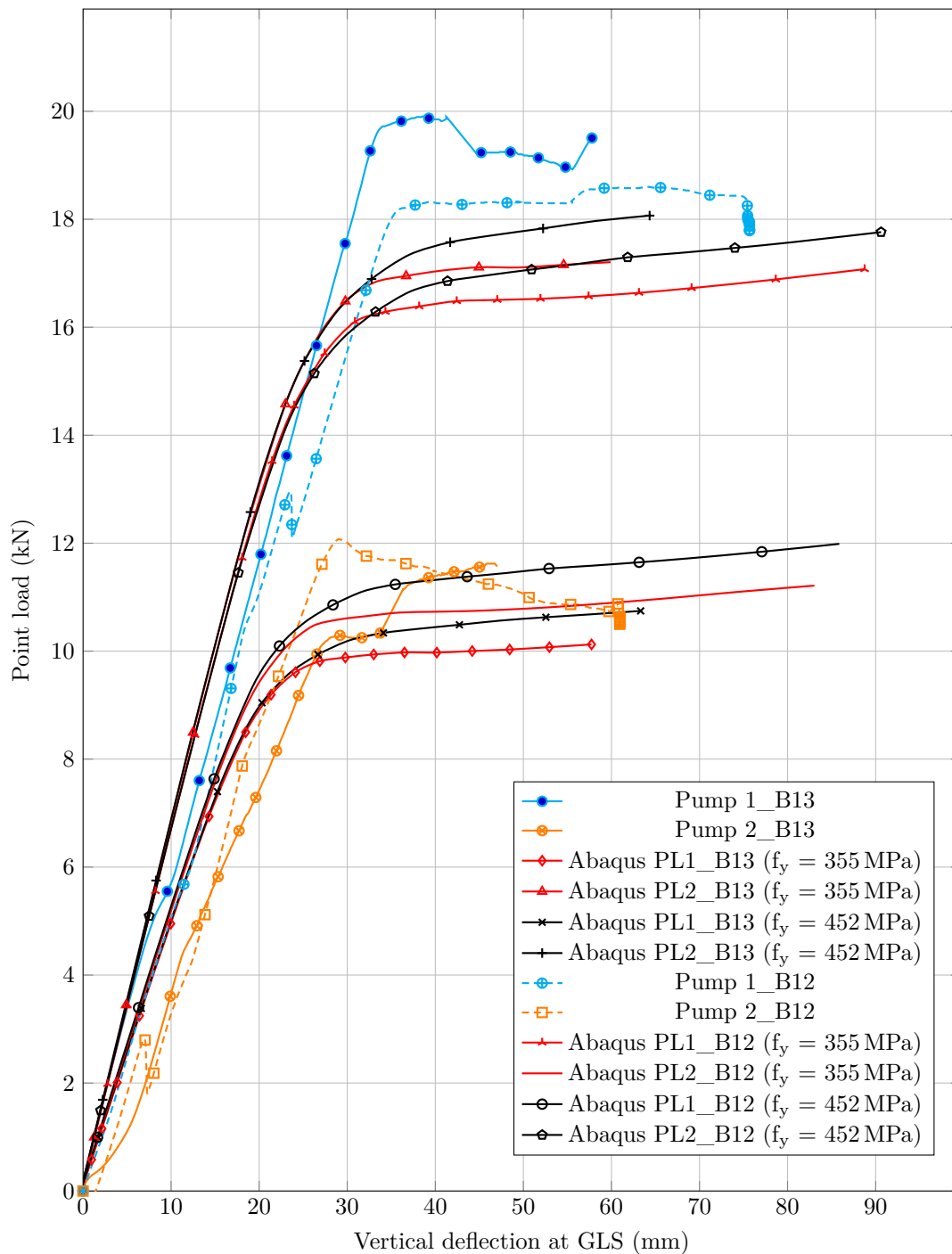


Figure C.13: Test specimens B12 & B13 - Pump 1 & Pump 2 refers to the hydraulic pumps used for each test, while PL1 & PL2 refers to the applied point load at each end of the FE model in order to simulate Pump 1 & Pump 2.

## Appendix D

# Sample calculation for determining $C_b$

This appendix presents a sample calculation for the determination of the  $C_b$  value as in Section 6.2. It includes the methods outlined in all four steel specifications, as well as the method used for the numerical results.

### D.1 End moment and distributed load

A total of 525 point loads were applied at each node along the centre of the web of the FE model. Each point load has a magnitude of 44.4 N, generating a distributed load of  $3.7 \text{ kN m}^{-1}$ .

The calculation is for  $\beta = 1.0$ :

$$\frac{\beta WL^2}{8} = \frac{1.0 \times 3.7 \times 6.3^2}{8} = 18.3 \text{ kN m}$$

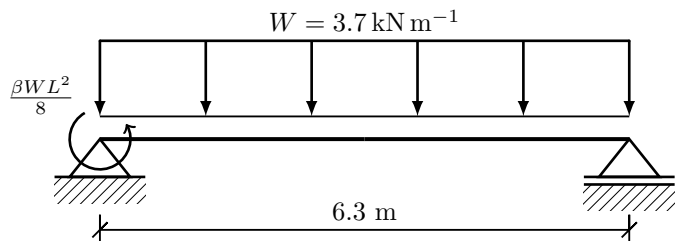
LPF obtained from Abaqus = 2.0245

End moment =  $2.0245 \times 18.3 = 37.08 \text{ kN m}$

Buckling moment for beam subjected to uniform moment distribution;  $M_u = 17.8 \text{ kN m}$

The  $C_b$  value is then calculated:  $C_b = \frac{37.08}{17.8} = 2.083$

$C_b$  values determined by the various steel specifications:



Moment at a distance  $x$ :

$$M_x = \frac{W}{2} \left( Lx - \beta \frac{L^2}{6} - x^2 \right)$$

Absolute values of quarter-point moments:

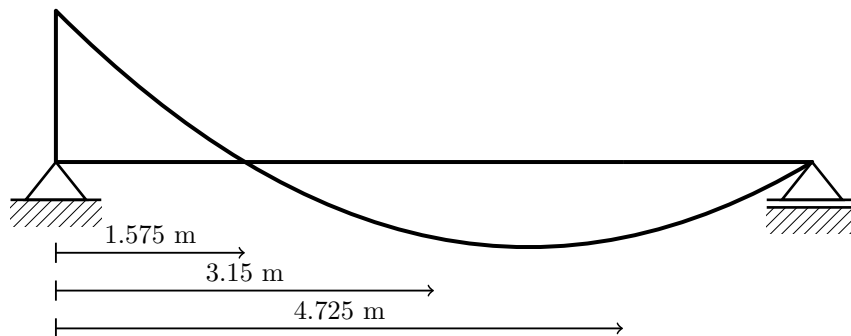
$$M_{1.575} = 0 \text{ kN m}$$

$$M_{3.15} = 18.54 \text{ kN m}$$

$$M_{4.725} = 18.54 \text{ kN m}$$

$$M_{max} = 37.08 \text{ kN m}$$

**Bending moment distribution:**



**SANS 10162-1:2011**

$$C_b = 1.75$$

**AISC 360-05**

$$C_b = \frac{12.5M_{max}}{2.5M_{max} + 3M_a + 4M_b + 3M_c} = \frac{12.5(37.08)}{2.5(37.08) + 3(0) + 4(18.54) + 3(18.54)} = 2.08$$

**EN1993-1-1**

$$C_b = 2.2$$

**CSA S16-09**

$$C_b = \frac{4M_{max}}{\sqrt{M_{max}^2 + 4M_a^2 + 7M_b^2 + 4M_c^2}} = \frac{4(37.08)}{\sqrt{(37.08)^2 + 4(0)^2 + 7(18.54)^2 + 4(18.54)^2}} = 2.07$$

## Appendix E

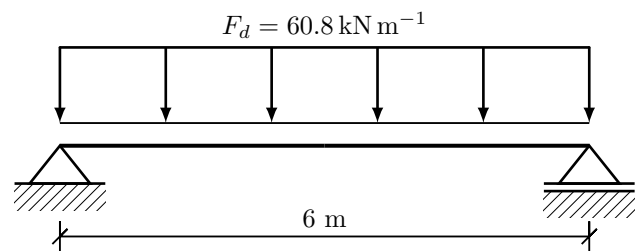
# Determination of the moment resistance

## resistance

This appendix presents a detailed set of calculations to determine the moment resistance of a steel beam for the three cases mentioned in Section 6.3. For each of the three cases, namely a simply supported beam, crane girder and rafter beam, the procedures for determining the moment resistance as discussed in Section 2.5 are presented.

### E.1 Simply supported beam

This case demonstrates the design of a laterally unrestrained beam. The beam is 6 m long and it is assumed that the loading is not destabilising. The design value for the permanent actions on the beam is  $60.8 \text{ kN m}^{-1}$ , which includes the self weight of the beam. The steel beam is a  $457 \times 191 \times 98$  section, of grade S355JR (Brown, 2011).



**E.1.1 SANS 10162-1:2011****Section classification:**

Table 4

$$\text{Flanges: } \left[ \frac{192.8}{2 \cdot 19.6} = 4.92 \right] \leq \left[ \frac{145}{\sqrt{355}} = 7.7 \right]$$

$$\text{Web: } \left[ \frac{467.6 - 2 \cdot 19.6}{11.4} = 37.58 \right] \leq \left[ \frac{1100}{\sqrt{355}} = 58.38 \right]$$

∴ Class 1

**Bending resistance:**

§13.6

$$\omega_2 = 1.0$$

$$M_{cr} = \frac{\omega_2 \pi}{KL} \sqrt{EI_y GJ + \left(\frac{\pi E}{KL}\right)^2 I_y C_w}$$

$$M_{cr} = \frac{1.0 \cdot \pi}{6000} \sqrt{200E3 \cdot 23.5E6 \cdot 7.7E4 \cdot 1220E3 + \left(\frac{\pi \cdot 200E3}{6000}\right)^2 \cdot 23.5E6 \cdot 1180E9} = 452.1 \text{ kN m}$$

$$M_{cr} \leq 0.67 \cdot M_p = 0.67(2230E3)(355) = 530.4 \text{ kN m}$$

$$\therefore M_r = 0.9 \cdot M_{cr} = 0.9 \cdot 452.1 = 406.89 \text{ kN m}$$

∴  $M_r = 407 \text{ kN m}$ **E.1.2 CSA S16-09****Section classification:**

Same as for SANS 10162-1:2011

**Bending resistance:**

§13.6

$$\omega_2 = \frac{4M_{max}}{\sqrt{M_{max}^2 + 4M_a^2 + 7M_b^2 + 4M_c^2}}$$

$$\omega_2 = \frac{4 \cdot 273.6}{\sqrt{273.6^2 + 4 \cdot 205.2^2 + 7 \cdot 273.4^2 + 4 \cdot 205.2^2}} = 1.131 \leq 2.5$$

$$M_{cr} = \frac{\omega_2 \pi}{KL} \sqrt{EI_y GJ + \left(\frac{\pi E}{KL}\right)^2 I_y C_w}$$

$$M_{cr} = \frac{1.131 \cdot \pi}{6000} \sqrt{200E3 \cdot 23.5E6 \cdot 7.7E4 \cdot 1220E3 + \left(\frac{\pi \cdot 200E3}{6000}\right)^2 \cdot 23.5E6 \cdot 1180E9} = 511.35 \text{ kN m}$$

$$M_{cr} \leq 0.67 \cdot M_p = 0.67(2230E3)(355) = 530.4 \text{ kN m}$$

$$\therefore M_r = 0.9 \cdot M_{cr} = 0.9 \cdot 511.35 = 460.22 \text{ kN m}$$

∴  $M_r = 460 \text{ kN m}$

**E.1.3 AISC 360-05****Section classification:**

Table B4.1

$$\text{Flanges: } \left[ \frac{192.8}{2 \cdot 19.6} = 4.92 \right] \leq \left[ 0.38 \sqrt{\frac{200E3}{355}} = 9.02 \right]$$

$$\text{Web: } \left[ \frac{408}{11.4} = 35.79 \right] \leq \left[ 3.76 \sqrt{\frac{200E3}{355}} = 89.2 \right]$$

∴ Compact section

**Bending resistance:**

Chapter F.2

$$L_b = 6000 \text{ mm}$$

$$L_p = 1.76 r_y \sqrt{\frac{E}{f_y}} = 1.76 \cdot 43.4 \cdot \sqrt{\frac{200E3}{355}} = 1809 \text{ mm}$$

$$r_{ts}^2 = \frac{\sqrt{I_y C_w}}{Z_x} = \frac{\sqrt{23.5E6 \cdot 1180E9}}{1960E3} = 2686.7 \Rightarrow r_{ts} = 51.83$$

$$L_r = 1.95 r_{ts} \frac{E}{0.7 f_y} \sqrt{\frac{J}{Z_x h_0}} \sqrt{1 + \sqrt{1 + 6.76 \left( \frac{0.7 f_y}{E} \cdot \frac{Z_x h_0}{J} \right)^2}}$$

$$L_r = 1.95 \cdot 51.83 \cdot \frac{200E3}{0.7 \cdot 355} \sqrt{\frac{1220E3}{1960E3 \cdot 448}} \sqrt{1 + \sqrt{1 + 6.67 \left( \frac{0.7 \cdot 355}{200E3} \cdot \frac{1960E3 \cdot 448}{1220E3} \right)^2}} = 5686 \text{ mm}$$

$$L_b = 6000 \geq L_r = 5686$$

$$C_b = \frac{12.5 M_{max}}{2.5 M_{max} + 3 M_a + 4 M_b + 3 M_c}$$

$$C_b = \frac{12.5 \cdot 273.6}{2.5 \cdot 273.5 + 3 \cdot 205.2 + 4 \cdot 273.6 + 3 \cdot 205.2} = 1.136$$

$$F_{cr} = \frac{C_b \pi^2 E}{\left( \frac{L_b}{r_{ts}} \right)^2} \sqrt{1 + 0.078 \frac{J}{Z_x h_0} \left( \frac{L_b}{r_{ts}} \right)^2}$$

$$F_{cr} = \frac{1.136 \cdot \pi^2 \cdot 200E3}{\left( \frac{6000}{51.83} \right)^2} \sqrt{1 + 0.078 \frac{1220E3}{1960E3 \cdot 448} \left( \frac{6000}{51.83} \right)^2} = 262.03 \text{ MPa}$$

$$M_u = F_{cr} Z_e = 262.03 \cdot 1960E3 = 513.58 \text{ kN m} < M_p$$

$$M_r = 0.9 \cdot 513.58 = 462 \text{ kN m}$$

∴  $M_r = 462 \text{ kN m}$

**E.1.4 EN 1993-1-1****Section classification:**

Table 5.2

$$\varepsilon = \sqrt{\frac{235}{355}} = 0.8136$$

$$\text{Outstand flange: } c = \frac{b - 2r - t_w}{2} = \frac{192.8 - 2 \cdot 10.2 - 11.4}{2} = 80.5 \text{ mm}$$

$$\frac{c}{b_f} = \frac{80.5}{19.6} = 4.107 \leq [9\varepsilon = 9 \cdot 0.8136 = 7.3224]$$

Internal compression part:  $c = h_w = 408$ 

$$\frac{c}{t_w} = \frac{408}{11.4} = 35.79 \leq [72\varepsilon = 72 \cdot 0.8136 = 58.58]$$

∴ Class 1

**Partial factors:**

Note B2, p.45

$$\gamma_{m0} = 1.00$$

$$\gamma_{m1} = 1.00$$

**Bending Resistance:**

§6.3.2

$$\frac{M_{Ed}}{M_{c,Rd}} \leq 1.0$$

$$M_{c,Rd} = M_{pl,Rd} = \frac{W_{pl} f_y}{\gamma_{m0}} = \frac{2230E3 \cdot 355}{1.0} = 761.65 \text{ kN m}$$

$$\frac{M_{Ed}}{M_{c,Rd}} = \frac{273.6}{761.65} = 0.3456 \leq 1.0$$

∴ OK

**Lateral-torsional buckling resistance:**

SN003a-EN-EU

$$M_{cr} = \frac{C_1 \pi^2 E I_y}{(kL)^2} \sqrt{\frac{C_w}{I_y} + \frac{L^2 G J}{\pi^2 E I_y}}$$

$$M_{cr} = \frac{1.127 \cdot \pi^2 \cdot 200E3 \cdot 23.5E6}{(6000)^2} \sqrt{\frac{1180E9}{23.5E6} + \frac{6000^2 \cdot 7.7E4 \cdot 1220E3}{\pi^2 \cdot 200E3 \cdot 23.5E6}} = 509.54 \text{ kN m}$$

§6.3.2.3



$$\text{Non-dimensional slenderness: } \bar{\lambda}_{LT} = \sqrt{\frac{W_y f_y}{M_{cr}}} = \sqrt{\frac{2230E3 \cdot 355}{509.54E6}} = 1.246$$

$$\text{Imperfection factor: } \frac{h}{b} \geq 2 \therefore \text{Buckling curve c} \Rightarrow \alpha_{LT} = 0.49$$

$$\Phi_{LT} = 0.5[1 + \alpha_{LT}(\bar{\lambda}_{LT} - \bar{\lambda}_{LT,0}) + \beta \bar{\lambda}_{LT}^2]; \text{ with } \beta = 0.75 \text{ and } \bar{\lambda}_{LT,0} = 0.4$$

$$\Phi_{LT} = 0.5[1 + 0.49(1.264 - 0.4) + 0.75 \cdot 1.264^2] = 1.289$$

$$\chi_{LT} = \frac{1}{\Phi_{LT} + \sqrt{\Phi_{LT}^2 - \beta \bar{\lambda}_{LT}}} = \frac{1}{1.289 + \sqrt{1.289^2 - 0.75 \cdot 1.246^2}} = 0.501$$

$$f = 1 - 0.5(1 - k_c)[1 - 2.0(\bar{\lambda}_{LT} - 0.8)^2] = 1 - 0.5(1 - 0.94)[1 - 2.0(1.246 - 0.8)^2] = 0.9819 \leq 1.0$$

$$\chi_{LT,mod} = \frac{\chi_{LT}}{f} = \frac{0.501}{0.9818} = 0.51$$

$$M_{b,Rd} = \chi_{LT,mod} W_{pl,y} \frac{f_y}{\gamma_{m1}} = 0.51 \cdot 2230E3 \cdot 355 = 404 \text{ kN m}$$

$$\therefore M_r = 404 \text{ kN m}$$

## E.2 Crane girder

### E.2.1 General problem outline

Presented in this section is the general problem outline and variables used in the design of the crane girder. It should be kept in mind that the design for the girder is only for the bending strength of the section under consideration. The wheel loads applied to the top flange are considered to be normal, refer to Section 6.3.2. The section used for the girder beam is a wide flange I-beam as shown in figure E.1 (MacCrimmon, 2009).

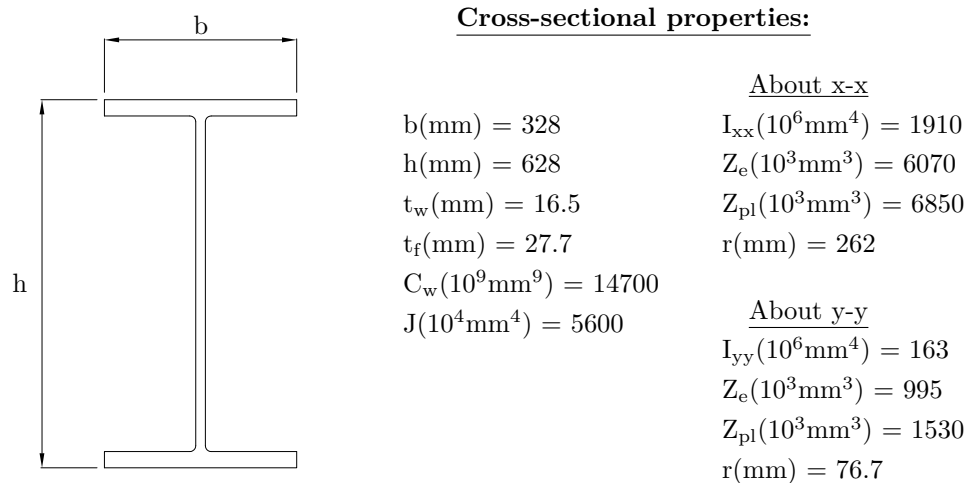


Figure E.1: W610×217

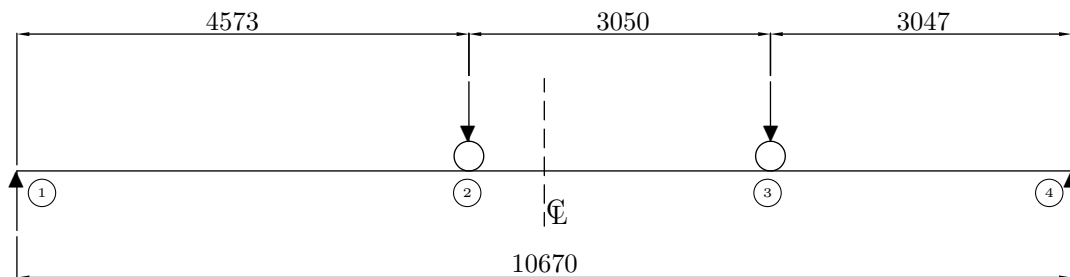


Figure E.2: Crane girder

#### For maximum moment:

Red Book: Table 5.19

$$M_{max} @ a = 10670 - \left[ \frac{10670}{2} + \frac{3050}{4} \right] = 4573 \text{ mm}$$

$$M_{max} = M_2 = \frac{169 \cdot 10.67}{8} \left( 2 - 2 \cdot \frac{1.525}{10.67} \right)^2 = 662.3 \text{ kN m}$$

$$M_3 = \frac{2 \cdot 169 \cdot 6.098}{10.67} (4.573 - 1.525) = 588.78 \text{ kN m}$$

Bending moment diagram:

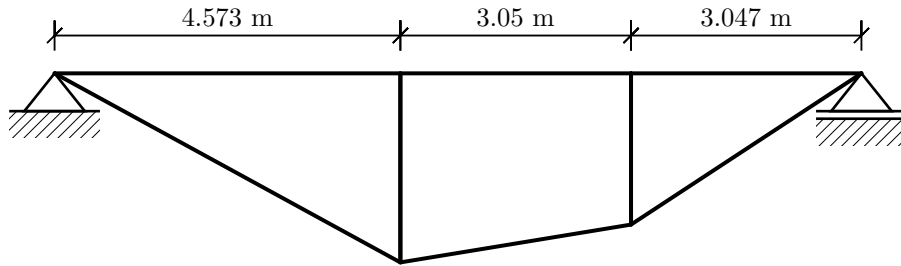


Figure E.3: Bending moment distribution along girder

Quarter-point moments:

$$M_{max} = 662.3 \text{ kN m}$$

$$M_a = 386.3 \text{ kN m}$$

$$M_b = 643.9 \text{ kN m}$$

$$M_c = 515.4 \text{ kN m}$$

## E.2.2 SANS 10162-1:2011

Section classification:

Table 4

$$\text{Flanges: } \left[ \frac{328}{2 \cdot 27.7} = 5.9 \right] \leq \left[ \frac{145}{\sqrt{355}} = 7.7 \right]$$

$$\text{Web: } \left[ \frac{640.7 - 2 \cdot 27.7}{16.5} = 35.47 \right] \leq \left[ \frac{1100}{\sqrt{355}} = 58.38 \right]$$

∴ Class 1

Bending resistance:

§13.6

$$\omega_2 = 1.0$$

$$M_{cr} = \frac{\omega_2 \pi}{KL} \sqrt{EI_y GJ + \left( \frac{\pi E}{KL} \right)^2 I_y C_w}$$

$$M_{cr} = \frac{1.0 \cdot \pi}{10670} \sqrt{200E3 \cdot 163E6 \cdot 7.7E4 \cdot 5600E3 + \left( \frac{\pi \cdot 200E3}{10670} \right)^2 \cdot 163E6 \cdot 14700E9} = 1160.3 \text{ kN m}$$

$$M_{cr} \leq 0.67 \cdot M_p = 0.67(6850E3)(355) = 1629.27 \text{ kN m}$$

$$\therefore M_r = 0.9 \cdot M_{cr} = 0.9 \cdot 1160.3 = 1044 \text{ kN m}$$

$$\therefore M_r = 1044 \text{ kN m}$$

**E.2.3 CSA S16-09****Section classification:**

Same as for SANS 10162-1:2011

**Bending resistance:**

§13.6

$$\omega_2 = \frac{4M_{max}}{\sqrt{M_{max}^2 + 4M_a^2 + 7M_b^2 + 4M_c^2}}$$

$$\omega_2 = \frac{4 \cdot 662.3}{\sqrt{662.3^2 + 4 \cdot 386.3^2 + 7 \cdot 643.9^2 + 4 \cdot 515.4^2}} = 1.185 \leq 2.5$$

$$M_{cr} = \frac{\omega_2 \pi}{KL} \sqrt{EI_y GJ + \left(\frac{\pi E}{KL}\right)^2 I_y C_w}$$

$$M_{cr} = \frac{1.185 \cdot \pi}{10670} \sqrt{200E3 \cdot 163E6 \cdot 7.7E4 \cdot 5600E3 + \left(\frac{\pi \cdot 200E3}{10670}\right)^2 \cdot 163E6 \cdot 14700E9} = 1650.05 \text{ kN m}$$

$$M_{cr} \geq 0.67 \cdot M_p = 0.67(6850E3)(355) = 1629.27 \text{ kN m}$$

$$\therefore M_r = 1.15 \phi M_p \left[ 1 - \frac{0.28 M_p}{M_{cr}} \right]$$

$$\therefore M_r = 1.15 \cdot 0.9 \cdot 2431.05 \left[ 1 - \frac{0.28 \cdot 2431.75}{1650.05} \right] = 1477.86 \text{ kN m}$$

$$\therefore M_r = 1478 \text{ kN m}$$

**E.2.4 AISC 360-05****Section classification:**

Table B4.1

$$\text{Flanges: } \left[ \frac{328}{2 \cdot 27.7} = 5.92 \right] \leq \left[ 0.38 \sqrt{\frac{200E3}{355}} = 9.02 \right]$$

$$\text{Web: } \left[ \frac{610.8 - 2 \cdot 27.7}{16.5} = 33.66 \right] \leq \left[ 3.76 \sqrt{\frac{200E3}{355}} = 89.2 \right]$$

∴ Compact section

**Bending resistance:**

Chapter F.2

$$L_b = 10670 \text{ mm}$$

$$L_p = 1.76 r_y \sqrt{\frac{E}{f_y}} = 1.76 \cdot 76.7 \cdot \sqrt{\frac{200E3}{355}} = 3204 \text{ mm}$$

$$r_{ts}^2 = \frac{\sqrt{I_y C_w}}{Z_x} = \frac{\sqrt{163E6 \cdot 14700E9}}{6070E3} = 8064.25 \Rightarrow r_{ts} = 89.8$$

$$L_r = 1.95 r_{ts} \frac{E}{0.7 f_y} \sqrt{\frac{J}{Z_x h_0}} \sqrt{1 + \sqrt{1 + 6.76 \left( \frac{0.7 f_y}{E} \cdot \frac{Z_x h_0}{J} \right)^2}}$$

$$L_r = 1.95 \cdot 89.8 \cdot \frac{200E3}{0.7 \cdot 355} \sqrt{\frac{5600E3}{6070E3 \cdot 600.3}} \sqrt{1 + \sqrt{1 + 6.67 \left( \frac{0.7 \cdot 355}{200E3} \cdot \frac{6070E3 \cdot 600.3}{5600E3} \right)^2}} = 10\,060 \text{ mm}$$

$$L_b = 10670 \geq L_r = 10060$$

$$C_b = \frac{12.5 M_{max}}{2.5 M_{max} + 3 M_a + 4 M_b + 3 M_c}$$

$$C_b = \frac{12.5 \cdot 662.3}{2.5 \cdot 662.3 + 3 \cdot 386.3 + 4 \cdot 643.9 + 3 \cdot 515.4} = 1.194$$

$$F_{cr} = \frac{C_b \pi^2 E}{\left( \frac{L_b}{r_{ts}} \right)^2} \sqrt{1 + 0.078 \frac{J}{Z_x h_0} \left( \frac{L_b}{r_{ts}} \right)^2}$$

$$F_{cr} = \frac{1.194 \cdot \pi^2 \cdot 200E3}{\left( \frac{10670}{89.8} \right)^2} \sqrt{1 + 0.078 \frac{5600E3}{6070E3 \cdot 600.3} \left( \frac{10670}{89.8} \right)^2} = 273.92 \text{ MPa}$$

$$M_u = F_{cr} Z_e = 273.92 \cdot 6070E3 = 1662.7 \text{ kN m} < M_p$$

$$M_r = 0.9 \cdot 1662.7 = 1496.4 \text{ kN m}$$

$$\therefore M_r = 1496 \text{ kN m}$$

## E.2.5 EN 1993-1-1

### Section classification:

Table 5.2

$$\varepsilon = \sqrt{\frac{235}{355}} = 0.8136$$

$$\text{Outstand flange: } c = \frac{b - t_w}{2} = \frac{328 - 16.5}{2} = 155.75 \text{ mm}$$

$$\frac{c}{b_f} = \frac{155.75}{27.7} = 5.62 \leq [9\varepsilon = 9 \cdot 0.8136 = 7.3224]$$

$$\text{Internal compression part: } c = h_w = 585.3$$

$$\frac{c}{t_w} = \frac{600.3}{16.5} = 36.38 \leq [72\varepsilon = 72 \cdot 0.8136 = 58.58]$$

$\therefore$  Class 1

### Partial factors:

Note B2, p.45

$$\gamma_{m0} = 1.00$$

$$\gamma_{m1} = 1.00$$

**Bending Resistance:**

## §6.3.2

$$\frac{M_{Ed}}{M_{c,Rd}} \leq 1.0$$

$$M_{c,Rd} = M_{pl,Rd} = \frac{W_{pl}f_y}{\gamma_{m0}} = \frac{6850E3 \cdot 355}{1.0} = 2431.75 \text{ kN m}$$

$$\frac{M_{Ed}}{M_{c,Rd}} = \frac{662.3}{2431.75} = 0.272 \leq 1.0$$

∴ OK

**Lateral-torsional buckling resistance:**

SN003a-EN-EU

$$M_{cr} = \frac{C_1\pi^2EI_y}{(kL)^2} \sqrt{\frac{C_w}{I_y} + \frac{L^2GJ}{\pi^2EI_y} + (C_2z_g)^2} - C_2z_g$$

$$M_{cr} = \frac{1.348 \cdot \pi^2 \cdot 200E3 \cdot 163E6}{(10670)^2} \sqrt{\frac{14700E9}{163E6} + \frac{10670^2 \cdot 7.7E4 \cdot 5600E3}{\pi^2 \cdot 200E3 \cdot 163E6} + (0.63 \cdot 305.35)^2} - 0.63 \cdot 305.35 = 1282.15 \text{ kN m}$$

## §6.3.2.3

$$\text{Non-dimensional slenderness: } \bar{\lambda}_{LT} = \sqrt{\frac{W_y f_y}{M_{cr}}} = \sqrt{\frac{6850E3 \cdot 355}{1282.15E6}} = 1.377$$

$$\text{Imperfection factor: } \frac{h}{b} \leq 2 \therefore \text{Buckling curve b} \Rightarrow \alpha_{LT} = 0.34$$

$$\Phi_{LT} = 0.5[1 + \alpha_{LT}(\bar{\lambda}_{LT} - \bar{\lambda}_{LT,0}) + \beta \bar{\lambda}_{LT}^2]; \text{ with } \beta = 0.75 \text{ and } \bar{\lambda}_{LT,0} = 0.4$$

$$\Phi_{LT} = 0.5[1 + 0.34(1.377 - 0.4) + 0.75 \cdot 1.377^2] = 1.3771$$

$$\chi_{LT} = \frac{1}{\Phi_{LT} + \sqrt{\Phi_{LT}^2 - \beta \bar{\lambda}_{LT}^2}} = \frac{1}{1.3771 + \sqrt{1.3771^2 - 0.75 \cdot 1.377^2}} = 0.484$$

$$f = 1 - 0.5(1 - k_c)[1 - 2.0(\bar{\lambda}_{LT} - 0.8)^2] = 1 - 0.5(1 - 0.94)[1 - 2.0(1.377 - 0.8)^2] = 0.9899 \leq 1.0$$

$$\chi_{LT,mod} = \frac{\chi_{LT}}{f} = \frac{0.484}{0.9899} = 0.489$$

$$M_{b,Rd} = \chi_{LT,mod} W_{pl,y} \frac{f_y}{\gamma_{m1}} = 0.489 \cdot 6850E3 \cdot 355 = 1188.88 \text{ kN m}$$

∴  $M_r = 1189 \text{ kN m}$

## E.3 Rafter beam

### E.3.1 General problem outline

Design considerations:

- Frame subjected to dead loads + across wind loads.
- Bending resistance for rafter beam shown in figure E.4 will be determined.
- Purlins provide lateral restraint to top flange.
- Lateral support for bottom flange at node 1, 5 and 9, see figure E.5.
- Calculations only consider bending resistance of the rafter beam, interaction with the axial forces are ignored.
- Beam segments are taken as the length between the lateral support of the compression flange, as indicated in figure E.5.
- The bending moment for each node due to the applied loads on the frame is shown in the table.

Node	$M_u$ (kN m)
①	-13.80
②	-15.93
③	-17.51
④	-14.51
⑤	-10.96
⑥	-2.83
⑦	5.840
⑧	19.08
⑨	32.84

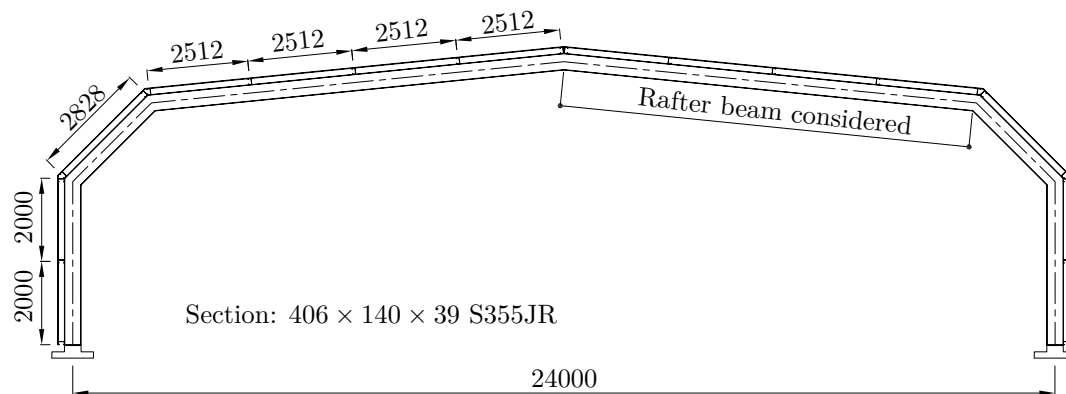


Figure E.4: Typical portal frame

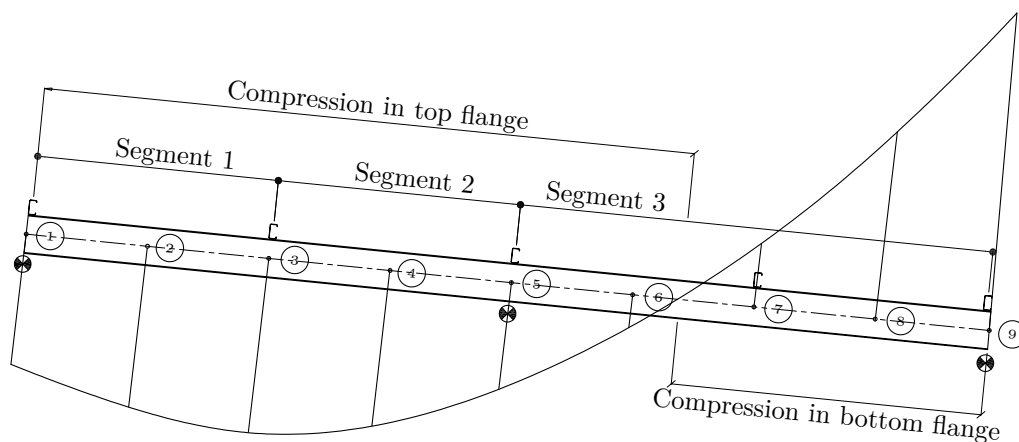


Figure E.5: Rafter bending moment diagram

**E.3.2 SANS 10162-1:2011****Section classification:**

Table 4

$$\text{Flanges: } \left[ \frac{141.8}{2 \cdot 8.6} = 8.24 \right] \leq \left[ \frac{170}{\sqrt{355}} = 9.02 \right]$$

$$\text{Web: } \left[ \frac{397.3 - 2 \cdot 8.6}{6.30} = 60.3 \right] \leq \left[ \frac{1700}{\sqrt{355}} = 90.3 \right]$$

∴ Class 2

**Segment 1:****Bending resistance:**

§13.6

$$\kappa = \frac{-13.80}{17.51} = -0.788$$

$$\omega_2 = 1.75 + 1.05(-0.788) + 0.3(-0.788)^2 = 1.109$$

$$M_{cr} = \frac{\omega_2 \pi}{KL} \sqrt{EI_y GJ + \left( \frac{\pi E}{KL} \right)^2 I_y C_w}$$

$$M_{cr} = \frac{1.109 \cdot \pi}{2512} \sqrt{200E3 \cdot 4.1E6 \cdot 7.7E4 \cdot 108E3 + \left( \frac{\pi \cdot 200E3}{2512} \right)^2 \cdot 4.1E6 \cdot 155E9} = 299.33 \text{ kN m}$$

$$M_{cr} \geq 0.67 \cdot M_p = 0.67(718E3)(355) = 170.78 \text{ kN m}$$

$$\therefore M_r = 1.15\phi M_p \left( 1 - \frac{0.28M_p}{M_{cr}} \right) = 1.15 \cdot 0.9 \cdot 254.89 \left( 1 - \frac{0.28 \cdot 254.89}{299.33} \right) = 201 \text{ kN m}$$

∴  $M_r = 201 \text{ kN m}$ **Segment 2:****Bending resistance:**

§13.6

$$\kappa = \frac{-10.96}{17.51} = -0.626$$

$$\omega_2 = 1.75 + 1.05(-0.626) + 0.3(-0.626)^2 = 1.210$$

$$M_{cr} = \frac{\omega_2 \pi}{KL} \sqrt{EI_y GJ + \left( \frac{\pi E}{KL} \right)^2 I_y C_w}$$

$$M_{cr} = \frac{1.210 \cdot \pi}{2512} \sqrt{200E3 \cdot 4.1E6 \cdot 7.7E4 \cdot 108E3 + \left( \frac{\pi \cdot 200E3}{2512} \right)^2 \cdot 4.1E6 \cdot 155E9} = 326.59 \text{ kN m}$$

$$M_{cr} \geq 0.67 \cdot M_p = 0.67(718E3)(355) = 170.78 \text{ kN m}$$

$$\therefore M_r = 1.15\phi M_p \left( 1 - \frac{0.28M_p}{M_{cr}} \right) = 1.15 \cdot 0.9 \cdot 254.89 \left( 1 - \frac{0.28 \cdot 254.89}{326.59} \right) = 206 \text{ kN m}$$

∴  $M_r = 206 \text{ kN m}$



**Segment 3:****Bending resistance:**

§13.6

$$\kappa = \frac{10.96}{32.84} = 0.334$$

$$\omega_2 = 1.75 + 1.05(0.334) + 0.3(0.334)^2 = 2.134 \leq 2.5$$

$$M_{cr} = \frac{\omega_2 \pi}{KL} \sqrt{EI_y GJ + \left(\frac{\pi E}{KL}\right)^2 I_y C_w}$$

$$M_{cr} = \frac{2.134 \cdot \pi}{2 \cdot 2512} \sqrt{200E3 \cdot 4.1E6 \cdot 7.7E4 \cdot 108E3 + \left(\frac{\pi \cdot 200E3}{2 \cdot 2512}\right)^2 \cdot 4.1E6 \cdot 155E9} = 172.75 \text{ kN m}$$

$$M_{cr} \geq 0.67 \cdot M_p = 0.67(718E3)(355) = 170.78 \text{ kN m}$$

$$\therefore M_r = 1.15\phi M_p \left(1 - \frac{0.28M_p}{M_{cr}}\right) = 1.15 \cdot 0.9 \cdot 254.89 \left(1 - \frac{0.28 \cdot 254.89}{172.75}\right) = 153.54 \text{ kN m}$$

$$\therefore M_r = 154 \text{ kN m}$$

**E.3.3 CSA S16-09****Section classification:**

Same as for SANS 10162-1:2011

**Segment 1:****Bending resistance:**

§13.6

$$\omega_2 = \frac{4M_{max}}{\sqrt{M_{max}^2 + 4M_a^2 + 7M_b^2 + 4M_c^2}}$$

$$\omega_2 = \frac{4 \cdot 17.51}{\sqrt{17.51^2 + 4 \cdot 16.9^2 + 7 \cdot 15.93^2 + 4 \cdot 14.98^2}} = 1.090 \leq 2.5$$

$$M_{cr} = \frac{\omega_2 \pi}{KL} \sqrt{EI_y GJ + \left(\frac{\pi E}{KL}\right)^2 I_y C_w}$$

$$M_{cr} = \frac{1.09 \cdot \pi}{2512} \sqrt{200E3 \cdot 4.1E6 \cdot 7.7E4 \cdot 108E3 + \left(\frac{\pi \cdot 200E3}{2512}\right)^2 \cdot 4.1E6 \cdot 155E9} = 294.2 \text{ kN m}$$

$$M_{cr} \geq 0.67 \cdot M_p = 0.67(718E3)(355) = 170.78 \text{ kN m}$$

$$\therefore M_r = 1.15\phi M_p \left[1 - \frac{0.28M_p}{M_{cr}}\right]$$

$$\therefore M_r = 1.15 \cdot 0.9 \cdot 254.89 \left[1 - \frac{0.28 \cdot 254.89}{294.2}\right] = 200 \text{ kN m}$$

$$\therefore M_r = 200 \text{ kN m}$$

**Segment 2:****Bending resistance:**

§13.6

$$\omega_2 = \frac{4M_{max}}{\sqrt{M_{max}^2 + 4M_a^2 + 7M_b^2 + 4M_c^2}}$$

$$\omega_2 = \frac{4 \cdot 17.51}{\sqrt{17.51^2 + 4 \cdot 16.3^2 + 7 \cdot 14.51^2 + 4 \cdot 12.78^2}} = 1.184 \leq 2.5$$

$$M_{cr} = \frac{\omega_2 \pi}{KL} \sqrt{EI_y GJ + \left(\frac{\pi E}{KL}\right)^2 I_y C_w}$$

$$M_{cr} = \frac{1.184 \cdot \pi}{2512} \sqrt{200E3 \cdot 4.1E6 \cdot 7.7E4 \cdot 108E3 + \left(\frac{\pi \cdot 200E3}{2512}\right)^2 \cdot 4.1E6 \cdot 155E9} = 319.58 \text{ kN m}$$

$$M_{cr} \geq 0.67 \cdot M_p = 0.67(718E3)(355) = 170.78 \text{ kN m}$$

$$\therefore M_r = 1.15 \phi M_p \left[ 1 - \frac{0.28 M_p}{M_{cr}} \right]$$

$$\therefore M_r = 1.15 \cdot 0.9 \cdot 254.89 \left[ 1 - \frac{0.28 \cdot 254.89}{319.58} \right] = 205 \text{ kN m}$$

$$\therefore M_r = 205 \text{ kN m}$$

**Segment 3:****Bending resistance:**

§13.6

$$\omega_2 = \frac{4M_{max}}{\sqrt{M_{max}^2 + 4M_a^2 + 7M_b^2 + 4M_c^2}}$$

$$\omega_2 = \frac{4 \cdot 32.84}{\sqrt{32.84^2 + 4 \cdot 2.83^2 + 7 \cdot 5.84^2 + 4 \cdot 19.08^2}} = 2.48 \leq 2.5$$

$$M_{cr} = \frac{\omega_2 \pi}{KL} \sqrt{EI_y GJ + \left(\frac{\pi E}{KL}\right)^2 I_y C_w}$$

$$M_{cr} = \frac{2.48 \cdot \pi}{2 \cdot 2512} \sqrt{200E3 \cdot 4.1E6 \cdot 7.7E4 \cdot 108E3 + \left(\frac{\pi \cdot 200E3}{2 \cdot 2512}\right)^2 \cdot 4.1E6 \cdot 155E9} = 200.76 \text{ kN m}$$

$$M_{cr} \geq 0.67 \cdot M_p = 0.67(718E3)(355) = 170.78 \text{ kN m}$$

$$\therefore M_r = 1.15 \phi M_p \left[ 1 - \frac{0.28 M_p}{M_{cr}} \right]$$

$$\therefore M_r = 1.15 \cdot 0.9 \cdot 254.89 \left[ 1 - \frac{0.28 \cdot 254.89}{200.76} \right] = 170 \text{ kN m}$$

$$\therefore M_r = 170 \text{ kN m}$$

**E.3.4 AISC 360-05****Section classification:**

Table B4.1

$$\text{Flanges: } \left[ \frac{141.8}{2 \cdot 8.6} = 8.24 \right] \leq \left[ 0.38 \sqrt{\frac{200E3}{355}} = 9.02 \right]$$

$$\text{Web: } \left[ \frac{360}{6.3} = 57.14 \right] \leq \left[ 3.76 \sqrt{\frac{200E3}{355}} = 89.2 \right]$$

∴ Compact section

**Segment 1:****Bending resistance:**

Chapter F.2

$$L_b = 2512 \text{ mm}$$

$$L_p = 1.76 r_y \sqrt{\frac{E}{f_y}} = 1.76 \cdot 28.9 \cdot \sqrt{\frac{200E3}{355}} = 1207 \text{ mm}$$

$$r_{ts}^2 = \frac{\sqrt{I_y C_w}}{Z_x} = \frac{\sqrt{4.1E6 \cdot 155E9}}{625E3} = 1275 \Rightarrow r_{ts} = 35.71$$

$$L_r = 1.95 r_{ts} \frac{E}{0.7 f_y} \sqrt{\frac{J}{Z_x h_0}} \sqrt{1 + \sqrt{1 + 6.76 \left( \frac{0.7 f_y}{E} \cdot \frac{Z_x h_0}{J} \right)^2}}$$

$$L_r = 1.95 \cdot 35.71 \cdot \frac{200E3}{0.7 \cdot 355} \sqrt{\frac{108E3}{625E3 \cdot 389}} \sqrt{1 + \sqrt{1 + 6.76 \left( \frac{0.7 \cdot 355}{200E3} \cdot \frac{625E3 \cdot 389}{108E3} \right)^2}} = 3411 \text{ mm}$$

$$L_p \leq L_b \leq L_r$$

$$C_b = \frac{12.5 M_{max}}{2.5 M_{max} + 3 M_a + 4 M_b + 3 M_c}$$

$$C_b = \frac{12.5 \cdot 17.51}{2.5 \cdot 17.51 + 3 \cdot 16.9 + 4 \cdot 15.93 + 3 \cdot 14.98} = 1.077$$

$$M_n = C_b \left[ M_p - (M_p - 0.7 f_y Z_e) \left( \frac{L_b - L_p}{L_r - L_p} \right) \right]$$

$$M_n = 1.077 \left[ 255E6 - (255E6 - 0.7 \cdot 355 \cdot 625E3) \left( \frac{2512 - 1207}{3411 - 1207} \right) \right] = 211 \text{ kN m} < M_p$$

$$M_r = 0.9 \cdot 211 = 190 \text{ kN m}$$

∴  $M_r = 190 \text{ kN m}$ **Segment 2:****Bending resistance:**

Chapter F.2

$$L_b = 2512 \text{ mm}$$

$$L_p = 1207 \text{ mm}$$

$$L_r = 3411 \text{ mm}$$

$$L_p \leq L_b \leq L_r$$

$$C_b = \frac{12.5M_{max}}{2.5M_{max} + 3M_a + 4M_b + 3M_c}$$

$$C_b = \frac{12.5 \cdot 17.51}{2.5 \cdot 17.51 + 3 \cdot 16.3 + 4 \cdot 14.51 + 3 \cdot 12.78} = 1.158$$

$$M_n = C_b \left[ M_p - (M_p - 0.7f_y Z_e) \left( \frac{L_b - L_p}{L_r - L_p} \right) \right]$$

$$M_n = 1.158 \left[ 255E6 - (255E6 - 0.7 \cdot 355 \cdot 625E3) \left( \frac{2512 - 1207}{3411 - 1207} \right) \right] = 227 \text{ kN m} < M_p$$

$$M_r = 0.9 \cdot 277 = 204 \text{ kN m}$$

$$\therefore M_r = 204 \text{ kN m}$$

### Segment 3:

#### **Bending resistance:**

Chapter F.2

$$L_b = 5024 \text{ mm}$$

$$L_p = 1207 \text{ mm}$$

$$L_r = 3411 \text{ mm}$$

$$L_b \geq L_r$$

$$C_b = \frac{12.5M_{max}}{2.5M_{max} + 3M_a + 4M_b + 3M_c}$$

$$C_b = \frac{12.5 \cdot 32.84}{2.5 \cdot 32.84 + 3 \cdot 2.83 + 4 \cdot 5.84 + 3 \cdot 19.08} = 2.398$$

$$F_{cr} = \frac{C_b \pi^2 E}{\left( \frac{L_b}{r_{ts}} \right)^2} \sqrt{1 + 0.078 \frac{J}{Z_x h_0} \left( \frac{L_b}{r_{ts}} \right)^2}$$

$$F_{cr} = \frac{2.398 \cdot \pi^2 \cdot 200E3}{\left( \frac{5024}{35.71} \right)^2} \sqrt{1 + 0.078 \frac{108E3}{625E3 \cdot 389} \left( \frac{5024}{35.71} \right)^2} = 310.05 \text{ MPa}$$

$$M_u = F_{cr} Z_x = 310.05 \cdot 625E3 = 194.06 \text{ kN m} < M_p$$

$$M_r = 0.9 \cdot 194.06 = 175 \text{ kN m}$$

$$\therefore M_r = 175 \text{ kN m}$$

**E.3.5 EN 1993-1-1****Section classification:**

Table 5.2

$$\varepsilon = \sqrt{\frac{235}{355}} = 0.8136$$

$$\text{Outstand flange: } c = \frac{b - 2r - t_w}{2} = \frac{141.8 - 2 \cdot 10.2 - 16.5}{2} = 57.55 \text{ mm}$$

$$\frac{c}{b_f} = \frac{57.55}{8.6} = 6.69 \leq [9\varepsilon = 9 \cdot 0.8136 = 7.3224]$$

Internal compression part:  $c = h_w = 360$ 

$$\frac{c}{t_w} = \frac{360}{6.3} = 57.14 \leq [72\varepsilon = 72 \cdot 0.8136 = 58.58]$$

∴ Class 1

**Partial factors:**

Note B2, p.45

$$\gamma_{m0} = 1.00$$

$$\gamma_{m1} = 1.00$$

**Section 1: Lateral-torsional buckling resistance:**

SN003a-EN-EU

$$M_{cr} = \frac{C_1 \pi^2 E I_y}{(kL)^2} \sqrt{\frac{C_w}{I_y} + \frac{L^2 G J}{\pi^2 E I_y}}$$

$$M_{cr} = \frac{1.12 \cdot \pi^2 \cdot 200E3 \cdot 4.1E6}{(2512)^2} \sqrt{\frac{155E9}{4.1E6} + \frac{2512^2 \cdot 7.7E4 \cdot 108E3}{\pi^2 \cdot 200E3 \cdot 4.1E6}} = 302.3 \text{ kN m}$$

§6.3.2.3

$$\text{Non-dimensional slenderness: } \bar{\lambda}_{LT} = \sqrt{\frac{W_y f_y}{M_{cr}}} = \sqrt{\frac{718E3 \cdot 355}{302.3E6}} = 0.918$$

Imperfection factor:  $\frac{h}{b} \leq 2$  ∴ Buckling curve c  $\Rightarrow \alpha_{LT} = 0.49$ 

$$\Phi_{LT} = 0.5[1 + \alpha_{LT}(\bar{\lambda}_{LT} - \bar{\lambda}_{LT,0}) + \beta \bar{\lambda}_{LT}^2]; \text{ with } \beta = 0.75 \text{ and } \bar{\lambda}_{LT,0} = 0.4$$

$$\Phi_{LT} = 0.5[1 + 0.49(0.918 - 0.4) + 0.75 \cdot 0.918^2] = 0.943$$

$$\chi_{LT} = \frac{1}{\Phi_{LT} + \sqrt{\Phi_{LT}^2 - \beta \bar{\lambda}_{LT}^2}} = \frac{1}{0.943 + \sqrt{0.943^2 - 0.75 \cdot 0.918^2}} = 0.6896$$

$$f = 1 - 0.5(1 - k_c)[1 - 2.0(\bar{\lambda}_{LT} - 0.8)^2] = 1 - 0.5(1 - 0.91)[1 - 2.0(0.918 - 0.8)^2] = 0.955 \leq 1.0$$

$$\chi_{LT,mod} = \frac{\chi_{LT}}{f} = \frac{0.6896}{0.955} = 0.721$$

$$M_{b,Rd} = \chi_{LT,mod} W_{pl,y} \frac{f_y}{\gamma_{m1}} = 0.721 \cdot 718E3 \cdot 355 = 184 \text{ kN m}$$

$$\therefore M_r = 184 \text{ kN m}$$

**Section 2: Lateral-torsional buckling resistance:**

SN003a-EN-EU

$$M_{cr} = \frac{C_1 \pi^2 EI_y}{(kL)^2} \sqrt{\frac{C_w}{I_y} + \frac{L^2 GJ}{\pi^2 EI_y}}$$

$$M_{cr} = \frac{1.22 \cdot \pi^2 \cdot 200E3 \cdot 4.1E6}{(2512)^2} \sqrt{\frac{155E9}{4.1E6} + \frac{2512^2 \cdot 7.7E4 \cdot 108E3}{\pi^2 \cdot 200E3 \cdot 4.1E6}} = 329.29 \text{ kN m}$$

§6.3.2.3

$$\text{Non-dimensional slenderness: } \bar{\lambda}_{LT} = \sqrt{\frac{W_y f_y}{M_{cr}}} = \sqrt{\frac{718E3 \cdot 355}{329.29E6}} = 0.880$$

$$\text{Imperfection factor: } \frac{h}{b} \leq 2 \therefore \text{Buckling curve c} \Rightarrow \alpha_{LT} = 0.49$$

$$\Phi_{LT} = 0.5[1 + \alpha_{LT}(\bar{\lambda}_{LT} - \bar{\lambda}_{LT,0}) + \beta \bar{\lambda}_{LT}^2]; \text{ with } \beta = 0.75 \text{ and } \bar{\lambda}_{LT,0} = 0.4$$

$$\Phi_{LT} = 0.5[1 + 0.49(0.880 - 0.4) + 0.75 \cdot 0.880^2] = 0.908$$

$$\chi_{LT} = \frac{1}{\Phi_{LT} + \sqrt{\Phi_{LT}^2 - \beta \bar{\lambda}_{LT}^2}} = \frac{1}{0.908 + \sqrt{0.908^2 - 0.75 \cdot 0.880^2}} = 0.7135$$

$$f = 1 - 0.5(1 - k_c)[1 - 2.0(\bar{\lambda}_{LT} - 0.8)^2] = 1 - 0.5(1 - 0.91)[1 - 2.0(0.880 - 0.8)^2] = 0.956 \leq 1.0$$

$$\chi_{LT,mod} = \frac{\chi_{LT}}{f} = \frac{0.7135}{0.956} = 0.747$$

$$M_{b,Rd} = \chi_{LT,mod} W_{pl,y} \frac{f_y}{\gamma_{m1}} = 0.747 \cdot 718E3 \cdot 355 = 190 \text{ kN m}$$

$$\therefore M_r = 190 \text{ kN m}$$

**Section 3: Lateral-torsional buckling resistance:**

SN003a-EN-EU

$$M_{cr} = \frac{C_1 \pi^2 EI_y}{(kL)^2} \sqrt{\frac{C_w}{I_y} + \frac{L^2 GJ}{\pi^2 EI_y}}$$

$$M_{cr} = \frac{2.42 \cdot \pi^2 \cdot 200E3 \cdot 4.1E6}{(5024)^2} \sqrt{\frac{155E9}{4.1E6} + \frac{5024^2 \cdot 7.7E4 \cdot 108E3}{\pi^2 \cdot 200E3 \cdot 4.1E6}} = 195.9 \text{ kN m}$$

§6.3.2.3

$$\text{Non-dimensional slenderness: } \bar{\lambda}_{LT} = \sqrt{\frac{W_y f_y}{M_{cr}}} = \sqrt{\frac{718E3 \cdot 355}{195.9E6}} = 1.141$$

$$\text{Imperfection factor: } \frac{h}{b} \leq 2 \therefore \text{Buckling curve c} \Rightarrow \alpha_{LT} = 0.49$$

$$\Phi_{LT} = 0.5[1 + \alpha_{LT}(\bar{\lambda}_{LT} - \bar{\lambda}_{LT,0}) + \beta \bar{\lambda}_{LT}^2]; \text{ with } \beta = 0.75 \text{ and } \bar{\lambda}_{LT,0} = 0.4$$

$$\Phi_{LT} = 0.5[1 + 0.49(1.141 - 0.4) + 0.75 \cdot 1.141^2] = 1.17$$

$$\chi_{LT} = \frac{1}{\Phi_{LT} + \sqrt{\Phi_{LT}^2 - \beta \bar{\lambda}_{LT}}} = \frac{1}{1.17 + \sqrt{1.17^2 - 0.75 \cdot 1.141^2}} = 0.557$$

$$f = 1 - 0.5(1 - k_c)[1 - 2.0(\bar{\lambda}_{LT} - 0.8)^2] = 1 - 0.5(1 - 0.91)[1 - 2.0(1.141 - 0.8)^2] = 0.965 \leq 1.0$$

$$\chi_{LT,mod} = \frac{\chi_{LT}}{f} = \frac{0.557}{0.965} = 0.577$$

$$M_{b,Rd} = \chi_{LT,mod} W_{pl,y} \frac{f_y}{\gamma_{m1}} = 0.577 \cdot 718E3 \cdot 355 = 147 \text{ kN m}$$

$$\therefore M_r = 147 \text{ kN m}$$

## Appendix F

# Detail drawings of experimental setup

The following CAD drawings are presented in this appendix:

- DWG 1: TESTING CONFIGURATIONS
- DWG 2: EXPERIMENTAL LAYOUT
- DWG 3: SECTION A-A, INSTRON END SUPPORT, WEIGHT FRAME
- DWG 4: ELEVATION VIEW
- DWG 5: BRACING DETAIL 5
- DWG 6: BRACING DETAIL 1; SWAY FRAME; FLOOR CONNECTION
- DWG 7: BRACING DETAIL 2; BEAM-TO-COLUMN DETAIL
- DWG 8: ROLLER DETAIL; HINGE DETAIL
- DWG 9: BEARING HOUSE DETAIL; BRACING DETAIL 4
- DWG 10: LATERAL END BRACING; ROLLER END DETAIL; LOADING FRAME 2
- DWG 11: LOADING FRAME 1
- DWG 12: BRACING DETAIL 3



DRAWN BY HJW SMALBERGER

DESCRIPTION OF DRAWING

TESTING CONFIGURATIONS

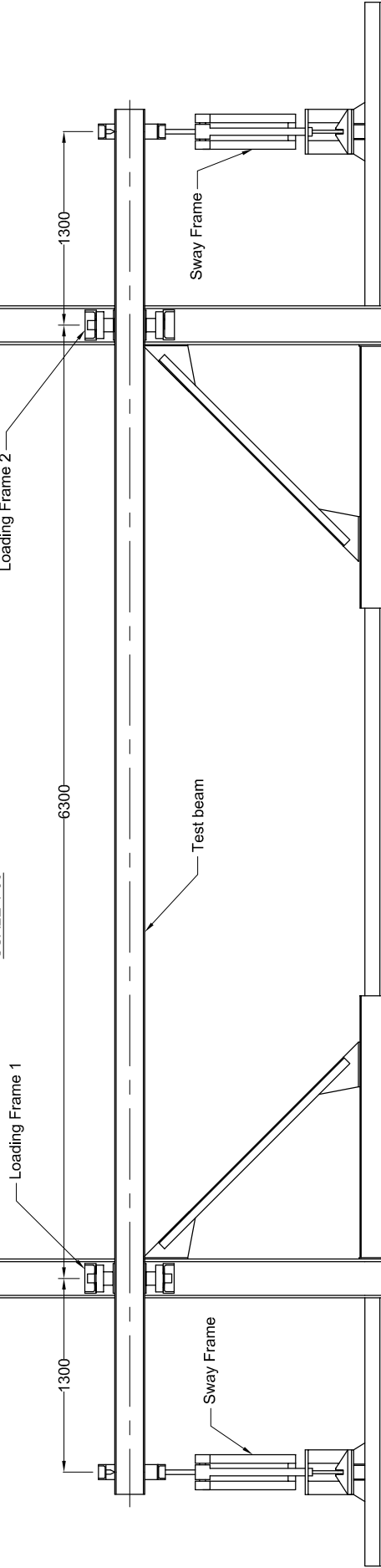
SCALE  
AS SHOWN

A4

DWG No.  
1

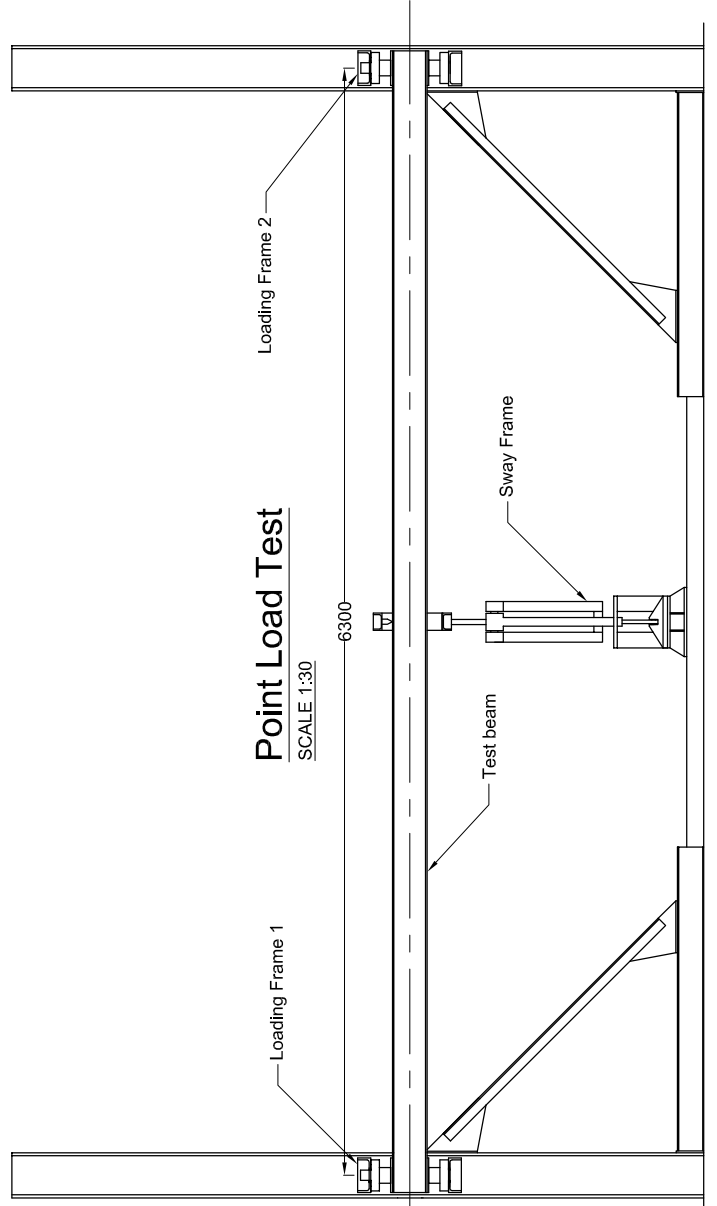
### Uniform Moment Test

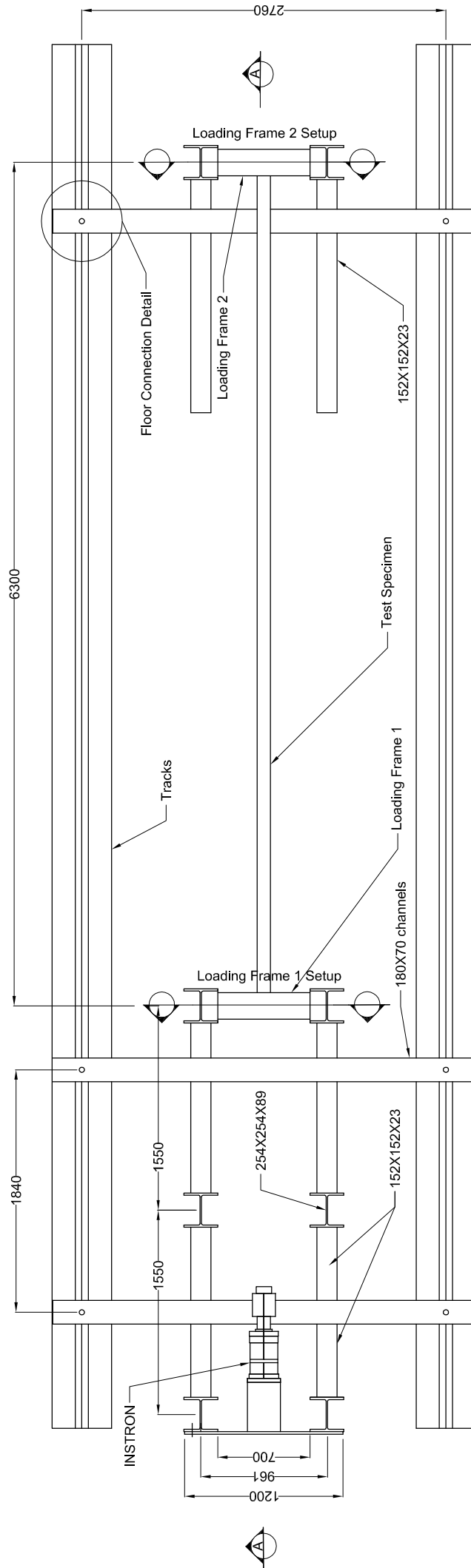
SCALE 1:30



### Point Load Test

SCALE 1:30

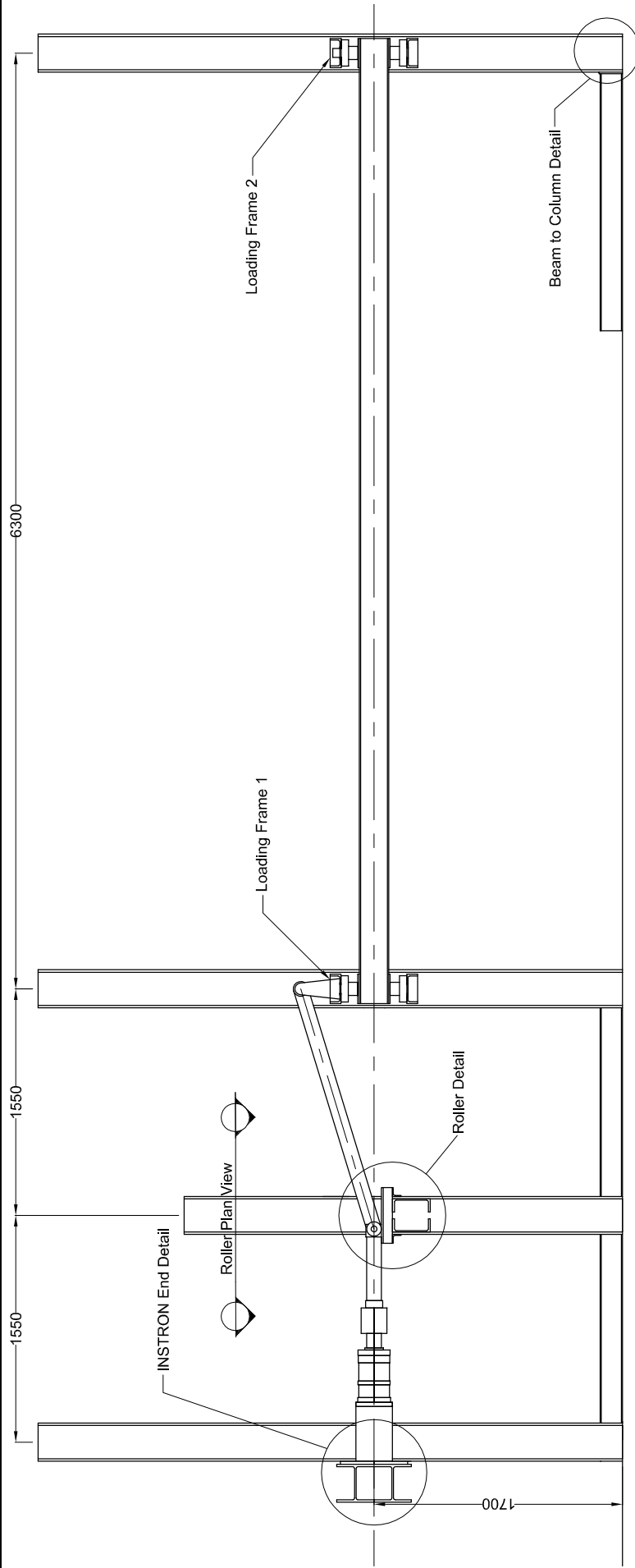




### Experimental Setup Layout

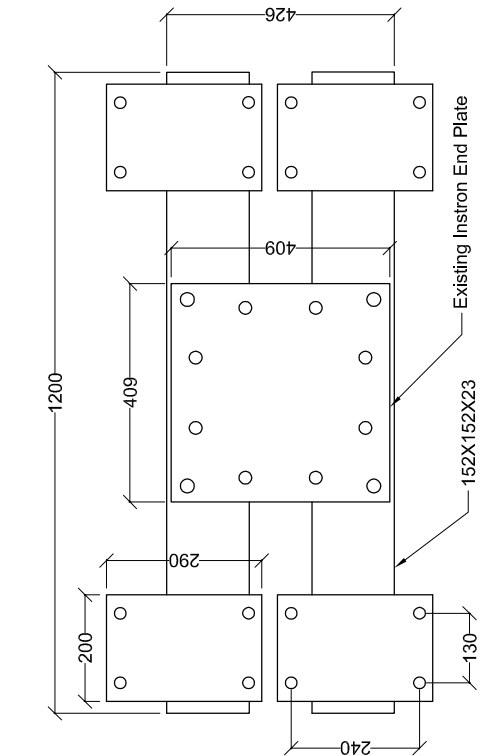
SCALE 1:30

DRAWN BY	H-JW SMALBERGER
DESCRIPTION OF DRAWING	
EXPERIMENTAL LAYOUT	
SCALE	AS SHOWN
SIZE	A4
DWG No.	2



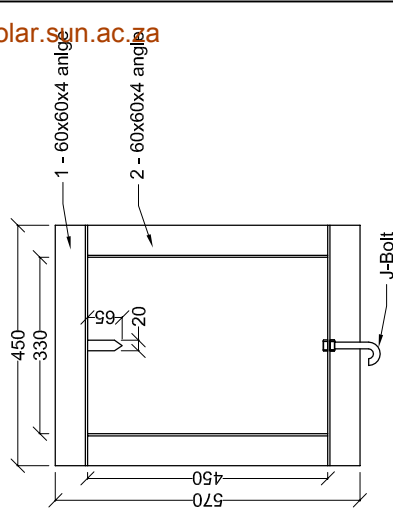
**Section A-A of Experimental Setup Layout**

SCALE 1:30



**INSTRON End Detail**

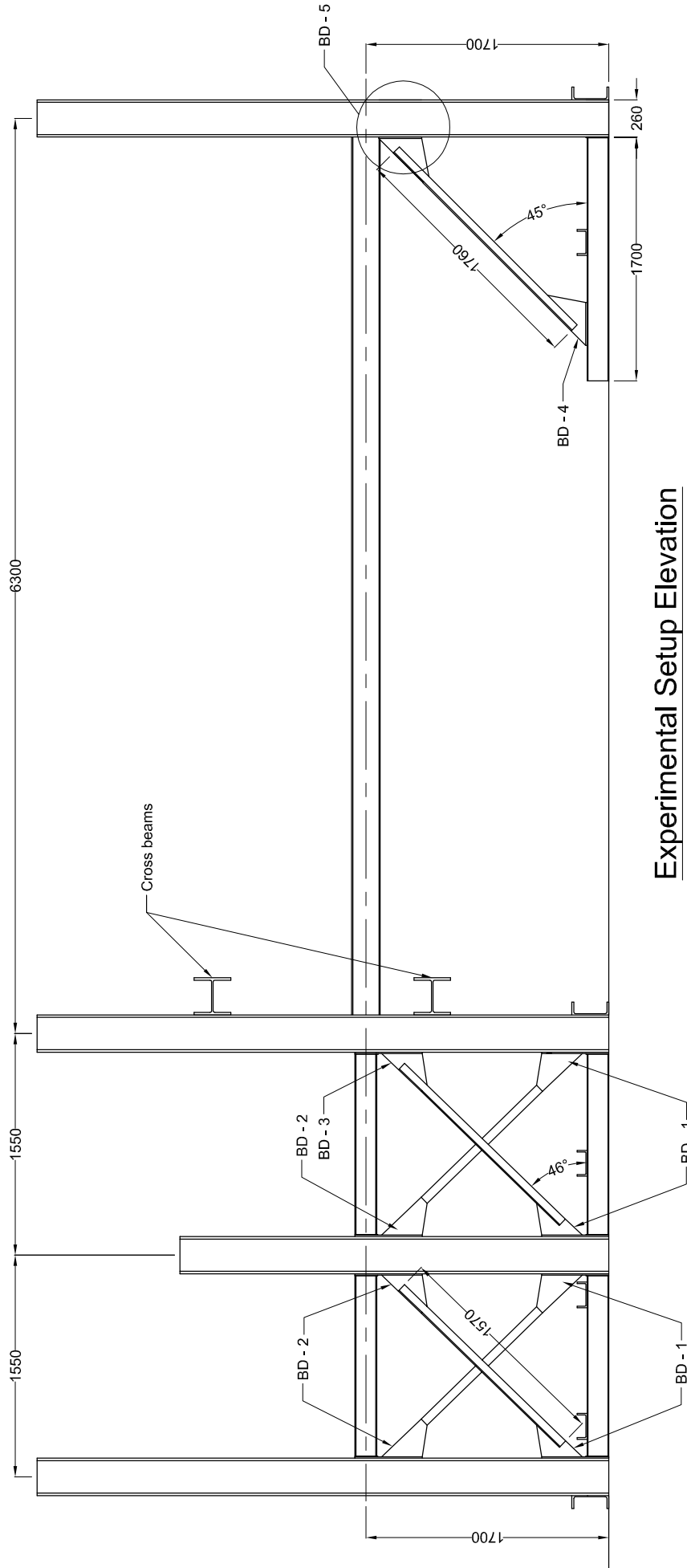
SCALE 1:10



**Lead Weight Frame**

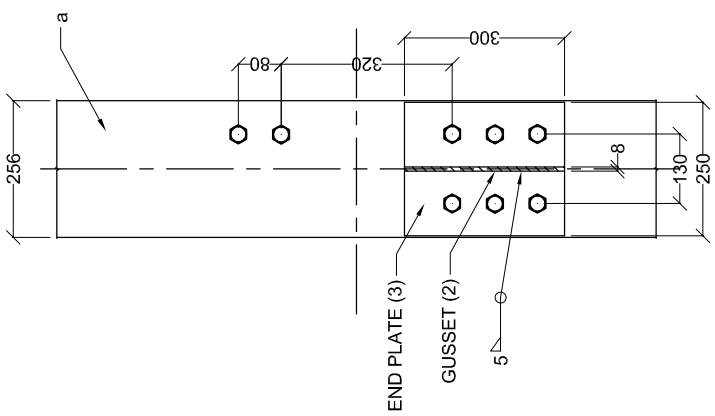
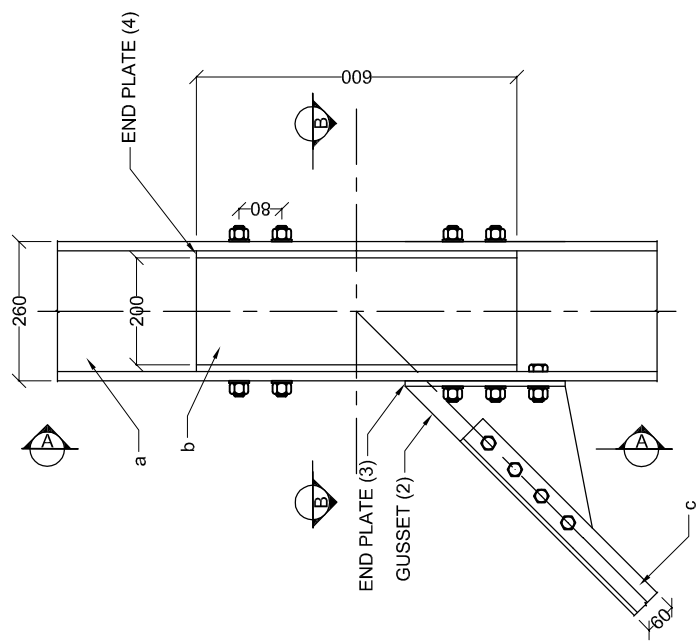
SCALE 1:10

DRAWN	H-JW SMALBERGER
DESCRIPTION OF DRAWING	
SECTION A-A: INSTRON END SUPPORT; WEIGHT FRAME	
SCALE	AS SHOWN
SIZE	A4
DWG No.	3

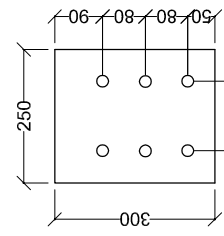


**Experimental Setup Elevation**  
SCALE 1:30

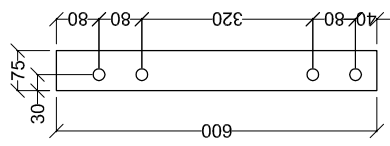
DRAWN BY	HJW SMALBERGER
DESCRIPTION OF DRAWING	ELEVATION VIEW
SCALE	AS SHOWN
SIZE	A4
DWG No.	4



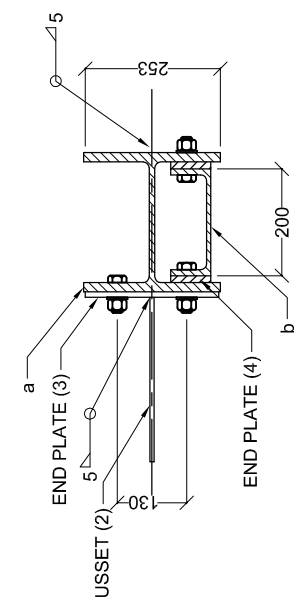
VIEW A-A



END PLATE (3) - 300X250X10



END PLATE (4) - 600X75X10



VIEW B-B

**ELEMENTS:**

- a - 254X254X89
- b - PC200X75
- c - 60X60X8

**NOTES:**

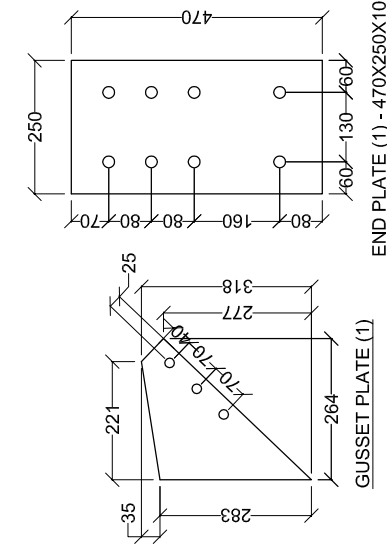
1. (b) is fixed between flanges of (a) to support roller bearings for loading frame, refer to Loading Frame 2.
2. End plate (4) fill space between flanges of (b) and flanges of (a).
3. End plate (3) that supports Gusset (2) is fixed to (a).
4. (c), bracing element, is fixed to Gusset (2) with X4 M16 8.8 bolts.
5. All bolts used to fixed elements to (a) is M20 8.8 bolts.
6. All welds are 5mm fillet welds, unless otherwise specified.
7. All steel is of grade S355JR, unless otherwise specified.

## Bracing Connection Detail 5

SCALE 1:10

DRAWN BY	HJW SMALBERGER
DESCRIPTION OF DRAWING	
BRACING DETAIL 5	
SCALE	AS SHOWN
SIZE	A4
DWG No.	5

DRAWN BY	HJW SMALBERGER
DESCRIPTION OF DRAWING	BRACING DETAIL 1; SWAY FRAME; FLOOR CONNECTION
SCALE	AS SHOWN
SIZE	A4
DWG No.	6



**END PLATE (1) - 470X250X10**

**GUSSET PLATE (1)**

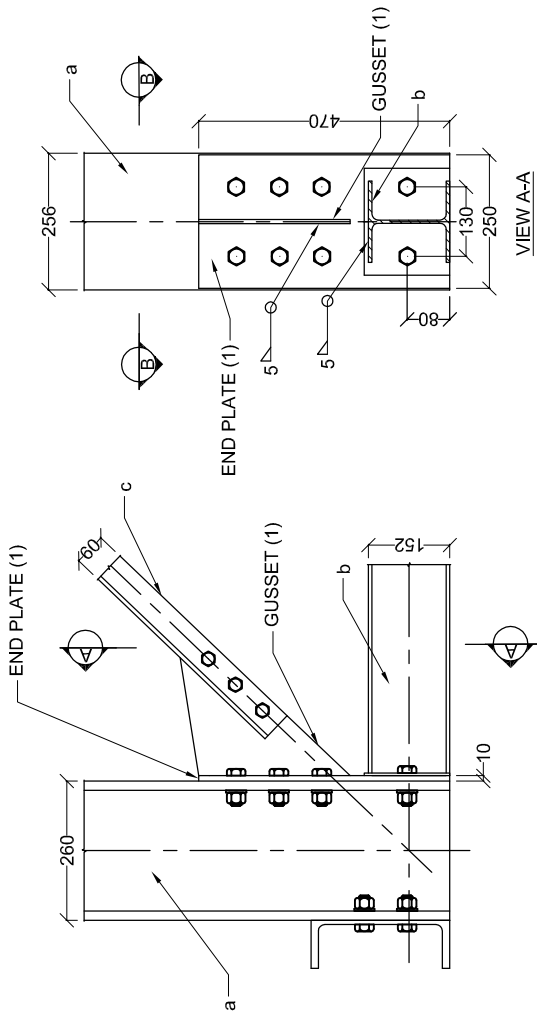
**NOTES:**

- ELEMENTS:**
- a - 254X254X89
  - b - 152X152X23
  - c - 60X60X8

1. (c) is fixed to Gusset (1) using X3 M16 8.8 bolts.
2. Gusset (1) is welded to End plate (1).
3. End plate (1) is bolted to (a) using X8 M20 8.8 bolts.
4. (b) is bolted to End plate (1).
5. All welds are 5mm fillet welds unless otherwise specified.
6. All steel are of grade S355JR unless otherwise specified.

**Bracing Connection Detail 1**

SCALE 1:10



**VIEW A-A**

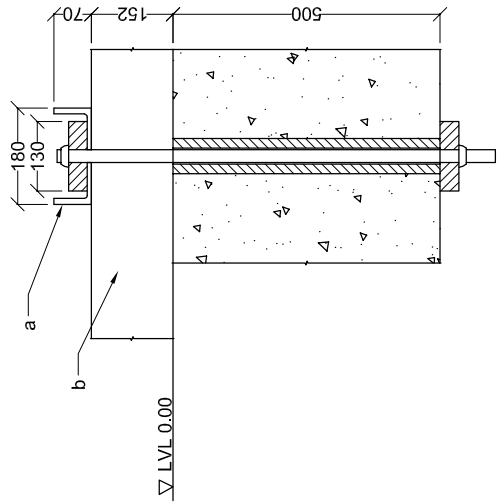
**VIEW B-B**

**NOTES:**

- ELEMENTS:**
- a - PC180X70
  - b - 152X152X23

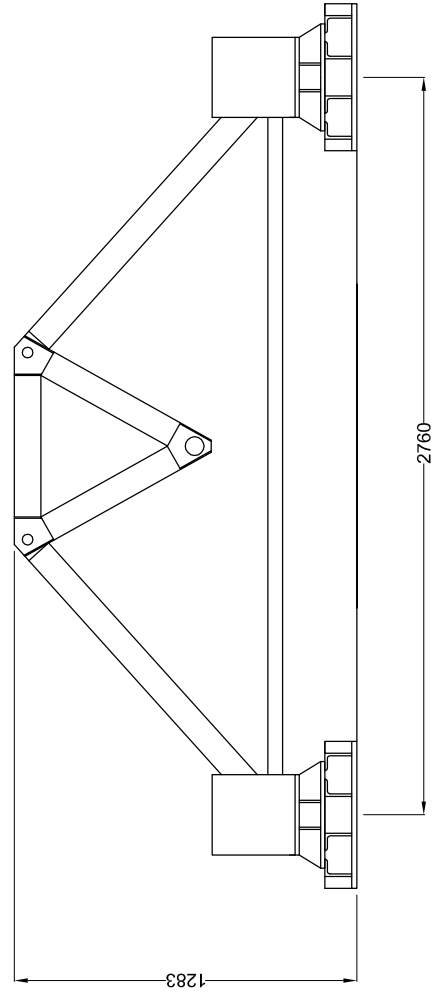
**NOTES:**

1. (a) fixed across on top of (b) on three places, refer to Experimental Setup Layout.
2. Bolts fixed on top of channel and bottom of lab floor.



**Floor Connection Detail**

SCALE 1:10



**Sway Frame**

SCALE 1:20

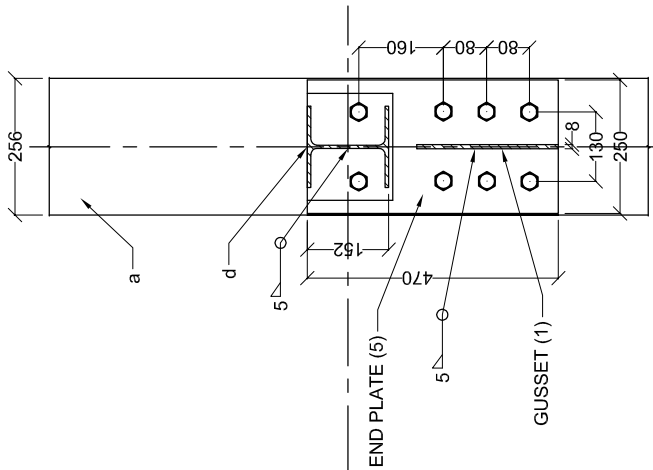
DRAWN BY	HJW SMALBERGER
DESCRIPTION OF DRAWING	BRACING DETAIL 2: BEAM-TO-COLUMN DETAIL
SCALE	AS SHOWN
SIZE	A3
DWG No.	7

**ELEMENTS:**

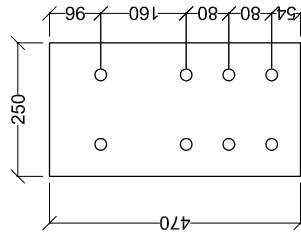
- a - 254X254X89
- c - 60X60X8
- d - 152X1452X23

**NOTES:**

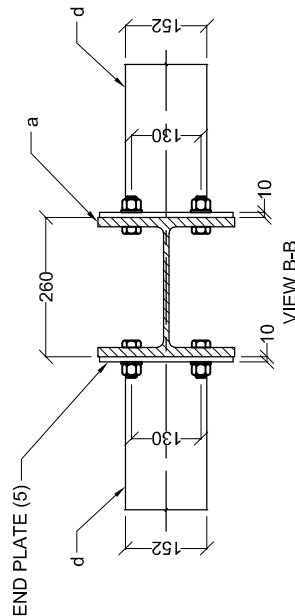
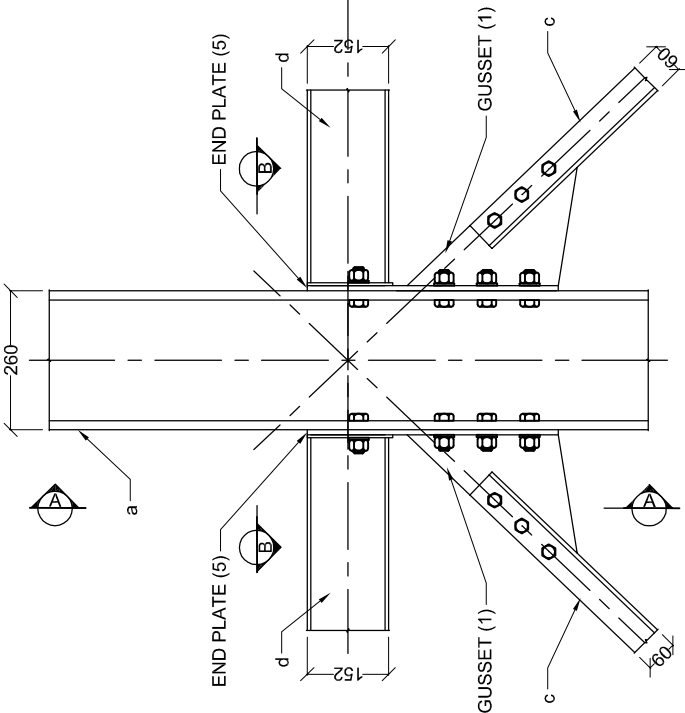
1. End plate (5) is fixed to (a) using X8 M20 8.8 bolts.
2. (d) is welded to End plate (5).
3. Gusset (1) is welded to End plate (5).
4. (c) is fixed to Gusset (1) using X3 M16 8.8 bolts.
5. All welds are 5mm fillet welds, unless otherwise specified.
6. All steel are of grade S355JR.



VIEW A-A



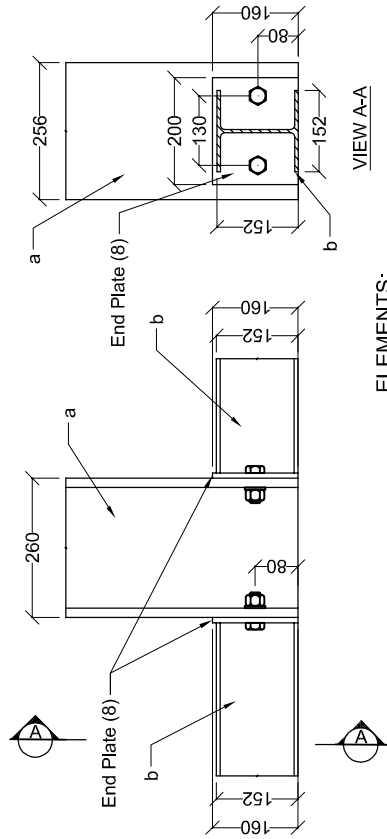
END PLATE (5) - 470X250X10



VIEW B-B

**Bracing Connection Detail 2**

SCALE 1:10



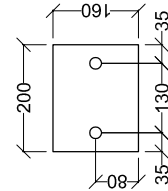
VIEW A-A

**ELEMENTS:**

- a - 254X254X89
- b - 152X1452X23

**NOTES:**

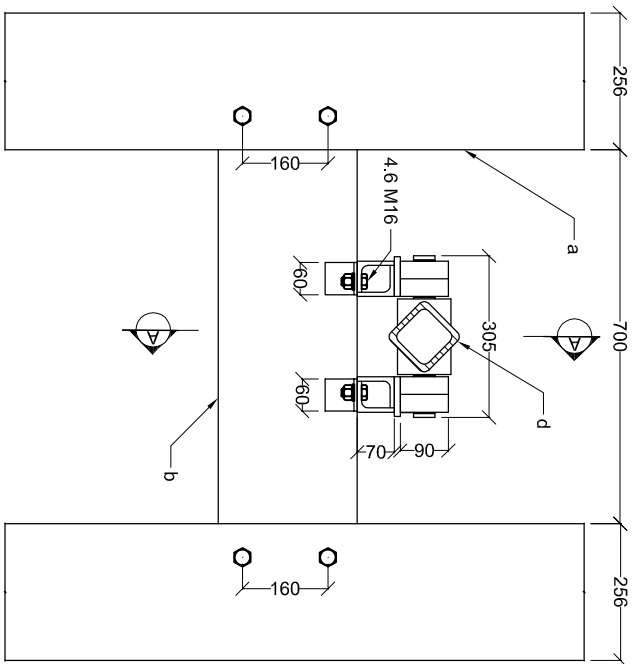
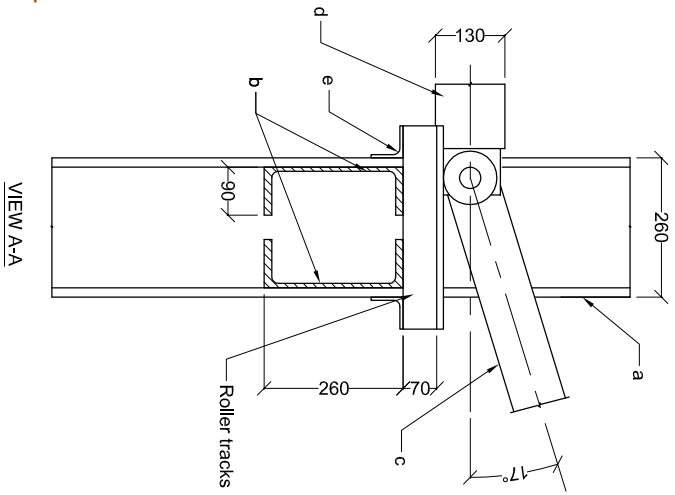
1. (b) is welded to End Plate (8).
2. End plate (8) is bolted to (a) using X2 M20 8.8 bolts.
3. All welds are 5mm fillet welds, unless otherwise specified.
4. All steel is of grade S355JR, unless otherwise specified.



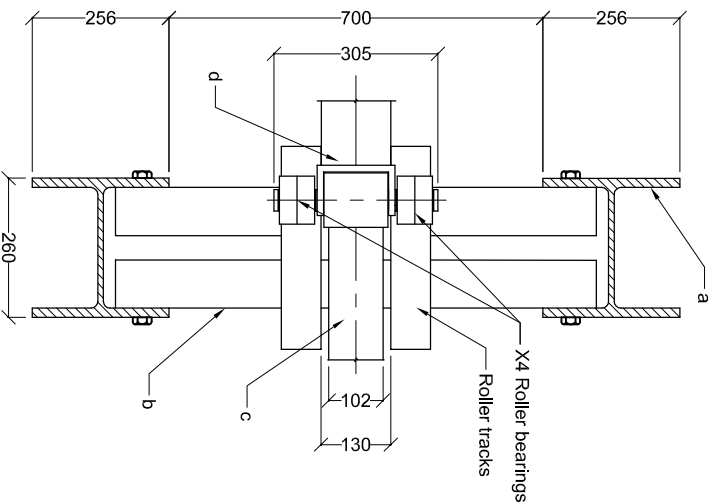
End Plate (8) - 200X160X10

**Beam to Column Detail**

SCALE 1:10



**Roller Detail**  
SCALE 1:10



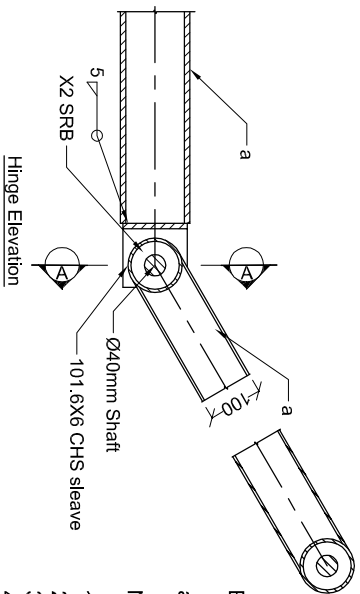
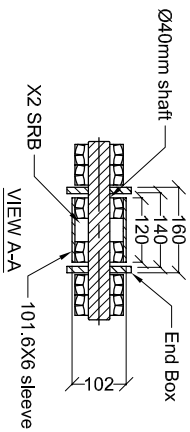
Roller Plan View

**ELEMENTS:**

- a - 254X254X89
- b - PC260X90
- c - 101.6X6 CHS
- d - 100X100X10 SHS
- e - 60X60X6 L

**NOTES:**

1. (b) is fixed to (a) using X4 M20 8.8 bolts.
2. Support angles are welded to (b).
3. Roller tracks are bolted to angles.
4. Spherical Roller Bearing (SRB) is kept in place using circlips.
5. All welds are 5mm fillet welds, unless otherwise specified.
6. All steel is of grade S355JR, unless otherwise specified.
7. SRB: 22308E



**Hinge Connection**

SCALE 1:10

**ELEMENTS:**

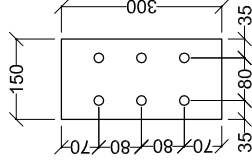
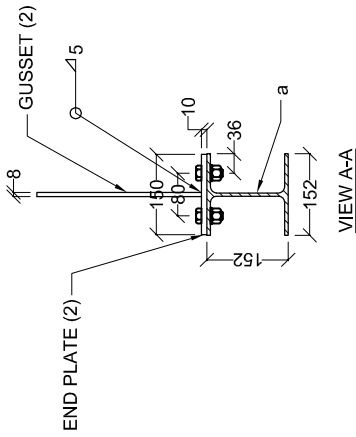
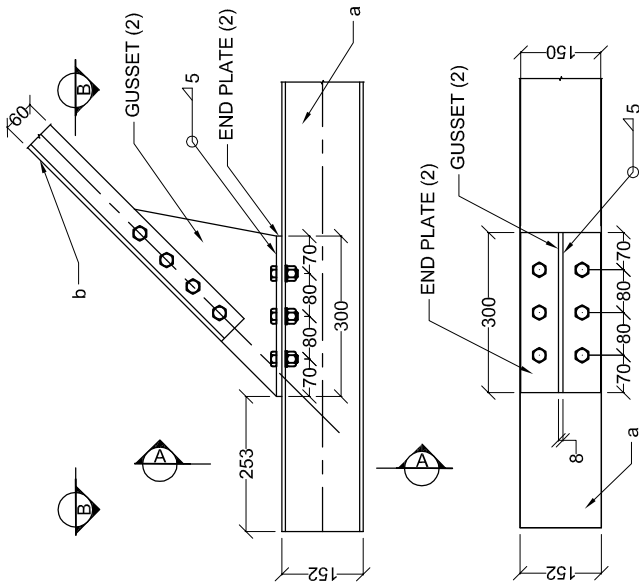
- a - 100X100X6 SHS

**NOTES:**

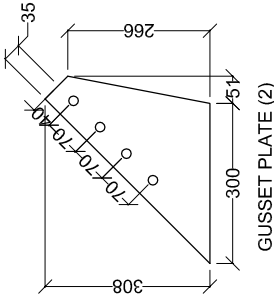
1. All welds 5mm fillet welds, unless specified otherwise.
2. Pin and bearings are positioned with circlips.
3. Spherical Bearings (SRB): 22308 E
4. (a) welded to back of End Box.
5. All steel of grade S355JR, unless otherwise specified.

DRAWN BY	HJW SMALBERGER
DESCRIPTION OF DRAWING	ROLLER DETAIL: HINGE DETAIL
SCALE	AS SHOWN
SIZE	A4
DWG No.	8





END PLATE (2) - 300X150X10



GUSSET PLATE (2)

NOTES:

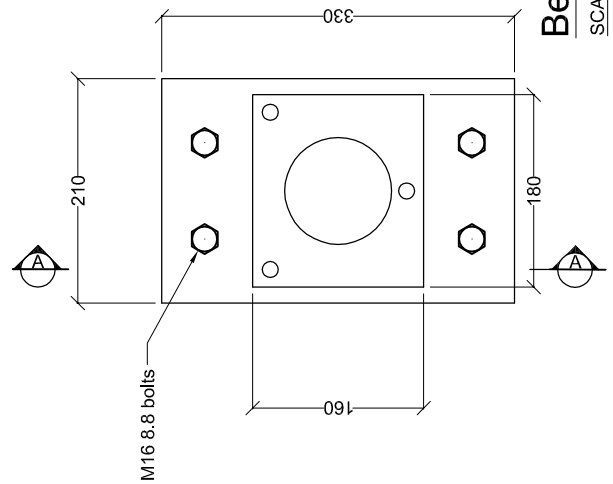
1. (b) is fixed to Gusset (2) using X4 M16 8.8 bolts.
2. Gusset (2) is welded to End plate (2).
3. End plate (2) is bolted to (a) using X6 M16 8.8 bolts.
4. All welds are 5mm fillet welds, unless otherwise specified.
5. All steel is of grade S355JR, unless otherwise specified.

ELEMENTS:

- a - 152X152X23
- b - 60X60X8

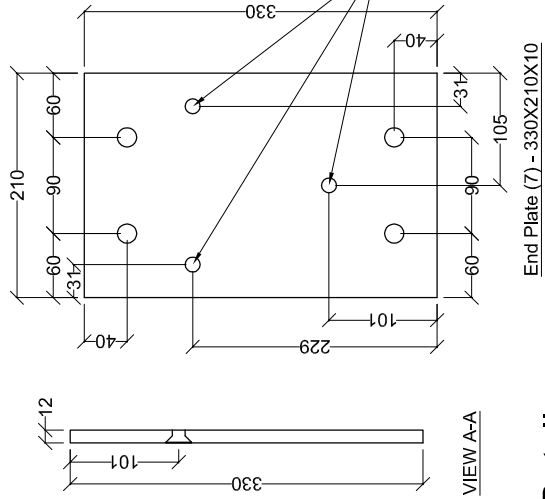
**Bracing Connection Detail 4**

SCALE 1:10



**Bearing House Detail**

SCALE 1:5



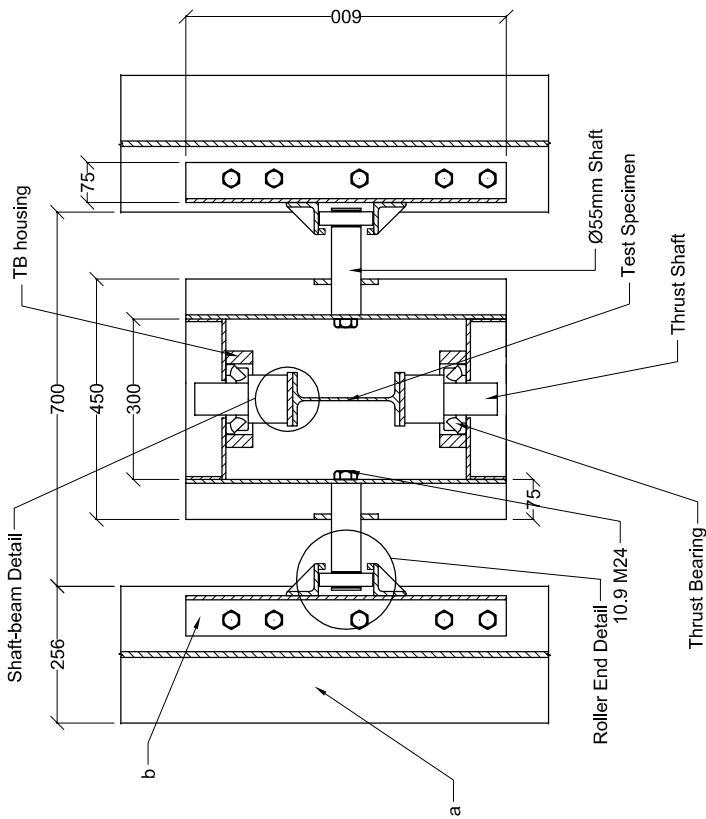
End Plate (7) - 330X210X10

NOTES:

1. Bearing housing appropriate for 22211E bearing with 55mm shaft.
2. Housing is fixed to End plate (7) using countersunk bolts.
3. Countersunk bolts: X3 M12 10.9.
4. End plate (7) is fixed to PC200X75 using X4 M16 8.8 bolts.
5. Refer to loading frame 1 for further information.

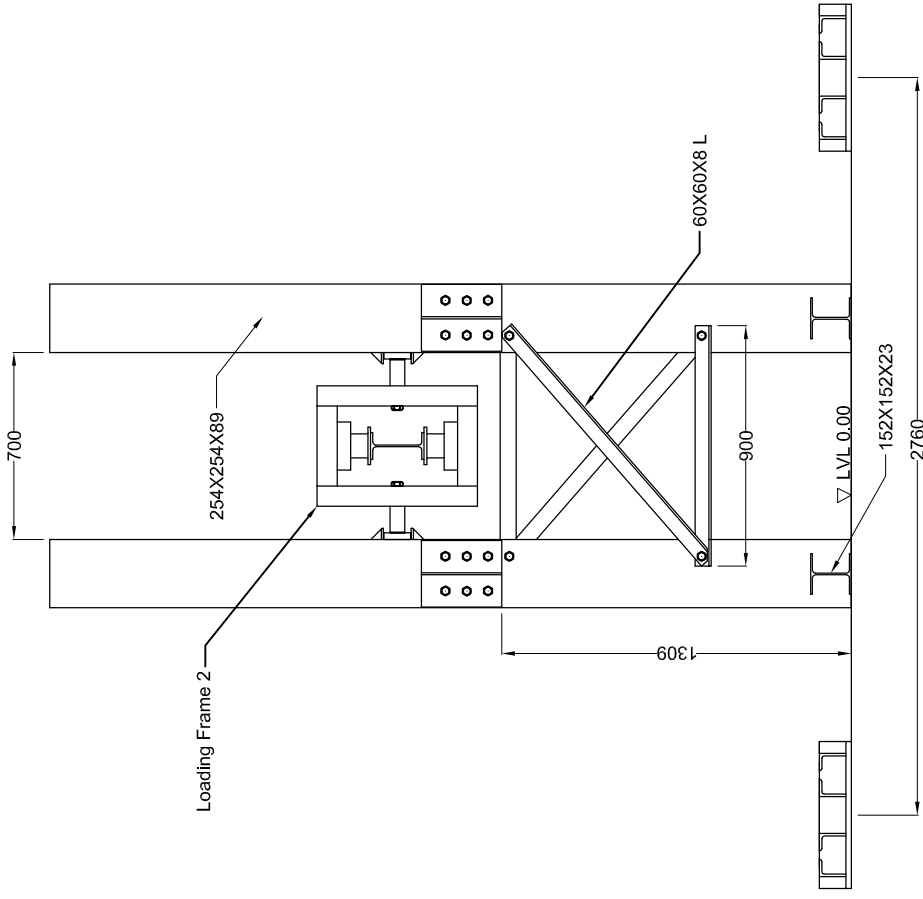
Holes for countersunk screws

DRAWN BY	HJW SMALBERGER
DESCRIPTION OF DRAWING	BEARING HOUSE DETAIL; BRACING DETAIL 4
SCALE	AS SHOWN
SIZE	A4
DWG No.	9



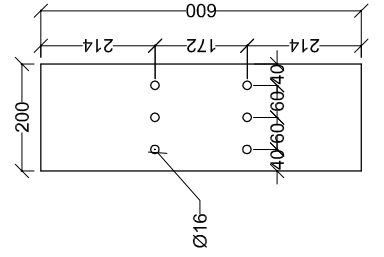
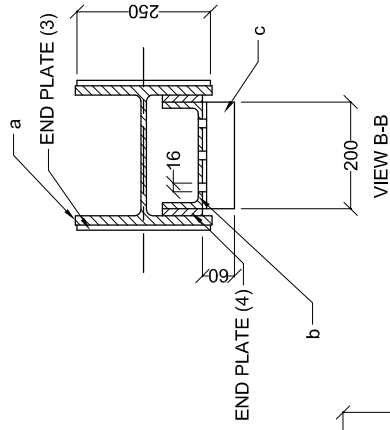
**Loading Frame 2 Setup**

SCALE 1:10



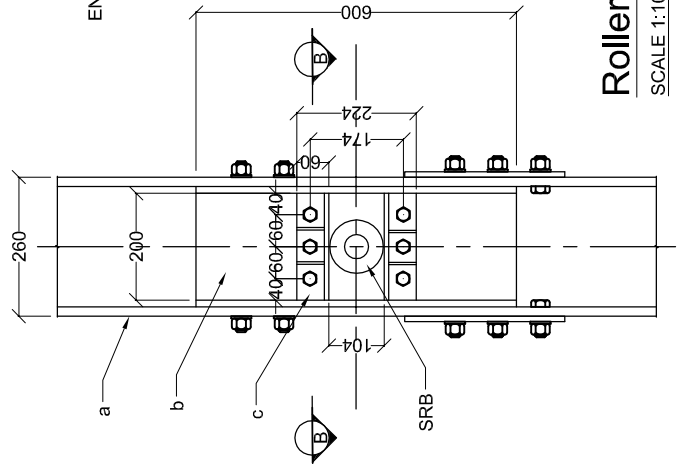
**Lateral Bracing at End**

SCALE 1:20

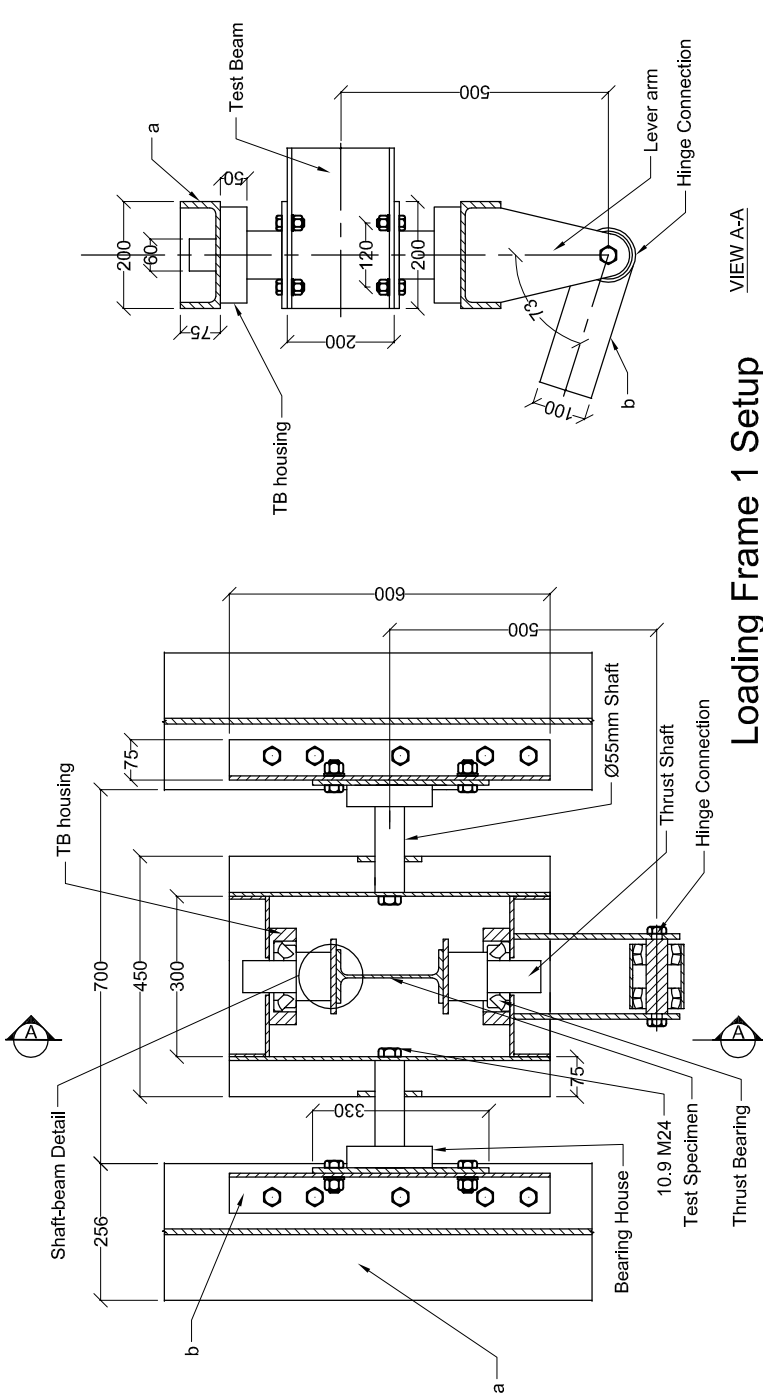


**Roller End Detail**

SCALE 1:10



DRAWN BY	HJW SMALBERGER
DESCRIPTION OF DRAWING	LATERAL END BRACING; ROLLER END DETAIL; LOADING FRAME 2
SCALE	AS SHOWN
SIZE	A4
DWG No.	10



**ELEMENTS:**

- a - 254X254X89
- b - PC200X75

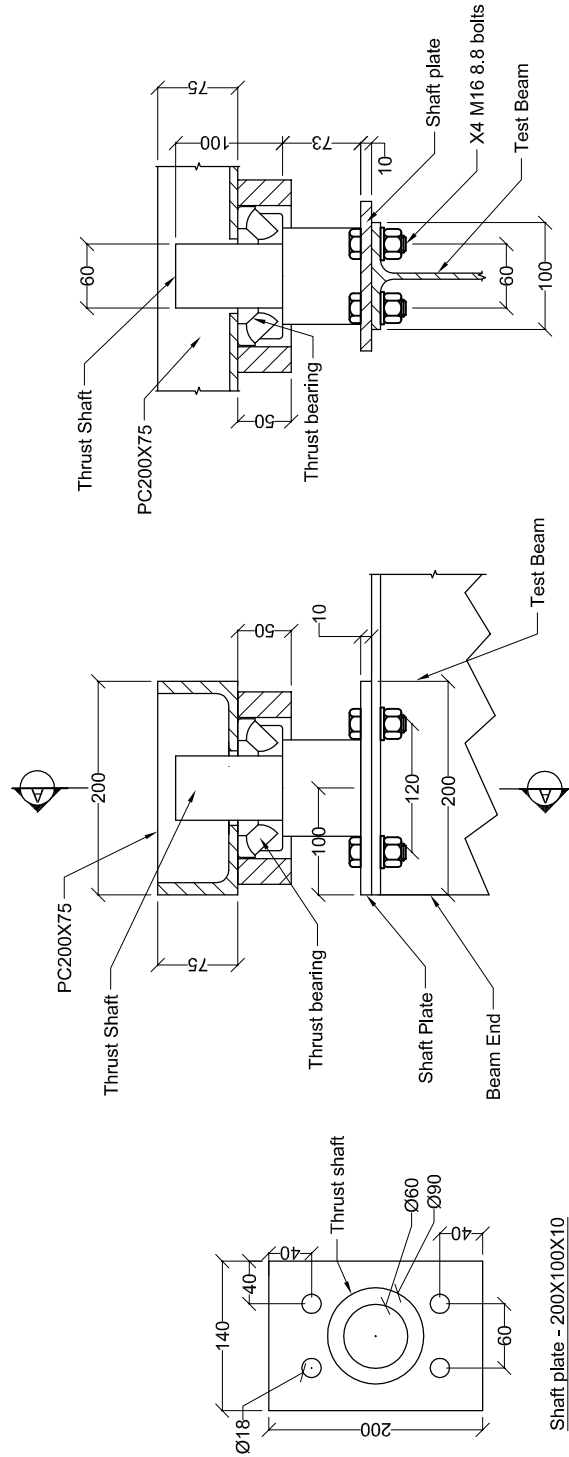
**NOTES:**

1. For connection of (b) to (a), refer to Bracing Detail 3.
2. Test beam is supported by shaft-beam connection.
3. Frame channels are bolted together using X8 M20 8.8 bolts.
4. Bearing house is fixed to channel, refer to Bracing Detail 3.
5. Thrust Bearing (TB) housing is constructed from 180X180X50 steel block.
6. All steel is of grade S355JR, unless otherwise specified.

VIEW A-A

**Loading Frame 1 Setup**

SCALE 1:10



**Shaft-beam Detail**

SCALE 1:5

VIEW A-A

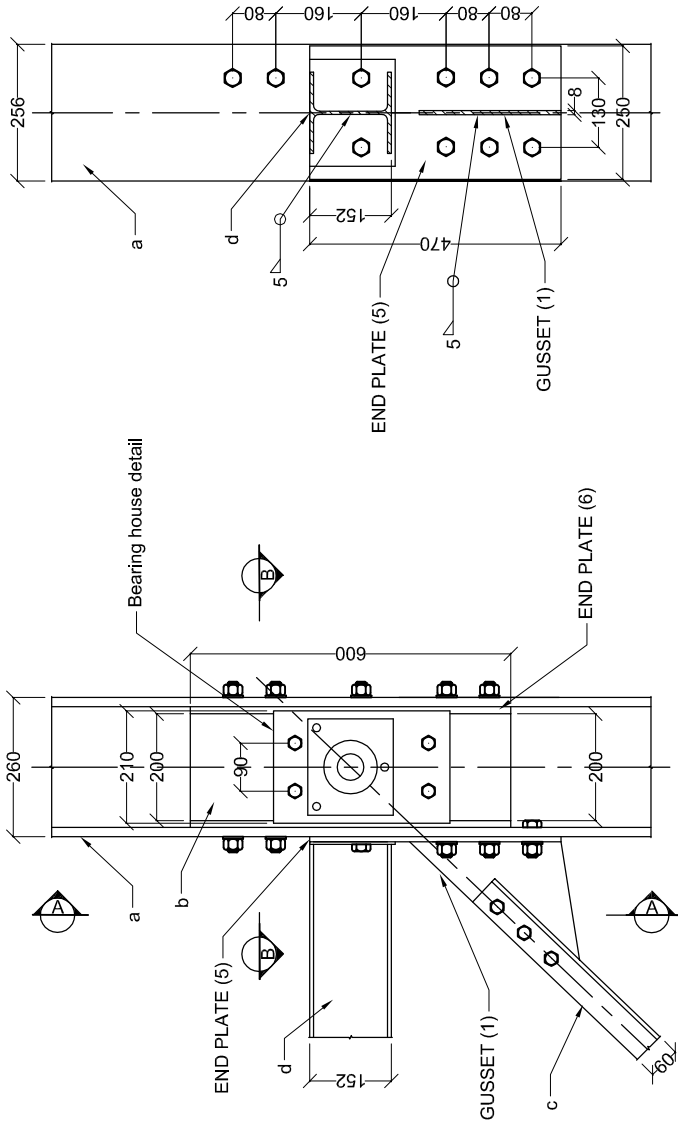
DRAWN BY	HJW SMALBERGER
DESCRIPTION OF DRAWING	LOADING FRAME 1
SCALE	AS SHOWN
SIZE	A4
DWG No.	11

**ELEMENTS:**

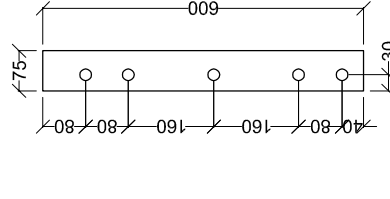
- a - 254X254X89
- b - PC200X75
- c - 60X60X8
- d - 152X1452X23

**NOTES:**

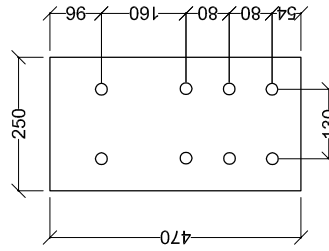
1. (b) is fixed between flanges of (a) to support bearing housing for loading frame, refer to Loading Frame 1.
2. End plate (6) fill space between flanges of (b) and flanges of (a).
3. End plate (5) that supports gusset (1) and (d), is fixed to (a) using X8 M20 8.8 bolts.
4. (c), bracing element, is fixed to Gusset (1) with X3 M16 8.8 bolts.
5. All bolts used to fixed elements to (a) is M20 8.8 bolts.
6. All welds are 5mm fillet welds, unless otherwise specified.
7. All steel is of grade S355JR, unless otherwise specified.



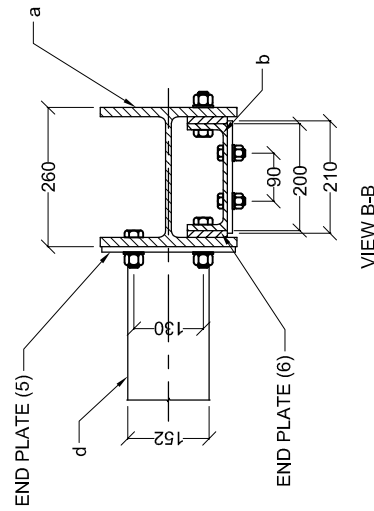
VIEW A-A



Channel (b) between flange of (a)



END PLATE (5) - 470X250X10



VIEW B-B

END PLATE (6) - 600X75X10

**Bracing Connection Detail 3**

SCALE 1:10

DRAWN BY	HJW SMALBERGER
DESCRIPTION OF DRAWING	
BRACING DETAIL 3	
SCALE	AS SHOWN
SIZE	A4
DWG No.	12